

MEASUREMENT OF THE FREQUENCY RESPONSE AND THERMAL
NEUTRON WAVE DISPERSION PARAMETERS IN WATER AND
WATER-VOID ASSEMBLIES

By

Mustafa Hasan ASHAA, B.Sc., M.Sc.

A Thesis submitted to the University of Aston
in Birmingham for the degree of

DOCTOR OF PHILOSOPHY

DEPARTMENT OF PHYSICS

AUGUST 1979.

SUMMARY

A square wave input of fast neutrons from the D-T reaction was supplied by a S.A.M.E.S. accelerator. The fast neutrons were thermalised by an iron-polypropylene arrangement which designed to provide a plane source of thermal neutrons with minimum pulse broadening. The thermal neutron waves were propagated axially in a water assembly with and without voids. The time profile of the thermal neutron pulse was recorded with lithium glass scintillation counters input to a multi-channel pulse high analyser used in a time sequence storage mode and synchronised with the source pulsing frequency.

From a Fourier analysis of the recorded thermal flux, the frequency response of the system was measured as a function of source frequency, position and void dimensions. This provided information on the space-dependent phase and amplitude of the wave, from which the attenuation factor and the phase shift per unit length were evaluated. The streaming factor of each water-void assembly was found to be a frequency-dependent quantity.

The dispersive properties of each assembly were expressed through the dispersion relation which relates the inverse complex relaxation length of the wave to the frequency of excitation and the nuclear properties of the system.

Three independent models were developed to calculate the dispersion parameters of the systems. The first model was a one group diffusion theory; the second model was based on a solution of Telegrapher's equation by P-1 approximation to account for transport effects, and the third model was to account for the thermalisation effects from the presence of a non-Maxwellian neutron energy spectrum. Calculations based on thermalisation theory predicted the experimental observations fairly well at frequencies less than 600 Hz.

KEYWORDS

Neutron wave, Streaming factor, Frequency response, Wave function, Neutron continuum.

ACKNOWLEDGMENTS

I should like to thank my supervisor, Dr. A. Bore, for his invaluable guidance and help throughout the course of this work. Thanks are also due to Dr. P.N. Cooper, for his useful advice and discussions and to Professor S.E. Hunt for his interest in this project.

I wish to express my gratitude to the technical staff of the nuclear physics laboratory, of the main workshop and of the computer centre of the University.

Finally, I would like to thank the Iraqi Atomic Energy Commission for providing me with leave of study throughout the period of this work.

To the memory of my parents

TABLE OF CONTENTS

	<u>Page</u>
SUMMARY	i
ACKNOWLEDGMENTS	iii
LIST OF SYMBOLS	1
CHAPTER ONE : TECHNIQUES RELATED TO NEUTRON STREAMING IN NUCLEAR SYSTEMS	2
1.1 An introduction to analysis technique for neutron streaming	2
1.2 The extent of the present work	3
1.3 A literature review	4
1.3.1 The static experimental and theoretical treatment	5
1.3.2 The dynamic experiment techniques and the theoretical treatment	7
1.3.2.1 Application of PST to neutron streaming problem	8
1.3.2.2 Application of NWT to neutron streaming problem	11
1.3.2.3 Comparison between PST and NWT	14
CHAPTER TWO : CONSTRUCTION OF A MODULATED THERMAL NEUTRON SOURCE ASSEMBLY	16
2.1 The fast neutron source	16
2.2 The external modulation of the fast neutron source	17
2.3 The required features of the thermal neutron source	22
2.4 Selection of the type of the neutron signal	23
2.5 Thermalisation using graphite	25
2.6 Neutron pulse shape measurements in graphite	28

	<u>Page</u>
2.7 Quantitative assessment of thermal neutron pulse broadening, (Computer code BROAD)	30
2.8 Fast neutron contamination of the thermal neutron pulse	33
2.9 Modification of thermalisation arrangement	36
2.9.1 Thermalisation with iron-graphite	38
2.9.2 Thermalisation with iron-polypropylene	39
 CHAPTER THREE : THE DESIGN OF A NON-MULTIPLYING ASSEMBLY WITH VOIDS	
3.1 The water moderator	41
3.2 The choice of void arrangements	42
3.3 Construction of the void cell	43
 CHAPTER FOUR : NEUTRON DETECTION AND DATA ACQUISITION SYSTEM	
4.1 The monitoring of the fast neutron production ...	48
4.2 Thermal neutron detection in the experimental assembly	49
4.3 The data acquisition system	56
4.3.1 Pulse generation and signal analysis	56
4.3.2 The frequency divider unit	57
4.3.3 The dual gate unit	57
4.3.4 The start-stop unit	59
4.3.5 Measurement procedure	59
 CHAPTER FIVE : EXPERIMENTAL MEASUREMENTS AND DATA ANALYSIS	
5.1 The measurement and the analysis of the experimental data	64
5.1.1 Data correction	66
5.1.2 Fourier analysis of the corrected data	66
5.2 The space dependent transfer function	68

	<u>Page</u>
5.2.1 Measurement of the frequency response parameters	69
5.2.2 The frequency response of the water moderator without voids	75
5.2.3 The frequency response of water-void assemblies	75
5.3 Determination of space-independent neutron wave parameters	82
5.3.1 The mathematical treatment	82
5.3.2 Application to the experimental data	85
5.4 Determination of diffusion and thermalisation parameters	91
5.4.1 The mathematical treatment	91
5.4.2 Application to the experimental data	97

CHAPTER SIX : THEORETICAL MODELS FOR THE CALCULATION OF
NEUTRON WAVE PARAMETERS

6.1 Fundamental concepts of neutron wave calculations.	111
6.2 The methods of calculation of neutron wave parameters	113
6.2.1 One group diffusion model	113
6.2.2 The one group P-1 approximation model	117
6.2.3 The thermalisation theory model	119
6.3 Evaluation of void effects on the neutron wave parameters	124
6.4 The frequency dependence of anisotropy	130
6.4.1 Evaluation of anisotropy by diffusion theory	130
6.4.2 Evaluation of anisotropy by P-1 theory	134
6.4.3 Evaluation of anisotropy by thermalisation theory	136

	<u>Page</u>
CHAPTER SEVEN : THE VALIDITY OF THE THEORETICAL MODELS	
7.1 Comparison between theoretical models	139
7.1.1 Calculations for water assembly without voids, (computer programme WAVE)	139
7.1.2 Comparison of theoretical results	141
7.2 Comparison between theoretical and experimental results, - water moderator without voids -	146
7.3 Determination of the diffusion and thermalisation parameters for water assembly without voids	157
7.4 Theoretical results for water-void assemblies, (computer programme VOIDWAVE)	159
7.5 Determination of the diffusion and thermalisation parameters for water-void assemblies	171
7.6 Discussion of errors	173
7.6.1 Errors associated with experimental technique	173
7.6.1.1 The changes in detector efficiency .	173
7.6.1.2 Errors in detector positions	175
7.6.2 Systematic errors	175
7.6.3 Statistical errors	176
7.6.4 Errors associated with the theoretical calculations	178
7.6.4.1 The energy dependence of the system nuclear parameters	178
7.6.4.2 Errors associated with streaming calculations	179
CHAPTER EIGHT : CONCLUSIONS AND RECOMMENDATIONS	
8.1 Conclusions	183
8.1.1 Frequency response measurements	183

	<u>page</u>
8.1.2 Thermal neutron wave parameters	
measurement	183
8.2 Recommendations for future work	186
APPENDIX I : Computer code - BROAD -	187
APPENDIX II : Computer code - WAVE -	193
APPENDIX III : Computer code - VOID -	200
BIBLIOGRAPHY	210

LIST OF SYMBOLS

- B^2 the geometrical buckling, cm^{-2}
- C Diffusion cooling coefficient, $\text{cm}^4 \text{s}^{-1}$
- D_0 Diffusion constant, cm
- d Extrapolation length cm
- F Spectrum hardening coefficient, $\text{cm}^6 \text{s}^{-1}$
- K Leakage factor, $\text{neutron} \cdot \text{s}^{-1} \text{cm}^{-2}$
- L^2 Diffusion area cm^2
- $M(E)$ Neutron Maxwellian energy distribution
- Σ_a Macroscopic absorption cross section, cm^{-1}
- Σ_s Macroscopic scattering cross section, cm^{-1}
- Σ_t Total Macroscopic cross section, cm^{-1}
- Σ_{tr} Transport macroscopic cross section, cm^{-1}
- $\Sigma_s(E' \rightarrow E)$ Scattering kernel for neutron of energy E' scattered into energy interval between E and $E+dE$, cm^{-1}
- α Amplitude attenuation per unit length constant, cm^{-1}
- ξ Phase shift per unit length, cm^{-1}
- ρ inverse complex relaxation length, cm^{-1}
- ω Source frequency, $\text{rad} \cdot \text{s}^{-1}$
- λ Neutron pulse decay constant, s^{-1}
- (||) Suffix to indicate the axial direction
- (⊥) Suffix to indicate the transverse direction.
- v Thermal neutron velocity at 22°C , $\text{cm} \cdot \text{s}^{-1}$
- \bar{u} Wave front velocity $\text{cm} \cdot \text{s}^{-1}$

CHAPTER ONE

TECHNIQUES RELATED TO NEUTRON STREAMING MEASUREMENT

IN NUCLEAR SYSTEMS

1.1 An introduction to analysis techniques for neutron streaming

The problem of neutron transport in heterogeneous media is one of great importance in reactor physics. The physical dimensions of any nuclear system depend largely upon the mean displacement of neutrons from their birth to the point of their capture or escape. The presence of empty spaces serves effectively to lengthen the neutron mean displacement and, consequently, increase the critical size of the reactor.

Voids in research reactors, in the form of irradiation holes, control rod sleeves and in-core instrumentation, are important design features. In power reactors, voids occur in the form of cooling ducts and sometimes as part of the control features. Therefore, an accurate knowledge of the effect of voids is important for the design, operation and safety of all reactors.

A first order effect of cavities can be found on the basis of the overall reduction in the density of the medium. A decrease in the average density means a corresponding reduction in the average macroscopic absorption, Σ_a , scattering, Σ_s , and transport, Σ_{tr} , cross sections. From diffusion theory one can predict that the diffusion area, (L^2) , will be increased accordingly. This is only an approximation, for when a void channel is introduced into a medium it will cause an anisotropic diffusion of neutrons due to streaming along the channel axis. Therefore, direction-dependent thermalisation and diffusion parameters are required for more accurate analysis.

Numerous attempts have been made to provide a theoretical basis for neutron streaming effects. Section 1.3 will deal in detail with these different approaches. Most of the experimental work has been with exponential or steady state sources, in which diffusion parameters were determined from the spatial distribution of the flux.

The dynamic approach to this problem promised more accuracy in measuring the thermalisation and diffusion parameters of the system under test. Two theoretically equivalent methods are used, namely, the pulsed sources technique, (PST), and the neutron wave technique, (NWT). In the PST, the neutron leakage rate is more directly measured by relating it to the time behaviour of the neutron flux following the introduction of a neutron burst into the assembly. In the NWT the neutron field is excited in some periodic fashion and the disturbance created is called a neutron wave. This disturbance describes the collective behaviour of the neutron field according to the mode of its interaction with the nuclei of the assembly. The inverse relaxation length, (ρ), of the neutron wave, i.e. the distance travelled by the wave to reduce the amplitude of the damped oscillation by a factor of e , the variation of the phase angle and the decay of the amplitude of the wave are dependent on the frequency of modulation, as well as on the diffusion and thermalisation parameters of the media in which the wave is propagated.

Although NWT has many advantages over PST, it has not been applied to the problem of neutron streaming in empty channels in a moderator. Moreover, the application of this technique for multiplying assemblies containing empty channels can be cited in very few publications, QUDDUS, et al (1969) and WARNER (1970).

1.2 The extent of the present work

The present work is an attempt to apply the NWT to study the

streaming of thermal neutrons along the vertical axis of long empty cylinders placed in a water moderator. The key to the quality of the measurements is the initial condition of the thermal neutron source employed in the experiment. A considerable effort was expended in construction of an optimum plane, thermal neutron source. The resultant source characteristics are presented in Chapter Two of this work. A lattice containing seven empty, parallel cylinders was placed vertically in a tank containing 800 litres of water. Four different lattices were used, of different cylinder radii but of the same effective height. The detail design of the assemblies is given in Chapter Three, while the neutron detection technique and the relevant electronic circuitry is employed in neutron flux measurements within the assembly presented in Chapter Four.

The frequency response of the system, with and without voids, was measured. The observed effects of the voids on the shape of the frequency response curves of the system and on the neutron wave parameters are presented in Chapter Five, as well as the methods developed for analysis of the experimental data are presented, together with the evaluated parameters of the neutron wave from which the diffusion and thermalisation of the system can be evaluated. Three theoretical models were employed to evaluate the experimental results. The development of the theoretical models is presented in Chapter Six. Chapter Seven deals with the comparison between theoretical results predicted by each model with those obtained experimentally. Finally, in Chapter Eight some principal conclusions drawn from this work are given, in addition to some experimental and analytical studies suggested to extend and compliment the present work.

1.3 A literature review

The work done in the field of neutron streaming through voids in a nuclear system can be classified according to the experimental

techniques employed by the authors. These can be divided into two main groups according to the initial condition of the neutron source employed:

- i. A static approach based on steady state sources;
- ii. A dynamic approach based on time-dependent, periodic or non-periodic sources.

1.3.1 The static experimental and theoretical treatment

In much of the theoretical work, the problem is treated by homogenising the heterogeneous effects created by the presence of voids. BEHRENS (1949) determined the characteristics of a theoretical medium in which the neutron distribution coincides with the distribution of a real medium averaged over a cell. Similar, but more detailed work was carried out by CARTER AND JARVIS (1961), which reached a different expression for the radial effects. However, better results are obtained by the application of the iteration methods: the Monte Carlo calculation used by SCHAEFER and PARKYN (1958) and the perturbation theory applied by MARTY and SCHNEEBERG (1962). Although the iteration calculation predicts better results, it is a lengthy computational approach.

In his early work BEHRENS (1949) derived a formula for cavities of any shape, assuming that the cavities were uniformly distributed in a homogeneous neutron flux and that all neutrons had identical probability of passing through them. Taking the diffusion area, (L^2), as a reference, Behrens obtained the following relations:

- i. For parallel cylindrical cavities of any cross sectional area located at a great distance apart so that the neutron does not traverse more than one cavity during the time of one free path, the axial ($S_{||}$) and the radial (S_{\perp}) streaming can be given as:

$$S_{\parallel} = \frac{L_{\parallel}^2}{L_m^2} = 1 + 2m + \frac{3}{2} m Q \frac{r}{\lambda_{tr}} \quad \dots\dots\dots 1.1$$

$$S_{\perp} = \frac{L_{\perp}^2}{L_m^2} = 1 + 2m + \frac{3}{4} m Q \frac{r}{\lambda_{tr}} \quad \dots\dots\dots 1.2$$

where L_{\parallel}^2 and L_{\perp}^2 are the parallel and perpendicular diffusion areas for the anisotropic lattice, L_m^2 is the diffusion area for a homogeneous lattice, m is void to material ratio, Q is a constant dependent on the shape of the void, r is the hydrolic radius of the void, which can be calculated for any void shape as:

$$r = \frac{2 \times \text{void volume}}{\text{void surface area}}$$

and λ_{tr} is the transport mean free path of the neutron in the moderator.

Although Behrens gave an approximation formula which can be used for any distance between cavities and any shape of cavity, equations (1.1) and (1.2) cannot be applied to the case of non-uniform distribution of holes or to the presence a small number of holes. GRANT (1958) proved that equation (1.2) is incorrect in slab geometry. CARTER (1961) applied appropriate boundary conditions for an asymptotic neutron flux on the cavity surface. He gave a different expression for the radial streaming:

$$S_{\perp} = \frac{L_{\perp}^2}{L_m^2} = 1 + m \left\{ 2 + \frac{r + m(2r + \frac{3}{2}\lambda_{tr})}{r + \lambda_{tr} + m(\frac{3}{2}\lambda_{tr})} \right\} \quad \dots\dots\dots 1.3$$

which gives lower values of (S_{\perp}) than those obtained from equation 1.2. Calculation of S_{\parallel} and S_{\perp} carried out by SCHAEFLER and PARKYN

(1958), using a Monte Carlo method, gave lower values for both streaming parameters.

BENOIST (1968) produced a general treatment for neutron transport in a heterogeneous medium which gives, as a first approximation, the same results as obtained by Behrens. Three corrections to the Behren's results are given to allow for:

- i. the consecutive passage of neutrons through the same channel;
- ii. the interaction between different channels;
- iii. the finite dimensions of the void cell.

More satisfactory results, based on an analytical model which allows for flux mapping inside the channels, and hence, for neutron currents along a channel wall, are given by ETEMAD et al (1964). He also reports a set of experimental results in good agreement with his theoretical prediction.

From the above discussion it is evident that there is not a single, general but rigorous theory to the problems presented by experimental work employing steady state neutron sources. This demanded a new approach; the problem was resolved by the dynamic experiment using periodic and non-periodic neutron sources.

1.3.2 The dynamic experiment techniques and theoretical treatment

Most of the experiments to be discussed in this section can be divided into two classes:

- i. Experiments using PST;
- ii. Experiments using NWT.

1.3.2.1 Application of PST to neutron streaming problems

Under certain limitations, explained by CORNGOLD (1964), a thermalised neutron field in a moderator in a true asymptotic state decays exponentially with time. The PST method is essentially the injection of a burst of neutrons into a system and measurement of the neutron population with thermal neutron detectors. This exponential decay, caused by leakage and absorption, depends on the size and the shape of the system i.e. on the geometrical buckling, (B_g^2) as well as on the nuclear properties of the moderator. It was assumed by DAUGHTRY and WALTNER (1965) and by JOSHI et al (1965) that the variation of the decay constant (λ) with the buckling at a given temperature can be expressed for a $(\frac{1}{v})$ moderator as:

$$\lambda = \lambda_0 + DB^2 - CB^4 + FB^6 + \dots \dots \dots 1.4$$

where $\lambda_0 = v\Sigma$, D is the diffusion coefficient, C is the diffusion cooling, which accounts for the higher probability of leakage of higher energy neutrons from the system boundary, and F is a constant which accounts for the spectral variation of neutron flux and is called the spectrum hardening constant. The PST method is to measure the time constant (λ) of the decay and to correlate it to the geometrical buckling, (B_g^2) , of the assembly. The resulting (λ) versus (B_g^2) curve is analysed in terms of the diffusion parameter of the moderator. In 1965 the Proceedings of the Symposium on Pulsed Neutron Research, organised by IAEA, were published. In the first volume there were many contributions to the application of PST to non-multiplying assemblies. The extensive theoretical work of CORNGOLD (1965), WOOD (1965) and PUROHIT (1965) provided a sound analytical model to the problem of the neutron thermalisation parameter. POOLE (1965) gave an excellent review of the application of PST to the measurement of neutron spectra in moderators and

reactor lattices. The common difficulties shared by all workers in applying (λ) versus (B_g^2) curve analysis were:

- i. the precise determination of (λ) in the presence of a non-asymptotic neutron flux and neutron background, especially in crystalline moderators like beryllium and graphite where the trapping of the low energy neutrons creates a limit beyond which (λ) cannot be detected discreetly;
- ii. the calculation of (B_g^2) from a given dimension of the scattering medium, where the extrapolation distance decreases with the increase of (B_g^2) due to diffusion cooling effects.
- iii. the statistical fitting of the (λ) versus (B_g^2) curve and the length of the (B_g^2) interval used.

BULL et al (1970) performed an experiment on a graphite system and suggested a solution to (i) by placing the system in cadmium-lined box with a borated polyethelene shield. To overcome (ii), the extrapolation distance (d) was calculated by an iterative method from the diffusion constant, D_0 , for a given energy distribution as:

$$d = 2.13 \frac{\overline{vD_0}}{v} \dots\dots\dots 1.5$$

To overcome (iii) it was suggested that $(B_g^2)^*$ intervals should be increased for small size systems and decreased for a large size system, to provide better statistical fitting.

The application of PST to study the effects of void channels in moderating media were reported by UTZINGER (1965), PAGE (1967), DENIZ (1968), BULL et al (1970), DANCE and CONNOLY (1971). They

* the g suffix to the buckling will be omitted hereafter

all used the principle suggested by BENOIST (1969) that, for streaming studies, direction-dependent diffusion parameters must be used.

Benoist defined a direction-dependent diffusion coefficient (D_k) in term of leakage (K) as:

$$K = \sum_{k=1}^3 D_k B_k^2 \iiint \phi_{(x,y,z)} dx dy dz \dots\dots\dots 1.6$$

where $\phi_{(x,y,z)}$ is the space dependent flux in an anisotropic system and k refers to the directions x, y and z. If the k direction is designated parallel and perpendicular to the axial direction of the channels, then:

$$D_{\perp} = D_{x,y} \quad \text{and} \quad D_{\parallel} = D_z$$

$$B_{\perp}^2 = \frac{\pi^2}{(x+2d)^2} + \frac{\pi^2}{(y+2d)^2} \dots\dots\dots 1.7$$

DANCE and CONOLLY (1971) solved the equation for neutron transport in the void channels and described the time behaviour of the neutron flux in the moderator in relation to the void dimensions. They found that a single decay constant cannot describe the neutron population decay following the introduction of a neutron pulse into a system containing void. The application of PST to evaluate the direction-dependent diffusion coefficients of a system requires a definition of the parallel and the perpendicular diffusion coefficient in terms of parallel and perpendicular leakage, i.e. K_{\parallel} and K_{\perp} . The parallel leakage K_{\parallel} per unit flux per unit volume can be found from the following relation:

$$K_{\parallel} = D_{\parallel} B_{\parallel}^2 \iiint \phi_{(x,y,z)} dx dy dz \dots\dots\dots 1.8$$

The total volume-intergrated flux refers only to the flux in the moderator, and the flux in the void should be included. This would require a prior knowledge of the flux space-time distribution in the void channel or, with certain limitations detailed by DANCE and CONOLLY (1971), the knowledge of the ratio of the actual volume-intergrated flux to the simple cosine flux that would exist without the void. Another approximation is to neglect the void-moderator interface flux variation. Therefore, the validity of extending the conventional PST to anisotropic system requires many approximations and assumptions.

1.3.2.2 Application of NWT to neutron streaming problems

In this type of experiment, the neutron field is excited in some periodic fashion. The resulting disturbance is called a neutron wave. When a periodic excitation of frequency (ω) is injected at the boundary of a moderator at the plane $Z=0$, an attenuated plane neutron wave travelling in the positive Z -direction can be represented as:

$$\phi(z,t) = A_0 \text{Exp. } -\{\alpha z - j(\omega t - \xi z)\} \dots\dots\dots 1.9$$

where, A_0 is a constant for a source symmetric along the Z -axis,

α is the attenuation constant, i.e. the reciprocal of the attenuation length of the envelope of the wave shape, and ξ is the phase constant, i.e. 2π divided by wave length.

HETRIC (1971) derived relationships between the wave parameters (α) and (ξ) and the nuclear properties of the medium in which the wave travels:

$$\alpha^2 - \xi^2 = \frac{\Sigma_a}{D} = \frac{1}{L^2} \dots\dots\dots 1.10$$

$$2\alpha\xi = \omega \cdot \frac{1}{2vD_0} \dots\dots\dots 1.11$$

Eq. (1.10) shows that $(\alpha^2 - \xi^2)$ is exclusively a function of thermalisation parameters, while Eq. (1.11) shows that $(2\alpha\xi)$ depends primarily on the diffusion parameters, and both equations suggest that (L^2) and (vD) could be experimentally found from observation of (α) and (ξ) .

PEREZ and UHRIG (1963) used a sinusoidal neutron source placed at the centre of the lower face of a rectangular-shaped moderator to study the thermalisation properties of a $(\frac{1}{v})$ moderator. They found that NWT is equivalent to a poisoning experiment, where the frequency of modulation is equivalent to the amount of the $(\frac{1}{v})$ poison. PEREZ and BOOTHE (1965) presented a series of measurements using graphite as a diffusion medium and indicated that diffusion theory is valid only for modulation frequencies smaller than the inverse of the time between two neutron collision.

Advances in the experimental and theoretical fields of NWT can be cited in the proceedings of a Symposium on Neutron Noise, Wave and Pulse Propagation edited by UHRIG (1967). The work of MOORE (1967), KUNAISH (1967) and BOOTH and PEREZ (1967) are of particular relevance to this work. MOORE (1964), (1965) and (1967) treated the problem by dealing with the dispersive nature of a neutron wave, (i.e. the dependence of the phase lag of the wave on the distance from the source). Moore defined (ρ) and $(\rho)^2$ dispersion laws as the plots of $(2\alpha\xi)$ versus (ω) and $(\alpha^2 - \xi^2)$ versus (ω) . From these plots Moore predicted the presence of exponential flux components in the neutron wave field. The analytical work of WILLIAMS (1968), and WOOD (1969) reached the same conclusion and interpreted the exponential flux as wave continuum in addition to the discrete mode of the wave. To include the continuum effects on the measurement of (α) and (ξ) , WARNER and ERDMAN (1969a) used the transport theory solution for neutron wave propagation and reported that there is a frequency limit

beyond which diffusion theory fails to explain the NWT experiments. This limit is when the source frequency is greater than the product $(v \sum_e)$ for a $(\frac{1}{v})$ moderator. Further work by WANER and ERDMAN (1969b) suggested that the frequency limitation depends on whether the moderator under investigation is a crystalline or non-crystalline moderator. The spatial dependence of (α) and (ξ) at different frequencies is investigated by RITCHIE and WHITTLESTONE (1972) and (1973). They found for beryllium oxide there is a limit of 520Hz below which the spatial dependence of (α) and (ξ) is of no significance and the N.W. has the properties of discrete mode of propagation. In the frequency range 520 - 720 Hz, the spatial dependence is noticeable, and beyond 720Hz diffusion theory failed to interpret the experimental results for the crystalline moderator. No similar work has been cited for non-crystalline moderator.

Pulsing the source in a square wave fashion can also be used in the same way as a sinusoidal input. Since the square wave can be fourier analysed into an infinite number of harmonics of the fundamental frequency, it can be considered as a superposition of sinusoidal inputs. For a linear system the output will be the superposition of the outputs due to individual components of the input. It has the advantage that the data for many frequencies can be taken simultaneously. However, it was reported by GIL RAMOS (1974) that the number of frequencies for which the measurement can be taken is limited because the amplitude of the higher harmonics decrease linearly with the order of harmonics. UHRIG (1970) suggests the use of a random square wave to overcome this difficulty.

The application of NWT to study the quantitative effects of neutron streaming in a moderator containing voids is very limited. The most relevant work that can be cited is that carried out by WAGNER (1970). However, this work was devoted to a measurement of

the degree of anisotropy as an overall parameter of a multiplying system with void channels. Moreover, the analysis is handicapped by a low upper limit to the modulation frequency.

1.3.2.3 Comparison between PST and NWT

It can be said that both PST and NWT are theoretically equivalent. PEREZ and UHRIG (1967) stated that the location of the neutron source makes necessary an essentially different analytical model for NWT. The equivalence of PST and NWT is detailed by MICHAEL and MOORE (1968). The coupling mathematical relationships described in this work will be presented in Chapter Six. The time-dependent form of the source in NWT is not relevant and it is a matter of convenience, so long as it is square integrable and can be Fourier analysed. The different types of periodic source will be discussed in Chapter Two. Some of the experimental features which distinguish one method from the other are summarised in Table 1.1.

TABLE 1.1

Comparison of experimental features of PST and NWT methods

PST	NWT
<p>The energy associated with the signal has a continuous spectrum.</p>	<p>The energy associated with the signal has a discrete spectrum.</p>
<p>The accuracy of the results is dependent on the noise level in nuclear system under test.</p>	<p>The test signals are assymmetric and will discriminate against background noise in the system.</p>
<p>The frequency response is obtained by taking the ratio of the Fourier transform of the output to the Fourier transform of the input.</p>	<p>The frequency response is obtained by taking the ratio of the Fourier integral of the output to the Fourier integral of the input.</p>
<p>It is a time-domain technique where the neutron population is a transient quantity.</p>	<p>It is a variable frequency technique where a quasi-static state can be established.</p>
<p>The fundamental mode prevails during the decay of neutron population.</p>	<p>The disturbance propagates away from the source and the dynamic behaviour of neutron population is spatially dependent.</p>
<p>One quantity (i.e. the decay constant) can be measured.</p>	<p>Two quantities (i.e. amplitude attenuation and phase lag) can be measured simultaneously.</p>

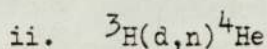
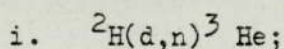
CHAPTER TWO

CONSTRUCTION OF A MODULATED THERMAL NEUTRON SOURCE ASSEMBLY

The experimental arrangements to provide an optimised source are described in this Chapter. A brief outline of the method of fast neutron production is given prior to a description of the source external modulation technique. The greater part of this chapter is devoted to the description of the construction of the thermalisation systems and their performance. Three types of moderating materials were tested and their characteristics are compared.

2.1 The fast neutron source

With the use of particle accelerators, it is possible to produce neutrons with energies from a few kev up to about 20 Mev. Accelerated charged particles such as protons, deuterons or tritons produce fast neutrons copiously with the lightest elements as targets. Two principle reactions are widely used. These are:



Both reactions can be achieved with a deuteron beam of energy of 150 kev. In reaction (i), also called the D/D reaction, neutrons of energies around 2.5 Mev are produced. In reaction (ii), also called T/D reaction, neutrons with energies between 13.6 - 15.8 Mev are produced. For a particular deuteron beam energy, the T/D reaction offers higher neutron yield compared with the D/D reaction, which makes it more desirable in the present work, despite the need to thermalise the 14 Mev neutrons.

The deuteron beam was furnished by a type-J S.A.M.E.S.

electrostatic accelerator with high voltage generating capacity up to 160 Kv. A description of the accelerator is given by DOUKAS (1971).

The target assembly consisted of a thin, circular titanium-tritide target (type TRT51, manufactured by Radiochemical Centre, Amersham, U.K.) and integral water-cooling system, coupled to the S.A.M.E.S. accelerator by a 65 cm long flight tube. The target assembly was placed on a graphite pedestal under the layers of moderator material to be tested. A detailed description of the target mounting and its cooling system is given by TWUM-DANCO (1969).

2.2 The external modulation of the fast neutron source

The important feature of the neutron detection technique used in this work is that the output from the neutron detectors had to be sampled by a multiscaler at regular intervals during each cycle of the neutron pulse. Therefore, it was necessary for the pulsing frequency to be a sub-multiple of that frequency controlling the channel advance command of the analyser. An external pulse generator and associated electronic units were used to maintain this synchronisation.

The method of pulsing the S.A.M.E.S. accelerator was adapted from COOPER and DOUKAS (1971), and GIL RAMOS and COOPER (1974). In the later work, a light signal of the same shape as the driving signal was produced by a light emitting diode (LED), type 1A48, which has an output of 40 uW at 100 mA peak current and a peak wavelength of 930 nm. The signal was transmitted to the high voltage terminal of the accelerator where it was detected by a light sensitive diode, type LS400. This was accomplished by means of a rigid PVC tube housing two lenses to improve the light collection and to provide adequate focussing onto the LS400 diode. The signal detected by LS400 diode was subsequently amplified by means of an integrated circuit

amplifier to drive the base of a high voltage transistor, type BU105. This transistor switched the voltage to the ion source oscillator of the accelerator on and off periodically, at the required pulsing frequency. In this way the beam pulse was always in-phase with the transmitted pulse.

This method of external pulsing was improved by the following modifications:

- i. the 1A48 LED was replaced with a lead-framed narrow beam LED, type FPE104, which provided a higher output of 10mW/sr at 100mA. This permitted the removal of the focussing lenses from the pipe coupling the two LEDs;
- ii. the single BU105 transistor was replaced with a Darlington pair to reduce the sensitivity of the pulsing system to impedance variations;
- iii. adequate screening was provided against the intense RF field produced by the ion source oscillator of the S.A.M.E.S. accelerator.

These modifications improved both the reliability and the performance of the S.A.M.E.S. external pulsing circuitry.

The driving signal to the LED was taken from the output of the frequency dividing circuit network constructed from two SN 7490AN and two SN 7493AN integrated circuits. The circuit diagram of the dividing network will be presented as a part of the data acquisition system in Chapter Four. The circuit diagrams of the light receiver are shown in Figures 2.1 and 2.2, and a photograph of the S.A.M.E.S. light coupling system is provided in Figure 2.3.

Ideally, the fast neutron production should follow the shape of the external pulsing signal and, therefore the manner in which the

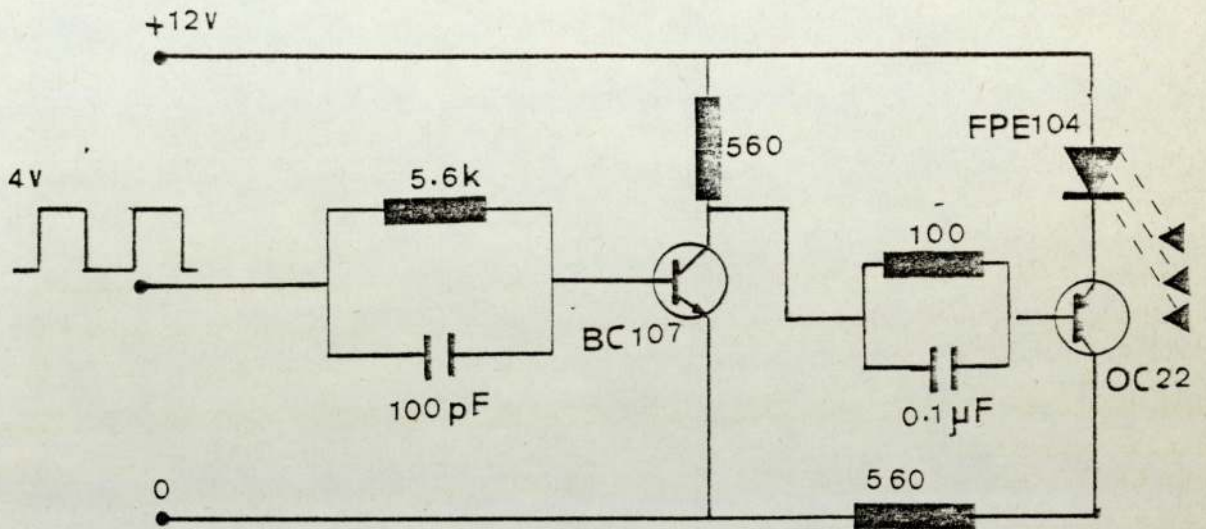


Fig.2.1 Light transmitter circuit.

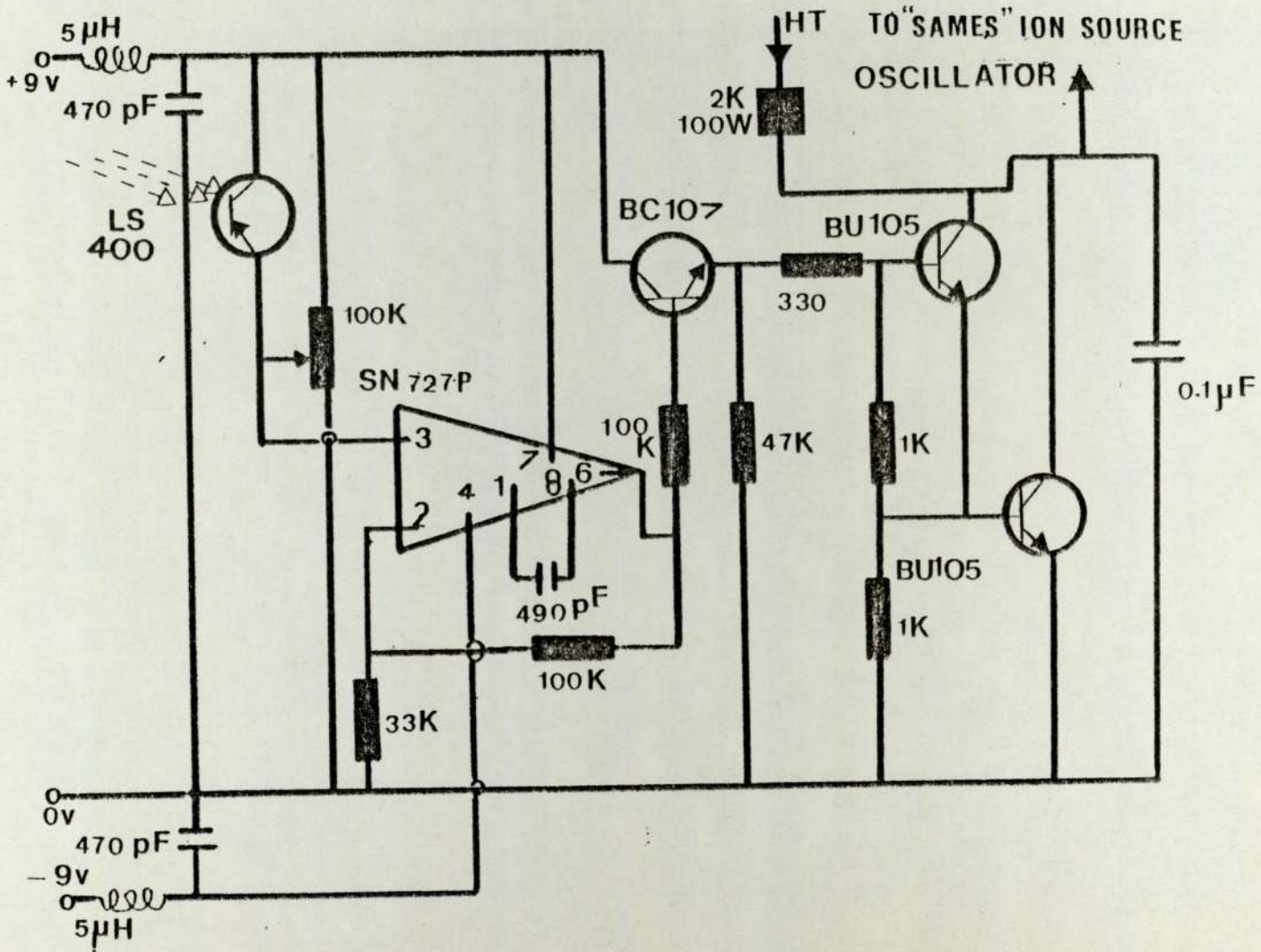


Fig. 2.2. Light receiver circuit.

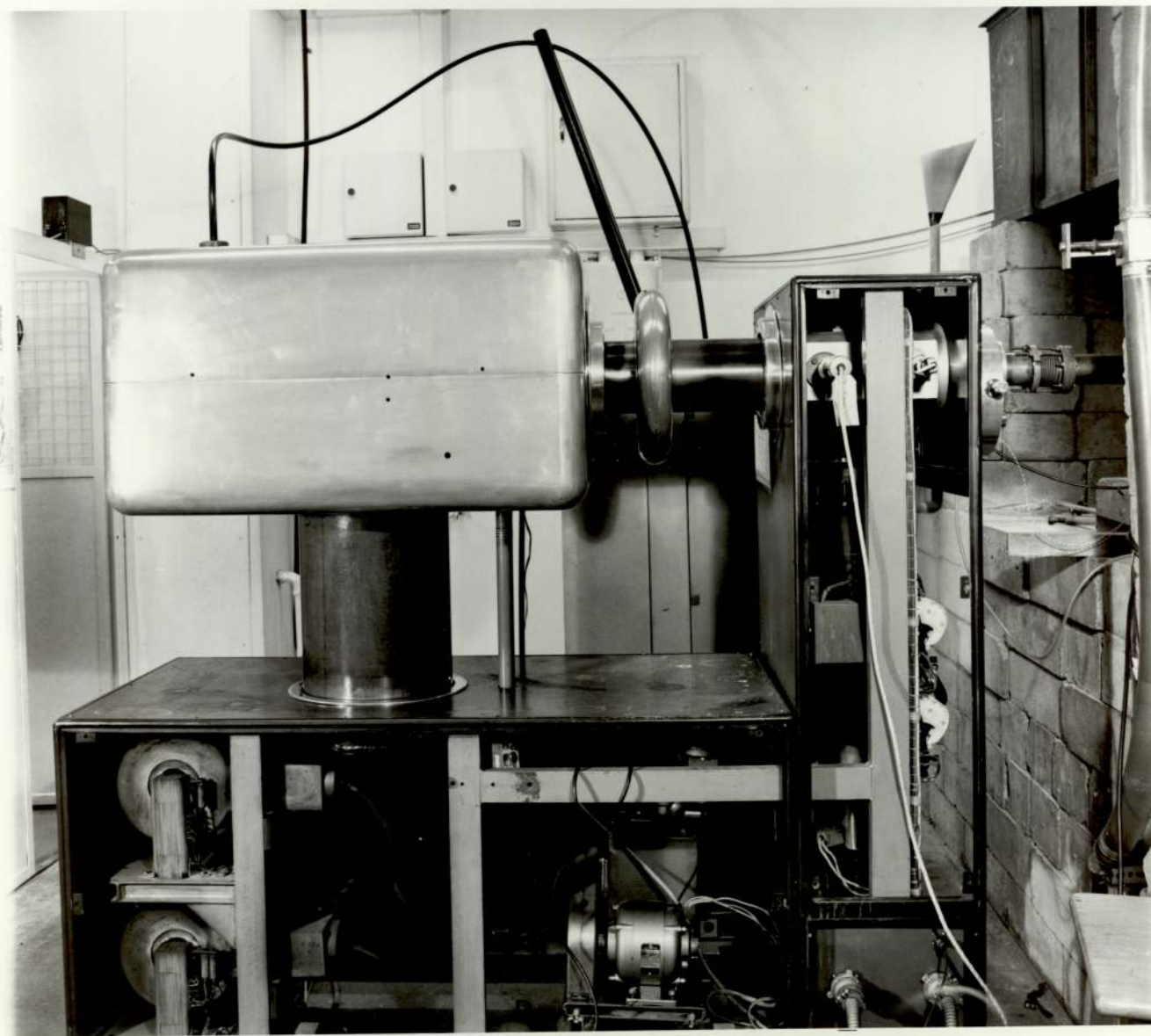


FIG. 2.3. THE S.A.M.E.S. ACCELERATOR

high tensions is applied to the S.A.M.E.S. oscillator circuit. These characteristics were investigated before any modifications were introduced into the pulsing circuits. It was found that with the previous circuitry the performance of the external pulsing system was reliable up to frequency of 1000 Hz, above which a distortion in the pulse shape onto the ion source was noticed. By the introduction of (i) and (ii) above, pulse shape distortion was not significant below 1500 Hz. The distortion above 1500 Hz was attributed to the instability of the output voltage of the oscillator power supply. This instability was corrected by the provision of a better stabilised power supply, and extended the upper frequency limit to 2700 Hz. With all these changes incorporated, the distortion in the voltage pulse shape applied to the ion source oscillator of the S.A.M.E.S. was insignificant below 10KHz, which is far beyond the desired experimental frequency range mentioned.

2.3 The required features of the thermal neutron source

The NWT has been employed in this work, using a square pulse which can be Fourier analysed into an infinite number of harmonics of the fundamental frequency. Ideally, the thermal neutron source in such experiments should have three basic characteristics. In the first instance the source should have a high intensity to overcome reduced neutron flux intensities at spatial distances far from the source. Secondly, it should have a large modulation depth for better Fourier analysis. Thirdly, it should be a well-thermalised source with minimum contribution of neutrons of higher energy. It was reported by PEREZ and BOOTH (1965), that the presence of high percentage of higher energy neutrons will create a distributed source of thermal neutrons throughout the assembly, which would mask the original propagation from the plane ($Z=0$) boundary.

Unfortunately, it is not possible to optimise all three requirements in a single design because one requirement may conflict with another. It is necessary to compromise, having in mind the following design objectives:

- i. thermalisation of the 14 Mev neutrons;
- ii. maximum thermal-to-fast neutron ratio;
- iii. planer uniformity of the thermal neutron wavefront;
- iv. maintenance of the thermal neutron pulse shape.

2.4 Selection of the type of the neutron signal

The quality of the results in neutron wave experiment depends partly on the source conditions described in section 2.3, and on the duration, shape and the amplitude of the neutron pulse, i.e. the test signal. The quality of any signal can be specified by the signal energy at selected frequencies. The signal energy at a particular frequency is determined by the total energy in the signal and the distribution of this energy over the frequency range. The total energy in a periodic signal can be given as:

$$E = \int_0^T (f_{(t)})^2 dt \quad \dots\dots\dots 2.1$$

where $f_{(t)}$ is the signal measured relative to its average value and T is the time over which the signal is input to the system. Thus, for a signal with amplitude of A, the total energy (E) is given as:

$$E = A^2.T \quad \dots\dots\dots 2.2$$

In selecting a particular signal the following points must be considered:

- i. the signal must contain many harmonics, permitting the determination of the frequency response at a number of frequencies in a single test,
- ii. the signal amplitude determines the amplitude and the location of the harmonics to be evaluated, therefore better analysis with higher modulation depth,
- iii. the lowest desired frequency determine the duration of the test (T), which can be related as:

$$T = \frac{2 \pi n}{\omega_{\min}}$$

where n is the number of the cycles,

- iv. the minimum signal duration in the pulse train is determined by the highest frequency desired in the test, for shorter pulses give a larger fraction of signal energy at high frequencies,
- v. the required level of discrimination against the noise in the nuclear system is determined by the signal symmetry, the best discrimination can be achieved by non-symmetric signals, e.g. the square pulse.

The mathematical analysis for different signal spectra is given by KERLIN (1972), who showed that the square wave has the following spectrum:

$$\left. \begin{aligned} E_k &= \frac{0.81 A^2 T \cdot n}{K^2} && \text{for odd } K \\ E_k &= 0 && \text{for even } K \end{aligned} \right\} \dots\dots\dots 2.3$$

where E_k is the energy associated with the kth harmonic, n is the

number of cycles, A is signal amplitude and T its duration.

A square wave can be Fourier analysed to allow simultaneous measurement of the frequency response of a nuclear system over many frequencies. However, the signal energy is concentrated in the first harmonic, as can be seen from Eq. (2.3), i.e. for $K = 1$ the first harmonic contains 81% of the signal energy. This limits the number of harmonics that can be evaluated since the amplitude of the higher harmonics decrease rapidly with the order of harmonic, as shown in Figure 2.4. For this work the square wave was selected as the shape of the input signal because it fulfilled all the requirements listed in (i) to (v) above.

2.5 Thermalisation using graphite

In the previous experiments performed by DOUKAS (1971), the 14 Mev neutrons were thermalised by using graphite as the moderating material. The neutron source was placed on the graphite pedestal at a distance 13.5 cm below the centre of the lower face of the nuclear assembly, similar to the arrangement shown in Figure 2.5. The characteristics of this arrangement were investigated in relation to the requirements listed in section 2.3.

The shape of the neutron of neutron wavefront passing into the assembly was measured by obtaining values for the relative thermal neutron intensity along two perpendicular axis drawn in the plane of the assembly base (Figure 2.5). The origin is that point directly above the source; one of the axis (Y-axis) is fixed parallel to the direction of beam entry. The neutron flux was measured at different (x,y) points on the $Z=0$ plane. The thermal neutron intensity was measured using two ${}^6\text{Li}$ scintillators, with measurements taken simultaneously at two points on either side of the source at the same radial distance. (The detection circuitry and technique will be

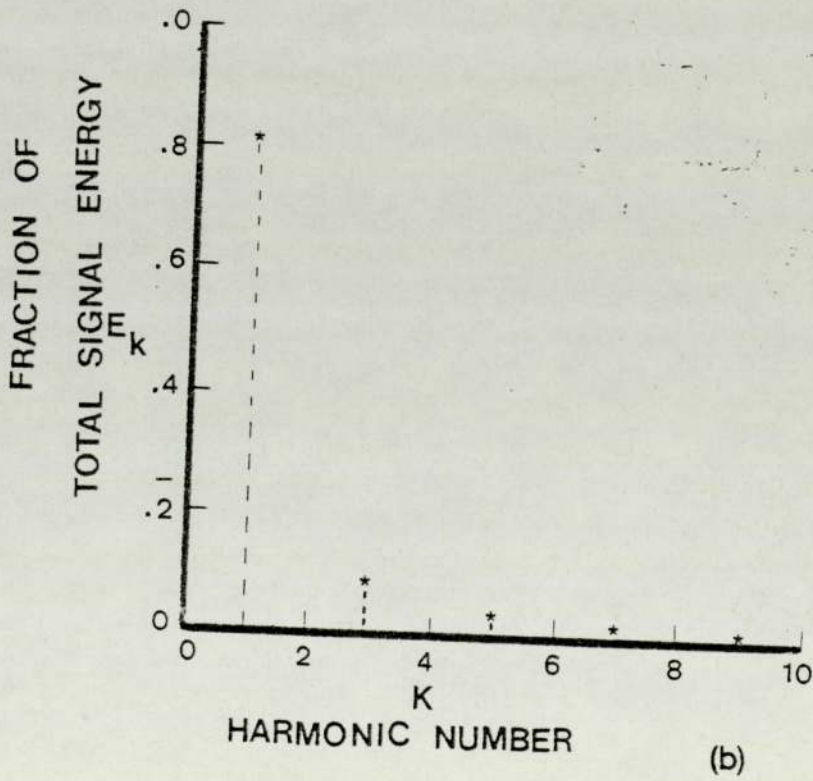
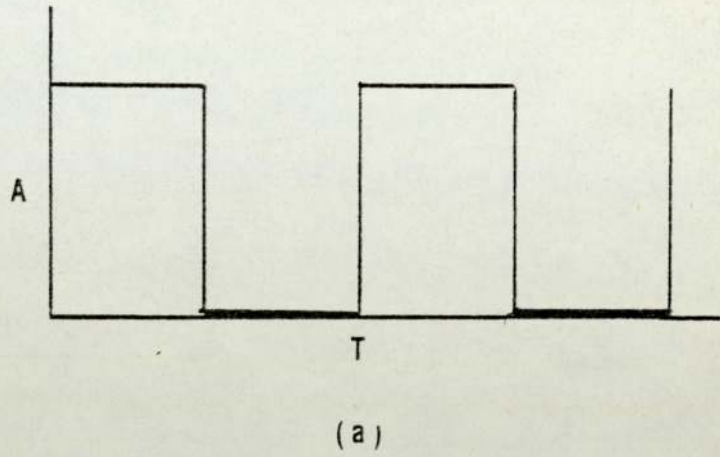


Fig.2.4. A square wave (a) and its energy spectrum (b).

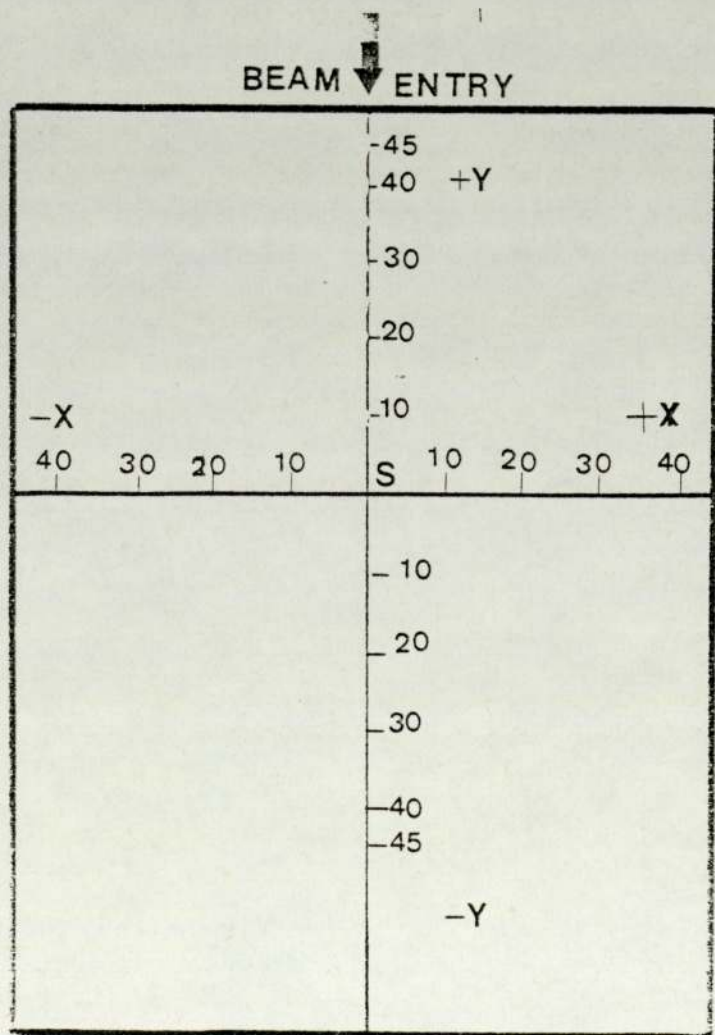
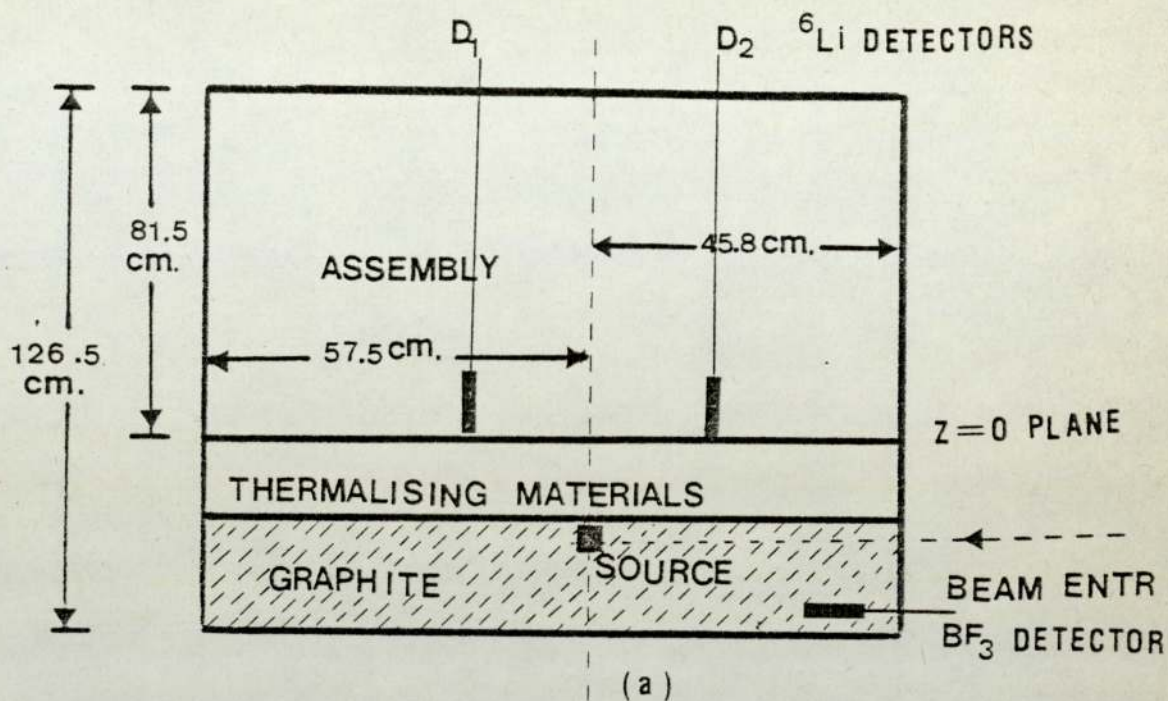


Fig. 2.5. Neutron pulse-shape investigation, (a), the experimental arrangement, (b), detection points on $Z=0$ plane.

detailed in Chapter Four). The measured fluxes were normalised to account for the relative efficiency of the detectors, different counting times, and the variation of neutron production rates. The neutron production rate was monitored by a BF_3 counter, shielded with a 2 cm thick layer of wax and placed just inside the graphite pedestal. The relative thermal neutron intensity was measured for modulation frequencies ranging from 1Hz to 2kHz. The results are shown in Figure 2.6.

It can be seen from Figure 2.6 that with 13.5 cm of graphite, the thermal neutron wavefront is markedly non-planar with assymetrical distribution ~~around~~ the Z-axis due to assymetrical leakage from the graphite pedestal. It was found that by pulsing the source, that the radius of curvature of the wave front increased with pulse repetition frequency. This is because the diffusion time of thermal neutrons in graphite (0.017 s) becomes comparable to the length of the 'ON' period of neutron pulse.

2.6 Neutron pulse-shape measurements in graphite

The number of harmonics which can be successfully evaluated depends on the propagation properties of the medium and on the frequency content of the initial pulse. By Fourier analysis of a square pulse, of height (A) and ratio (S) of the pulse duration time to the pulse repetition time, WAGNER (1970) derived the expression for the square pulse as:

$$F(t) = A.S + 2A.S \sum_{n=1}^{\infty} \frac{\sin nTS}{n\pi S} \cos n\omega_0(t - \frac{1}{2}\pi S) \dots\dots 2.4$$

where $\omega_0 = 2\pi/T$, and T is the Pulse Period

This equation was taken into account in designing the pulsing system for the accelerator. However, the broadening suffered by the square pulse during moderation, when it passes through the

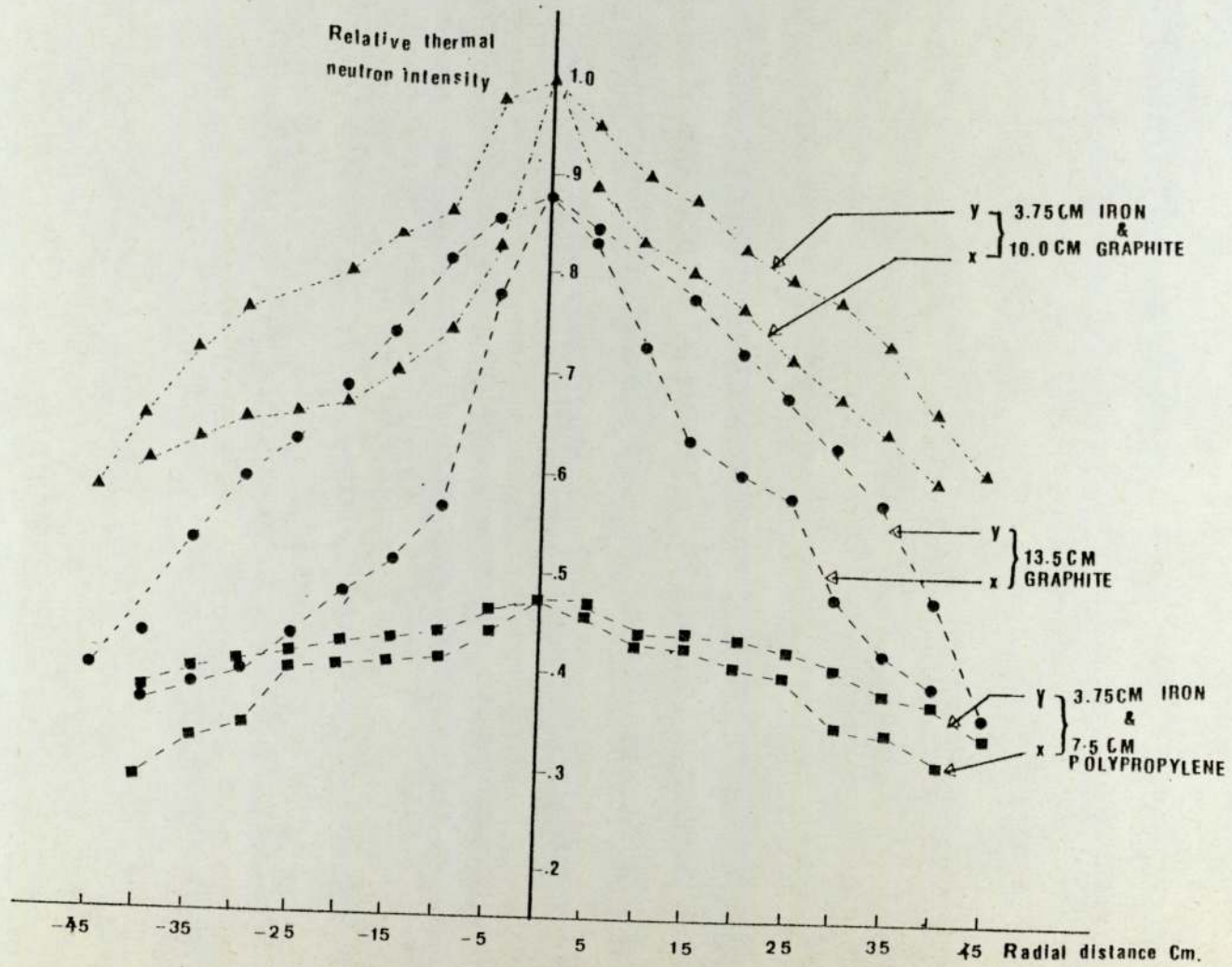


Fig.2.6. Thermal neutron wavelronts emerging from differnt moderators, source frequency = 200 Hz.

graphite pedestal, is important to the measurement of the frequency response of the system. This broadening is due to the relatively long moderation and diffusion times in graphite.

The broadening was measured from the time variation of the thermal neutron flux leaving the graphite moderator. The flux variation was measured over a pulsing frequency range from 1 Hz to 2000 Hz, and at different radial distances.

The broadening increased with distance from the source but it is more sensitive to the increase in pulsing frequency. It was found that at frequencies less than 100 Hz the pulse shape could be regarded as a constant amplitude square wave pulse. At frequencies greater than 100 Hz the pulse exhibited longer rise and fall times, effects which increased rapidly above 500 Hz. At frequencies greater than 1000 Hz the modulation depth decreased to such an extent that no wave-like properties could be observed. The results are shown in Figure 2.7 for frequencies of 100, 300 and 1500 Hz, and at a radial distance of 25 cm from the source.

2.7 Quantitative assessment of thermal neutron pulse broadening

(Computer Code BROAD)

In order to determine the suitability of the moderating material being used to slow down and thermalise the 14 Mev neutrons, it was necessary to undertake a quantitative assessment of the thermal neutron pulse characteristics. A detailed understanding of the physical processes in neutron wave propagation can be gained from the pulse shape. WOOD and LAWRENCE (1971) used the pulse data to study the neutron wave interference effect; BEYNON and MONDAL (1971) studied the relation between the pulse shape and neutron slowing times; HINO and OZAWA (1974) used pulse shape data to study the superposition of the neutron wave.

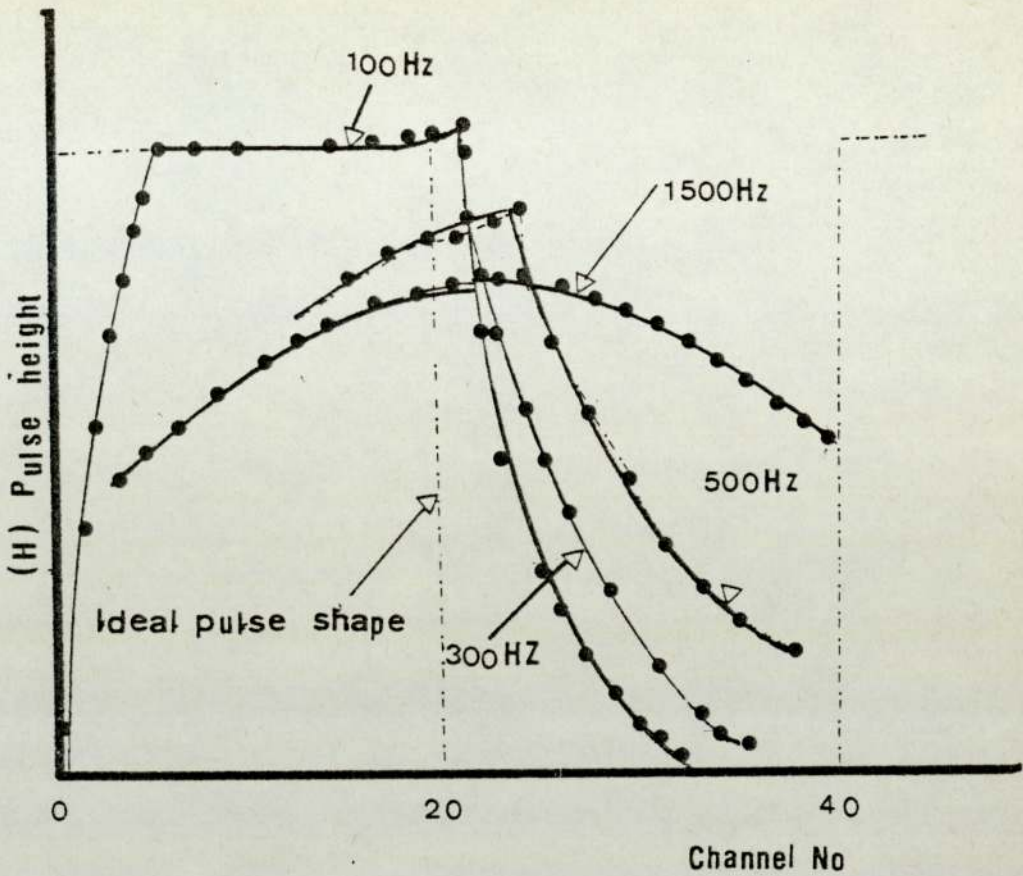


Fig.2.7. Pulse broadening in graphite at 25 cm. radial distance.

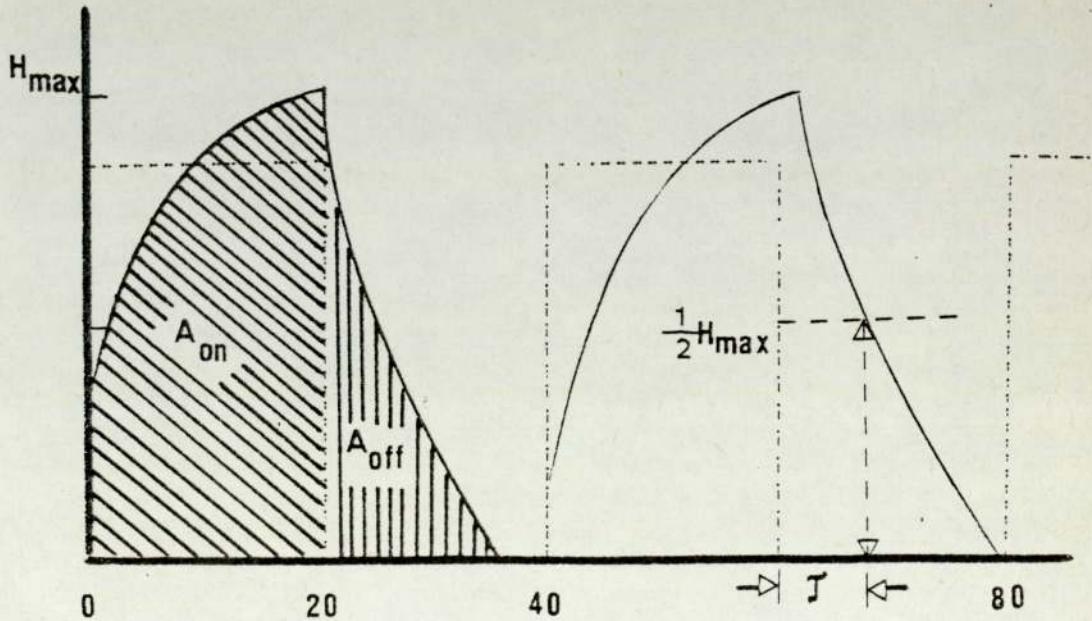


Fig.2.8 Schematic representation of pulse distortion and broadening

As illustrated in Figure 2.8, if the neutron population during the ON part of the cycle is ' A_{on} ', and that during the OFF part is ' A_{off} ', then a distortion factor can be defined as:

$$D_{(r,f)} = \frac{A_{off}}{A_{on}} \dots\dots\dots 2.2$$

For minimum distortion of the neutron pulse, $D(r,f)$ should be small. The distortion factor will vary with the pulse repetition frequency and the position from the source.

Pulse broadening can be quantified by measuring the time needed for the count in the last channel of the ON part of the cycle to reach its half value, i.e. by measuring the decay constant of the distorted square pulse. In multi-scaler analysis the accumulation time for each channel is equal. Hence, the channel number axis in Figure 2.7 and 2.8 represents the time axis.

A FORTRAN computer code, BROAD, was written to perform the following steps:

- i. to provide a background correction for each channel;
- ii. to calculate the values of A_{on} in the first 20 channel of the cycle and A_{off} in the second 20 channels;
- iii. to calculate $D_{(r,f)}$ according to equation 2.2.;
- iv. to fit the decay of the pulse to an exponential of the form:

$$H = A e^{-(B.t)} + C \dots\dots\dots 2.3$$

(This form of representation was found to be correct for frequencies between 100 and 1000 Hz). A least-squares method was used to provide the best values for the constants A, B and C;

- v. to calculate the number of channels required for the count in channel $20n$ (where $n = 1, 3, 5, \dots$), i.e. H_{\max} , to reach its half-value, such that when $H = \frac{1}{2} H_{\max}$, then $t = \tau$. For minimum broadening of the neutron pulse, (τ) should be small.
- vi. to repeat the calculation for each cycle, for each detector, and to print out the mean values of $D_{(r,f)}$ and $\tau_{(r,f)}$ for each frequency.

The computer programme BROAD is listed in Appendix I.

The results obtained are plotted in Figures 2.9 and 2.10 and illustrate the variation of $D_{(r,f)}$ and $\tau_{(r,f)}$ with pulsing frequency. Both measurements were performed at a radial distance of 25cm from the source. It is evident that both $D_{(r,f)}$ and $\tau_{(r,f)}$ increase with the source modulation frequency. For graphite, significant distortion occurs at frequencies just above 25Hz.

2.8 Fast neutron contamination of the thermal neutron pulse

The presence of non-thermal neutrons in the wave is an undesirable feature in neutron wave experiments. The episcadmium contamination in a thermal neutron wave injected into a moderator at its boundary can create a distributed source of thermal neutrons throughout the assembly. This additional source of thermal neutrons can then mask the original thermal neutron disturbance propagated from the system boundary. An analysis of the effects of a distributed source on wave propagation is given by PEREZ and BOOTH (1965). It is essential to investigate the degree of episcadmium contamination in the neutrons emerging from the moderator.

MEGAHID (1975) measured the neutron energy spectra behind different homogeneous and heterogeneous shields. These measurements

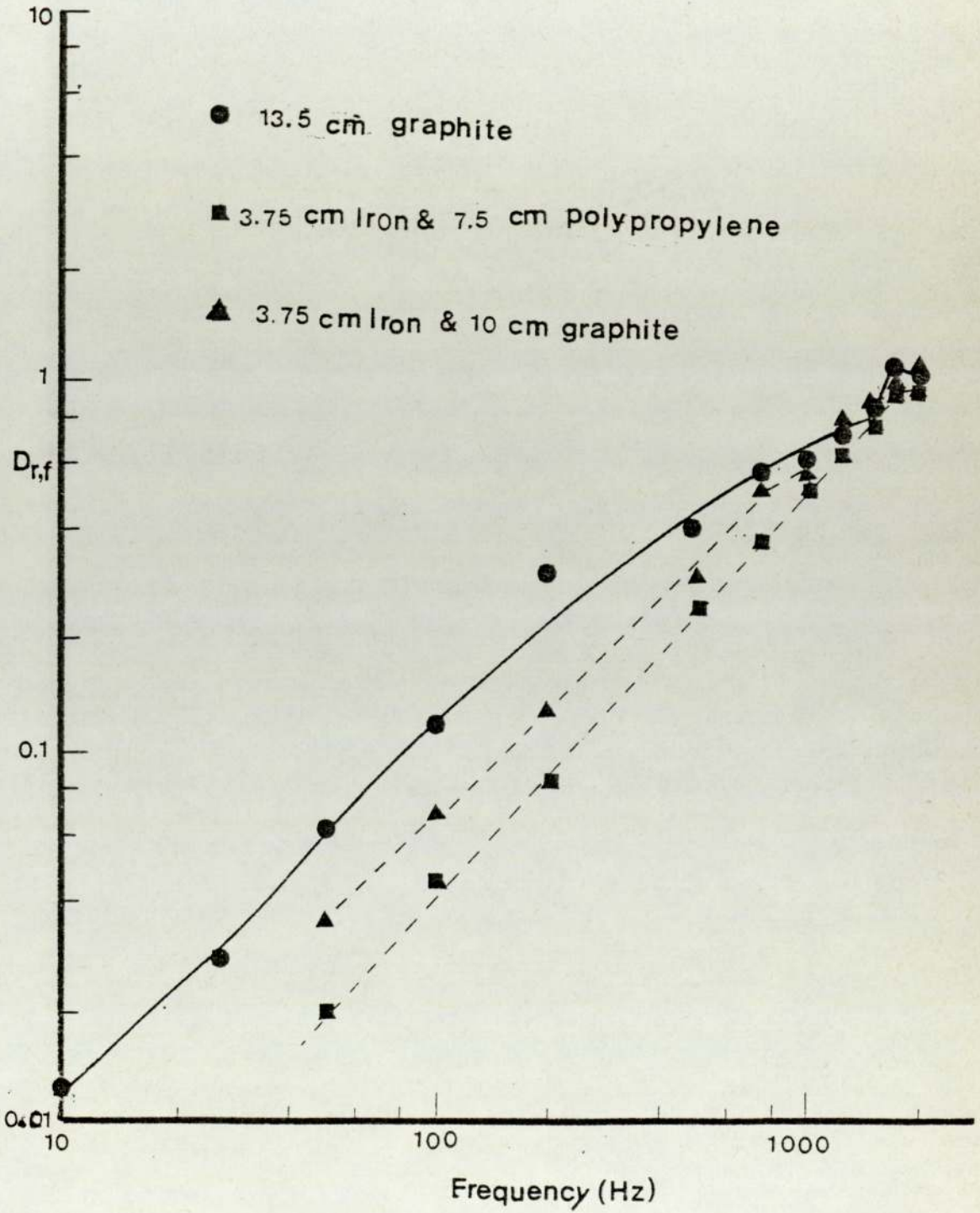


Fig.2.9 pulse distortion variation with modulation frequency at $r = 25$ cm.

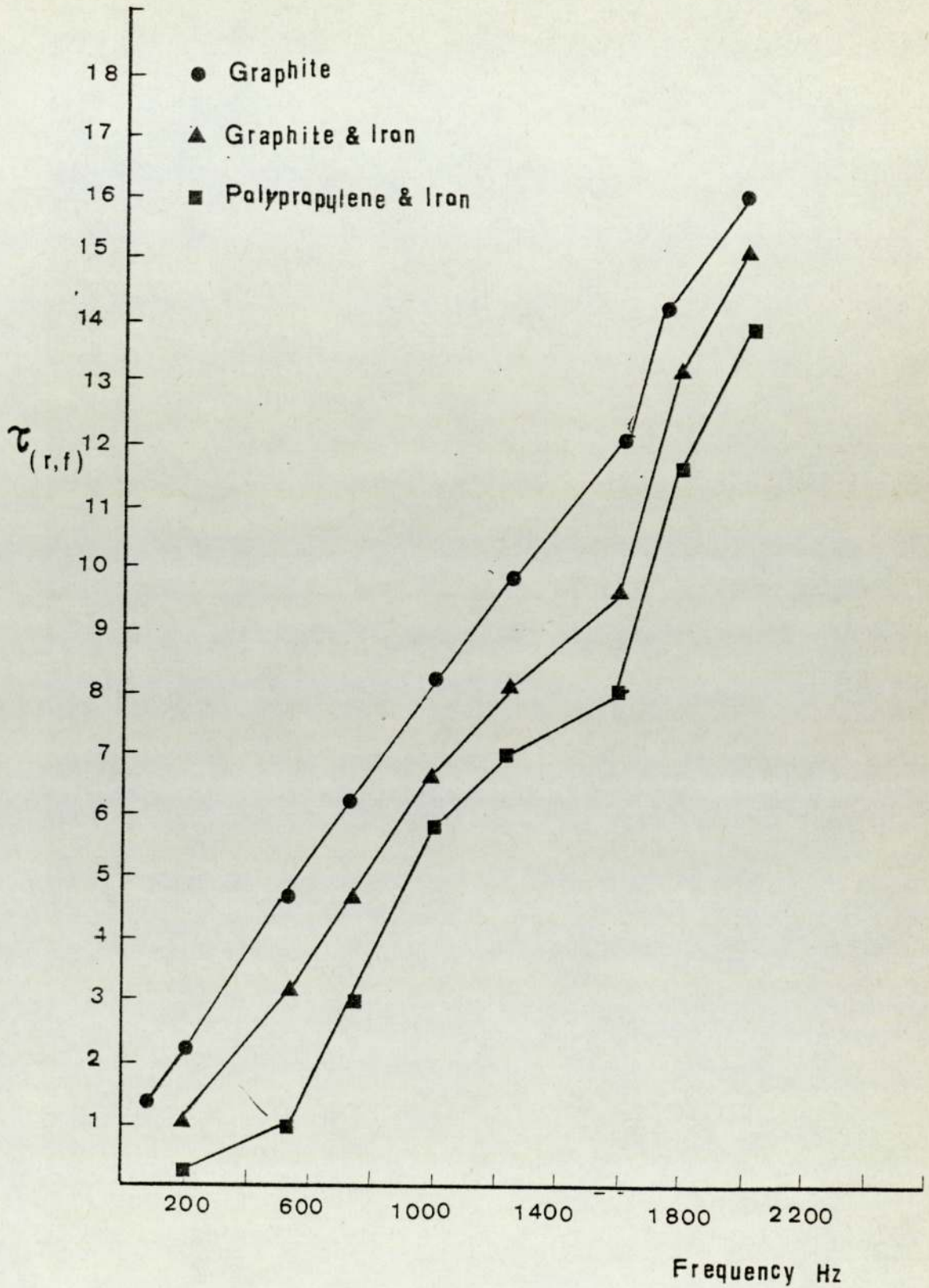


Fig. 2.10. Pulse decay time variation with modulation frequency at radial distance 25 CM.

were made with a small organic scintillator, type NE-213, and were based on a technique which discriminates between the neutron pulses and those pulses due to gamma interactions. A computer code FASTNSPEC was used to perform the transformation of the neutron pulse amplitude into a neutron energy distribution. The same method was adopted in this work, using a re-calibrated neutron spectrometer to measure the neutron spectra emerging from the graphite and other combinations of moderating materials. The results are shown in Figure 2.11 and indicate that there is a considerable fast neutron population in the neutrons injected into the experimental assembly. This must be regarded as undesirable feature of the source conditions and one which should be minimised.

2.9 Modification of the thermalisation arrangement

The investigations carried out in sections 2.4, 2.5, 2.6 and 2.7, to test the moderating properties of graphite, show that if the requirements listed in section 2.4 were to be achieved then modification to the thermalisation arrangement was necessary. The main reasons for the undesirable features exhibited by graphite, as compared to other known moderators, are that:

- i. it has a relatively longer moderation time, thermalisation time and diffusion time, which results in a non-planar wavefront and causes pulse distortion and broadening;
- ii. the low scattering cross sections for high energy neutrons results in incomplete thermalisation and fast neutron contamination of the source;
- iii. the polycrystalline structure ensures the existence of a critical frequency beyond which wave-like behaviour of the thermal neutron population fluctuation is not possible.

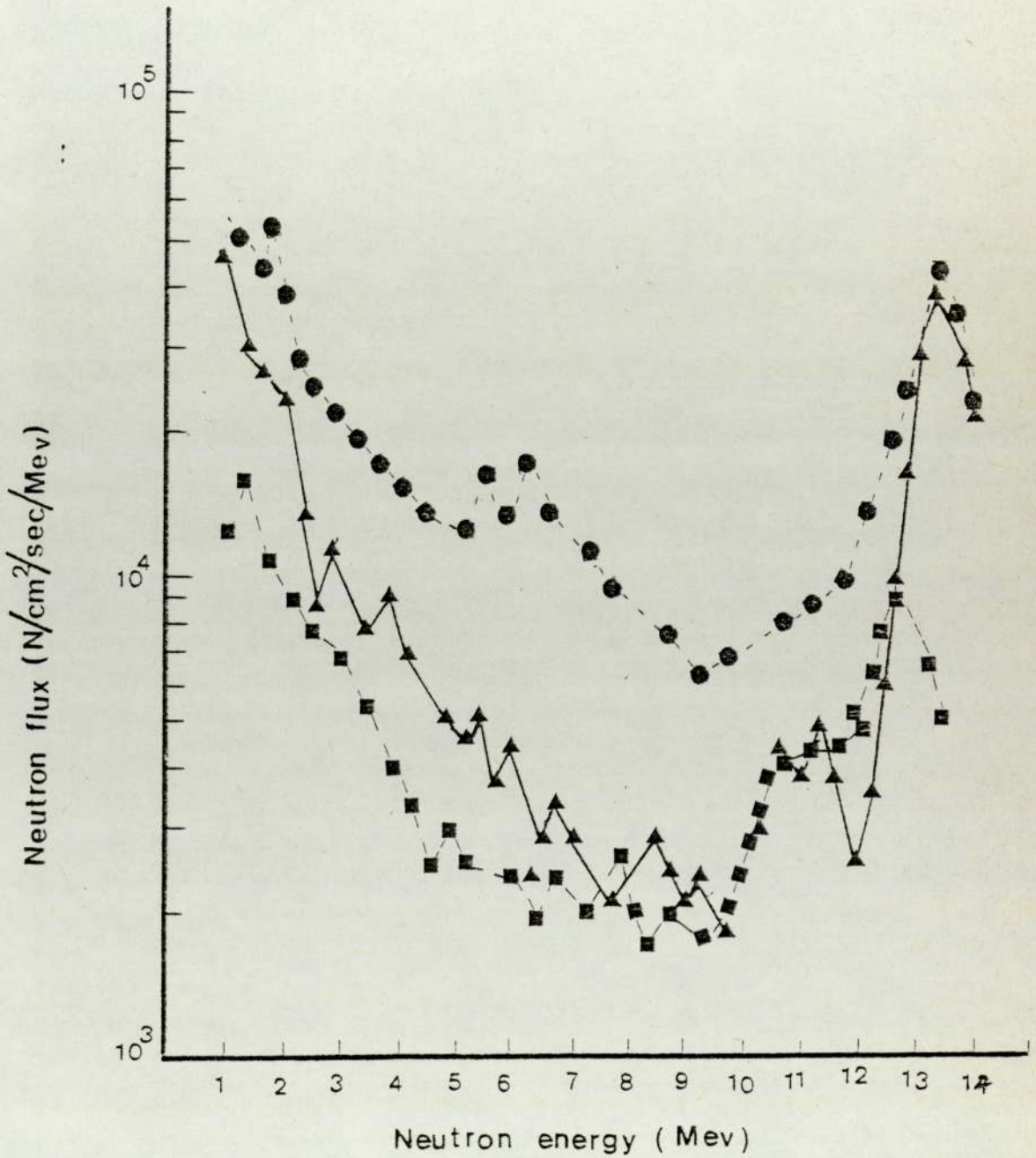


Fig.2.11. Energy spectra of neutrons emerging from:

- 13.5 cm. graphite only,
- ▲ 3.75 cm. iron + 10.5 cm. graphite,
- 3.75 cm. iron + 7.50 cm. polypropylene.

This frequency is lower than that which exists in other crystalline moderators

To overcome these difficulties, two heterogeneous combinations of iron-graphite and iron-polypropylene were tested as alternatives to the graphite-only arrangement.

2.9.1 Thermalisation with an iron-graphite

An arrangement was built whereby the tritium target rested on supporting graphite blocks. The target was covered with steel plates of total thickness 3.75 cm. The steel section was followed by graphite layers of total thickness of 10 cm and the final moderator assembly had dimensions of 120 x 100 x 13.75 cm³. The steel section offers the advantage of having a high inelastic cross section for high energy neutrons, so that the 14 Mev neutrons have a greater probability of being slowed down past the first few excited states of iron, i.e., 2.25, 2.09 and 0.85 Mev. The graphite section then acts to thermalise these neutrons.

The iron-graphite combination was tested as described in sections 2.4, 2.5, 2.6 and 2.7. The results have been included with those of graphite-only moderator, in Figures 2.6, 2.9, 2.10 and 2.11 and show that a significant improvement was achieved. Figure 2.6 shows a higher thermal neutron intensity and better planer uniformity for the iron-graphite arrangement. Although pulse distortion and broadening showed some improvement on graphite, it can be seen from Figures 2.9 and 2.10 that these features remain to a significant degree. Distortion and broadening of the pulse can be attributed to the long diffusion time of thermal neutrons in graphite. Hence, further improvements could be achieved with a moderator of much shorter thermal diffusion time.

2.9.2 Thermalisation with an iron-polypropylene moderator

Polypropylene is a hydrogenous material which has the chemical structure of $(C_{2n}H_{2n})$. When it is used in an appropriate thickness of a few mean free paths, it can slow down and thermalise neutrons more effectively and more rapidly than graphite. The 3.75 cm layer of iron and 10.0 cm graphite layer was replaced with 3.75 cm iron and layers of polypropylene of total thickness of 7.50 cm. This heterogeneous combination was tested as above. The results are plotted with those of graphite and iron-graphite moderators in Figures 2.6, 2.9, 2.10 and 2.11. Although the presence of hydrogenous material reduces the thermal neutron intensity, the other desirable characteristics exhibited in these figures makes the iron-polypropylene combination the most appropriate thermalisation column, i.e. it has the best planer uniformity, minimum pulse distortion and broadening, in addition to minimum fast neutron contamination. A numerical comparison between the three moderating arrangements is listed in Table 2.1.

TABLE 2.1

Comparison between thermalisation columns properties

Parameter	Graphite moderator	Iron-Graphite moderator	Iron- $\frac{C}{2n} \frac{H}{2n}$ moderator
Thickness	13.5 cm	3.75 cm iron + 10.0 cm graphite	3.75 cm iron + 7.50 cm. polypropylene
Relative thermal neutron intensity at $r = 0$ cm.	0.865	1.000	0.470
Planar uniformity of pulse at radial distance of:			
$r = 10$ cm	0.820	0.915	0.450
$r = 20$ cm	0.720	0.825	0.435
$r = 30$ cm	0.625	0.775	0.415
$r = 40$ cm	0.475	0.675	0.380
Pulse broadening for $\tau(r, f)$ frequencies:			
10 Hz	0.350	0.005	0.004
50 Hz	1.225	0.007	0.006
100 Hz	2.245	1.052	0.015
500 Hz	4.985	3.450	1.010
1000 Hz	8.200	6.255	3.820
Pulse distortion for $D(r, f)$ frequencies			
10 Hz	0.020	0.000	0.000
50 Hz	0.070	0.035	0.020
100 Hz	0.150	0.062	0.042
500 Hz	0.375	0.175	0.100
1000 Hz	0.855	0.550	0.470
No. of fast neutrons in energy range of: 1 Mev to 12 Mev for thermal count 2.65×10^8	5.4×10^4	3.3×10^3	1.08×10^3

CHAPTER THREE

THE DESIGN OF A NON-MULTIPLYING ASSEMBLY WITH VOIDS

The literature review presented in section 1.3 shows that the measurements of anisotropic effects of void channels in diffusing media were carried out mostly by the application of PST, with the majority of these measurements performed in crystalline media. A few experiments have been performed to quantify the streaming effects in water and the reported results show a considerable disagreement (AHMAD (1969), and KANEKO et al (1974)). However, the application of NWT promises better accuracy in crystalline moderators, as shown by RITCHIE and WHITTLESTONE (1973), and for non-crystalline moderators as shown by WAGNER (1970).

The physical design of the experimental assembly used in this work was chosen in order to obtain accurate data for anisotropic diffusion parameters for a hexagonal lattice of empty channels in a water moderator, since such a combination of moderator and lattice has not been examined previously. Also to allow a comparison between experimental and theoretical values of the thermalisation and diffusion constants of the medium, the design had to be sufficiently simple to allow a theoretical model of the system to be prepared.

3.1 The water moderator

Water is the most-used moderator in nuclear systems. It is non-crystalline moderator and has many advantages over others in terms of cost, availability and existing nuclear data. The water was contained in a stainless steel tank of 0.3 cm wall thickness, with the tank placed directly above the thermalising column. The dimensions of the water assembly were $86.5 \times 112.0 \times 81.5 \text{ cm}^3$,

i.e. about 800 litres of water. The geometrical buckling of the system was calculated using the relation:

$$B^2 = \left(\frac{\pi}{A + 2d}\right)^2 + \left(\frac{\pi}{B + 2d}\right)^2 + \left(\frac{\pi}{C + 2d}\right)^2$$

where A, B and C are the lengths of the sides of the assembly, and d is its extrapolation length, defined as:

$$d = 0.71 \lambda_{tr}$$

The geometrical buckling of the assembly is $3.537 \times 10^{-3} \text{ cm}^{-2}$, assuming a value for λ_{tr} of 0.475 cm.

3.2 The choice of void arrangements

The size and shape of the voids were influenced by the desire to simplify the anisotropic calculation in any theoretical model of the system and by practicality of the void arrangement to nuclear systems. The effects of voids depend on their location with respect to the neutron source and on the nuclear properties of the system. These effects are reflected in an increase in the net diffusion current per unit gradient of the flux. The current through a void channel depends on the dimension and on the orientation of the channel with respect to the neutron flux gradient, as well as on the scattering properties of the medium and the initial flux distribution in the moderator.

The presence of circular cylindrical empty channels is a common feature in most reactors. The streaming effect of a cylindrical channel has been investigated in a square lattice with PST. Hence the choice of a hexagonal lattice and the application of NWT can be justified.

3.3 Construction of the void cells

The void cells were constructed of a regular lattice of seven empty channels of internal radius (r) and triangular pitch giving the hexagonal-shaped arrangement shown in Figure 3.1. The void tubes and the two neutron detectors used for neutron flux measurements were held vertical and parallel to each other by means of three thin aluminium grids as lattice spacers; both detectors were positioned at fixed radial positions, one detector at an axial height $H=0$ and the second detector at an adjustable axial height, calibrated within 0.1 cm. In this way, the radial distance between each detector and the centre of the central channel in the lattice was maintained at 13.6 cm during all measurements. The lattice was inserted in the water tank with the channel axis perpendicular to the plane of neutron propagation i.e. perpendicular to the thermal neutron wavefront.

Four lattices were constructed, with different void radii and triangular pitch. The water level in the tank was the same for all lattices when the lattices were inserted in the water tank. The centre of the central channel was placed at a fixed point marked on the base of the tank, which ensured identical initial source conditions for all lattices. Hence, any change in the frequency response of the system would be due to the changes in the void dimensions.

The minimum separation between the void tube walls in the smallest lattice was 4.75 cm. Since the transport mean free path for thermal neutrons in water is 0.475 cm, the probability of a thermal neutron traversing more than one channel was very low. By maintaining a constant ratio of the cell radius (R) to the void channel radius (r) and a constant void channel length, the void to moderator ratio within the cell boundary was the same for all

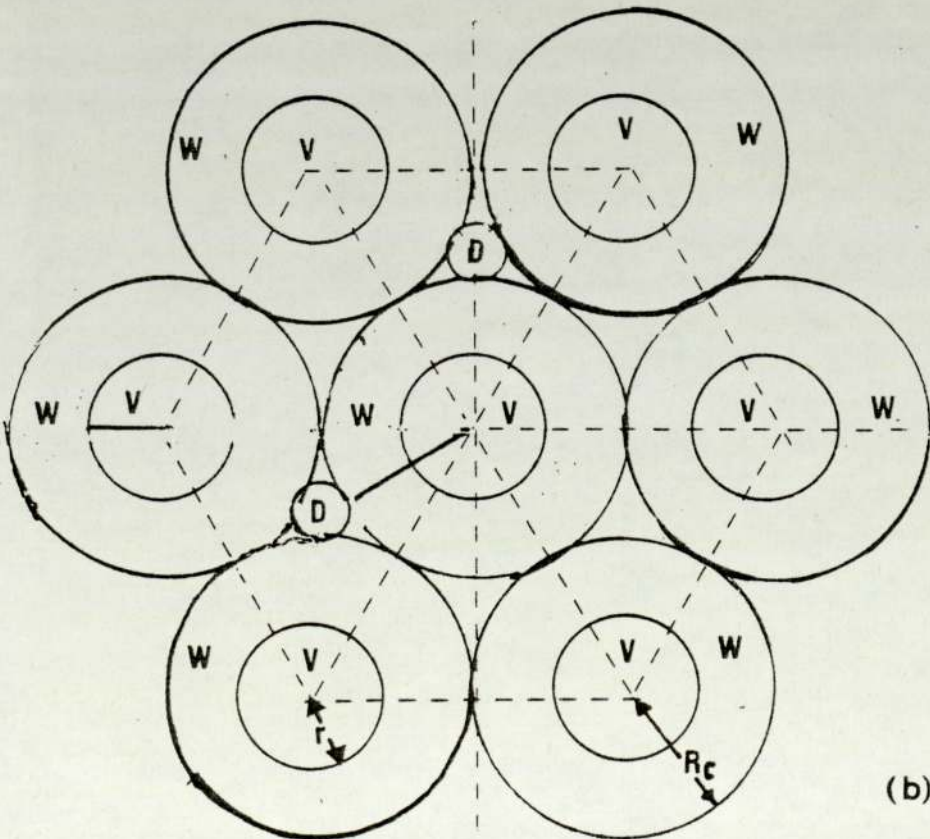
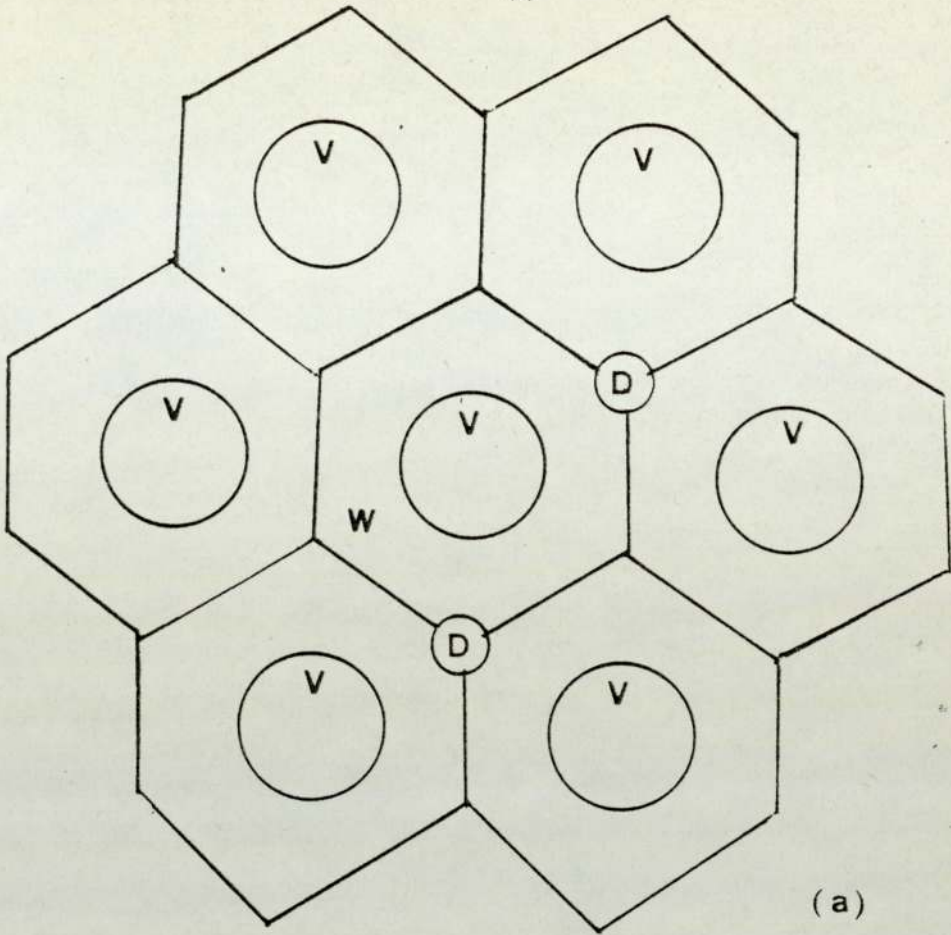


Fig.3.1. Hexagonal cell, a, and its approximation, b.

lattices. Any change in leakage from the cell would be due to the effects of neutron streaming. The physical characteristics of the cells are summarised in table 3.1 and a photographs of the cells is provided in Figures 3.2. and 3.3.

Neutron streaming through the detectors was minimised by filling the detector cases with solid polyethelene, which has similar thermal neutron scattering and absorption properties as water.

Further details of the neutron detectors used in this work are given in Chapter Four.

TABLE 3.1

Void cell dimension

Cell No.	Cell radius (R_c)	Void channel radius (r)	$X = \frac{\text{void volume}}{\text{moderator volume}}$ $= \frac{r^2}{R_c^2 - r^2}$	$Y = \frac{r}{\text{Cell height}}$
1	3.925	1.550	0.184	0.019
2	4.475	1.750	0.183	0.021
3	6.175	2.400	0.180	0.032
4	9.250	3.550	0.178	0.045

(All dimensions are in cm)



FIG. 3.2. FOUR VOID CHANNEL ARRANGEMENTS



FIG. 3.3. THE RELATIVE DETECTOR POSITIONS IN A VOID CELL

CHAPTER FOUR

NEUTRON DETECTION AND DATA ACQUISITION SYSTEM

In this chapter, a brief description is given of the electronic circuitry involved in the detection of thermal neutron flux in the experimental assembly. This is divided into three parts, namely:

- i. the monitoring of the fast neutron production;
- ii. thermal neutron detection in the experimental assembly;
- iii. the data acquisition system.

4.1 The monitoring of the fast neutron production rate

Previous experimental work with the S.A.M.E.S. accelerator has shown that there is considerable drift in the machine conditions, affecting the rate of neutron production. These variations can be attributed to several factors, e.g. fluctuation in the deuteron beam intensity, instability in the accelerating voltage level and depletion of the tritium target. The fluctuations in the fast neutron production rate was monitored and these measurements were used for normalisation of the experiments, described in Chapter Two, to investigate the properties of the emerging neutron wave from the thermalising column.

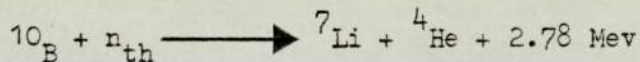
With the D/T reaction, two methods for monitoring the rate of fast neutron production were considered, namely:

- i. monitoring the associated alpha particles in the D/T
reaction;

- ii. monitoring the thermalised neutrons emerging in a particular solid angle at a particular distance from the source.

The second method has many advantages over the first, especially in the efficiency of the detection and the simplicity of the associated electronic circuitry.

A BF_3 counter is an efficient thermal neutron detector, as ^{10}B of a high thermal neutron cross section of 3840 barn for the $^{10}\text{B}(n,\alpha)^7\text{Li}$ reaction utilised in the detector:



It was reported by PRICE (1964) that BF_3 counters used for thermal neutron detection have a very low gamma ray sensitivity. This is very desirable in the present work since an intense gamma field is always present from the D/T reaction and from the interaction of fast neutrons with the steel section of the moderating column. In this work, a BF_3 counter of an active length of 9.5 cm is placed at the edge of the graphite pedestal at 40 cm from the D/T source. The neutron monitoring equipment, which assembled from standard electronic units, was independent of the rest of the detection system employed for flux measurements inside the non-multiplying assembly. A schematic diagram of neutron source monitoring and detection systems is shown in Figure 4.1.

4.2 Thermal neutron detection in the experimental assembly

Nowadays, a wide range of thermal neutron detectors are available. Their uses depend on the specific requirements of a particular detection system. The most familiar types of thermal neutron detectors and their characteristics are listed in Table 4.1. The

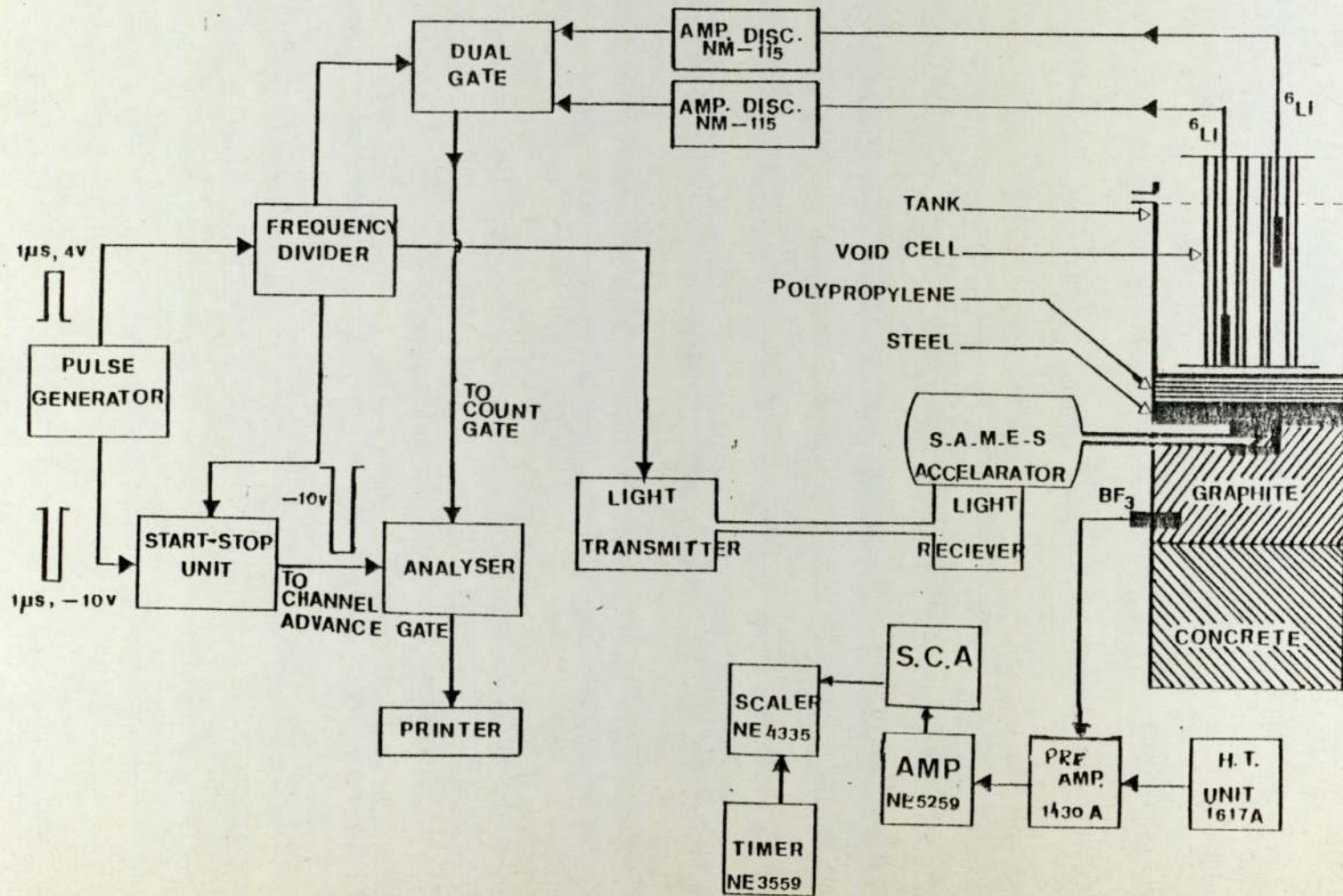


Fig. 4.1. Schematic diagram of neutron detection and data acquisition system.

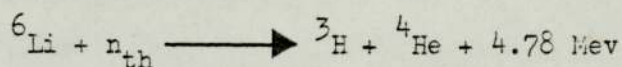
Detector type	Nuclear reaction utilised for neutron detection	Cross section for thermal neutrons and its energy dependence	Efficiency compared to BF ₃ counter	Gamma radiation sensitivity	Ref.
BF ₃	¹⁰ B(n,α) ⁷ Li	3840 barn ($\frac{1}{v}$) to 30 kev	1	very low	PRICE (1964)
³ He	³ He(n,p) ³ H	5400 barn ($\frac{1}{v}$) no resonance	20	low	BIRKS (1964)
Fission chambers	²³³ U(n,f) ²³⁵ U(n,f) ²³⁹ P(n,f)	²³³ U = 524 b ²³⁵ U = 590 b ²³⁹ P = 729 b ($\frac{1}{v}$)	0.01-0.1	very low	PRICE (1964)
⁶ Li	⁶ Li(n,α) ³ H	936 barn ($\frac{1}{v}$) up to 75 kev resonance at 243 kev σ = 3.2	varies with size and ⁶ Li content	low for thin crystal	BIRKS (1964) and FORT (1974)

Table 4.1. Summary of thermal neutron detectors properties

requirements of the present measurements can be listed as:

- i. maximum detection efficiency for thermal neutrons;
- ii. minimum detection efficiency for fast neutrons;
- iii. minimum detection efficiency for gamma rays and other secondary radiations;
- iv. minimum flux perturbation by the detector inside the assembly, and minimum neutron streaming through the detector.

The ${}^6\text{Li}$ glass scintillator was chosen for measurements of the thermal neutron flux within the assembly. Thermal neutron detection with ${}^6\text{Li}$ involves the following exothermic reaction:



The energy released is shared between the two products in inverse proportion to their masses. The cross section for this reaction is 936 barn at 0.025 eV, ($v=2.2 \times 10^5 \text{ cm}\cdot\text{sec}^{-1}$), and varies with $(\frac{1}{v})$ up to 30 keV. The variation of ${}^6\text{Li}(n,\alpha){}^3\text{H}$ cross section with neutron energy in a range 1 - 500 keV was studied by COATES et al (1974), and in the range 20 - 1700 keV by FORT and MARQUETTE (1974), using glass scintillators of thickness between 0.5 to 9.5 mm. Their measurements have shown that the $\frac{1}{v}$ variation can be extended to 75 keV and that there is a resonance peak at about 243 keV with a peak cross section value of 3.2 barn. No other peaks were detected up to neutron energy of 1700 keV.

The principal advantage of Li glass scintillator detectors is the high thermal neutron detection efficiency, (e.g. it was reported by PRICE (1964) that 1 cm thick crystal of natural lithium has an efficiency of 69%). The efficiency can be effectively improved by

^6Li -enrichment, (e.g. it was reported by BIRKS (1964) that a 2mm thick, 96% ^6Li -enriched crystal had thermal neutron efficiency of 95%). The principal disadvantage of this detector is its high efficiency to both alpha particles and electrons. Thus, a high gamma ray level of energies higher than 3.5 Mev can cause a pile up of pulses, which leads to spurious counts in the data acquisition system. However, the use of thin and highly enriched crystals can minimise this problem effectively.

Two ^6Li glass scintillators were available for the present work and satisfy the compromise between efficiency, size and gamma-fast neutron discrimination. Their characteristics are listed in Table 4.2. The scintillators were optically coupled to EMI 9524B photomultipliers of the same diameter as the crystals and 12 cm in length, and housed inside aluminium tubes of diameter 2.62 cm and length 93 cm. To minimise the streaming through the detector tubes, the tubes were filled with a solid polyethelene material of similar neutron absorption and scattering properties as water. A photograph of the detector system is shown in Figure 4.2.

The two detectors were used for simultaneous measurements of thermal neutron fluxes at two positions in the assembly as described in section 3.3. The signal from each detector was input to a charge sensitive amplifier-discriminator before further processing. In order to minimise the acquisition of counts from the detection of gamma rays, the discrimination levels were set after a careful examination of the pulse height spectra of the two detectors. The pulse height distribution from thermalised Am-Be source neutrons measured by the ^6Li glass scintillators is shown in Figure 4.3. It can be seen from Figure 4.3 that there is a well-defined thermal neutron peak, below which the amplifier discriminator level is set.

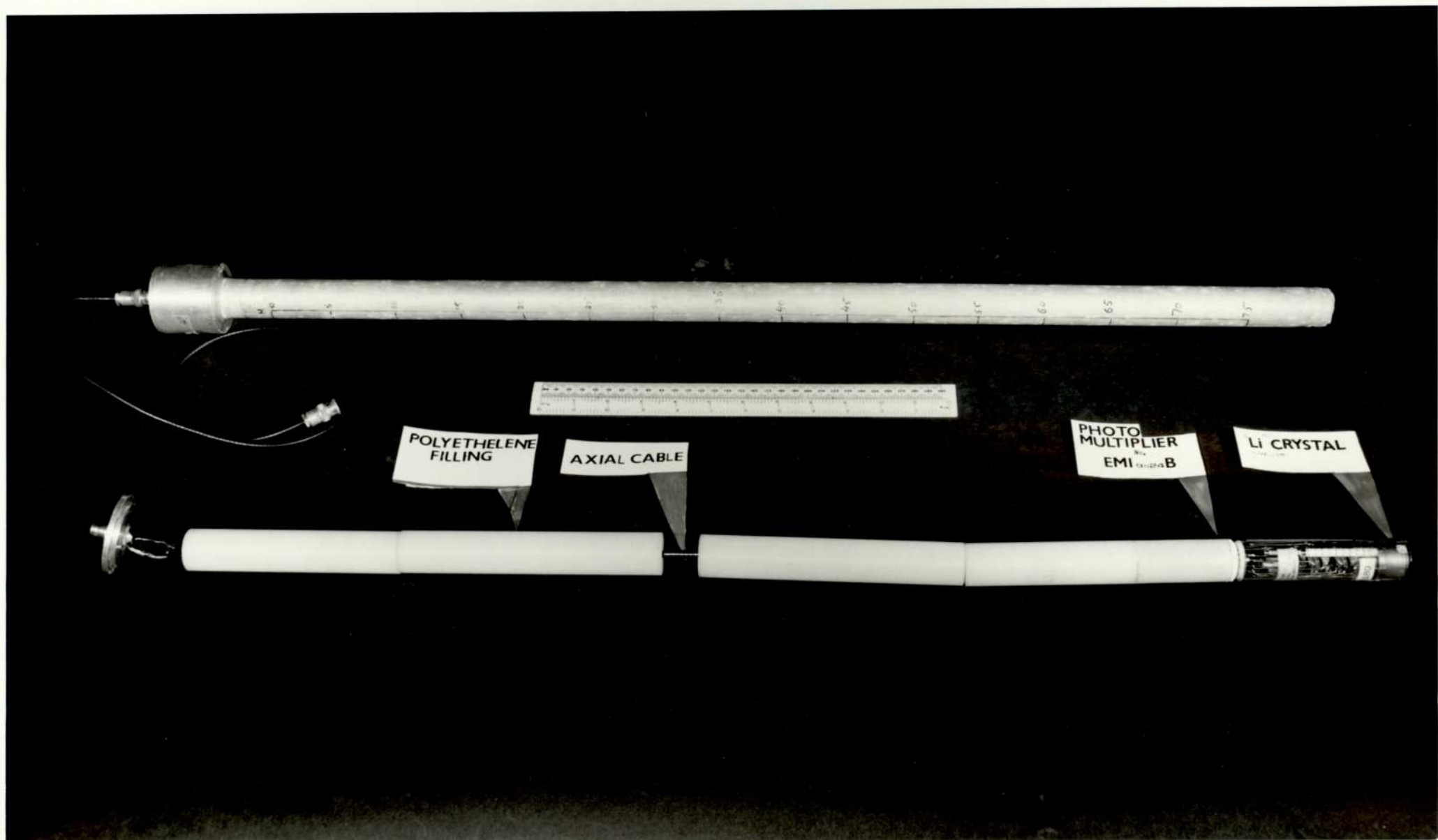


FIG.4.2. ^6Li DETECTOR HOUSING ARRANGEMENTS.

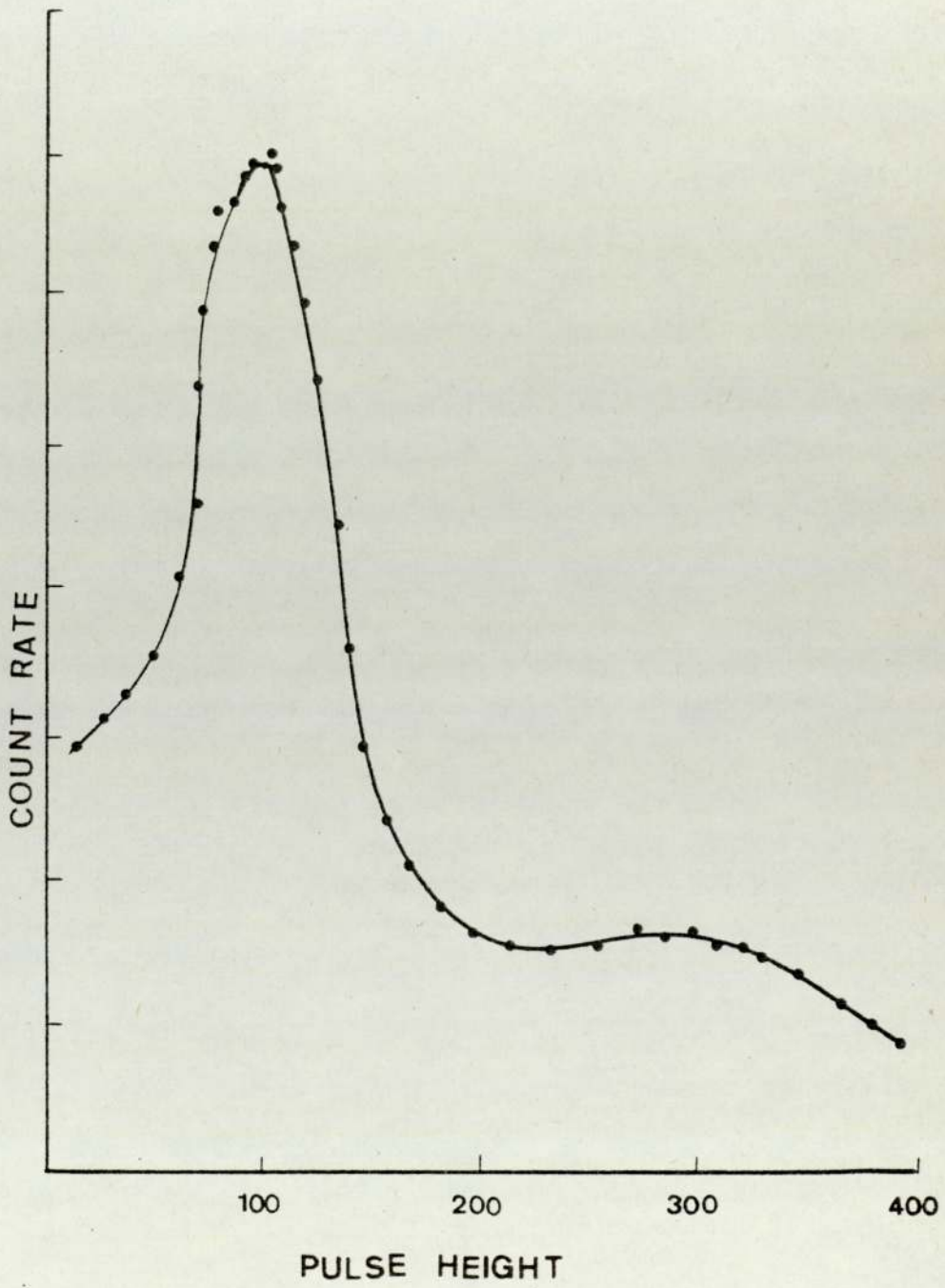


Fig.4.3. ${}^6\text{Li}$ scintillation spectrum from Am-Be source

TABLE 4.2

Properties of the ^6Li glass scintillators

Crystal type	Cerium activated lithium silicate glass type NE905
Lithium content	6.6%
^6Li enrichment	95%
Dimensions	2.53 cm diameter x 0.3 cm thick
Scintillation time resolution	0.3 micro-sec.
Photo-multiplier	EMI 9524B, operating voltage 930 v.

4.3 The data acquisition system

A brief description of the data acquisition system is given within this section; the function of each individual unit and its mode of operation is described. Several electronic units are standard, commercial modules but the key control units were modified versions of those previously used by GIL-RAMOS (1974), rebuilt as standard (NIM) modules.

4.3.1 Pulse generation and signal analysis

A RIDL 400-channels analyser was used in a Time Sequence Storage mode, (TSS), to record the time-variation of the neutron flux in the non-multiplying assemblies. In the TSS mode each channel accepts a number of pulses delivered to the analyser during a fixed interval, between time (t) and (t+dt), where dt is the channel width. Two signals were input to the analyser: the channel advance signal and the processed detector signal. The total time required for a 400 channels sweep is (400 x dt). Since both detectors were used

simultaneously, the signal from each detector was fed into the analyser for an alternative period of $(200 \times dt)$, with each half of the analyser memory allocated to the same detector for the duration of the measurement period by means of the pulse processing sequence adopted in the remainder of the neutron detection and data acquisition system.

The experiment was controlled by FARNELL two-channel pulse generator. This unit provided, simultaneously, two signals identical in frequency but with different height and polarity. One signal, +4v and of 1 μ s duration, was input to a frequency dividing unit which was used to control the external pulsing system of the S.A.M.E.S accelerator (as described in section 2.2) and the other signal, -10v and of 1 μ s duration, was input to a unit which controlled the channel advance of the analyser.

4.3.2 The frequency divider unit

The +4v signal from the pulse generator, frequency F, was input to the frequency divider and pulse inverter circuit shown in Figure 4.4. The dividing part of the circuit produces square pulses of +4v amplitude and frequencies (F/n) where n is 20, 40, 80, 160, 200 and 400. The following output frequencies were used:

- i. $F/40$ to drive the light transmitter unit, which is part of the external pulsing system of S.A.M.E.S accelerator;
- ii. $F/200$ to a dual gate unit through a pulse inverter circuit;
- iii. $F/400$ to a start-stop unit.

4.3.3 The dual gate unit, (adapted from GIL-RAMOS (1974))

This unit was used to gate the input pulses from one detector while the pulses from the other detector were addressed into 200 channels of the analyser allocated to that detector. The PHA memory

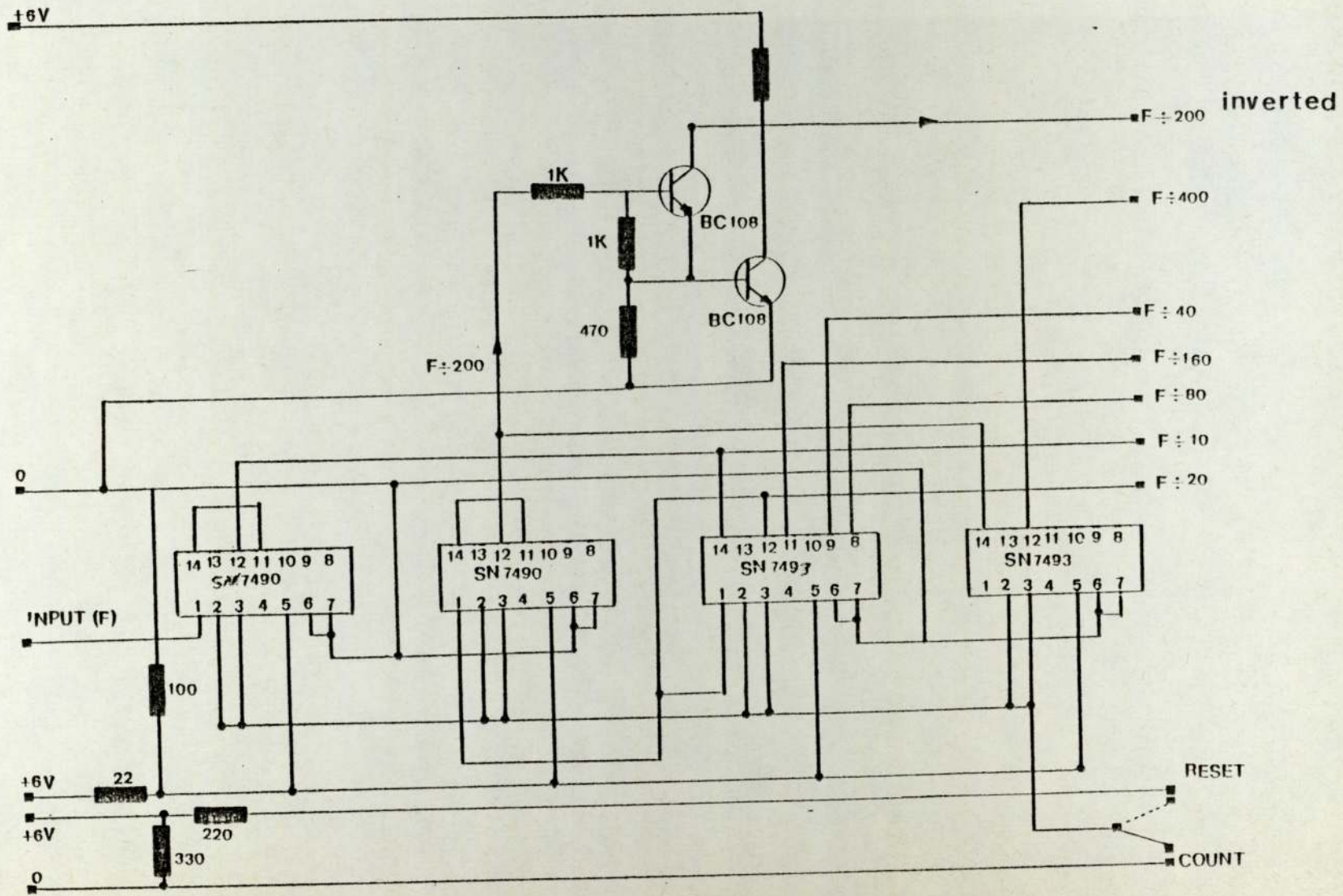


Fig.4.4. Frequency dividing and pulse inverter circuit

requires a signal of +12v in amplitude and 1 us duration, so the dual gate unit also amplifies and shapes the detector signals to be compatible to the analyser requirements. A circuit diagram of this unit is shown in Figure 4.5.

4.3.4 The start-stop unit

A start-stop unit was used to eliminate random starting of the PHA and to assign the first 200 channels to one detector and the other 200 channels to the second detector. The unit synchronises the first channel advance signal reaching the PHA with the dual gate (i.e. detector) pulse.

The output pulse shape and amplitude proved to be an important factor in the reliability of operation of this unit, so it was necessary to design a circuit which eliminated any pulse shape distortion, in order to make the start-stop unit output acceptable to the channel-advance gate of the PHA. The circuit diagram of this unit is shown in Figure 4.6.

A photograph of the data acquisition system is shown in Figure 4.7.

4.3.5 Measurement procedure

For each measurement of the neutron flux in the assembly, the following procedure was followed:-

- i. the start-stop unit was set so that no pulses reached the channel-advance gate of the PHA;
- ii. the PHA accumulation was initiated using the start pushbutton on the analyser - as the channel advance signal could not reach the PHA, all pulses reaching the PHA from the detectors, via the dual-gate unit, were stored in the first channel;

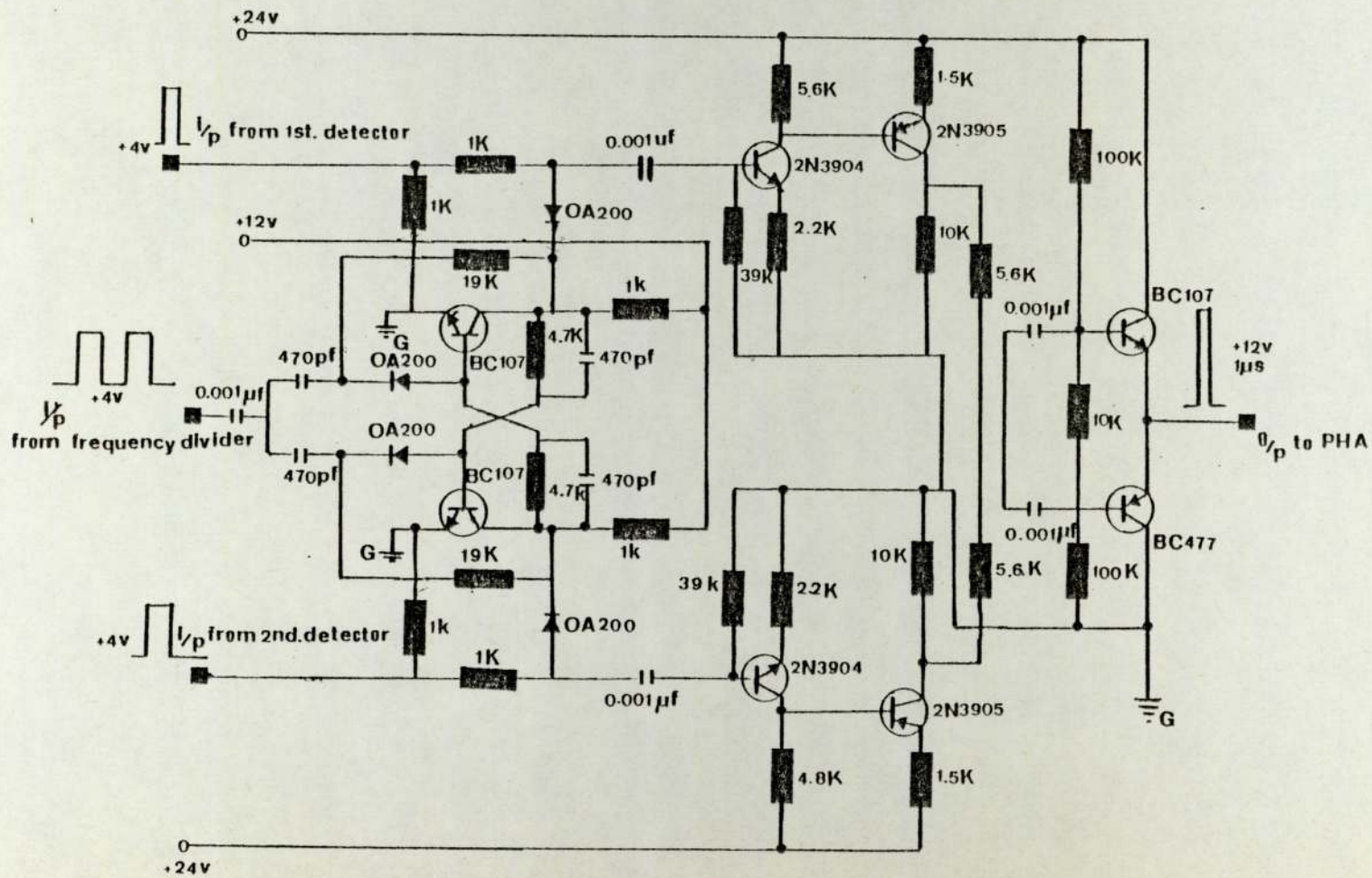


Fig.4.5. Dual-Gate circuit

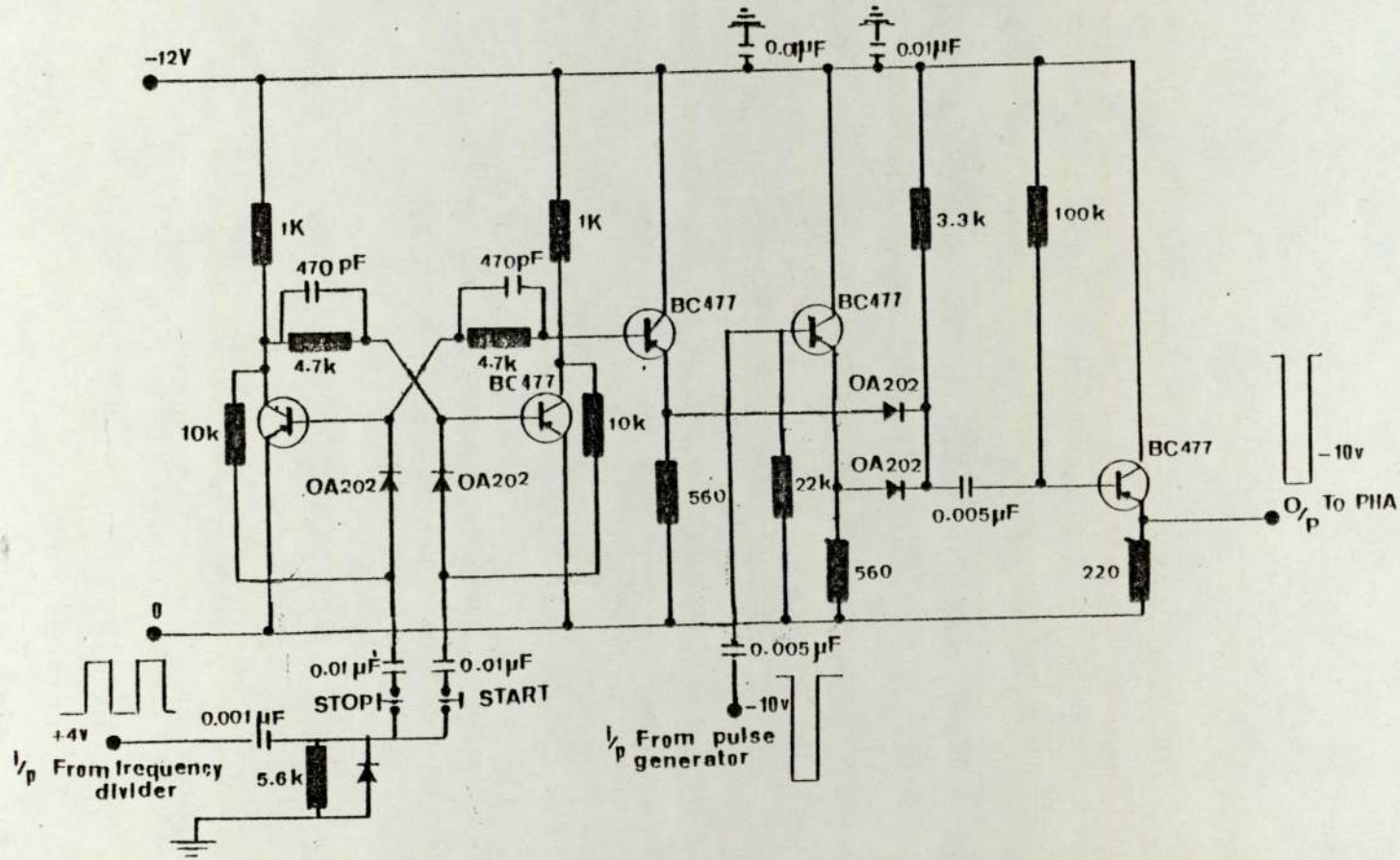


Fig.4.6 START-STOP unit circuit diagram

- iii. the start-stop unit was set to allow pulses to reach the channel advance gate of the analyser;
- iv. data accumulation was halted at any required time by stopping the PHA or, alternatively, the start-stop unit.

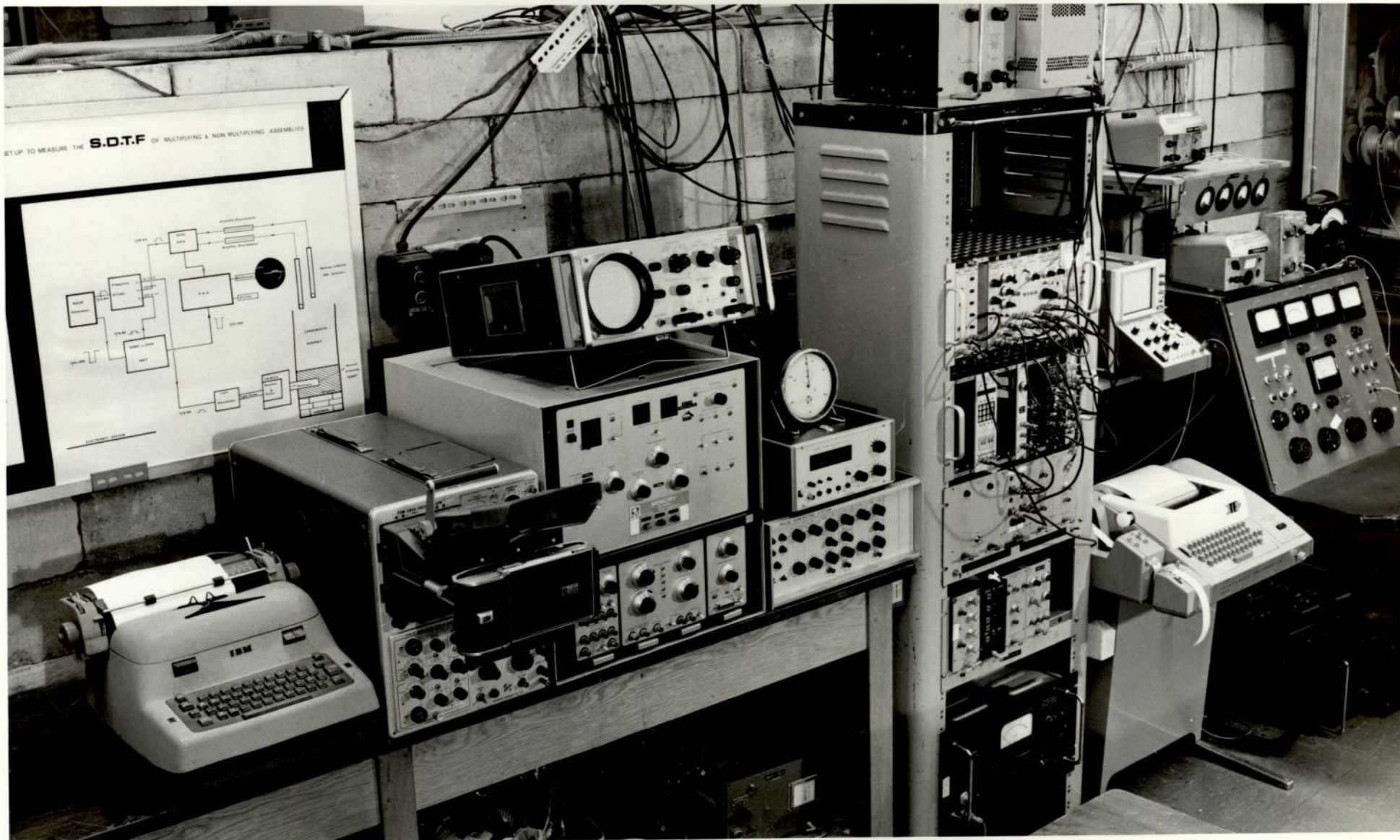


Fig.4.7. DATA ACQUISITION SYSTEM AND ASSOCIATED EQUIPMENTS

CHAPTER FIVE

EXPERIMENTAL MEASUREMENTS AND DATA ANALYSIS

The method by which the frequency response of the non-multiplying assembly was obtained is presented in this chapter. A Fourier analysis of the measured time and space dependent fluxes in the different lattice arrangements was extended to determine the frequency dependence of the wave parameters. The dispersion laws for each assembly are measured, and the effect of voids on the wave propagation are quantified, the degree of anisotropy caused by voids being related to the frequency of the source modulation.

5.1 The measurement and the analysis of the experimental data

The main function of the data acquisition system described in Chapter Four was to record the time profile of the thermal neutron pulse. The recorded time-variation of flux in different assemblies was corrected, first for the time resolution of the data acquisition system and, second, for detector background.

The time-variation of neutron population at positions in the non-multiplying assembly was recorded by using two ${}^6\text{Li}$ detectors as shown in Figure 5.1. One detector, (detector A), was at fixed position to record the pulse data at the system boundary; the second detector, (detector B), was moveable and could be located at several positions along the Z-axis, but with the same (X,Y) position. A BF_3 counter was located outside the system and was used to correct for source variation and to normalise the data recorded by the two ${}^6\text{Li}$ detectors.

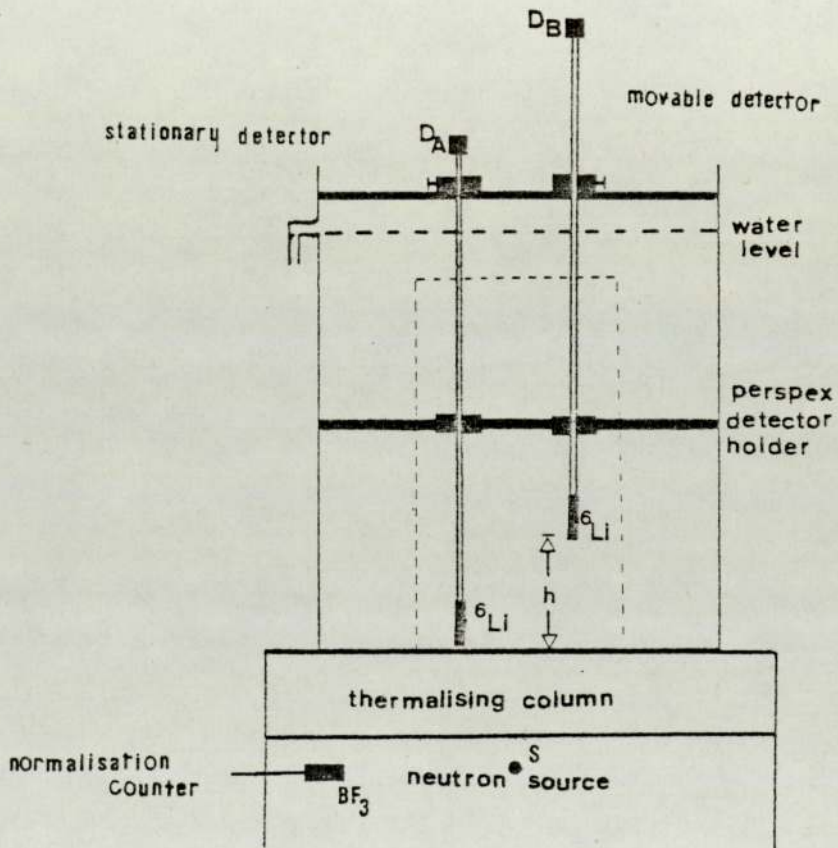


Fig.5.1. Experimental arrangement for measurement of the SDTF of the water assembly.

5.1.1 Data corrections

The most significant loss of counts in the acquisition system occurred in the analyser due to the dead time and memory transfer time. Each channel of the analyser records the counts between time (t) and (t+T) where T is the channel width. The average count (Q) that should be recorded in any given channel in (N) number of cycles is:

$$Q = NcT \dots\dots\dots 5.1$$

where c is the average count rate. However, the recorded counts per channel (Q^1) are somewhat smaller than (Q) due to the dead time (δ) and the memory transfer time (τ). (For the RIDL analyser τ is 12.5 us). The relationship between (Q) and (Q^1) are derived by GILRAMOS (1974) as:

$$\frac{Q^1}{Q} = \frac{1 - \frac{\tau}{T}}{1 + c \cdot \delta} + \frac{\tau}{T} \cdot \frac{1 - e^{-c\tau}}{c\tau} \dots\dots\dots 5.2$$

This relationship is a function of the mode of the operation of the analyser and depends on the maximum count rate per channel, as indicated by RITCHIE and WHITTLESTONE (1973). It is very difficult to obtain a unique resolution time for the data acquisition system when working with high time-varying count rates, as in recording a square pulse of thermal neutrons. However, Eq. (5.2) can be used to characterise the system if the count rate remains below 5×10^4 counts per channel per second. The maximum count rate per channel per second encountered in this work does not exceed 10^3 .

5.1.2 Fourier analysis of the corrected data

The recorded shape of the thermal neutron pulse after applying resolution time correction and background subtraction can be described

by square wave function $F(x)$ in the interval $-\pi \leq x \leq \pi$:

$$F(x) = 0, \text{ at } -\pi \leq x \leq 0$$

$$F(x) = a_0, \text{ at } 0 \leq x \leq \pi$$

An arbitrary function $F(x)$ can be represented by a trigonometric series as:

$$F(x) = \frac{a_0}{2} + \sum_{n=1}^{\infty} a_n \cos nx + \sum_{n=1}^{\infty} b_n \sin nx \dots\dots\dots 5.3$$

Eq. (5.3) is the Fourier expansion of the function $F(x)$ and a_0 , a_n and b_n are the Fourier coefficients, defined by ARFKEN (1973) as:

$$a_0 = \frac{1}{\pi} \int_{-\pi}^{\pi} F(x) dx$$

$$a_n = \frac{1}{\pi} \int_{-\pi}^{\pi} F(x) \cos nx dx \dots\dots\dots 5.4$$

$$b_n = \frac{1}{\pi} \int_{-\pi}^{\pi} F(x) \sin nx dx$$

For the square wave function in the intervals described above, $a_n = 0$ for $n \neq 0$ and

$$F(x) = \frac{1}{2} + \frac{2}{\pi} (\sin x + \frac{1}{3} \sin 3x + \frac{1}{5} \sin 5x + \dots) \dots\dots\dots 5.5$$

By expanding the measured thermal neutron flux as in Eq. (5.3) and performing a numerical evaluation of the Fourier coefficients, the thermal neutron wave parameters can be evaluated.

The wave amplitude (A_n), and the phase lag angle (θ), are determined from the relationship:



$$a_n \cos nx + b_n \sin nx = A_n \sin (nx + \theta) \dots\dots\dots 5.6$$

Then,

$$A_n = (a_n^2 + b_n^2)^{\frac{1}{2}} \dots\dots\dots 5.7$$

$$\theta_n = \arctan\left(\frac{a_n}{b_n}\right)$$

A modified version of a computer code DATACOR is used to perform the following operations:

- i. correction for background;
- ii. correction for dead time and memory transfer time of the analyser;
- iii. analysis of the corrected data, including numerical evaluation of the Fourier coefficients and determination of the wave amplitude and the phase angle for any source frequency, in accordance with Eqs. (5.6) and (5.7).

The output of the program provides the values of a_n , b_n , A_n and θ_n . The output also provides a function $H(\omega)$, which is the ratio of the amplitude of the nth harmonic to the amplitude of the zero harmonic, $\frac{A_n \neq 0}{A_n = 0}$. The function $H(\omega)$ is regarded as a measure of the

amplitude attenuation. The amplitude gain is defined in decibels as

$$\text{Gain} = 20 \text{ Log}_{10} H(\omega)$$

Program details of the code DATACOR can be found in GIL-RAMOS (1974).

5.2 The space-dependent transfer function of a non-multiplying system

When a modulated source of neutrons is introduced into a moderating medium, the response to the source can be measured by

measuring the ratio of any localised output to the original input to the system. This ratio is space dependent and is called the Space Dependent Transfer Function, (SDTF). The SDTF concept is of fundamental importance in the dynamic analysis and control of nuclear systems. The SDTF relates to a mathematical quantity, the ratio of the Laplace transform of the output to the Laplace transform of the input. In neutron wave experiments, the observation of the wave parameters at different locations in the system yields the frequency response of the system. This is an experimentally measurable quantity linked to the SDTF.

The most convenient way to assess the frequency content of the thermal neutron pulse is to provide separate graphs of wave amplitude and phase as a function of source frequency, assuming the neutron pulse to be a continuous spectrum from zero frequency to some high frequency cutoff.

5.2.1 Measurement of frequency response parameters

The amplitude attenuation function $H(\omega)$ and the phase angle of the neutron wave in the water assembly without voids is plotted in Figure 5.2 and Figure 5.3. The two figures represent the frequency response of the water moderator at 25 cm from the source-moderator boundary. These curves are drawn using the data of the fundamental frequency, ($n=1$) and harmonics up to and including the seventh, ($n=7$). It can be seen from Figure 5.2 that the higher harmonic data are in good agreement with the fundamental frequency data. This was the case for all measurements regardless of the axial distance from the source-moderator boundary. This can be attributed to the improvements in the source conditions described in Chapter Two. In Figure 5.3 the data were restricted to the fundamental and the third harmonic only. It was found that the data obtained by the higher

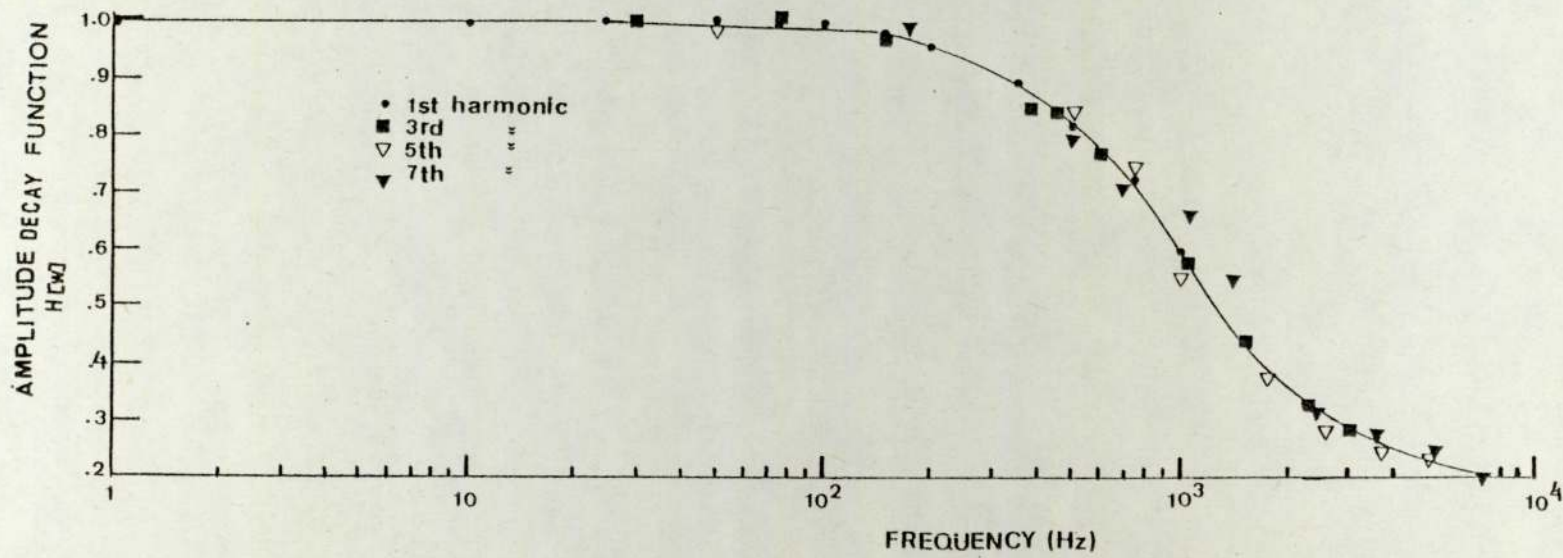


Fig. 5.2. The experimental SDTF, (Amplitude decay), for water assembly without voids, $h = 25$ cm.

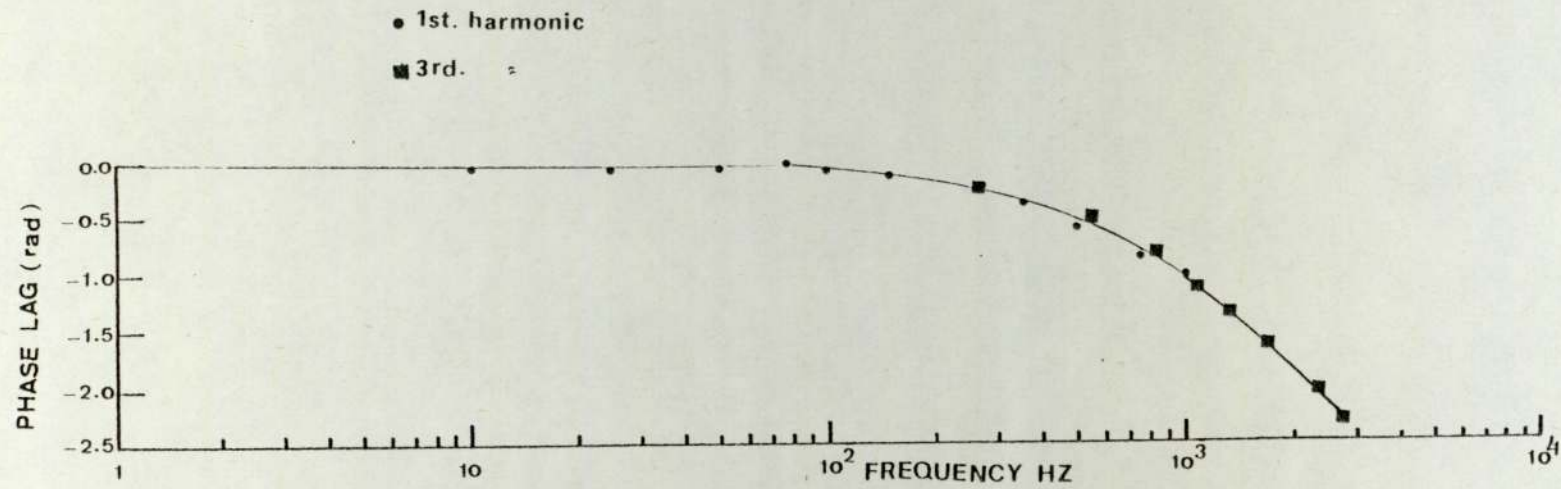


Fig. 5.3. The experimental SDTF, (Phase shift), for water assembly without voids,
 $h = 25$ cm.

harmonics of frequency were not always in agreement with the fundamental frequency data, especially at distances larger than 20 cm from the source-moderator boundary.

The variation of the amplitude decay function and the phase angle with frequency characterise the frequency response of the system. Two parameters have been introduced to quantify the characteristics of a moderator lattice: The break frequency (F_b) and the cut-off frequency (F_c). To evaluate F_b and F_c , consider the transfer function (G) for a time dependent input function of the form:

$$G(t)_{input} = K e^{-at}$$

The transfer function, i.e. the ratio of Laplace transform of the output to the Laplace transform of the input, can be written as:

$$G(s) = \frac{1}{s + a} \dots\dots\dots 5.8$$

where s is the Laplace parameter, which has the value of $(j\omega)$ for a sinusoidal input. The real and the imaginary part of the transfer function are derived by KERLIN (1974) as:

$$\text{Re}\{G(j\omega)\} = \frac{a}{a^2 + \omega^2} \dots\dots\dots 5.9$$

$$\text{Im}\{G(j\omega)\} = \frac{-\omega}{a^2 + \omega^2} \dots\dots\dots 5.10$$

The amplitude $A_{(j\omega)}$ and the phase angle $\theta_{(j\omega)}$ can be written as:

$$A_{(j\omega)} = \left\{ \frac{1}{a^2 + \omega^2} \right\}^{\frac{1}{2}} \dots\dots\dots 5.11$$

$$\theta_{(j\omega)} = \arctan \left(\frac{-\omega}{a} \right) \dots\dots\dots 5.12$$

These quantities have the same physical meaning as the amplitude and phase derived by Fourier analysis in Eqs. (5.6) and (5.7).

The break frequency F_b and the cut-off frequency can be found by examining the asymptotic values of $A(j\omega)$ and $\theta(j\omega)$.

i. for very small frequencies:

$$\left. \begin{aligned} \lim_{\omega \rightarrow 0} A(j\omega) &= \frac{1}{a} \\ \lim_{\omega \rightarrow 0} \theta(j\omega) &= \tan^{-1}(0) = 0 \end{aligned} \right\} \dots\dots\dots 5.13$$

ii. for very large frequencies:

$$\left. \begin{aligned} \lim_{\omega \rightarrow \infty} A(j\omega) &= \frac{1}{\omega} \\ \lim_{\omega \rightarrow \infty} \theta(j\omega) &= \tan^{-1}(\infty) = -90^\circ \end{aligned} \right\} \dots\dots\dots 5.14$$

Hence, the amplitude has a constant value of $(\frac{1}{a})$ at low frequencies and varies as $(\frac{1}{\omega})$ at higher frequencies. The asymptotic phase values are (0) at low frequencies and (-90°) at higher frequencies.

The asymptotic approximation is shown in Figure 5.4 for the frequency response curve of the water assembly without voids at a distance 20 cm from the source. The intersection of the two asymptotes determine the F_b value. It can be seen from Figure 5.4 that F_c can be defined as the frequency beyond which the wave amplitude attenuation, or, the phase angle, becomes independent of the frequency of modulation. However, F_c occurs at frequencies higher than 6000 Hz for water and it is difficult to determine its value because of phase and amplitude fluctuation at higher harmonics. Therefore, F_b is taken as a measure of the frequency response curves.

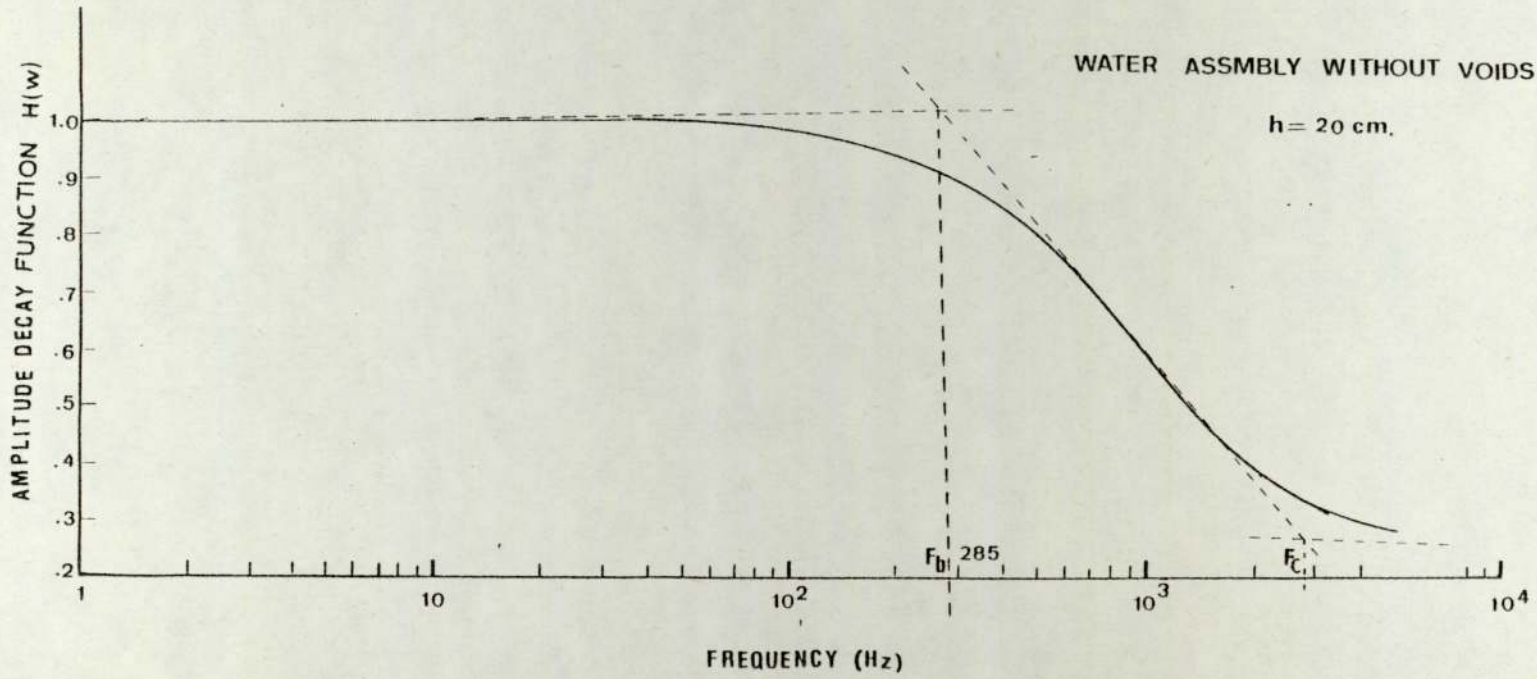


Fig.5.4. Determination of break, F_b , and cut off, F_c , frequencies

5.2.2 The frequency response of the water moderator without voids

The frequency response of the parallelepiped-shaped water assembly, of geometrical buckling $B^2 = 0.003565 \text{ cm}^{-2}$, was measured at seven axial distances from the moderator-source boundary. The results are plotted in Figure 5.5 and show that the general shape of the frequency response curve is characterised by gradual reduction in $H_{(w)}$ for frequencies up to 200 Hz. Above 200 Hz, amplitude function decreases more rapidly, up to the cut-off frequency, beyond which the variation becomes insignificant. The curves in Figure 5.5 indicate that:

- i. the general shape of the frequency response remains the same up to distance of 50 cm from the source-moderator boundary;
- ii. The spatial differences are more noticeable at higher frequencies;
- iii. the spatial differences are more noticeable at locations closer to the source-moderator boundary, i.e. small h ;
- iv. the break frequency (F_b) decreases with locations further from the source-moderator boundary.

A similar set of curves can be drawn to examine the spatial effects on the phase angle response of the system, and (i-iv) above remain valid for phase response.

5.2.3 The frequency response of waver-void assemblies

As described in Chapter 3, four water-void assemblies of different void channel radii were used to study the effects of the presence of voids in the water moderator. The results are shown in Figures 5.6, 5.7, 5.8 and 5.9.

In Figure 5.6 the amplitude decay function $H_{(w)}$ response for a water-void assembly (void radius 2.4 cm) is compared with the

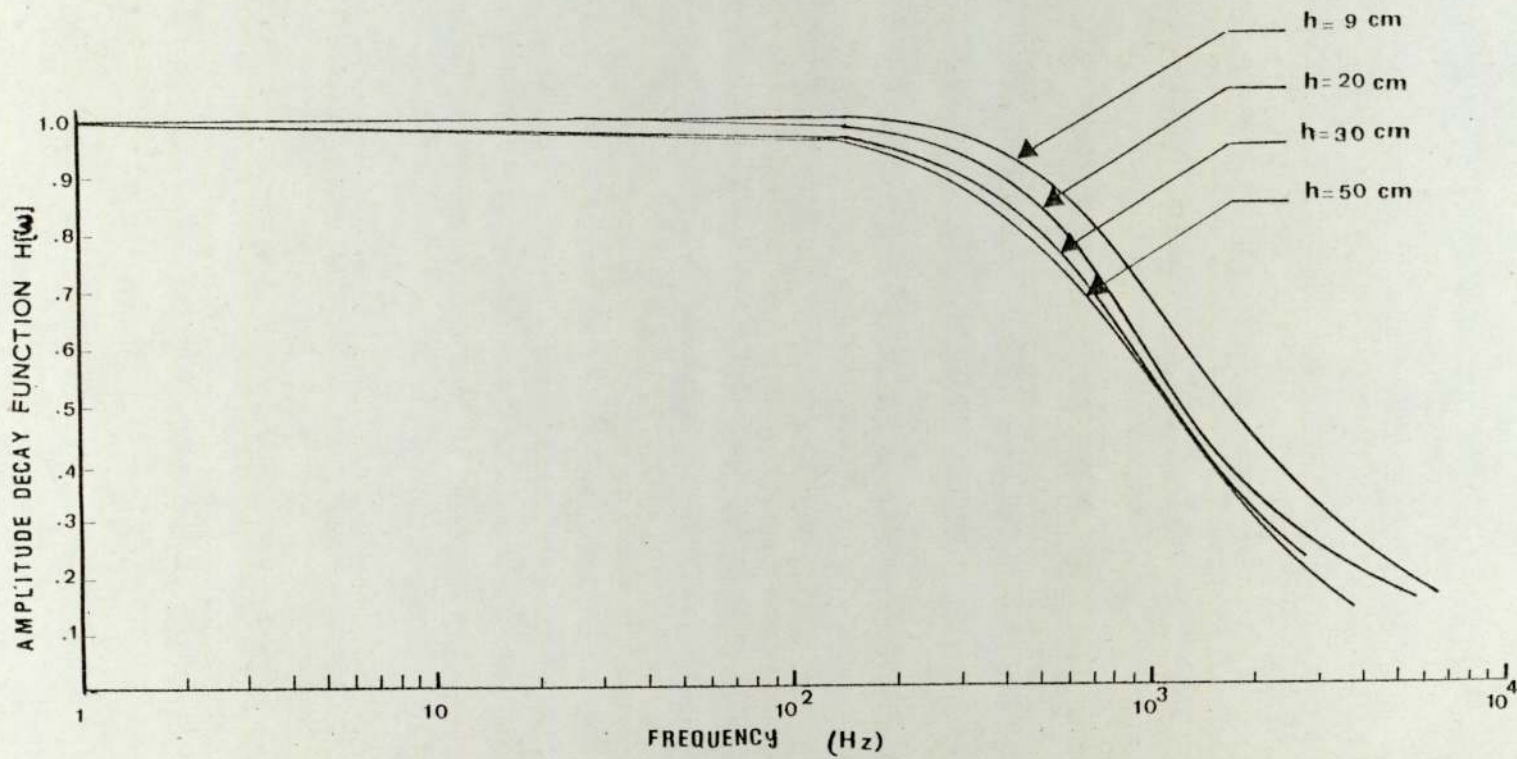


Fig.5.5. The spatial dependence of the measured frequency response of the water assembly without voids.

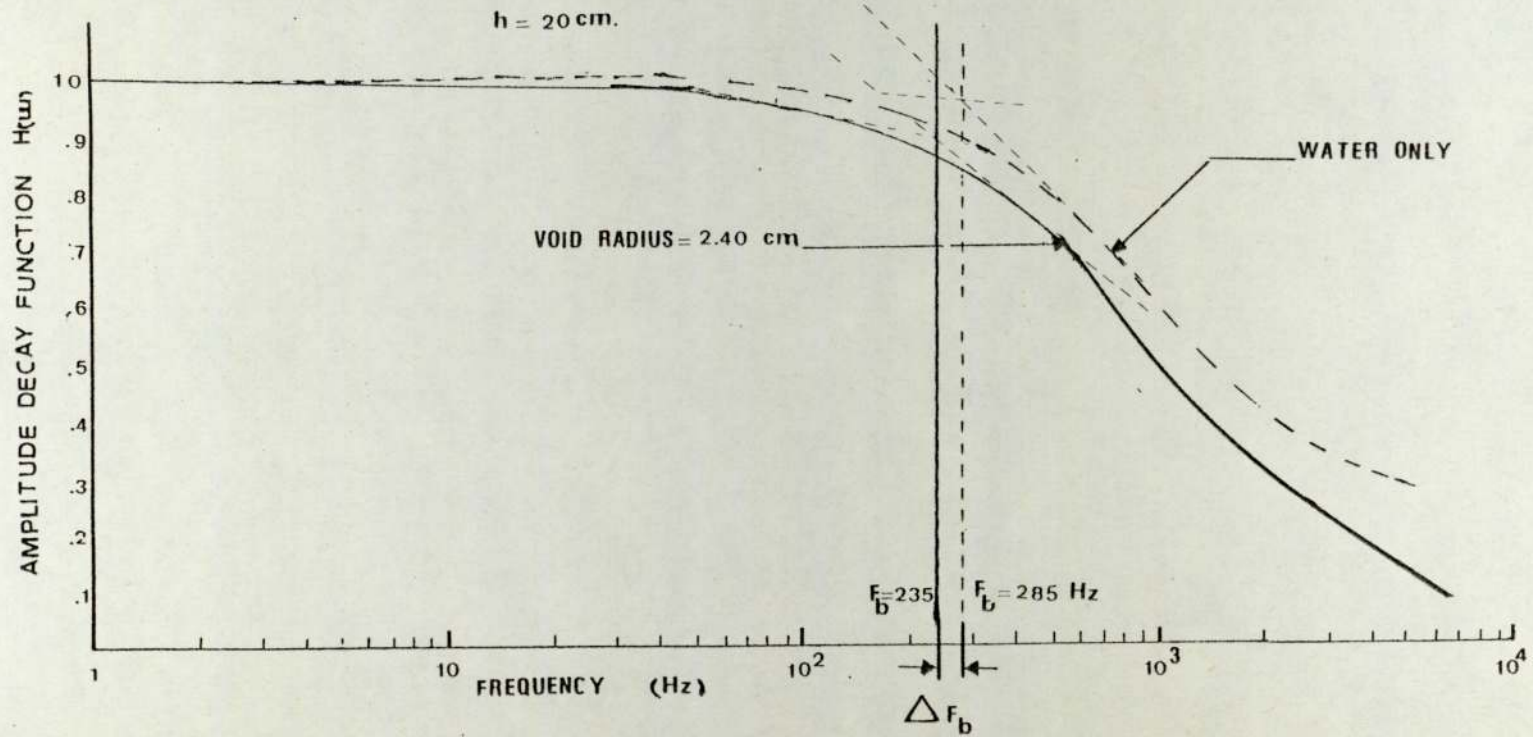


Fig.5.6. Comparison between water and water-void assemblies frequency response curves

amplitude response of the water moderator. Both responses were measured at a distance of 20 cm from the moderator-source boundary. It can be seen from Figure 5.6 that the presence of the void in the moderator increases the attenuation of the amplitude considerably. While the response at frequencies up to 10 Hz does not differ significantly with the introduction of voids, the void effect on the amplitude attenuation function, and the phase lag angle, is appreciable at frequencies larger than 50 Hz. The break frequency is also reduced by 50 Hz by the presence of voids.

The effect of void dimension is shown in Figure 5.7. It can be seen that, by increasing the void channel radius, the amplitude decay function attenuated more rapidly, and the break frequency decreases as the void radius increases.

The spatial effects on the frequency response, for the water-void assembly with void radius = 2.40 cm, can be seen in Figure 5.8. Unlike the water-only results presented in Figure 5.5, Figure 5.8 indicates that the spatial effects are more significant when void is present in the moderator, and more noticeable at distances far from the source. The break frequency decreases more rapidly with distance from the source. At distances more than 30 cm, the cut-off frequency (F_c) occurs within the source frequency range i.e. less than 1250 Hz.

Further examination of the spatial effect is presented by plotting the phase response in Figure 5.9. These results confirm the presence of the cut-off frequency below 1250 Hz at a distance 50 cm from the source. The phase response data is obtained from the first and third harmonics only, since the higher harmonics data for distances higher than 20 cm were unreliable.

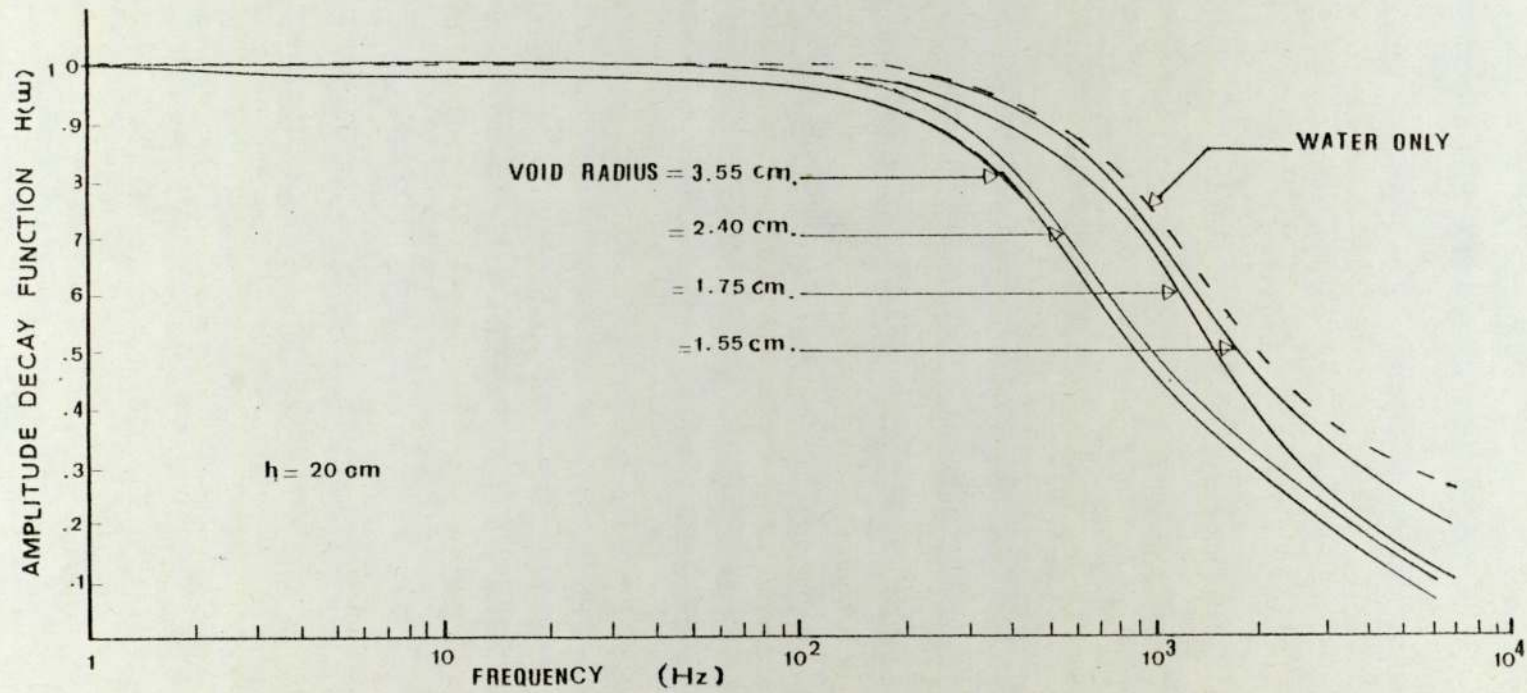


Fig.5.7. The effects of void dimension on the frequency response curves at 20cm axial height

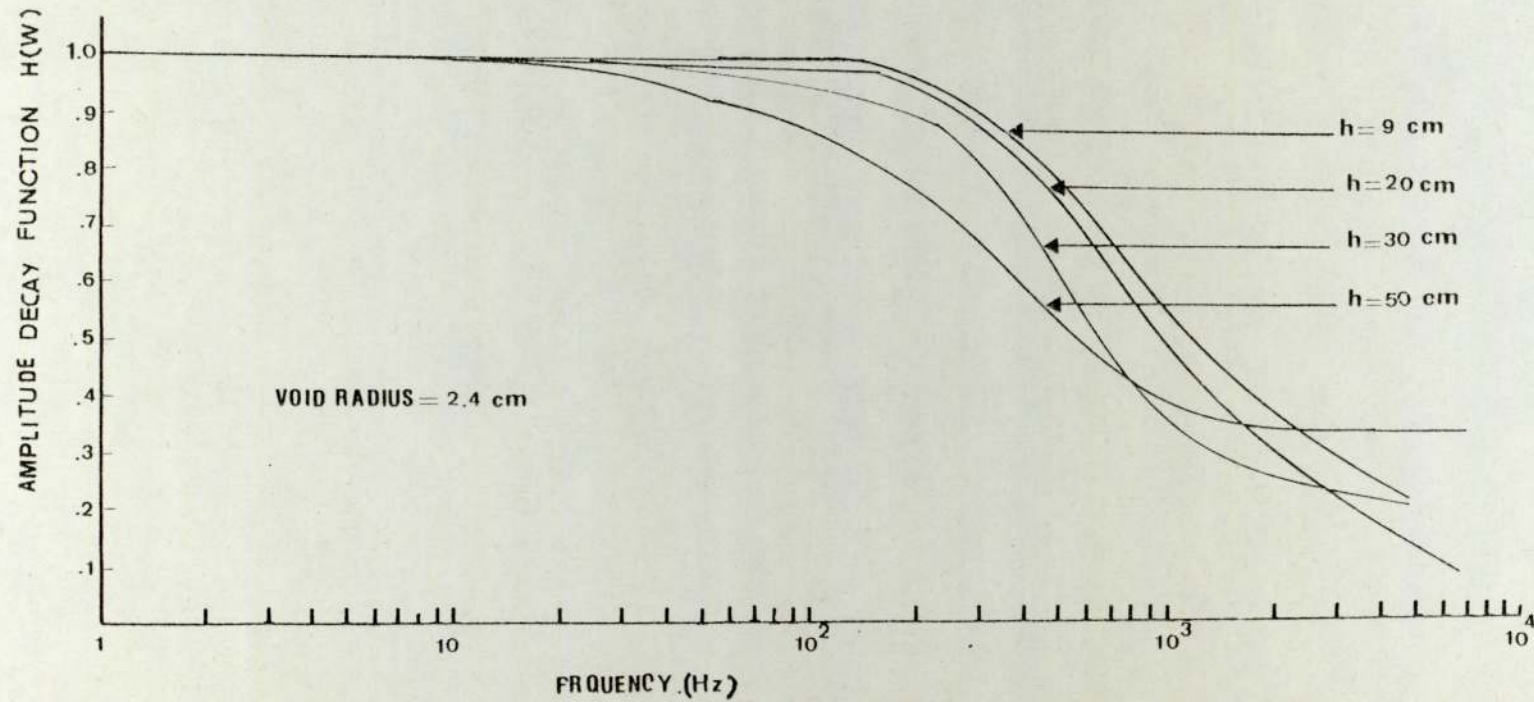


Fig.5.8. The spatial effects on the frequency response curves of water-void assembly No.3.

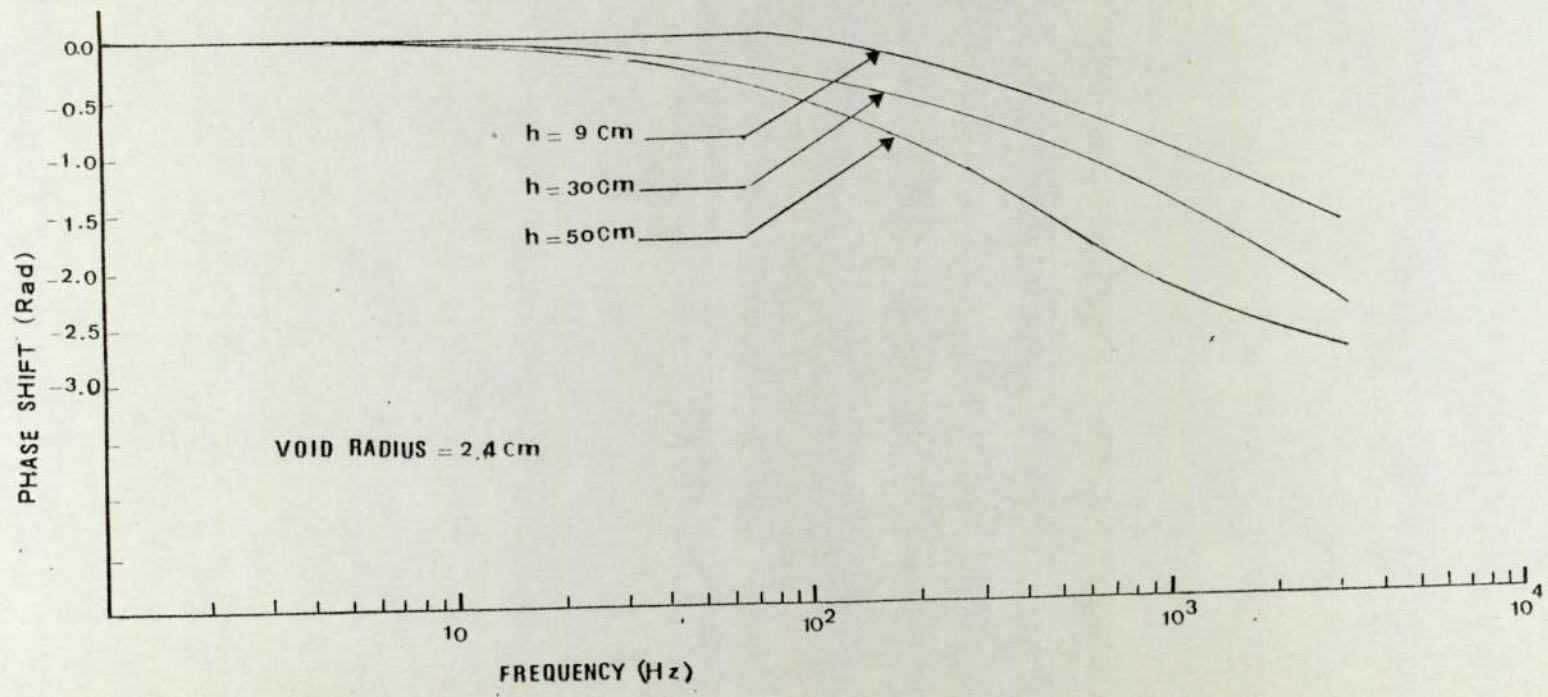


Fig.5.9. The spatial effects on phase response curves of water-void assembly No.3.

5.3 Determination of space-independent neutron wave parameters

As stated in Section 1.3.2.2, an attenuated plane wave travelling in the positive Z-direction can be represented as:

$$\phi(z,t) = A_0 e^{-\rho_\omega z} \cdot e^{j\omega t} \dots\dots\dots 5.15$$

where A_0 is constant for a given frequency (ω) and ρ_ω is the complex inverse relaxation length defined in terms of the amplitude attenuation α_ω and phase lag ξ_ω as:

$$\rho_\omega = \alpha_\omega + j \xi_\omega \dots\dots\dots 5.16$$

In a neutron wave experiment, a set of $\alpha(z,\omega)$ and $\xi(z,\omega)$ must be determined for each detector location. In this section, the measured values of $\alpha(\omega,z)$ and $\xi(\omega,z)$ are related to the complex inverse relaxation length $\rho(\omega)$ by reducing the measured wave parameters to frequency dependent parameters.

5.3.1 The mathematical treatment

The Fourier expansion of the function $F(x)$ presented in Eq. (5.3) can be represented in a complex form as:

$$F(t) = \sum_{n=1}^{\infty} c_n e^{j\omega_n t} \dots\dots\dots 5.17$$

where c_n is the complex Fourier coefficient, defined by KERLIN (1974) as:

$$c_n = \frac{1}{T} \int_{-\frac{1}{2}T}^{\frac{1}{2}T} F(t) e^{-j\omega_n t} dt \dots\dots\dots 5.18$$

where $\omega_n = \frac{2\pi n}{T}$

and T is the time duration of $F(t)$.

To compute the values of c_n for a square wave, the Fourier coefficients of the function $F(x)$ from Eq. (5.4) can be expressed as:

$$a_n = \frac{1}{2\pi} \int_{-\pi}^{\pi} F(x) (e^{jnx} + e^{-jnx}) dx \dots\dots\dots 5.19$$

$$b_n = \frac{1}{2\pi j} \int_{-\pi}^{\pi} F(x) (e^{jnx} - e^{-jnx}) dx \dots\dots\dots 5.20$$

by adding Eqs. (5.19) and (5.20);

$$\frac{1}{2}(a_n + jb_n) = \frac{1}{2\pi} \int_{-\pi}^{\pi} F(x) e^{-jnx} dx \dots\dots\dots 5.21$$

comparing Eq. (5.21) with Eq. (5.18), then,

$$c_n = \frac{1}{2}(a_n + jb_n) \dots\dots\dots 5.22$$

Eq. (5.22) shows that the complex Fourier coefficient c_n can be defined in terms of experimentally measured quantities, a_n and b_n .

To relate the complex Fourier coefficient to the complex inverse relaxation length of the wave, $\rho(\omega)$, we define a continuous complex function of position and frequency $G(z, \omega)$, where the measured c_n are complex numbers which represent the values of the function $G(z, \omega)$. The function $G(z, \omega)$ is related to the inverse relaxation length $\rho(\omega)$ by the expression:

$$G(z, \omega) = A(\omega) e^{-\rho(\omega) z} \dots\dots\dots 5.23$$

or:

$$G_{(z,\omega)} = A_{(\omega)} e^{-(\alpha_{(\omega)} + j \xi_{(\omega)}) z} \dots\dots\dots 5.24$$

where $A_{(\omega)}$ is a complex constant of proportionality with respect to a given value of ω .

The complex function $G_{(z,\omega)}$ can be regarded as having real and imaginary parts. An amplitude R_n and the phase B_n are defined in a way similar to Eq. (5.6) and Eq. (5.7) as:

$$R_{(z,\omega)} = \{ (\text{Re } \{ G_{(z,\omega)} \})^2 + (\text{Im } \{ G_{(z,\omega)} \})^2 \}^{\frac{1}{2}} \dots 5.25$$

$$B_{(z,\omega)} = \arctan \frac{\text{Im } \{ G_{(z,\omega)} \}}{\text{Re } \{ G_{(z,\omega)} \}} \dots\dots\dots 5.26$$

From Eq. (5.24)

$$\log (R_{(z,\omega)}) + jB_{(z,\omega)} = - (\alpha_{(\omega)} + \xi_{(\omega)})z + \log A_{(\omega)} \dots\dots 5.27$$

Separating Eq. (5.27) into real and imaginary parts and equating the equivalent terms for a given harmonic number yields:

$$\log R_{(z,\omega)} = - \alpha_{(\omega)}z + f_{(\omega)} \dots\dots\dots 5.28$$

$$B_{(z,\omega)} = - \xi_{(\omega)}z + g_{(\omega)} \dots\dots\dots 5.29$$

where $f_{(\omega)}$ is the logarithm of the modulus of $A_{(\omega)}$ and $g_{(\omega)}$ is the logarithm of the argument of $A_{(\omega)}$. Eqs. (5.28) and (5.29) can be applied to the experimental data to evaluate the experimental values of $\alpha_{(\omega)}$ and $\xi_{(\omega)}$, as will be discussed in the following section.

5.3.2 Application to the experimental data

The output data of computer code DATACOR provides the values of the wave amplitude gain (Section 5.1.2). These values can be taken as a measure of $\log_e R_{(z,\omega)}$ in Eq. (5.28). The slope of the plot of the gain versus the axial distance from the source-moderator boundary at a given frequency will yield the values of $\alpha_{(\omega)}$. Similarly, the values of $B_{(z,\omega)}$ in Eq. (5.29) are regarded to be equivalent to the measured phase lag angle $\theta_{(z,\omega)}$ in Eq. (5.7), and plots of $\theta_{(z,\omega)}$ versus the axial distance will yield a straight line whose slope is equal to $\xi_{(\omega)}$.

Figure 5.10 and 5.11 show the linear plot of Eqs. (5.28) and (5.29) respectively. The slope is obtained from a linear least squares fit of the experimental values of $\text{Gain}_{(z,\omega)}$ and $\theta_{(z,\omega)}$, for several frequencies of interest. It can be seen from Figure 5.10 that the amplitude gain attenuates more rapidly at higher frequencies. The phase response data are presented in Figure 5.11, from which a similar conclusion can be drawn. The neutron wave parameters for the water assembly without voids are listed in Table 5.1, the data being derived from the linear least squares fit of the experimental data.

The experimental data for the water-void assemblies are treated in a similar way. Figure 5.12 shows the amplitude gain variation with the axial distance for the waver-void assembly with void channel radius = 2.40 cm. The results of several water-void assemblies for a single frequency are presented in Figure 5.13 and indicate that the amplitude gain decays more rapidly for smaller void dimensions. Although Figure 5.13 represents the data obtained at a modulation frequency of 500 Hz, the results obtained at lower frequencies, (i.e. 200, 150, 100 and 75 Hz.), confirm this observation. At 75 Hz, the gain variation with the void dimension

Table 5.1

Neutron wave parameters for water assembly without voids

Harmonic No.	Frequency		$\alpha(\omega)$ cm ⁻¹	$\beta(\omega)$ cm ⁻¹	$\alpha^2(\omega) - \beta^2(\omega)$ cm ⁻²	$2\beta(\omega)\beta_2(\omega)$ cm
	Hz.	rad/sec.				
1st.	10	62.28	0.305	0.094	0.085	0.057
1st.	25	157.08	0.310	0.082	0.090	0.051
1st.	50	314.15	0.344	0.091	0.110	0.062
1st.	75	471.23	0.355	0.124	0.111	0.088
1st.	100	622.80	0.372	0.139	0.119	0.103
1st.	150	942.47	0.388	0.185	0.116	0.143
1st.	200	1256.63	0.389	0.205	0.109	0.159
3rd.	300	1884.94	0.430	0.253	0.120	0.217
1st.	350	2199.11	0.425	0.259	0.113	0.220
3rd.	450	2827.43	0.434	0.297	0.100	0.258
1st.	500	3141.59	0.455	0.308	0.113	0.280
3rd.	600	3769.91	0.471	0.327	0.115	0.308
1st.	750	4712.38	0.510	0.375	0.120	0.382
1st.	1000	6283.18	0.605	0.338	0.188	0.409
1st.	1250	7853.98	0.635	0.399	0.247	0.507
3rd.	1500	9424.77	0.782	0.362	0.274	0.559
3rd.	2250	14137.1	0.810	0.326	0.549	0.529
3rd.	3000	18849.5	0.847	0.371	0.579	0.629

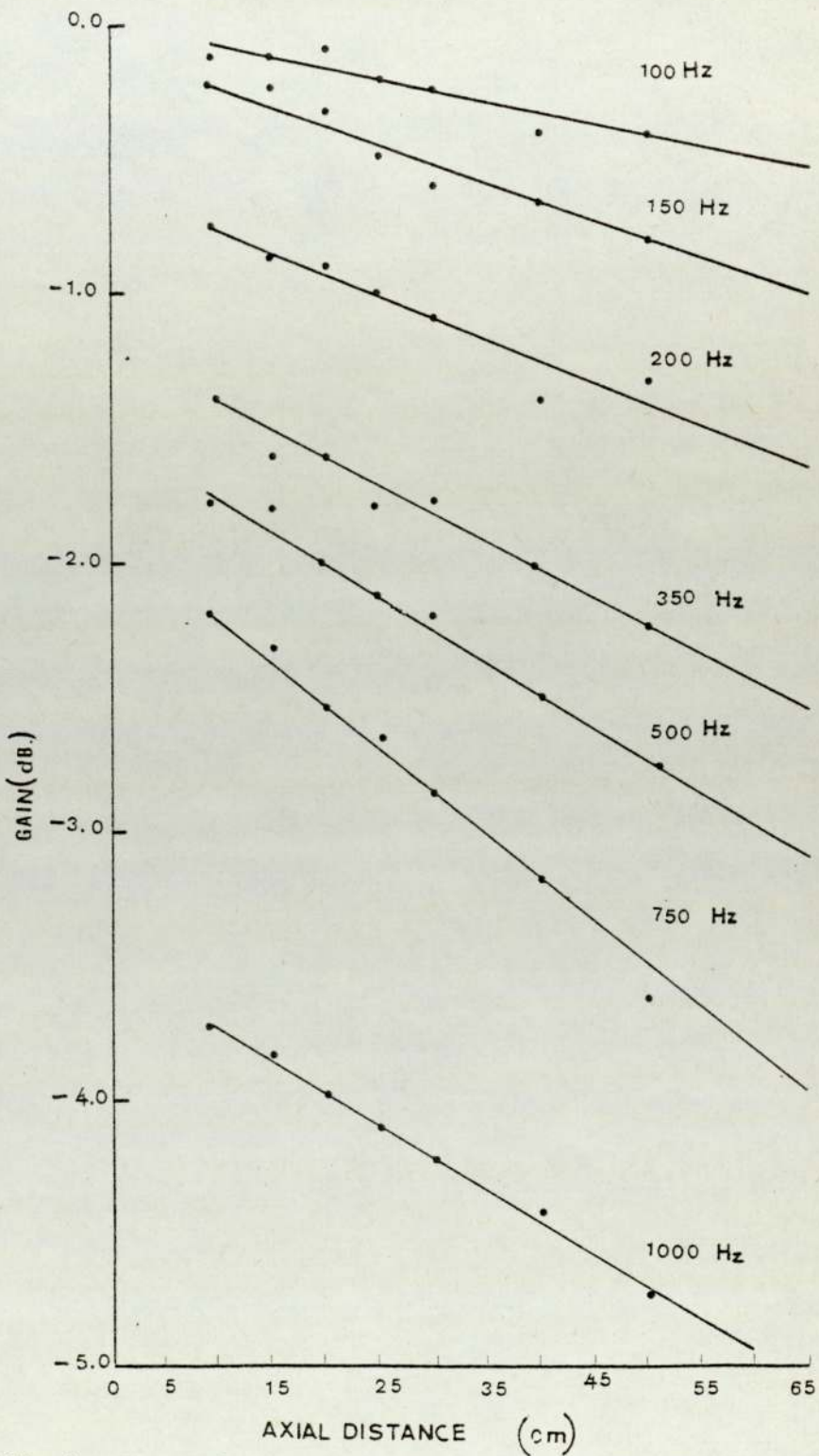


Fig.5.10. Amplitude gain variation with axial distance for several frequencies in water assembly without voids.

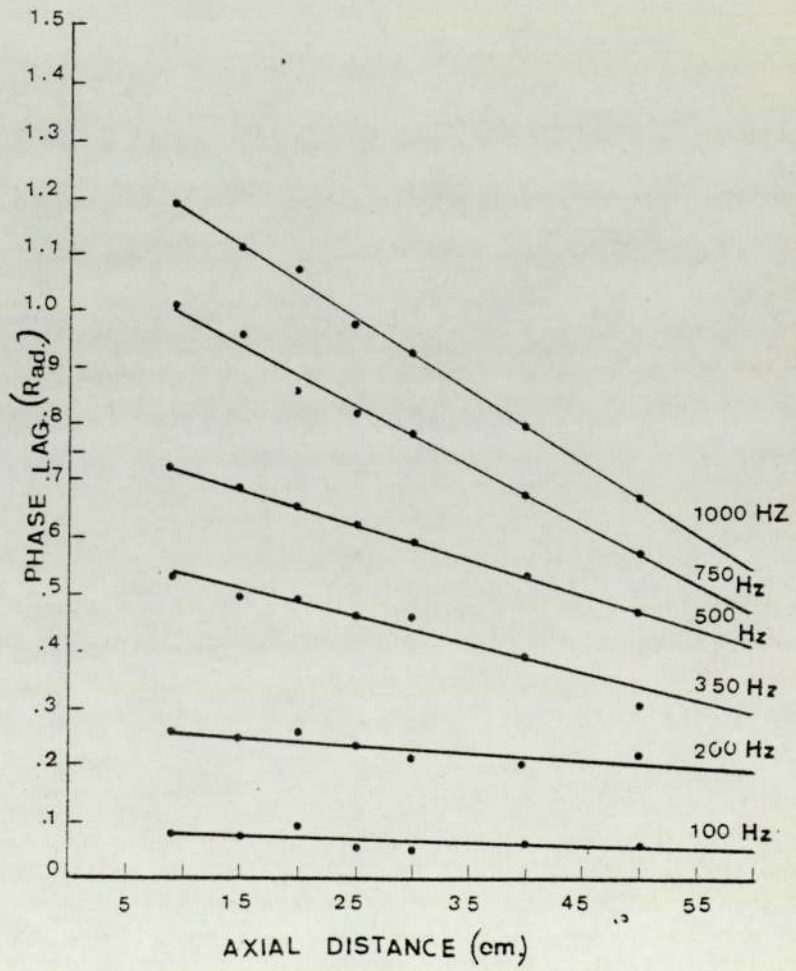


Fig.5.11. Phase lag variation with axial distance for several frequencies in water assembly without void.

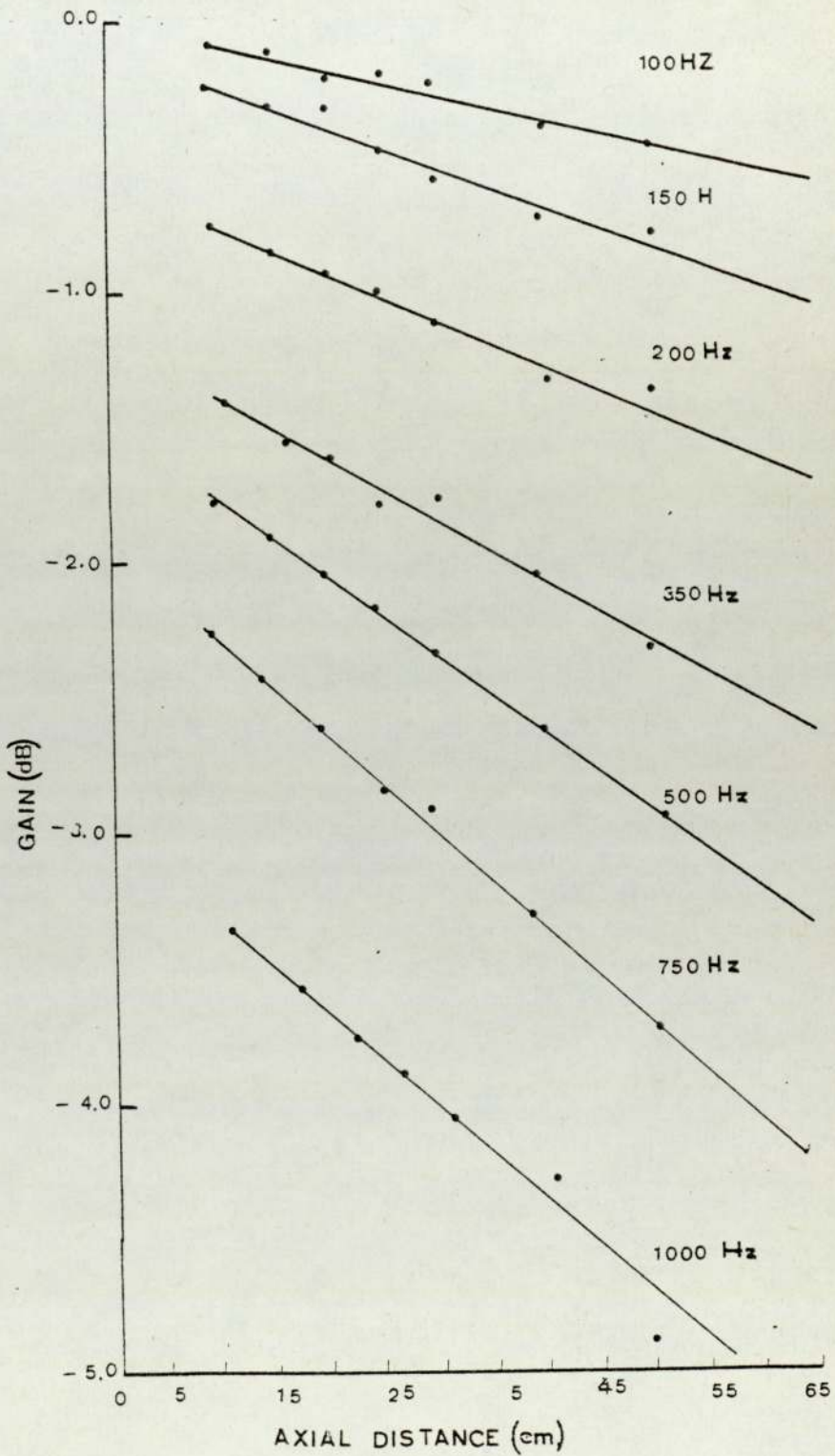


Fig.5.12. Amplitude gain variation with axial distance for several frequencies in water-void assembly (void radius=2.4 cm).

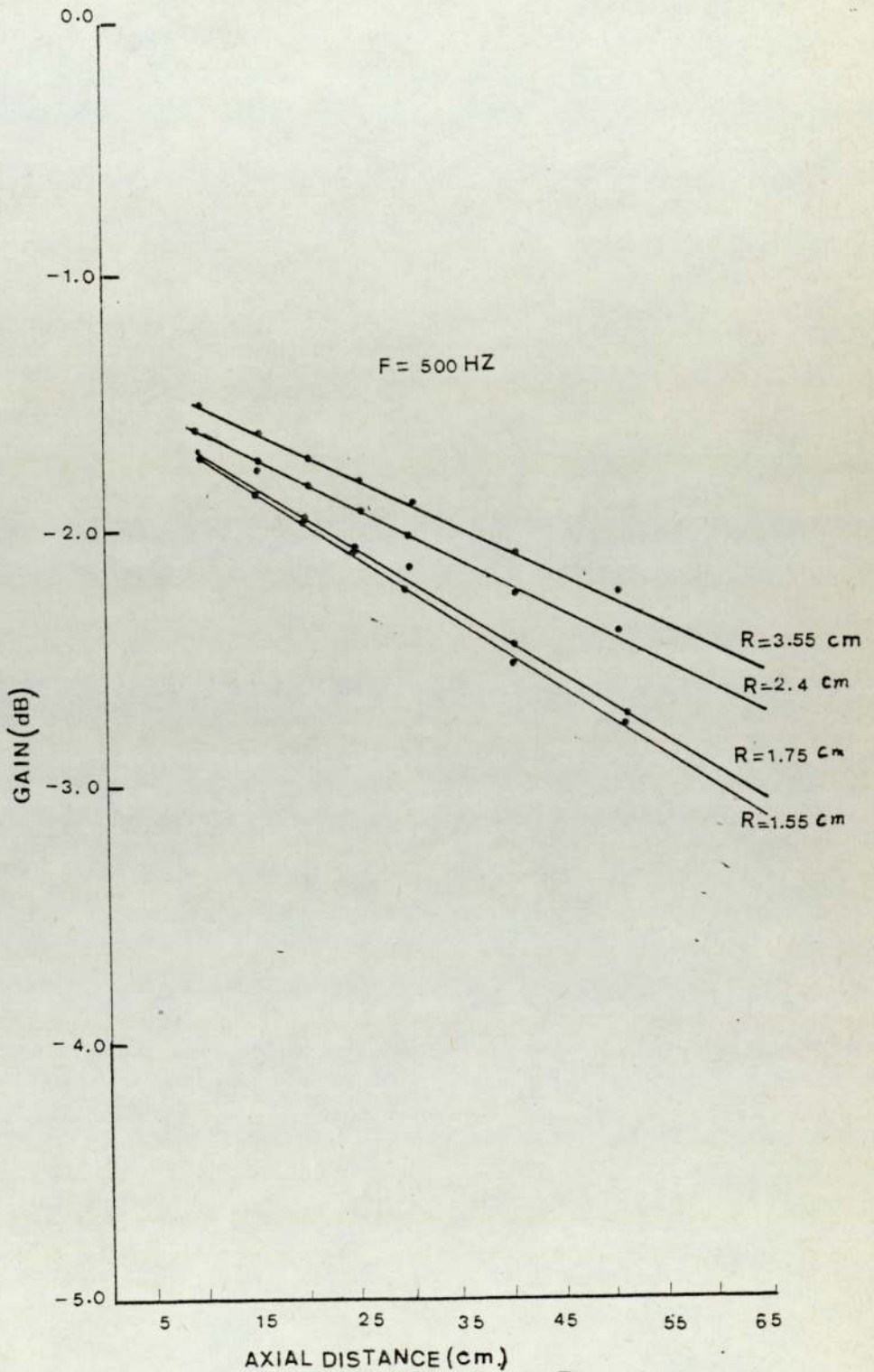


Fig.5.13. EFFECT OF VOID DIMENSIONS ON AMPLITUDE GAIN VARIATION WITH AXIAL DISTANCE

becomes difficult to detect. This indicates that, with a void cell producing significant neutron streaming, the amplitude attenuation becomes less noticeable at lower frequencies. At higher frequencies, (i.e. beyond 1250 Hz), the effects of void dimension become negligible. Similar conclusions can be drawn from the phase response presentations. The numerical values of $\alpha(\omega)$ and $\xi(\omega)$ for several water-void assemblies are listed in Tables 5.2, 5.3, 5.4 and 5.5, the values being obtained from the least squares fit of the experimental data.

5.4 Determination of diffusion and thermalisation parameters

The method used to determine the diffusion and thermalisation parameters of the water assembly without voids and several water-void assemblies is presented in this section. The mathematical treatment of the observed wave parameters is presented first, followed by its application to the experimental measurements.

5.4.1 The mathematical treatment

The time-dependent one group diffusion equation for a non-multiplying medium is given by LAMARSH (1967) as:

$$\bar{D}_0 \nabla^2 \phi(x,y,z,t) - \bar{\Sigma}_a \phi(x,y,z,t) = \frac{1}{v} \frac{\delta \phi(x,y,z,t)}{\delta t}$$

..... 5.30

where \bar{D}_0 and $\bar{\Sigma}_a$ are the thermal diffusion constant and the macroscopic absorption cross section of the moderator averaged over a Maxwellian energy spectrum. (The Maxwellian average is omitted hereafter).

Introducing the wave solution presented in Eq. (5.15) into Eq. (5.30) will yield:

Table 5.2
 Numerical results for void cell
 void channel radius = 1.55 cm.

Harmonics No.	Frequency		$\alpha(\omega)$ cm ⁻¹	$\rho(\omega)$ cm ⁻¹	$\alpha(\omega) - \rho(\omega)$ cm ⁻²	$2\alpha(\omega)\rho(\omega)$ cm ⁻²
	Hz	rad.s ⁻¹				
1st.	10	62.28	0.240	0.056	0.003	0.027
1st.	25	157.08	0.245	0.062	0.005	0.030
1st.	50	314.15	0.246	0.068	0.055	0.033
1st.	75	471.23	0.255	0.107	0.054	0.054
1st.	100	628.80	0.262	0.136	0.049	0.071
1st.	150	942.47	0.264	0.162	0.040	0.085
1st.	200	1256.63	0.286	0.179	0.037	0.102
3rd.	300	1884.94	0.291	0.208	0.038	0.121
1st.	350	2199.11	0.319	0.251	0.038	0.164
3rd.	450	2827.43	0.318	0.250	0.060	0.159
1st.	500	3141.59	0.320	0.222	0.060	0.142
3rd.	600	3769.91	0.344	0.240	0.048	0.165
1st.	750	4712.58	0.348	0.269	0.045	0.187
1st.	1000	6283.18	0.367	0.302	0.048	0.221
1st.	1250	7853.98	0.385	0.327	0.046	0.251
3rd.	1500	9424.77	0.472	0.337	0.065	0.318
3rd.	2250	14137.10	0.522	0.382	0.082	0.398
3rd.	3000	18849.50	0.563	0.495	0.123	0.557

Table 5.3

Numerical results for void cell
 Void Channel radius = 1.75 cm.

Harmonic No.	Frequency		$\alpha_{(w)}$ cm ⁻¹	$\bar{P}_{(w)}$ cm ⁻¹	$\alpha_{(w)}^2 - \bar{P}_{(w)}^2$ cm ⁻²	$2\alpha_{(w)}\bar{P}_{(w)}$ cm ⁻²
	Hz.	rad.s ⁻¹				
1st.	25	157.08	0.075	0.095	0.004	0.014
1st.	50	314.15	0.205	0.115	0.028	0.047
1st.	75	471.23	0.278	0.138	0.058	0.076
1st.	100	628.80	0.377	0.197	0.103	0.148
1st.	150	942.47	0.394	0.214	0.109	0.168
1st.	200	1256.63	0.409	0.251	0.104	0.205
3rd.	300	1884.94	0.434	0.279	0.111	0.242
1st.	350	2199.11	0.453	0.294	0.119	0.266
3rd.	450	2827.43	0.463	0.325	0.108	0.300
1st.	500	3141.59	0.472	0.333	0.112	0.314
3rd.	600	3769.91	0.488	0.356	0.111	0.347
1st.	750	4712.91	0.508	0.372	0.119	0.378
1st.	1000	6283.18	0.537	0.418	0.125	0.449
3rd.	1500	9424.77	0.584	0.419	0.165	0.489
3rd.	2250	14137.10	0.635	0.529	0.128	0.671
3rd.	3000	18849.50	0.680	0.579	0.137	0.787

Table 5.4

Numerical results for void cell

Void channel radius = 2.40 cm.

Harmonic No.	Frequency		α (w) cm ⁻¹	\bar{P} (w) cm ⁻¹	T^i (w) - T^e (w) cm ⁻²	2α (w) \bar{P} (w) cm ⁻²
	Hz	rad.s ⁻¹				
1st.	50	714.15	0.137	0.085	0.011	0.023
1st.	75	471.25	0.208	0.103	0.033	0.042
1st.	100	628.80	0.372	0.192	0.102	0.142
1st.	150	942.47	0.339	0.220	0.103	0.171
1st.	200	1256.63	0.405	0.248	0.102	0.201
3rd.	300	1884.94	0.430	0.287	0.102	0.247
1st.	350	2199.11	0.440	0.302	0.102	0.265
3rd.	450	2827.43	0.459	0.329	0.102	0.302
1st.	500	3141.59	0.468	0.341	0.102	0.319
3rd.	600	3769.91	0.483	0.361	0.103	0.348
1st.	750	4712.91	0.504	0.387	0.105	0.390
1st.	1000	6283.18	0.535	0.423	0.107	0.452
3rd.	1500	9424.77	0.556	0.477	0.116	0.531
3rd.	2250	14137.10	0.573	0.463	0.121	0.533
3rd.	3000	18849.50	0.626	0.581	0.137	0.726

Table 5.5

Numerical results for void cell

Void Channel radius = 3.55 cm.

Harmonic No.	Frequency		$\alpha_{(w)}$ cm^{-1}	$\bar{f}_{(w)}$ cm^{-1}	$\alpha_{(w)}^2 - \bar{f}_{(w)}^2$ cm^{-2}	$2\alpha_{(w)}\bar{f}_{(w)}$ cm^{-2}
	Hz.	rad. s^{-1}				
1st.	50	314.15	0.182	0.081	0.027	0.029
1st.	75	471.23	0.274	0.111	0.063	0.060
1st.	100	628.30	0.365	0.193	0.096	0.141
1st.	150	942.47	0.381	0.217	0.098	0.165
1st.	200	1256.63	0.397	0.246	0.097	0.195
3rd.	300	1884.94	0.422	0.286	0.097	0.241
1st.	350	2199.11	0.432	0.302	0.096	0.261
3rd.	450	2827.43	0.451	0.332	0.093	0.299
1st.	500	3141.59	0.460	0.341	0.095	0.313
3rd.	600	3769.91	0.475	0.365	0.093	0.346
1st.	750	4712.91	0.495	0.381	0.100	0.377
1st.	1000	6283.18	0.524	0.402	0.113	0.421
3rd.	1500	9424.77	0.569	0.451	0.121	0.513
3rd.	2250	14137.10	0.621	0.463	0.172	0.575
3rd.	3000	18849.50	0.663	0.561	0.126	0.744

$$\rho_{\omega}^2 = \frac{\Sigma_a}{D_0} + j \frac{\omega}{vD_0} \dots\dots\dots 5.31$$

By squaring Eq. (5.16) and comparing the result with Eq. (5.31), then:

$$\alpha_{\omega}^2 - \xi_{\omega}^2 = \frac{\Sigma_a}{D_0} = \frac{1}{L^2} \dots\dots\dots 5.32$$

$$2\alpha_{\omega}\xi_{\omega} = \frac{\omega}{vD_0} \dots\dots\dots 5.32a$$

where L^2 is the thermal diffusion area.

Eqs. (5.32) and (5.33) suggest that L^2 , Σ_a and D_0 can be determined by observation of $\alpha_{(\omega)}$ and $\xi_{(\omega)}$. To check the asymptotic behaviour of Eqs. (5.32) and (5.33) they can be combined to give:

$$\alpha_{(\omega)}^2 = \frac{1}{2L^2} + \frac{1}{2} \left(\frac{1}{L^4} + \frac{\omega^2}{v^2 D_0^2} \right)^{\frac{1}{2}} \dots\dots\dots 5.33$$

$$\xi_{(\omega)}^2 = \frac{-1}{2L^2} + \frac{1}{2} \left(\frac{1}{L^4} + \frac{\omega^2}{v^2 D_0^2} \right)^{\frac{1}{2}} \dots\dots\dots 5.33a$$

Eqs. (5.34) and (5.35) show that, when ω approaches zero, $\alpha_{(\omega)} \rightarrow \frac{1}{L}$ and $\xi_{(\omega)} \rightarrow 0$. For large frequencies, $\xi_{(\omega)}$ and $\alpha_{(\omega)}$ approach a common value of $\left(\frac{\omega}{2vD_0} \right)^{\frac{1}{2}}$.

The phase velocity (\bar{u}) is defined by ($\bar{u} = \frac{\omega}{\xi_{\omega}}$) has asymptotic values of $\left(\frac{1}{L} \right)$ as ω approaches zero and $(2vD_0\omega)^{\frac{1}{2}}$ for large frequencies.

To facilitate the comparison with theory, it is convenient to present the wave parameters in a plot of (α_{ω}) versus (ξ_{ω}) for

the range of the modulation frequencies of interest. The resultant diagram is called the (ρ) dispersion law. Similarly, the plot of $(\alpha_{\omega}^2 - \xi_{\omega}^2)$ versus $(2\alpha_{\omega}\xi_{\omega})$ is called the (ρ^2) dispersion law.

5.4.2 Application to the experimental data

The values of (α_{ω}) and (ξ_{ω}) of the thermal neutron wave propagated in the water assembly without voids are listed in Table 5.1. These values, which were obtained from a least squares fit of the experimental data, are used to plot the variation of $(2\alpha_{\omega}\xi_{\omega})$ and $(\alpha_{\omega}^2 - \xi_{\omega}^2)$ with modulation frequency. The results are shown in Figures 5.14 and 5.15. The solid curves are the least squares fit performed by a standard FORTRAN curve fitting routine UA01. This program fits a polynomial to a set of values of a function of one variable using the method of least squares via orthogonal polynomials. The dashed lines represent the linear fit of the experimental data for frequencies lower than, and including 600 Hz. Figure 5.14 indicates that the linear relationship between $(2\alpha_{\omega}\xi_{\omega})$ and the frequency holds up to 600 Hz. Beyond 600 Hz the relationship given by Eq. (5.33) is no longer valid. Figure 5.14 also indicates that even below 600 Hz, the best straight line through the experimental points does not pass through the origin as predicted by Eq. (5.33). The relationship between $(\alpha_{\omega}^2 - \xi_{\omega}^2)$ and frequency in Figure 5.15 deviates from the constant value predicted by Eq. (5.32) at frequencies larger than 600 Hz, where the sensitivity to change in frequency is greater than that of $(2\alpha_{\omega}\xi_{\omega})$.

It is apparent from Figures 5.14 and 5.15 that the diffusion approximation based on Eq. (5.30) can not interpret correctly the experimental observations in the entire experimental frequency range. Hence, a more comprehensive theoretical model is necessary.

The slope of the linear fit in Figure 5.14 should give the value

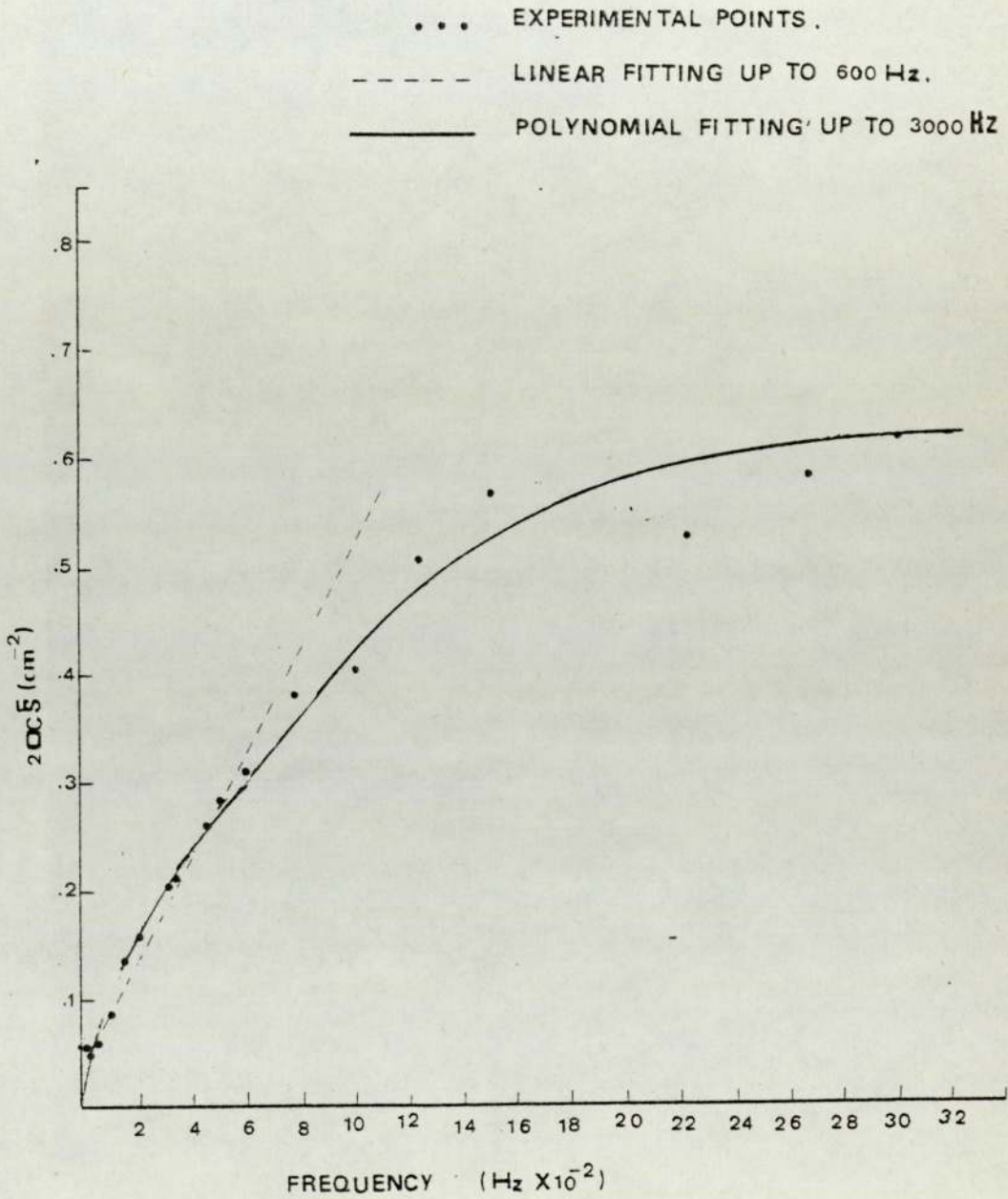


Fig. 5.14. Variation of wave parameters with frequency for water assembly.

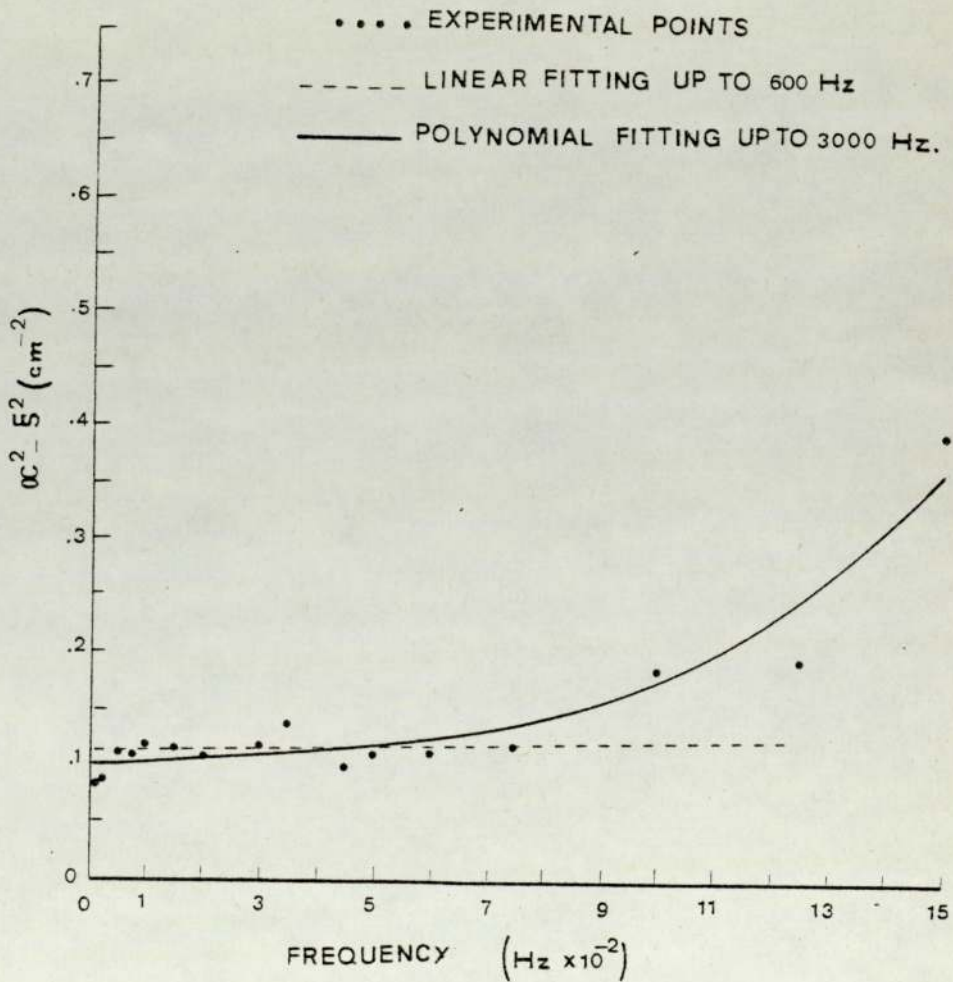


Fig.5.15. Variation of $\alpha_c^2 - S^2$ with frequency for water assembly without voids.

of $(\frac{1}{vD_0})$, and the zero frequency intercept in Figure 5.15 gives the value of $(\frac{\Sigma_a}{D_0})$ i.e. $(\frac{1}{L^2})$ for the water assembly without voids.

These values are found to be higher than the accepted values for water. This discrepancy is commented upon in Chapter Seven.

The first order dispersion law for water assembly without voids is presented in Figure 5.16, where the relation between (α_ω) and (ξ_ω) can be examined. The (α, ξ) plane can furnish some information about the presence of a discrete wavefront and continuum, as will be discussed in Chapter Seven. It can be seen from Figure 5.16 that at frequencies higher than 600 Hz, (or 3769 rad s^{-1}), a well defined cyclic behaviour occurs. This will be related to the attenuation of the discrete and the continuum modes of the thermal neutron wave in Chapter Seven.

The phase velocity ($\bar{u} \text{ cm s}^{-1}$), and the wave length ($\lambda \text{ cm}$) of the thermal neutron wave in water, are plotted in Figure 5.17 versus frequency in rad. s^{-1} . It can be seen from Figure 5.17 that the phase velocity is related to the modulation frequency and increases as frequency decreases. This indicates the dispersive nature of the thermal neutron wave. The wavelength variation with frequency is another way to show the dispersive nature of the thermal neutron wave. Both curves in Figure 5.17 indicate the presence of a finite wavefront velocity, which contradicts the diffusion theory assumption of the infinite wavefront velocity.

The measurements of the frequency response of several water-void assemblies were performed and the data obtained are presented in a way similar to those for water assembly without voids. The numerical values of the wave parameters are listed in Tables 5.2, 5.3, 5.4 and 5.5. The dependence of $(\alpha_\omega^2 - \xi_\omega^2)$ on the source frequency for one of the water-void assemblies is shown in Figure 5.18. This figure

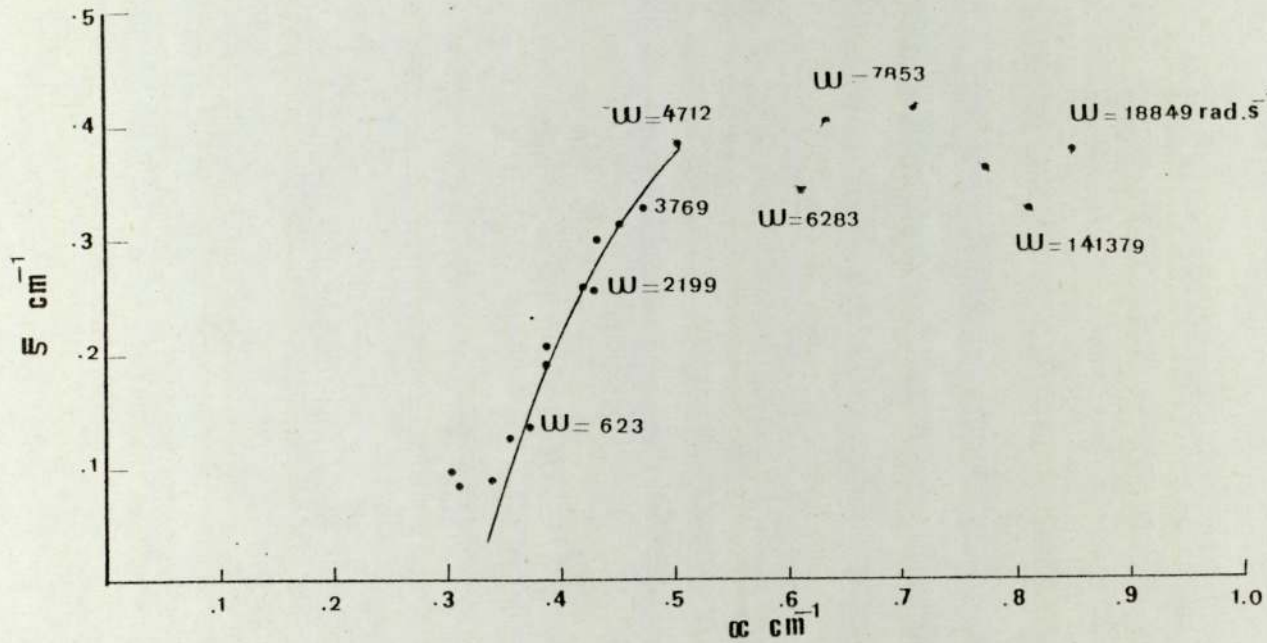


Fig.5.16. DISPERSION LAW FOR WATER ASSEMBLY WITHOUT VOIDS.

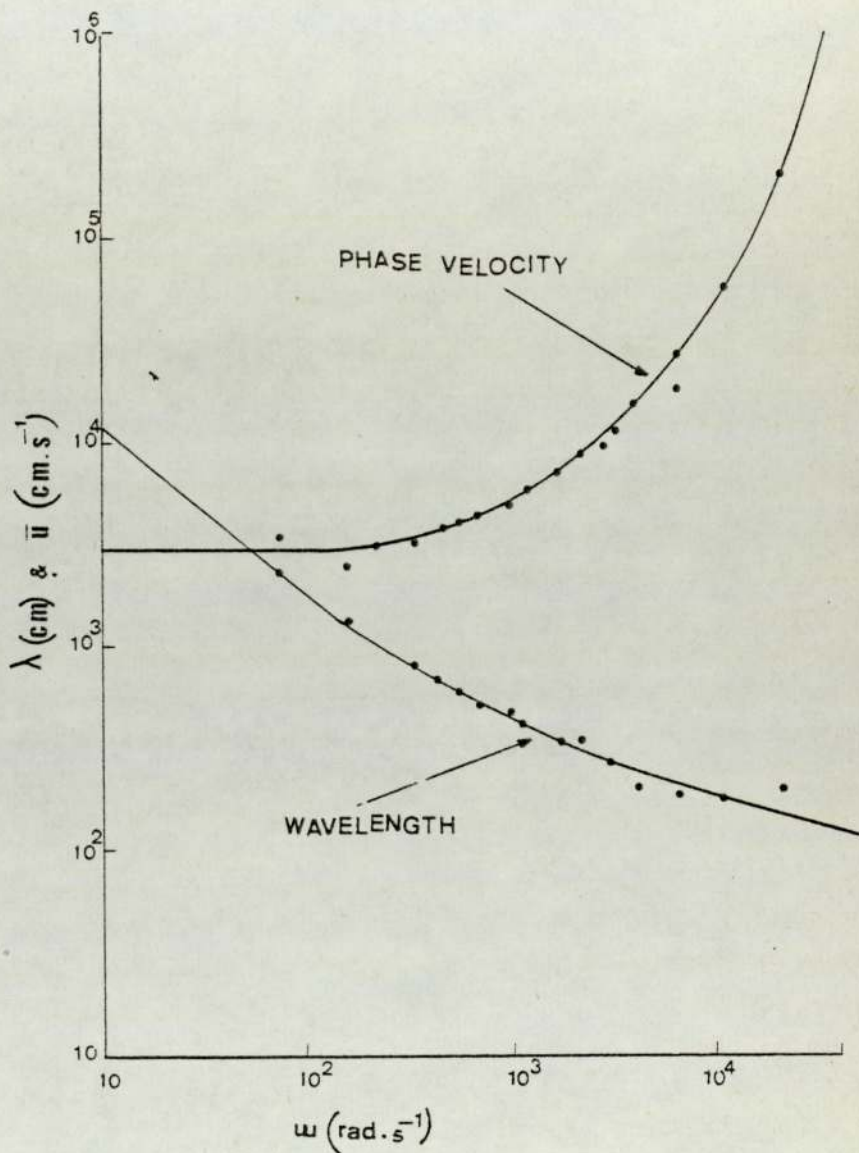


Fig. 5.17. Phase velocity, \bar{u} and wavelength, λ , for thermal neutron wave in water assembly, without voids.

shows that the relationship given in Eq. (5.32) holds satisfactorily for source frequencies up to and including 600 Hz. It was found that beyond this frequency the measured values of $(\alpha_{\omega}^2 - \xi_{\omega}^2)$ increase with frequency, as can be seen from the solid curve in Figure 5.18 which was obtained as a result of the polynomial fitting of the experimental data for frequencies up to and including 3000 Hz.

To investigate the effect of the void dimension on the variation of the wave parameters function $(2\alpha_{\omega} \xi_{\omega})$ with source frequency, the values of $(2\alpha_{\omega} \xi_{\omega})$, obtained over the range of the experimental frequencies, were plotted versus frequency for several water-void assemblies. The results are shown in Figure 5.19. The results of the water assembly without void is also drawn in Figure 5.19.

Figure 5.19 shows that by the introduction of voids into a moderator, the wave function $(2\alpha_{\omega} \xi_{\omega})$ becomes more sensitive to the source frequency. It was found that this sensitivity to the frequency increases by increasing the void dimensions. The linear relationship between $(2\alpha_{\omega} \xi_{\omega})$ and the source frequency for the water assembly was found to be valid up to 600 Hz. By the introduction of voids into the moderator, the frequency upper limit decreases to 450 Hz for a water-void assembly with void channel radius of 1.75 cm. It was found that further increase in the void dimension reduces the frequency upper limit below which Eq. (5.33) can be applied.

The effect of void on the variation of $(\alpha_{\omega}^2 - \xi_{\omega}^2)$ with frequency was examined by plotting the values of $(\alpha_{\omega}^2 - \xi_{\omega}^2)$ versus frequency for water assembly without void and three water-void assemblies of different void channel radius. The results can be seen in Figures 5.20 and 5.21. Figure 5.20 shows that below 600 Hz the size of the void channel has a little effect on $(\alpha_{\omega}^2 - \xi_{\omega}^2)$ curves. However, the effect of the voids on the zero-frequency intercepts is noticeable. Figure 5.20 provides the values

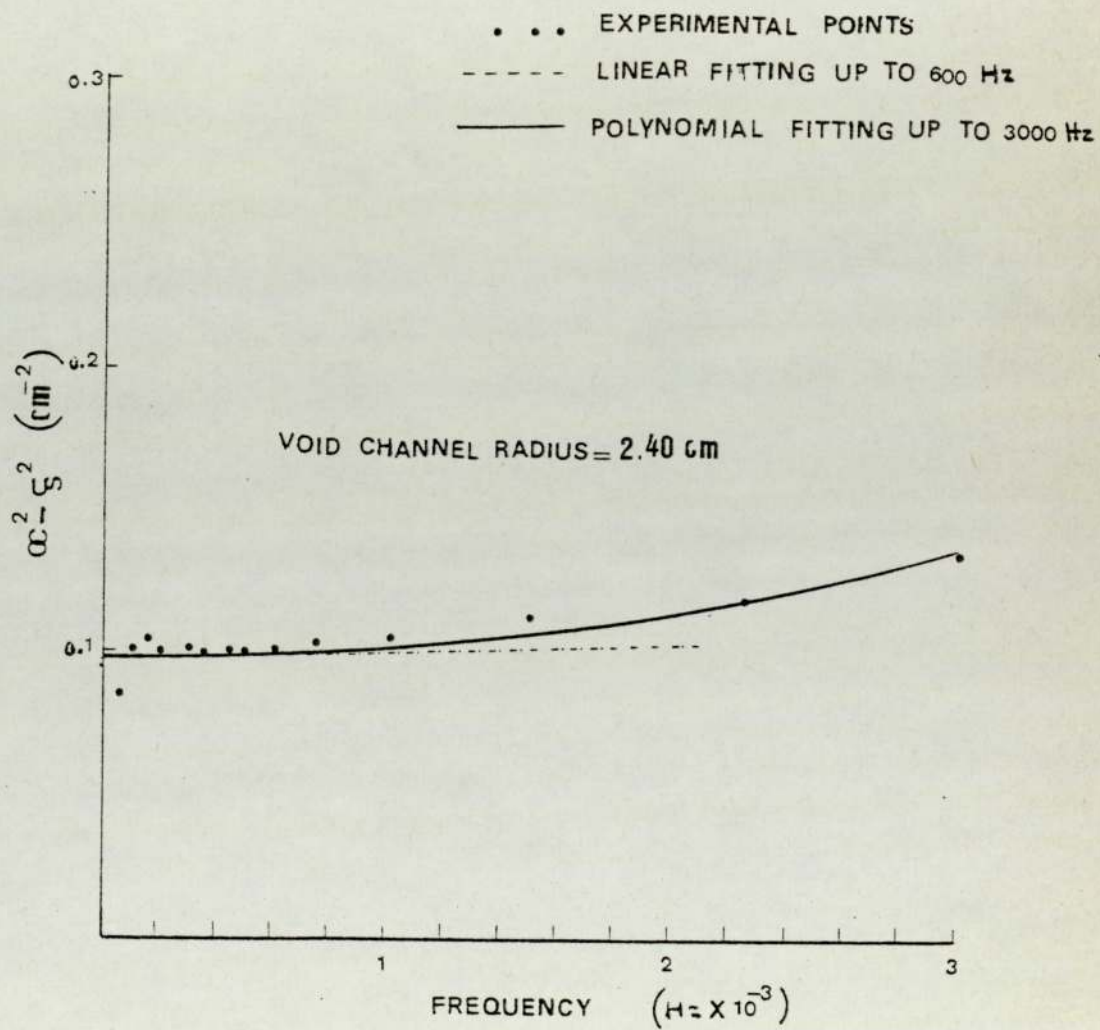


Fig.5.18. Variation of wave parameters with modulation frequency in water-void assembly.

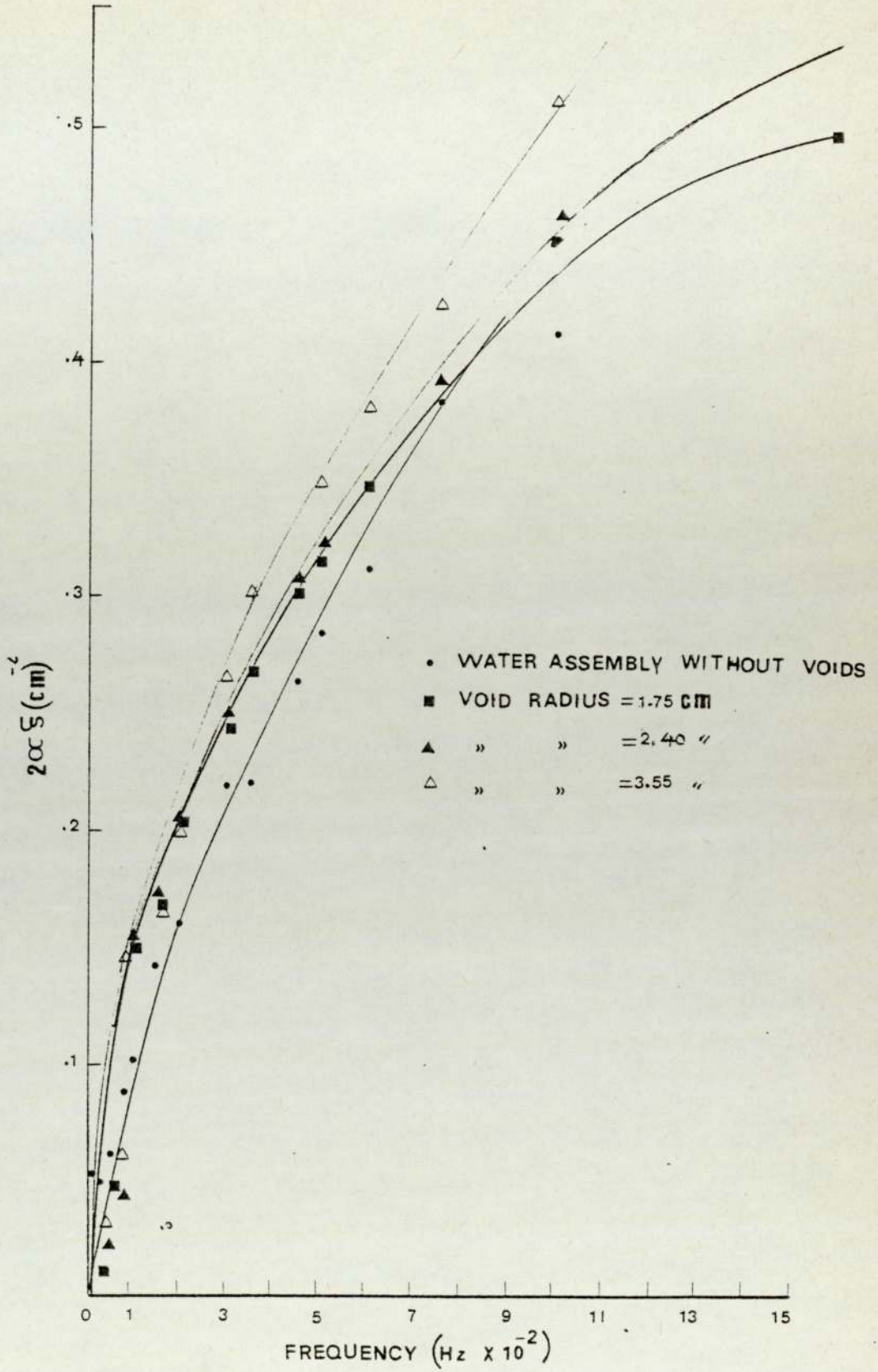


Fig.5.19 . Comparison between $(2\alpha\xi)$ and frequency relation for several assemblies of different void channe radius.

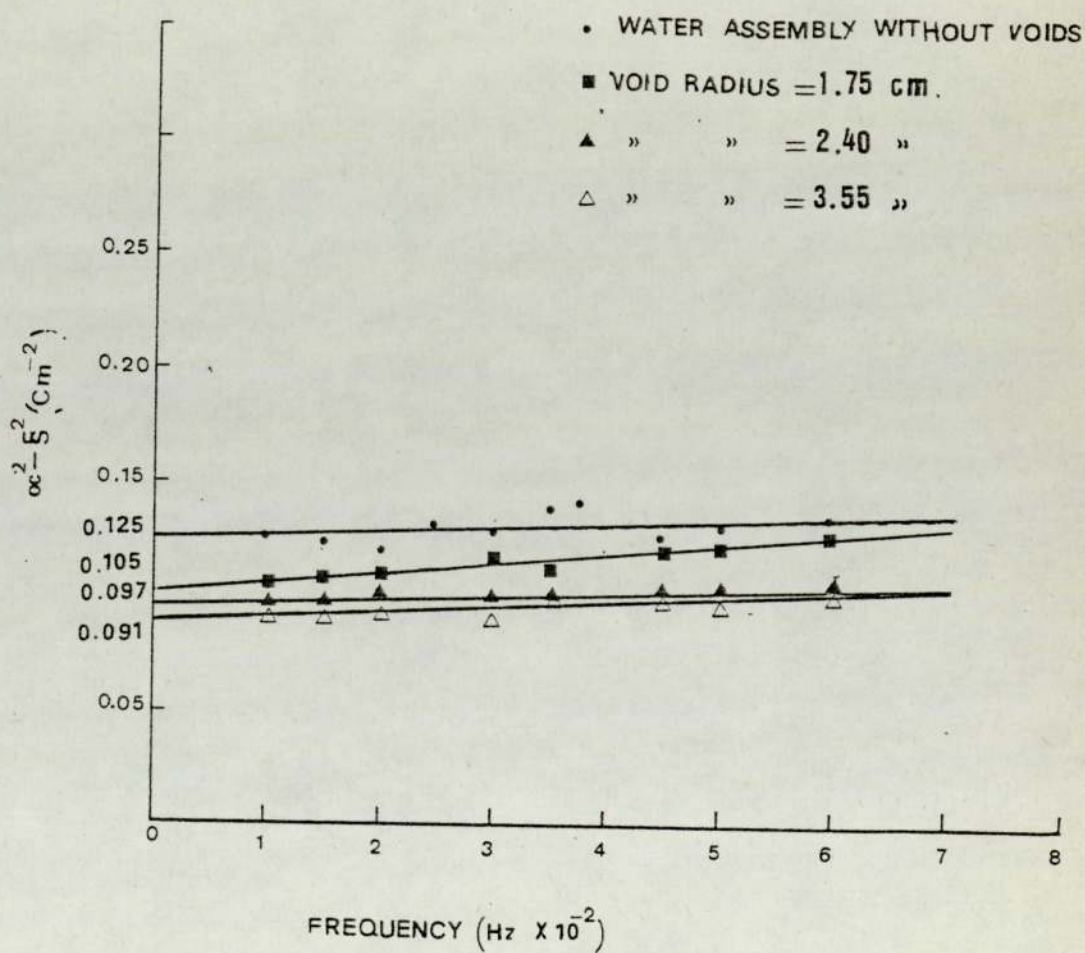


Fig.5.20. Comparison between the variation of $(\alpha^2 - S^2)$ with frequency for water and water-void assemblies.

of the axial diffusion area (L_z^2) for each assembly as the reciprocal of the zero-frequency intercept on ($\alpha_\omega^2 - \xi_\omega^2$) axis according to Eq. (5.32). Hence, the axial streaming factor can be found as:

$$S_z = \frac{(L_z^v)^2}{(L_z^m)^2} \dots\dots\dots 5.34$$

where, (L_z^v) is the axial diffusion area of the water-void assembly and (L_z^m)² is the axial diffusion area of the water assembly without voids.

Figure 5.21 shows that the values of ($\alpha_\omega^2 - \xi_\omega^2$) become frequency dependent for frequencies larger than 600 Hz. It can be seen from Figure 5.21 that by the introduction of voids into a moderating assembly, the values of ($\alpha_\omega^2 - \xi_\omega^2$) become less sensitive to frequency and this sensitivity drops further by increasing the void size. Figure 5.21 provides a mean of evaluating the frequency dependent axial streaming factor, (S_z^ω), which can be defined for a given frequency (F) as:

$$(S_z^\omega)_F = \frac{(L_z^v)^2}{(L_z^m)^2} = \frac{(\alpha_\omega^2 - \xi_\omega^2)_F}{(\alpha_\omega^2 - \xi_\omega^2)_F} \dots\dots\dots 5.35$$

The numerical values of ($\alpha_\omega^2 - \xi_\omega^2$) for water and water-void assemblies and the associated values of (S_z^ω) for certain frequencies are listed in Table 5.6. These values are drawn in Figure 5.22, which shows the variation of the axial streaming factor with source frequency. Figure 5.22 indicates that by increasing the frequency of modulation beyond certain value, the axial streaming increases significantly with the frequency. Hence, the increase in the source frequency is equivalent to an increase in the void dimension.

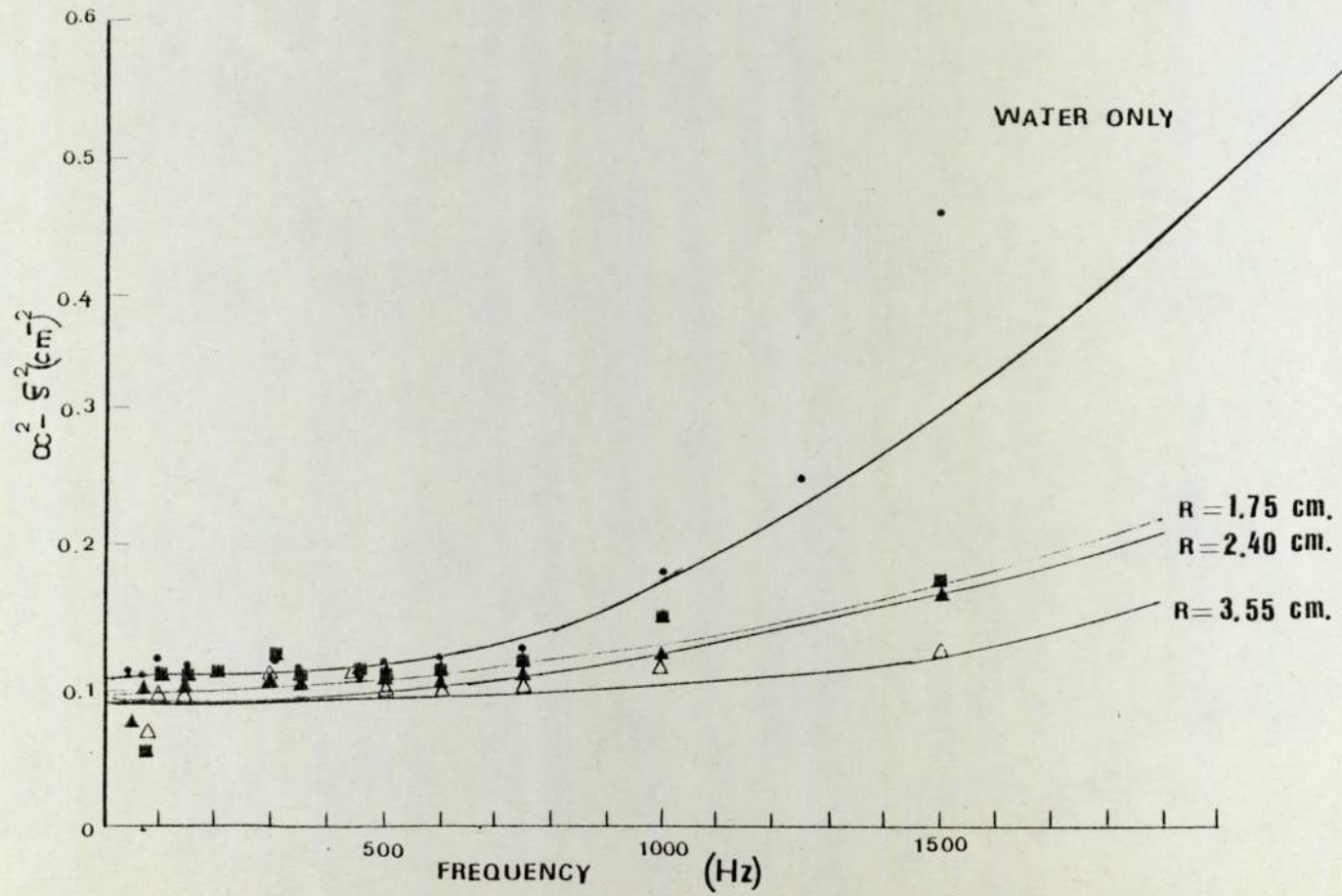


Fig. 5.21. The effect of void channel radius (R) on the $(cc^{-2} S^2)$ variation with frequency.

Table 5.6

Frequency dependent axial streaming factor (S_z^W)
for several water-void assemblies

Frequency (Hz)	Water assembly without voids $(\alpha^2 - \beta^2)$ cm^{-2}	water-void assemblies					
		R=1.75 cm.		R=2.40 cm.		R=3.55 cm.	
		$(\alpha^2 - \beta^2)$ cm^{-2}	(S_z^W)	$(\alpha^2 - \beta^2)$ cm^{-2}	(S_z^W)	$(\alpha^2 - \beta^2)$ cm^{-2}	(S_z^W)
0	0.125	0.105	1.190	0.097	1.288	0.091	1.373
100	0.126	0.106	1.192	0.098	1.295	0.092	1.380
300	0.126	0.106	1.196	0.098	1.296	0.093	1.376
500	0.128	0.107	1.195	0.099	1.292	0.093	1.380
700	0.136	0.114	1.192	0.104	1.307	0.098	1.387
1000	0.130	0.136	1.323	0.128	1.406	0.104	1.730
1200	0.220	0.148	1.436	0.144	1.527	0.108	2.037
1500	0.304	0.176	1.727	0.168	1.809	0.120	2.533

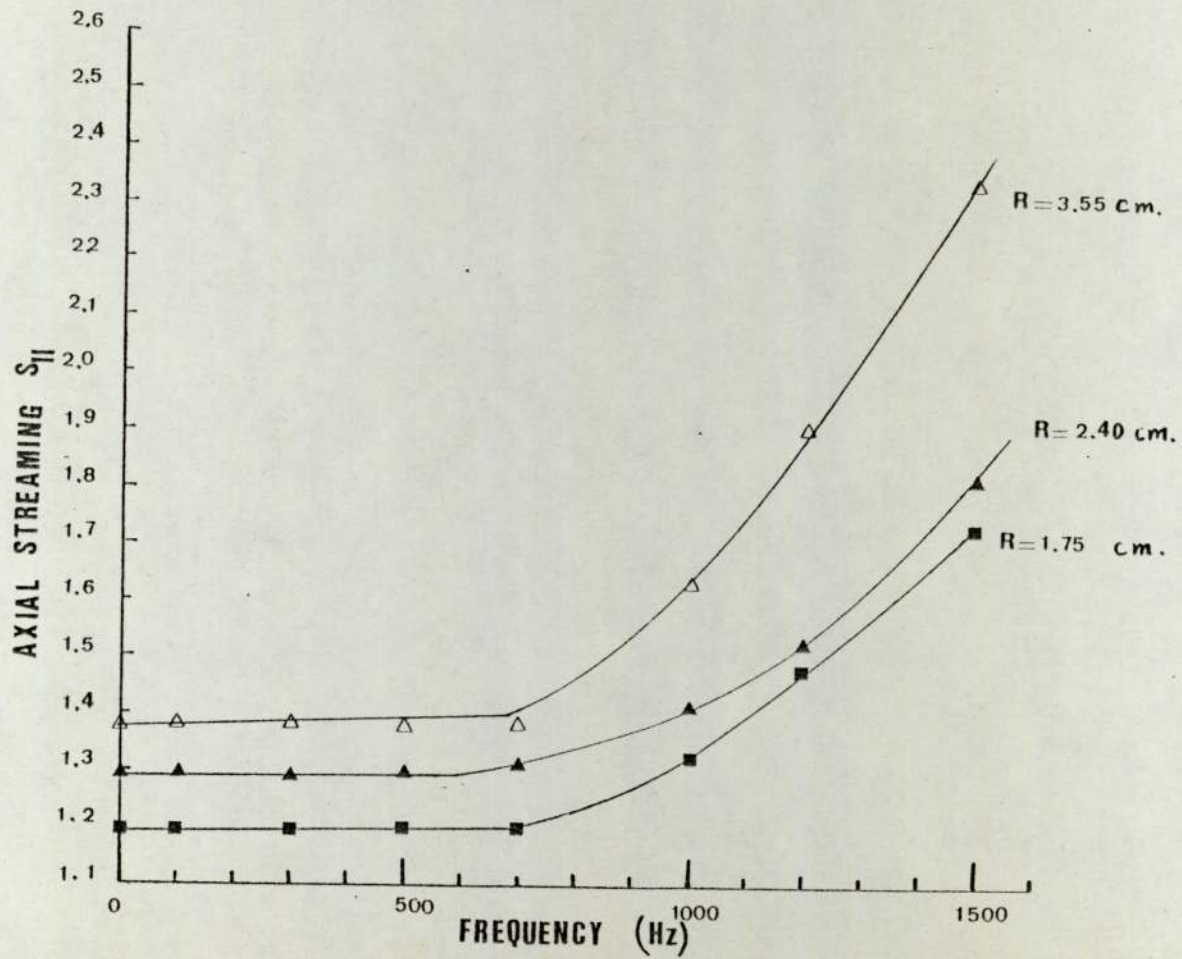


Fig. 5.22. Variation of axial streaming with frequency for several void radius.

CHAPTER SIX

THEORETICAL MODELS FOR CALCULATION OF NEUTRON WAVE PARAMETERS

The methods used to calculate the thermal neutron wave parameters for the different moderator assemblies are presented in this chapter. A one group time-dependent diffusion model for neutron wave propagation is developed, followed by a P_1 -approximation based on the solution of the Telegrapher's equation. A thermalisation model is developed to account for neutrons with a non-Maxwellian energy spectrum. The dispersion law for each model is derived to provide an accurate prediction of the wave parameter dependence on space and frequency, and to facilitate the comparison with the experimental observations. Finally, a set of parameters are derived to quantify the effects on the neutron wave parameters of voids in the moderator and the streaming of thermal neutrons along the vertical axis of the assembly.

6.1 Fundamental concepts of neutron wave calculations

The characteristics of a thermal neutron wave propagating in non-multiplying system were referred to in sections 1.3, 5.3 and 5.4. This analysis considers a parallelepiped moderator with a periodic plane thermal neutron source at the lower face of the parallelepiped, ($Z=0$). The source intensity, $S_{(z,t)}$, can be represented by a steady component, $S_{o(z)}$, and the real part of the oscillatory component, $S_{(z)} \cdot e^{j\omega t}$, i.e.

$$S_{(z,t)} = S_{o(z)} + \text{Re} \left[S_{(z)} \cdot e^{j\omega t} \right] \dots\dots\dots 6.1$$

where 'Re' refers to the real part of the complex number written as its argument, and $S_{(z)}$ is a complex amplitude.

PEREZ and UHRIG (1968) indicated that a quasi-static flux, $\phi_{(z,t)}$, will be introduced into the system and will comprise a time-independent component, $\phi_{o(z)}$, due to the steady source, and a propagating disturbance created by the real part of the source modulation, $\phi_{(z)} \cdot e^{j\omega t}$, i.e.

$$\phi_{(z,t)} = \phi_{o(z)} + \text{Re} \left[\phi_{(z)} \cdot e^{j\omega t} \right] \dots\dots\dots 6.2$$

where $\phi_{(z)}$ is a complex amplitude.

The neutron density near the source will oscillate in-phase with the source. These forced oscillations are produced by the collective behaviour of neutrons which, at the same time interact with the medium and travel with a finite velocity. Thus for regions far from the source, there is a delay in the oscillation. MOORE (1966) showed that because of the space-dependent phase, the disturbance possesses wave-like properties and can be described as a damped thermal neutron wave. HETRICK (1971) showed that an attenuated plane neutron wave travelling in the positive Z-direction can be represented as:

$$\phi_{(z,t)} = A_o e^{-\alpha_{(\omega)} Z} \cdot e^{j(\omega t - \xi_{(\omega)} Z)} \dots\dots\dots 6.3$$

where A_o is a constant and $(\alpha_{(\omega)})$ and $(\xi_{(\omega)})$ are the frequency dependent attenuation and the rate of change of the phase angle of the wave at a certain distance along Z-axis.

By defining a complex quantity (ρ_{ω}) as:

$$\left. \begin{aligned} \rho_{(\omega)} &= \alpha_{(\omega)} + j \xi_{(\omega)} \\ \text{or: } \rho_{(\omega)}^2 &= \alpha_{(\omega)}^2 - \xi_{(\omega)}^2 + j 2\alpha_{(\omega)} \xi_{(\omega)} \end{aligned} \right\} \dots\dots\dots 6.4$$

then, Eq. (6.3) can be written as:

$$\phi(z,t) = A_0 \cdot e^{j\omega t} \cdot e^{-\rho z} \dots\dots\dots 6.5$$

It is evident from Eq. (6.5) that (ρ) is the complex inverse relaxation length of the wave.

The time-dependent one group neutron diffusion equation at a point (x,y,z) in a non-multiplying medium can be written as:

$$D_0 \nabla^2 \phi(x,y,z,t) - \sum_a \phi(x,y,z,t) = \frac{1}{v} \frac{d\phi(x,y,z,t)}{dt} \dots\dots 6.6$$

where D_0 is the thermal diffusion constant, and \sum_a is the macroscopic absorption cross section. Both D_0 and \sum_a are averaged over a Maxwellian energy spectrum.

It has been shown in Section 5.4, that by substituting Eq. (6.5) into Eq. (6.6), the squared inverse relaxation length (ρ^2) of the wave can be expressed in terms of diffusion and thermalisation parameters of the non-multiplying medium as in Eqs. (5.32) and (5.33).

Plots of ($\alpha(\omega)$) versus ($\xi(\omega)$) and ($\alpha(\omega)^2 - \xi(\omega)^2$) versus ($2\alpha(\omega) \cdot \xi(\omega)$) are often referred to as the (ρ) and (ρ^2) dispersion laws. These will be derived independently for any theoretical models in the following sections.

6.2 The methods of calculation of neutron wave parameters

The theoretical models developed to calculate the thermal neutron wave parameters ($\alpha(\omega)$) and ($\xi(\omega)$) are presented in this section. A parallelepiped-shaped moderator with a plane, thermal neutron source at the lower face is assumed.

6.2.1 One group diffusion model

The laplacian operator, (∇^2), used in Eq. (6.6) can be written as:

$$\nabla^2 = \frac{\partial^2}{\partial x^2} + \frac{\partial^2}{\partial y^2} + \frac{\partial^2}{\partial z^2} = \nabla^2_{(x,y)} + \nabla^2_{(z)} \dots\dots\dots 6.7$$

If:

$$\phi_{(x,y,z,t)} = \phi_{(x,y)}\phi_{(z,t)} \dots\dots\dots 6.8$$

then Eq. (6.6) can be written as:

$$\begin{aligned} & \phi_{(z,t)} D_0 \nabla^2_{(x,y)} \phi_{(x,y)} + \phi_{(x,y)} D_0 \nabla^2_{(z)} \phi_{(z,t)} \\ & - \sum_a \phi_{(x,y)} \phi_{(z,t)} = \phi_{(x,y)} \frac{1}{v} \frac{\partial \phi_{(z,t)}}{\partial t} \dots\dots\dots 6.9 \end{aligned}$$

LAMARSH (1967) indicated that it is possible to solve such an equation by an eigenfunction method, in which the solution can be found in terms of solutions to another differential equation;

$$\nabla^2 \phi + B^2 \phi = 0 \dots\dots\dots 6.10$$

where B^2 is a constant and the function ϕ satisfies the same initial and boundary conditions as in Eq. (6.9). The fundamental eigenvalue B^2 known in reactor physics as the geometrical buckling. For a parallelepiped moderator it can be written as:

$$B^2 = B_{||}^2 + B_{\perp}^2 \dots\dots\dots 6.11$$

where the (||) and (\perp) suffixes indicate parallel and the normal direction to the neutron motion. Eq. (6.10) can be separated into two equations by using Eq. (6.7) and Eq. (6.11), such that:

$$-\nabla^2_{(x,y)} \phi_{(x,y)} = B_{\perp}^2 \phi_{(x,y)} \dots\dots\dots 6.12$$

$$-\nabla^2_{(z)} \phi_{(z,t)} = B_{||}^2 \phi_{(z,t)} \dots\dots\dots 6.13$$

Substituting Eqs. (6.12) and (6.13) into Eq. (6.9), then:

$$D_0 \nabla^2 \phi_{(z,t)} - (D_0 B_1^2 + \sum_a) \phi_{(z,t)} = \frac{1}{v} \frac{\partial \phi_{(z,t)}}{\partial t} \dots\dots\dots 6.14$$

Eq. (6.14) is a one-dimension diffusion equation which accounts for the change in the transverse buckling, a feature which is very desirable in this work and especially in void calculations. Eq. (6.14) is a parabolic differential equation which does not have a true wave solution, (UHRIG (1967)). A familiar technique to obtain a wave-like solution is to introduce a complex source term, as reported by COHN (1966). The Complex Source Method, (CSM), is based on the transformation of the time-dependent equation into a set of complex equations dependent on space and frequency, but not on time. CSM has been tested by many workers, BRIDGES (1972) showed that the CSM predicts accurate results in studying space-independent phenomena, e.g. reactivity of multiplying system and systems in which a secondary source of neutron exists. GIL-RAMOS (1974) applied a multigroup version of CSM and showed that CSM predicts with good accuracy the core region of a subcritical system. However, the CSM leads to a complicated analysis which involves long computation time.

Substituting Eq. (6.5) into Eq. (6.14) yields:

$$\rho^2 = \left(B_1^2 + \frac{\sum_a}{D_0} + j \frac{\omega}{v D_0} \right) \dots\dots\dots 6.15$$

By comparing Eq. (6.15) with the squared of Eq. (6.4), the two wave parameters can be related to the system parameters as:

$$\alpha_{(\omega)}^2 - \xi_{(\omega)}^2 = B_1^2 + \frac{\sum_a}{D_0} \dots\dots\dots 6.16$$

and:

$$2\alpha_{(\omega)} \xi_{(\omega)} = \frac{\omega}{v D_0} \dots\dots\dots 6.17$$

Using the general result that:

$$\sqrt{\beta + j\gamma} = \frac{1}{\sqrt{2}} \sqrt{\sqrt{\beta^2 + \gamma^2} + \beta} + \frac{j}{\sqrt{2}} \sqrt{\sqrt{\beta^2 + \gamma^2} - \beta}$$

and by defining :

$$\beta = B_1^2 + \frac{\sum a}{D_0} \quad \text{and} \quad \gamma = \frac{\omega}{v D_0}$$

Therefore:

$$\alpha(\omega) = \frac{1}{\sqrt{2}} \left[\left\{ \left(B_1^2 + \frac{\sum e}{D_0} \right)^2 + \left(\frac{\omega^2}{v D_0} \right)^2 \right\}^{\frac{1}{2}} + \left(B_1^2 + \frac{\sum e}{D_0} \right) \right]^{\frac{1}{2}} \dots\dots\dots 6.18$$

$$\xi(\omega) = \frac{1}{\sqrt{2}} \left[\left\{ \left(B_1^2 + \frac{\sum e}{D_0} \right)^2 + \left(\frac{\omega^2}{v D_0} \right)^2 \right\}^{\frac{1}{2}} - \left(B_1^2 + \frac{\sum e}{D_0} \right) \right]^{\frac{1}{2}} \dots\dots\dots 6.19$$

From Eq. (6.18) and (6.19), $\alpha(\omega)$ and $\xi(\omega)$ can be calculated from the knowledge of the system parameters and the source frequency.

This method was first used by UHRIG (1965) to calculate the system transfer function using isotropic point source conditions, and later by MILES (1974) to calculate the dispersion laws for berellyium at frequencies below 1000 Hz. The method is extended

in this work to calculate the wave parameters of a thermal neutron wave propagating in the positive Z-direction with plane source conditions, and as a theoretical base for sections 6.3.2 and 6.3.3 following.

6.2.2 The one group p_1 -approximation model

The equation which described the time behaviour of neutron populations in energy-phase-space parameters is called Boltzmann's Transport Equation, (BTE). The diffusion equation is a simplified version of BTE which can be used satisfactorily to describe neutron transport in a system under certain conditions. These conditions include the assumption that the flux is isotropic and does not change rapidly with position, the neglect of absorption cross section in comparison to the scattering cross section, and the avoidance of flux calculations of the system boundaries and near to the source.

The use of a diffusion approximation in the treatment of an external wave-like neutron disturbance introduced into system predicts that the disturbance travels instantaneously in all directions with an infinite velocity, i.e. no initial wave-front expected. Therefore, the use of a more refined theory which will predict the wave properties of a disturbance is essential in NWT treatment.

Another simplified version of BTE is by the well-known P_1 -approximation in which the angular distribution of flux is expanded in Legendre polynomials restricted to the first two terms of the expansion, as detailed by WEINBERG and WIGNER (1958). The propagation of mon-energetic neutrons through a system is considered by averaging the energy dependent parameters over a Maxwellian spectrum, which leads to the familiar Telegrapher's equation:

$$\frac{3D_0}{v^2} \frac{\partial^2 \phi}{\partial t^2}(x,y,z,t) + \frac{1}{v} (1 + 3D_0 \sum_a) \frac{\partial \phi}{\partial t}(x,y,z,t)$$

$$D_0 \nabla^2 \phi(x,y,z,t) - \sum \phi(x,y,z,t) \dots\dots\dots 6.20$$

A one-dimensional Telegrapher's equation can be determined for a rectangular moderator with source symmetry along the Z-axis by using the approach detailed in Eqs. (6.9) to (6.14);

$$\frac{3D_0}{v^2} \frac{\partial^2 \phi(z,t)}{\partial t^2} + \frac{(1 + 3D_0 \sum_a)}{v} \frac{\partial \phi(z,t)}{\partial t} =$$

$$D_0 \nabla_z^2 \phi(z,t) - (D_0 B_1^2 + \sum_a) \phi(z,t) \dots\dots\dots 6.21$$

WEINBERG and WIGNER (1958) have indicated that the solution of Eq. (6.21) shows a phenomenon of retardation, i.e. the solution has a well-defined wave front in addition to a residual disturbance. Thus the solution of Eq. (6.21) must represent a damped wave travelling with finite velocity as:

$$\phi(z,t) = A_0 e^{j\omega t - \rho z} \dots\dots\dots 6.22$$

Introducing Eq. (6.22) into Eq. (6.21) yields:

$$\rho^2 = \left[(B_1^2 + \frac{\sum_a}{D_0} - \frac{3\omega^2}{v^2}) + \frac{j\omega}{vD_0} (1 + 3D_0 \sum_a) \right] \dots\dots 6.23$$

By comparing Eq. (6.23) with Eq. (6.4) and using the same method as in the previous section, the wave parameters as a function of frequency and system constant can be given as:

$$\alpha_{(\omega)} = \frac{1}{\sqrt{2}} \left[\left\{ \left(B_1^2 + \frac{\Sigma_a}{D_0} - \frac{3\omega^2}{v^2} \right)^2 + \frac{\omega^2}{v^2 D_0^2} (1 + 3 D_0 \Sigma_a)^2 \right\}^{\frac{1}{2}} + \left(B_1^2 + \frac{\Sigma_a}{D_0} - \frac{3\omega^2}{v^2} \right) \right]^{\frac{1}{2}} \dots\dots\dots 6.24$$

$$\bar{F}_{(\omega)} = \frac{1}{\sqrt{2}} \left[\left\{ \left(B_1^2 + \frac{\Sigma_a}{D_0} - \frac{3\omega^2}{v^2} \right)^2 + \frac{\omega^2}{v^2 D_0^2} (1 + 3 D_0 \Sigma_a)^2 \right\}^{\frac{1}{2}} - \left(B_1^2 + \frac{\Sigma_a}{D_0} - \frac{3\omega^2}{v^2} \right) \right]^{\frac{1}{2}} \dots\dots\dots 6.25$$

6.2.3 The thermalisation theory model

In a non-multiplying system, the main processes experienced by the slowed-down neutrons are thermalisation and absorption. Recent work by RITCHIE and WHITTLESTONE (1973) and KOBAYASHA et al (1975) has indicated that the presence of a non-Maxwellian energy distribution affects the discrete mode of the propagation, i.e. the values of $\alpha_{(\omega)}$ and $\bar{F}_{(\omega)}$. Moreover, the presence of voids in the moderator requires a correction to the Maxwellian-averaged parameters as reported by WARNER and ERDMANN (1969). In present work, the effects of the energy distribution of the neutrons in a moderator will be taken into account by means of a thermalisation theory.

The diffusion approximation to the Boltzman equation, describing the neutron field in a rectangular moderator of

extrapolated dimensions a, b and c and having a plane source of thermal neutrons in the Z=0 plane, is given by WEINBERG and WIGNER (1958) as:

$$D_{0(E)} \nabla^2 \phi(x,y,z,E,t) - (\Sigma_a(E) + \Sigma_s(E)) \phi(x,y,z,E,t) + \int_E \Sigma_{s(E' \rightarrow E)} \phi(x,y,z,E,t) dE' = \frac{\partial \phi(x,y,z,E,t)}{\partial t} \quad \dots\dots 6.26$$

where, Σ_a is the Macroscopic absorption cross section of the medium,
 Σ_s is the macroscopic scattering cross section of the medium,
 $\Sigma_{s(E' \rightarrow E)}$ is the scattering kernel for a neutron of energy E' scattered into energy interval between E and E+dE.

Eq. (6.26) can be solved applying the following boundary conditions:

$$\phi(x=\frac{a}{2}, y, z, E, t) = \phi(x, y=\frac{b}{2}, z, E, t) = 0 \quad \dots\dots 6.27$$

$$- D_{0(E)} \left. \frac{d \phi(x,y,z,E,t)}{dz} \right|_{z=0} = \frac{1}{2} S(x,y,E,t) \quad \dots\dots 6.28$$

where S is the neutron source. A third boundary condition can be formulated by assuming that, if $c \gg \lambda_{tr}$, then:

$$\phi(x,y,z=c \rightarrow \infty, E, t) = 0 \quad \dots\dots 6.29$$

Following the method described in sections 6.2.1 and 6.2.2, Eq. (6.26) can be written in one dimension as:

$$D_{o(E)} \nabla^2 (z) \phi(z, E, t) - (\sum_{a(E)} + \sum_{s(E)} + D_{o(E)} B_{\perp}^2) \phi(z, E, t) + \int_E S(E' \rightarrow E) \phi(z, E, t) dE' = \frac{1}{v} \frac{\partial \phi(z, E, t)}{\partial t} \dots\dots\dots 6.30$$

where the integration is to be performed over all possible energy intervals into which the neutron might be scattered.

To generalise the treatment it is convenient to carry out the theoretical analysis in the frequency domain. The Fourier transform of the neutron field $\phi(z, E, \omega)$, and of the source $S(x, y, E, \omega)$, are defined as:

$$\phi(z, E, \omega) = \int_{-\infty}^{\infty} e^{-j\omega t} \phi(z, E, t) dt \dots\dots\dots 6.31$$

$$S(x, y, E, \omega) = \int_{-\infty}^{\infty} e^{-j\omega t} S(x, y, E, t) dt \dots\dots\dots 6.32$$

By using the relationship in Eq. (6.31), it can be shown that the Fourier transform of Eq. (6.30) can be written as:

$$D_{o(E)} \nabla^2 (z) \phi(z, E, \omega) - (\sum_{a(E)} + \sum_{s(E)} + D_{o(E)} B_{\perp}^2 + j \frac{\omega}{v}) \phi(z, E, \omega) + \int_E S(E' \rightarrow E) \phi(z, E, \omega) dE' = 0 \dots\dots\dots 6.33$$

Eq. (6.33) is an integro-differential equation which describes the neutron field in terms of space, energy and frequency. The convenient method to solve Eq. (6.33) is by the elimination of the integral term.

This was performed by PEREZ and BOOTH (1965), with a solution based on the symmetrisation of the scattering kernel, $\sum_{s(E' \rightarrow E)}$. It can be shown that, by following the method suggested by PEREZ and BOOTH, the solution of Eq. (6.33) for a discrete mode of the neutron wave can be expressed as:

$$\phi_{(z,E,\omega)} = A_0 \left(\frac{vM(E)}{D(E)} \right)^{\frac{1}{2}} e^{-\rho(\omega)z} \dots\dots\dots 6.34$$

where A_0 is a constant for the discrete mode of the wave,

$\rho(\omega)$ is the complex inverse relaxation length of the wave and

$M(E)$ is the neutron Maxwellian energy distribution which can be defined for $n(E')$ neutrons per unit volume per unit energy interval at the energy (E'). If n is the total number of thermal neutrons of energy (E) per unit volume, then:

$$M(E) = \frac{n(E')}{n(E)} = \frac{2}{\sqrt{\pi}} \frac{\sqrt{E'}}{(\sqrt{E})^3} e^{-E'/E} \dots\dots\dots 6.35$$

UHRIG (1965) derived an expression for the squared complex inverse relaxation length for the thermalisation model in terms of the source frequency and the system parameters as:

$$\rho(\omega)^2 = B_1^2 + \frac{\sqrt{\pi}}{2} \left\{ \frac{1}{L_T^2} \left[1 - \frac{\pi C}{4vD_0} \left(\frac{1}{L_T^2} + j\frac{\omega}{vD_0} \right) \right] + j \frac{\omega}{vD_0} \left[1 - j \frac{\pi \omega C}{4v^2 D_0^2} \right] \right\} \dots\dots\dots 6.36$$

where C is the diffusion cooling coefficient expressed in $\text{cm}^4 \text{s}^{-1}$ and L_T^2 is the thermal diffusion area in cm^2 . Eq.(6.36) can be separated into real and imaginary components and by comparing with Eq.(6.4):

Real:

$$\alpha_{(\omega)}^2 - \xi_{(\omega)}^2 = \left\{ B_1^2 + \frac{\sqrt{\pi}}{2L^2} \left[1 + \frac{\pi C}{4vD_0 L^2} \right] \right\} + \left[\frac{\sqrt{\pi}}{2vD_0} \right]^3 c\omega^2 \dots\dots 6.37$$

Imaginary:

$$2\alpha_{(\omega)} \xi_{(\omega)} = \frac{\sqrt{\pi}}{2vD_0} \left[1 - \frac{C}{4vD_0 L^2} \right] \omega \dots\dots 6.38$$

The expressions for $\alpha_{(\omega)}$ and $\xi_{(\omega)}$ in terms of the system parameters and the modulation frequency can be found by the same method expressed in sections 6.2.1 and 6.2.2, as:

$$\alpha_{(\omega)} = \frac{1}{\sqrt{2}} \left\{ \left[\left[B_1^2 + \frac{\sqrt{\pi}}{2L^2} \left\{ 1 + \frac{\pi C}{4vD_0 L^2} \right\} + \left\{ \frac{\sqrt{\pi}}{2vD_0} \right\}^3 c\omega^2 \right]^2 + \frac{\sqrt{\pi}}{2vD_0} \left\{ 1 - \frac{\pi C}{4vD_0 L^2} \right\} \omega \right]^{\frac{1}{2}} + \left[B_1^2 + \frac{\sqrt{\pi}}{2L^2} \left\{ 1 + \frac{\pi C}{4vD_0 L^2} \right\} + \left\{ \frac{\sqrt{\pi}}{2vD_0} \right\}^3 c\omega^2 \right]^{\frac{3}{2}} \right\} \dots\dots 6.39$$

and

$$\xi_{(\omega)} = \frac{1}{\sqrt{2}} \left\{ \left[\left[B_1^2 + \frac{\sqrt{\pi}}{2L^2} \left\{ 1 + \frac{\pi C}{4vD_0 L^2} \right\} + \left\{ \frac{\sqrt{\pi}}{2vD_0} \right\}^3 c\omega^2 \right]^2 + \frac{\sqrt{\pi}}{2vD_0} \left\{ 1 - \frac{\pi C}{4vD_0 L^2} \right\} \omega \right]^{\frac{1}{2}} - \left[B_1^2 + \frac{\sqrt{\pi}}{2L^2} \left\{ 1 + \frac{\pi C}{4vD_0 L^2} \right\} + \left\{ \frac{\sqrt{\pi}}{2vD_0} \right\}^3 c\omega^2 \right]^{\frac{3}{2}} \right\} \dots\dots 6.40$$

6.3 Evaluation of void effects on the neutron wave parameters

The space-time distribution of the thermal neutron flux in the moderator in neutron wave experiments has been expressed as:

$$\phi(z,t) = A_1 e^{-\rho z} .e^{j\omega t} \dots\dots\dots 6.41$$

where A_1 is a constant for the first discrete mode of the neutron wave travelling in the positive Z-direction.

In neutron pulse experiments, e.g. WAGNER (1970), the space-time distribution of the thermal neutron flux is given as:

$$\phi(z,t) = A_2 e^{jB_{||} z} .e^{-\lambda t} \dots\dots\dots 6.42$$

where A_2 is a constant for the first discrete mode of the neutron pulse travelling in the positive Z-direction, $B_{||}^2$ is the system axial buckling and λ is the pulse decay constant.

PEREZ and OHANIAN (1968) have shown that, in NWT, the squared complex inverse relaxation length (ρ^2) associated with a given discrete mode of the wave can be expressed in a power series in frequency as:

$$\rho^2 = \sum_{n=0}^N P_n(j\omega)^n \dots\dots\dots 6.43$$

In PST, e.g. BULL (1970), the decay constant (λ) associated with a given discrete mode of pulse propagation can be expressed in a power series in system buckling as:

$$\lambda = v \sum a + vD_0 B^2 - CB^4 + FB^6 + \dots\dots\dots 6.44$$

It was shown in Chapter One that both NWT and PST are theoretically equivalent. The analogy between NWT and PST was detailed analytically

by MICHAEL and MOORE (1968), they showed that the coefficients P_n in the frequency expansion in Eq. (6.43) can be written as a linear combination of the terms that appear as coefficients of the buckling in Eq. (6.44). Therefore, it is possible theoretically to express the thermal neutron flux measured in NWT, Eq. (6.41), with parameters measured in PST. Hence, by comparing Eqs. (6.41) and (6.42), the coupling relationships between the two methods can be expressed as:

$$\left. \begin{aligned} -\rho &= jB_{\parallel} \\ -\lambda &= j\omega \end{aligned} \right\} \dots\dots\dots 6.45$$

When a void is introduced into moderating medium, anisotropic diffusion is observed because there is streaming of neutrons along the void axis. This phenomena requires direction-dependent neutron transport parameters. In the present work, the k number of directions mentioned in Eq. (1.6) is reduced to two directions, i.e. (\parallel) and (\perp), designated the directions parallel and perpendicular to the void channel axis. Therefore, for an anisotropic medium, the first three terms of Eq. (6.44) can be written as:

$$\lambda = v \sum_a + vD_{\perp} B_{\perp}^2 + vD_{\parallel} B_{\parallel}^2 - C_{\perp} B_{\perp}^4 - C_{\parallel} B_{\parallel}^4 \dots\dots\dots 6.46$$

Introducing Eq. (6.45) into Eq. (6.46) results in:

$$-j\omega = v \sum_a + vD_{\perp} B_{\perp}^2 - vD_{\parallel} \rho^2 - C_{\perp} B_{\perp}^4 - C_{\parallel} \rho^4 \dots\dots\dots 6.47$$

Eq. (6.47) relates (ρ^2) to the direction-dependent diffusion and thermalisation parameters of the moderator in which the wave propagates. Thus, the wave parameters can be evaluated for each model as follows:

- i. For the diffusion model, Eq.(6.47) can be terminated at the third term, (i.e $C_{\parallel} = C_{\perp} = 0$), therefore:

$$\rho^2 = B_{\perp}^2 \frac{D_{o\perp}}{D_{o\parallel}} + \frac{\sum_a}{D_{o\parallel}} + j \frac{\omega}{v D_{o\parallel}} \dots\dots\dots 6.48$$

Therefore:

$$\alpha(\omega) = \frac{1}{\sqrt{2}} \left\{ \left[\left\{ B_{\perp}^2 \frac{D_{o\perp}}{D_{o\parallel}} + \frac{\sum_a^v}{D_{o\parallel}} \right\}^2 + \frac{\omega^2}{v^2 D_{o\parallel}^2} \right]^{\frac{1}{2}} + \left\{ B_{\perp}^2 \frac{D_{o\perp}}{D_{o\parallel}} + \frac{\sum_a^v}{D_{o\parallel}} \right\} \right\}^{\frac{1}{2}} \dots\dots\dots 6.49$$

$$\xi(\omega) = \frac{1}{\sqrt{2}} \left\{ \left[\left\{ B_{\perp}^2 \frac{D_{o\perp}}{D_{o\parallel}} + \frac{\sum_a^v}{D_{o\parallel}} \right\}^2 + \frac{\omega^2}{v^2 D_{o\parallel}^2} \right]^{\frac{1}{2}} - \left\{ B_{\perp}^2 \frac{D_{o\perp}}{D_{o\parallel}} + \frac{\sum_a^v}{D_{o\parallel}} \right\} \right\}^{\frac{1}{2}} \dots\dots\dots 6.50$$

ii. For the P-1 model:

$$\rho^2 = B_{\perp}^2 \frac{D_{o\perp}}{D_{o\parallel}} + \frac{\sum_a^v}{D_{o\parallel}} - \frac{3\omega^2}{v^2} + j \frac{\omega}{v D_{o\parallel}} (1 + 3 D_{o\parallel} \sum_a^v) \dots\dots\dots 6.51$$

The wave parameters are:

$$\alpha(\omega) = \frac{1}{\sqrt{2}} \left\{ \left[\left\{ B_{\perp}^2 \frac{D_{o\perp}}{D_{o\parallel}} + \frac{\sum_a^v}{D_{o\parallel}} - \frac{3\omega^2}{v^2} \right\}^2 + \frac{2}{v^2 D_{o\parallel}^2} \left\{ 1 + 3 D_{o\parallel} \sum_a^v \right\}^2 \right]^{\frac{1}{2}} + \left\{ B_{\perp}^2 \frac{D_{o\perp}}{D_{o\parallel}} + \frac{\sum_a^v}{D_{o\parallel}} - \frac{3\omega^2}{v^2} \right\} \right\}^{\frac{1}{2}} \dots\dots\dots 6.52$$

$$\xi(\omega) = \frac{1}{\sqrt{2}} \left\{ \left[\left[B_{\perp}^2 \frac{D_{o\perp}}{D_{o\parallel}} + \frac{\sum_a^v}{D_{o\parallel}} - \frac{3\omega^2}{v^2} \right]^2 + \frac{\omega^2}{v^2 D_{o\parallel}^2} \left\{ 1 + 3 D_{o\parallel} \sum_a^v \right\}^2 \right]^{\frac{1}{2}} - \left\{ B_{\perp}^2 \frac{D_{o\perp}}{D_{o\parallel}} + \frac{\sum_a^v}{D_{o\parallel}} - \frac{3\omega^2}{v^2} \right\} \right\} \dots\dots\dots 6.53$$

Eqs. (6.49 to (6.53) can be reduced to Eqs. (6.18), (6.19), (6.24) and (6.25) by putting, $D_o = D_o = D_{om}$, which is valid for homogeneous moderators.

iii. For thermalisation theory, the procedure followed to obtain an expression for (ρ^2) for anisotropic lattice with voids can be summarized as follows:

First, Eq. (6.47) can be rewritten as:

$$a \rho^4 + b \rho^2 + c = 0 \dots\dots\dots 6.54$$

where,

$$a = C_{\parallel}, b = v D_{o\parallel} \text{ and } c = C_{\perp} B_{\perp}^4 - v D_{o\perp} B_{\perp}^2 - v \sum_a^v - j\omega$$

Eq. (6.54) can be solved for the positive value of (ρ^2) as:

$$\rho^2 = \frac{-v D_{o\parallel}}{2C_{\parallel}} + \frac{1}{2C_{\parallel}} \sqrt{v^2 D_{o\parallel}^2 - 4C_{\parallel} (C_{\perp} B_{\perp}^4 - v D_{o\perp} B_{\perp}^2 - v \sum_a^v) - j(4C_{\parallel} \omega)} \dots\dots\dots 6.55$$

If:

$$x = v^2 D_{o\parallel}^2 - 4C_{\parallel} (C_{\perp} B_{\perp}^4 - v D_{o\perp} B_{\perp}^2 - v \sum_a^v) \dots\dots\dots 6.56$$

then:

$$\begin{aligned}
 x^2 = & (16 C_{\parallel}^2 C_{\perp}^2) E_{\perp}^8 - (32 C_{\parallel}^2 C_{\perp} v D_{o\perp}) E_{\perp}^6 \\
 & + (16 C_{\parallel}^2 v^2 D_{o\perp}^2 - 32 C_{\parallel}^2 C_{\perp} v \sum_a^v - 8 C_{\parallel} v^2 D_{o\parallel}^2 C_{\perp}) E_{\perp}^4 \\
 & + (32 C_{\parallel}^2 v^2 \sum_a^v D_{o\perp} + 8 C_{\parallel} v^3 D_{o\parallel}^2 D_{o\perp}) E_{\perp}^2 \\
 & + (16 C_{\parallel}^2 v^2 (\sum_a^v)^2 + v^4 D_{o\parallel}^4 + 8 C_{\parallel} v^3 D_{o\parallel}^2 \sum_a^v) \dots\dots 6.57
 \end{aligned}$$

If $y = 4C_{\parallel}\omega$ 6.58

then $y^2 = 16 C_{\parallel}^2 \omega^2$ 6.59

Therefore, by applying the relationship:

$$\sqrt{x + jy} = \frac{1}{\sqrt{2}} \sqrt{\sqrt{x^2 + y^2} + x} + \frac{j}{\sqrt{2}} \sqrt{\sqrt{x^2 + y^2} - x}$$

then the real and the imaginary parts of (ρ^2) can be written as:

$$\alpha_{(\omega)}^2 - \xi_{(\omega)}^2 = \frac{vD_{o\parallel}}{-2C_{\parallel}} + \frac{1}{2\sqrt{2} C_{\parallel}} \sqrt{\sqrt{x^2 + y^2} + x} \dots\dots\dots 6.60$$

and

$$2\alpha_{\omega} \xi_{(\omega)} = \frac{1}{2\sqrt{2} C_{\parallel}} \sqrt{\sqrt{x^2 + y^2} - x} \dots\dots\dots 6.61$$

If $K_{(E_0)}$ is the value of an energy-dependent nuclear parameter measured at the neutron most probable velocity, ($v_0 = 2200 \text{ m.s}^{-1}$), then the average value of that parameter over a Maxwellian energy distribution, $K_{(M)}$, can be evaluated

as:

$$K_{(M)} = \frac{\int K_{(E)} E e^{-\left(\frac{E}{E_0}\right)} dE}{\int E e^{-\left(\frac{E}{E_0}\right)} dE} = \frac{2}{\sqrt{\pi}} K_{(E_0)} \dots\dots\dots 6.62$$

where (E) is any possible energy the neutron can take.

Hence, each energy-dependent parameter in Eqs.(6.60) and (6.61) must be evaluated at neutron velocity of 2200 m.s^{-1} , by using Eq.(6.62). The wave parameters $(\alpha_{(\omega)}^v)$ and $(\xi_{(\omega)}^v)$ for thermal neutron wave in a moderator containing voids are taken

as:

$$\alpha_{(\omega)}^v = \frac{1}{\sqrt{2}} \left\{ \left[\left\{ \frac{\sqrt{\pi}}{4\sqrt{2} C_{||}} \sqrt{\sqrt{x_o^2 + y_o^2} + x_o} - \frac{\sqrt{\pi} v D_{o||}}{4C_{||}} \right\}^2 + \left\{ \frac{\sqrt{\pi}}{4\sqrt{2} C_{||}} \sqrt{\sqrt{x_o^2 + y_o^2} - x_o} \right\}^2 \right]^{\frac{1}{2}} + \left\{ \frac{\sqrt{\pi}}{4\sqrt{2} C_{||}} \sqrt{\sqrt{x_o^2 + y_o^2} + x_o} - \frac{v D_{o||}}{4C} \right\} \right]^{\frac{1}{2}} \dots\dots\dots 6.63$$

$$\xi_{(\omega)}^v = \frac{1}{\sqrt{2}} \left\{ \left[\left\{ \frac{\sqrt{\pi}}{4\sqrt{2} C_{||}} \sqrt{\sqrt{x_o^2 + y_o^2} + x_o} - \frac{\sqrt{\pi} v D_{o||}}{4C_{||}} \right\}^2 + \left\{ \frac{\sqrt{\pi}}{4\sqrt{2} C_{||}} \sqrt{\sqrt{x_o^2 + y_o^2} - x_o} \right\}^2 \right]^{\frac{1}{2}} - \left\{ \frac{1}{4} \frac{x_o^2 + y_o^2 + x_o}{2C} - \frac{v D_o}{4C} \right\} \right]^{\frac{1}{2}} \dots\dots\dots 6.64$$

where x_o and y_o are the values of x and y at $v = v_o = 2200 \text{ m.s}^{-1}$. Eqs.(6.63) and (6.64) can be reduced to Eqs.(6.39) and (6.40) for homogeneous moderator by putting:

$$C_{||} = C_{\perp} = C$$

$$D_{o||} = D_{o\perp} = D_{om}$$

and putting the values of B_{\perp}^{δ} and B_{\perp}^{δ} to zero.

6.4 The frequency dependence of anisotropy

It has been shown in Chapter One that a convenient way for the evaluation of the degree of anisotropy in a lattice is to introduce a correction factor to the diffusion area L^2 . The ratio $\frac{L_{||}^2}{L_m^2}$ in Eq. (1.1) and the ratio $\frac{L_{\perp}^2}{L_m^2}$ in Eq. (1.2) are a measure of the parallel and perpendicular anisotropy in a moderator containing voids. An alternative form for the anisotropy measurement is suggested by BENOIST (1968) as the ratio of the diffusion constants of the lattice with and without voids. BENOIST (1968) defined the diffusion constant for a moderating medium with void channels of a radius (r) as:

$$D_{om} = \frac{1}{3} (2D_{o\perp} + D_{o||}) \dots\dots\dots 6.65$$

provided that r is much greater than the transport mean free path λ_{tr} . By assuming that the macroscopic absorption cross section for a material with void, \sum_a^v , decreases with the void-material fraction, X, as:

$$\sum_a^v = \frac{\sum_a^m}{1 + X} \dots\dots\dots 6.66$$

BEHRENS (1954) reduced Eq. (1.1) to give an axial streaming factor, $S_{||}$, as:

$$S_{||} = \frac{D_{o||}}{D_{om}} = 1 + X + 2Q \left(\frac{r}{H \lambda_{tr}} \right) \dots\dots\dots 6.67$$

H is the effective void channel height, and Q is a geometrical factor equal to $\frac{4}{3}$ for a long circular cylinder.

6.4.1 Evaluation of anisotropy by diffusion theory

To investigate the anisotropy of a lattice in which the thermal

neutron flux is time dependent, as in neutron wave experiment, it is necessary to develop a theoretical model which relates the effect of the source frequency to the degree of anisotropy in the lattice with voids and to assess the effects of voids on the neutron wave parameters $\alpha_{(\omega)}$ and $\xi_{(\omega)}$; In the present work, this theoretical model has been developed by following a procedure which can be summarised as:

- i. the frequency dependent amplitude decay of a thermal neutron wave propagating in the axial direction of the void lattice, $\alpha_{(\omega)}^V$, was defined by Eq. (6.49) for diffusion theory model, by Eq. (6.52) for P-1 theory model and by Eq. (6.63) for thermalisation theory.
- ii. the frequency dependent amplitude decay of a thermal neutron wave propagating in the axial direction of a homogeneous moderator, $\alpha_{(\omega)}$, was defined by Eq. (6.18) for diffusion theory model, by Eq. (6.24) for P-1 theory model and by (6.39) for thermalisation theory.
- iii. from Eqs. (6.65) and (6.67):

$$\left. \begin{aligned} D_{o||} &= D_{om} \cdot S_{||} \\ \frac{D_o}{D_{o||}} &= \frac{1}{2} \left(\frac{3}{S_{||}} - 1 \right) \end{aligned} \right\} \dots\dots\dots 6.68$$

Then, by introducing Eqs. (6.66) and (6.68) into Eq. (6.49), it follows that:

$$\alpha_{\omega}^v = \frac{1}{\sqrt{2}} \left\{ \left[\left\{ B_{\perp}^2 \left(\frac{1}{2} \left(\frac{3}{S_{\parallel}} - 1 \right) \right) + \frac{\sum_a^m}{(1+X)(D_{om} \cdot S_{\parallel})} \right\}^2 + \frac{\omega^2}{v^2 D_{om}^2 S_{\parallel}^2} \right]^{\frac{1}{2}} + \left\{ B_{\perp}^2 \left(\frac{1}{2} \left(\frac{3}{S_{\parallel}} - 1 \right) \right) + \frac{\sum_a^m}{(1+X)(D_{om} \cdot S_{\parallel})} \right\}^{\frac{1}{2}} \right\} \dots\dots 6.69$$

iv. the frequency dependent amplitude streaming factor calculated by diffusion theory can be evaluated as:

$$\alpha_{\omega}^s = \frac{\alpha_{\omega}^v}{\alpha_{\omega}^e} = \frac{\text{Eq. (6.69)}}{\text{Eq. (6.18)}}$$

or:

$$\alpha_{\omega}^s = \left\{ \left[\left\{ B_{\perp}^2 \left(\frac{1}{2} \left(\frac{3}{S_{\parallel}} - 1 \right) \right) + \frac{\sum_a^m}{(1+X)(D_{om} \cdot S_{\parallel})} \right\}^2 + \frac{\omega^2}{v^2 D_{om}^2 S_{\parallel}^2} \right]^{\frac{1}{2}} + \left\{ B_{\perp}^2 \left(\frac{1}{2} \left(\frac{3}{S_{\parallel}} - 1 \right) \right) + \frac{\sum_a^m}{(1+X)(D_{om} \cdot S_{\parallel})} \right\}^{\frac{1}{2}} \right\} + \left\{ \left[\left[B_{\perp}^2 + \frac{\sum_a^m}{D_{om}} + \frac{\omega^2}{v^2 D_m^2} \right]^{\frac{1}{2}} + B_{\perp}^2 + \frac{\sum_a^m}{D_m} \right]^{\frac{1}{2}} \right\} \dots\dots 6.70$$

Similarly, ξ_{ω} , the frequency dependent phase lag of a thermal neutron wave propagating in the axial direction of the void lattice was defined by Eq. (6.50) for the diffusion theory model and can be written as:

$$\xi_{\omega}^v = \frac{1}{\sqrt{2}} \left\{ \left[\left\{ B_{\perp}^2 \left(\frac{1}{2} \left(\frac{3}{S_{\parallel}} - 1 \right) \right) + \frac{\sum_a^m}{(1+X)(D_{om} \cdot S_{\parallel})} \right\} + \frac{\omega^2}{v^2 D_{om}^2 \cdot S_{\parallel}^2} \right]^{\frac{1}{2}} - \left\{ B_{\perp}^2 \left(\frac{1}{2} \left(\frac{3}{S_{\parallel}} - 1 \right) \right) + \frac{\sum_a^m}{(1+X)(D_{om} \cdot S_{\parallel})} \right\}^{\frac{1}{2}} \right\} \dots\dots\dots 6.71$$

The phase lag of the thermal neutron wave propagating in a homogeneous moderator was defined by Eq.(6.19). Therefore, the frequency dependent phase lag streaming factor is defined as:

$$\xi_{\omega} \Big|_{\text{diff.}} = \frac{\xi_{\omega}^v}{\xi_{\omega}} = \frac{\text{Eq. (6.71)}}{\text{Eq. (6.19)}}$$

or:

$$\left\{ \left[\left\{ B_{\perp}^2 \left(\frac{1}{2} \left(\frac{3}{S_{\parallel}} - 1 \right) \right) + \frac{\sum_a^m}{(1+X)(D_{om} \cdot S_{\parallel})} \right\} + \frac{\omega^2}{v^2 D_{om}^2 \cdot S_{\parallel}^2} \right]^{\frac{1}{2}} - \left\{ B_{\perp}^2 \left(\frac{1}{2} \left(\frac{3}{S_{\parallel}} - 1 \right) \right) + \frac{\sum_a^m}{(1+X)(D_{om} \cdot S_{\parallel})} \right\}^{\frac{1}{2}} \right\}$$

$$\div \left\{ \left[\left\{ B_{\perp}^2 + \frac{\sum_a^m}{D_{om}} \right\}^2 + \frac{\omega^2}{v^2 D_{om}^2} \right]^{\frac{1}{2}} - \left\{ B^2 + \frac{a^m}{D_{om}} \right\}^{\frac{1}{2}} \right\} \dots\dots\dots 6.72$$

6.4.2 Evaluation of anisotropy by P-1 theory

To obtain expressions for the frequency dependent amplitude and phase streaming factors in P-1 theory, the procedure explained in

(i) - (iv) above is followed, resulting in the following expressions:

$$S_{\epsilon R} \Big|_{P-1} = \left\{ \left[\left\{ B_{\perp}^2 \left(\frac{1}{2} \left(\frac{3}{S_{\parallel}} - 1 \right) \right) + \frac{\sum_a^m}{(1+x)(D_{om} S_{\parallel})} - \frac{3\omega^2}{v^2} \right\}^2 + \frac{\omega^2}{v^2 D_{om}^2 S_{\parallel}^2} \left\{ 1 + 3D_{om} S_{\parallel} \frac{\sum_a^m}{(1+x)} \right\}^2 \right]^{\frac{1}{2}} + \left\{ B_{\perp}^2 \left(\frac{1}{2} \left(\frac{3}{S_{\parallel}} - 1 \right) \right) + \frac{\sum_a^m}{(1+x)(D_{om} S_{\parallel})} - \frac{3\omega^2}{v^2} \right\}^{\frac{1}{2}} \right\}$$

$$\div \left\{ \left[\left\{ B_{\perp}^2 + \frac{\sum_a^m}{D_{om}} - \frac{3\epsilon^2}{v^2} \right\}^2 + \frac{\omega^2}{v^2 D_{om}^2} \left\{ 1 + 3D_{om} \sum_a^m \right\}^2 \right]^{\frac{1}{2}} + \left\{ B_{\perp}^2 + \frac{\sum_a^m}{D_{om}} - \frac{3\epsilon^2}{v^2} \right\}^{\frac{1}{2}} \right\} \dots\dots\dots 6.73$$

Similarly:

$$S_{\epsilon S} \Big|_{P-1} = \left\{ \left[\left\{ B_{\perp}^2 \left(\frac{1}{2} \left(\frac{3}{S} - 1 \right) \right) + \frac{\sum_a^m}{(1+x)(D_{om} S_{\parallel})} - \frac{3\omega^2}{v^2} \right\}^2 + \dots \right]^{\frac{1}{2}} + \dots \right\}$$

$$\frac{\omega^2}{v^2 D_{om}^2 S_{||}^2} \left\{ 1 + 3D_{om} S_{||} \frac{\sum_a^m}{(1+x)} \right\}^2 \Bigg]^{-\frac{1}{2}} -$$

$$B_{\perp}^2 \left(\frac{1}{2} \left(\frac{3}{S_{||}} - 1 \right) + \frac{\sum_a^m}{(1+x)(D_{om} S_{||})} - \frac{3\omega^2}{v^2} \right) \Bigg]^{-\frac{1}{2}} \div$$

$$\left\{ \left[\left\{ B_{\perp}^2 + \frac{\sum_a^m}{D_{om}} - \frac{3\omega^2}{v^2} \right\} + \frac{\omega^2}{v^2 D_{om}^2} \left(1 + 3D_{om} \sum_a^m \right) \right]^2 \right\}^{-\frac{1}{2}} - \left\{ B_{\perp}^2 + \frac{\sum_a^m}{D_{om}} - \frac{3\omega^2}{v^2} \right\} \Bigg]^{-\frac{1}{2}}$$

..... 6.74

Eqs. (6.71) and (6.73) relate the frequency dependent streaming factor to the void dimensions, the nuclear parameters of the system and the modulation frequency. It can be seen from Eq. (6.67) that the value of $(S_{||})$ is always greater than unity and increases with the channel radius (r). Hence, it follows from Eqs. (6.71) and (6.73) that:

$$S_{\omega}^{\alpha} \Big|_{diff.} \quad \text{and} \quad S_{\omega}^{\alpha} \Big|_{P-1} < 1$$

$$\text{or,} \quad \alpha_{\omega}^v < \alpha_{\omega}^m ,$$

which indicates that the amplitude of the thermal neutron wave decays less rapidly over all frequencies. Eqs. (6.72) and (6.74) show that the presence of voids decreases the phase lag of the wave for all frequencies.

6.4.3 Evaluation of anisotropy by thermalisation theory

The direction dependence of the diffusion cooling coefficient, C, its relation to the system size and its relation to the diffusion coefficient, vD_o , were investigated by PUROHIT (1961). He suggested that for a large system, i.e. $(B_{||}^2)^2$ and $(B_{\perp}^2)^2$ are very small, and with a Maxwellian energy distribution, the relation between the diffusion cooling coefficients for a moderator with and without voids can be expressed as:

$$C_m = C_{||}^{\frac{1}{2}} C_{\perp}^{\frac{1}{2}} = C_{\perp} \frac{vD_{o||}}{vD_{o\perp}} \dots\dots\dots 6.75$$

Combining Eq. (6.75) with Eq. (6.68) yields:

$$\sqrt{\frac{C_{\perp}}{C_{||}}} = \frac{1}{2} \left(\frac{3}{S_{||}} - 1 \right) \dots\dots\dots 6.76$$

From Eq. (6.75):

$$\frac{C_m}{C_{\perp}} = \frac{vD_{o||}}{vD_{o\perp}} \dots\dots\dots 6.77$$

To evaluate the effect of voids on the neutron wave parameters and to evaluate the frequency dependent anisotropy, the procedure detailed in Section 6.3 is followed after substituting Eqs. (6.75), (6.76) and (6.77) in Eq. (6.57). Therefore Eq. (6.57) can be wrottem as:

$$\begin{aligned} x^2 = & (16C_m^4)B_{\perp}^8 \\ & - (32 C_m^3 vD_{o||})B_{\perp}^6 \\ & + (16 C_m^2 v^2 D_{o||}^2 - 32 C_m^3 vD_{o||} \frac{\sum_a^v}{D_{o\perp}} - 8C_m^2 v^2 D_{o||}^2)B_{\perp}^4 \\ & + (32 C_m^2 v^2 D_{o||}^2 \frac{\sum_a^v}{D_{o\perp}} + 8 C_m v^3 D_{o||}^3)B_{\perp}^2 \end{aligned}$$

$$+ (v_{D_{o11}}^4 + 16C_m^2 v_{D_{o11}}^2 v_{D_{o11}}^2) \frac{\sum_a^v}{D_{o11}^2} + 8 C_m v_{D_{o11}}^3 \frac{\sum_a^v}{D_{o11}} \dots\dots\dots 6.78$$

Similarly, Eq. (6.59) can be written as:

$$y^2 = 16 C_m^2 \omega^2 \frac{v_{D_{o11}}^2}{v_{D_{o11}}^2} = 16 C_m^2 \left(\frac{2S_{||}}{3 - S_{||}} \right)^2 \omega^2 \dots\dots\dots 6.79$$

It can be shown that by following the method detailed in Section 6.3 and using Eq. (6.66) and by defining the thermal diffusion area in a moderator containing void, (L_v^2) as:

$$L_{v||}^2 = \frac{D_{o11}}{\sum_a^v}, L_{v\perp}^2 = \frac{D_{o11}}{\sum_a^v} \text{ and } \frac{L_v^2}{L_m^2} = S_{||}$$

where \sum_a^v is related to the void fraction, X, by:

$$\sum_a^v = \frac{\sum_a^m}{1 + X}$$

then the wave parameters as a function of system nuclear parameters, source frequency and void dimensions can be written as:

$$\Omega_{\epsilon^v} = \frac{1}{\sqrt{2}} \left\{ \left[\left\{ A + B(1+C) + D \right\}^2 + E \right]^{\frac{1}{2}} + \left\{ A + B(1+C) + D \right\} \right\}^{\frac{1}{2}} \dots\dots\dots 6.80$$

and:

$$\nu_{\epsilon^v} = \frac{1}{\sqrt{2}} \left\{ \left[\left\{ A + B(1+C) + D \right\}^2 + E \right]^{\frac{1}{2}} - \left\{ A + B(1+C) + D \right\} \right\}^{\frac{1}{2}} \dots\dots\dots 6.80a$$

where:

$$A = E_{\perp}^2 \left\{ \frac{1}{2} \left(\frac{3}{S_{\parallel}} - 1 \right) \right\}$$

$$B = \frac{\sqrt{\pi} \sum_a^m}{(1+X)(D_{om} \cdot S_{\parallel})}$$

$$C = \left\{ 1 + \pi C_m \cdot \left(\frac{2S_{\parallel}}{3 - S_{\parallel}} \right) \right\}$$

$$D = \left(\frac{\sqrt{\pi}}{2vD_{om}S_{\parallel}} \right)^3 \cdot C_m \left(\frac{2S_{\parallel}}{3 - S_{\parallel}} \right) \omega^2$$

$$E = \left(\frac{\sqrt{\pi}}{2vD_{om}S_{\parallel}} \right) (1 - C) \omega$$

It can be shown that Eqs. (6.79) and (6.80) can be reduced to Eqs. (6.39) and (6.40) for a moderator without voids by putting:

$$D_{o\parallel} = D_{o\perp} = D_{om}$$

$$S_{\parallel} = S_{\perp} = 1$$

$$X = 0$$

$$L_{\parallel}^2 = L_{\perp}^2 = L_m^2 = \frac{D_{om}}{\sum_a^m}$$

The effect of the source modulation frequency on the streaming can be evaluated as in the previous sections as:

$$\left. S_{\omega}^x \right]_{\text{Thermalisation}} = \frac{\alpha_{\omega}^v}{\alpha_{\omega}^m} = \frac{\text{Eq. (6.79)}}{\text{Eq. (6.39)}} \dots\dots\dots 6.81$$

$$\left. S_{\omega}^{\xi} \right]_{\text{Thermalisation}} = \frac{\xi_{\omega}^v}{\xi_{\omega}^m} = \frac{\text{Eq. (6.80)}}{\text{Eq. (6.40)}} \dots\dots\dots 6.82$$

CHAPTER SEVEN

THE VALIDITY OF THE THEORETICAL MODELS

The theoretical models, which were detailed in the previous chapter, are compared to each other in this chapter. The results obtained by each model are compared with those obtained in the experimental measurements to establish the validity of the model. This procedure is applied to the experiments with the water moderator without voids and several water-void assemblies. The discrepancy between the theoretical results and the experimental observations is discussed with reference to the physical characteristics of each assembly and the frequency of modulation. Finally, an attempt to explore the possibility of thermal neutron wave interference has been made by examining the dispersion relation of each assembly under investigation.

7.1 Comparison between theoretical models

The calculations of thermal neutron wave parameters, i.e. $\alpha(\omega)$ and $\xi(\omega)$ for a neutron wave propagating in the axial direction of a water assembly without voids, are presented in this section. The calculations are performed using the formula which relate the wave parameters to the nuclear characteristics of the assembly and the modulation frequency. A comparison between the numerical results is given.

7.1.1 Calculations for water assembly without voids (computer programme WAVE)

The wave parameters were calculated by means of a computer code WAVE. This programme is written in FORTRAN to perform the calculation

of $\alpha(\omega)$ and $\bar{f}(\omega)$ from Eqs. (6.18) and (6.19) for the diffusion theory model, Eqs. (6.24) and (6.25) for the P-1 approximation model and Eqs. (6.39) and (6.40) for the thermalisation theory model. The calculations were performed over a range of modulation frequency of 0 - 10000 Hz, in steps of 50 Hz. The diffusion and thermalisation parameters used in the calculations are listed in Table 7.1. The code WAVE evaluates the wave functions $2 \frac{\bar{f}(\omega)}{\alpha(\omega)}$ and $\alpha(\omega) - \bar{f}(\omega)^2$ for each model and provides the numerical values of the function $G(\omega)$, which is defined as:

$$G(\omega) = \frac{\text{The wave amplitude at frequency } = \omega}{\text{The amplitude at frequency } = 0} \dots\dots\dots 7.1$$

The values of $G(\omega)$ were taken as a measure of the amplitude damping with modulation frequency. A listing of the programme WAVE and a sample of the output data is provided in Appendix II.

Table 7.1

Diffusion and thermalisation parameters of water corrected to 22°C

Transverse buckling B_I^2	0.002087 cm ⁻²	
Axial buckling B_{II}^2	0.001483 cm ⁻²	
Thermal neutron velocity v	220500 cm s ⁻¹	
Diffusion constant D_0	0.1593 cm	LAMARSH (1967)
Absorption cross section Σ_a	0.01913 cm ⁻¹	KANEKO (1974)
Maxwellian averaged $\bar{\Sigma}_a$	0.0221 cm ⁻¹	WARNER (1969)
Scattering cross section Σ_s	2.3551 cm ⁻¹	KANEKO (1974)
Maxwellian averaged $\bar{\Sigma}_s$	2.6715 cm ⁻¹	WARNER (1969)
Thermal diffusion area L^2	8.245 cm ²	LAMARSH (1967)
Diffusion cooling coefficient C	3380 cm ⁴ s ⁻¹	PAINO (1968)

7.1.2 Comparison of theoretical results

The numerical values of the amplitude decay function, $G(\omega)$, evaluated by different theoretical models, are plotted against the modulation frequency in Figure 7.1. Both the diffusion and the P-1 approximation models, (denoted by D and P-1), predicted no effective amplitude decay of the thermal neutron wave in water up to modulation frequencies of 200 Hz. Beyond this frequency, the amplitude decay becomes more noticeable but both models predicted the same results up to 600 Hz. At larger frequencies, the transport effects associated with the P-1 model tend to minimise the amplitude decay.

The thermalisation theory results (denoted by T in Figure 7.1), are more sensitive to the modulation frequency. A noticeable amplitude decay appears at frequencies as low as 20 Hz. The amplitude decreases more rapidly with frequency than the diffusion or the P-1 models. It can be concluded from Figure 7.1 that the correction to the diffusion theory introduced by thermalisation theory (i.e. due to the non-Maxwellian energy distribution) is much more important than transport effects correction introduced into the diffusion model.

The analytical interpretation of the theoretical models can be presented by plotting the real and the imaginary parts of the squared complex inverse relaxation length, (ρ^2) , i.e. $(\alpha_\omega^2 - \xi_\omega^2)$ and $2\alpha_\omega \xi_\omega$, versus modulation frequency. These plots are presented in Figures 7.2. and 7.3. In Figure 7.2 the zero frequency intercept on $(\alpha_\omega^2 - \xi_\omega^2)$ axis has the following values:

$$A_1 = B_1^2 + \frac{\sum a}{D_0} \quad \text{for diffusion theory, and}$$

$$A_1 = B_1^2 + \frac{\sum a}{D_0} - \frac{3\omega^2}{v^2} \quad \text{for P-1 approximation theory.}$$

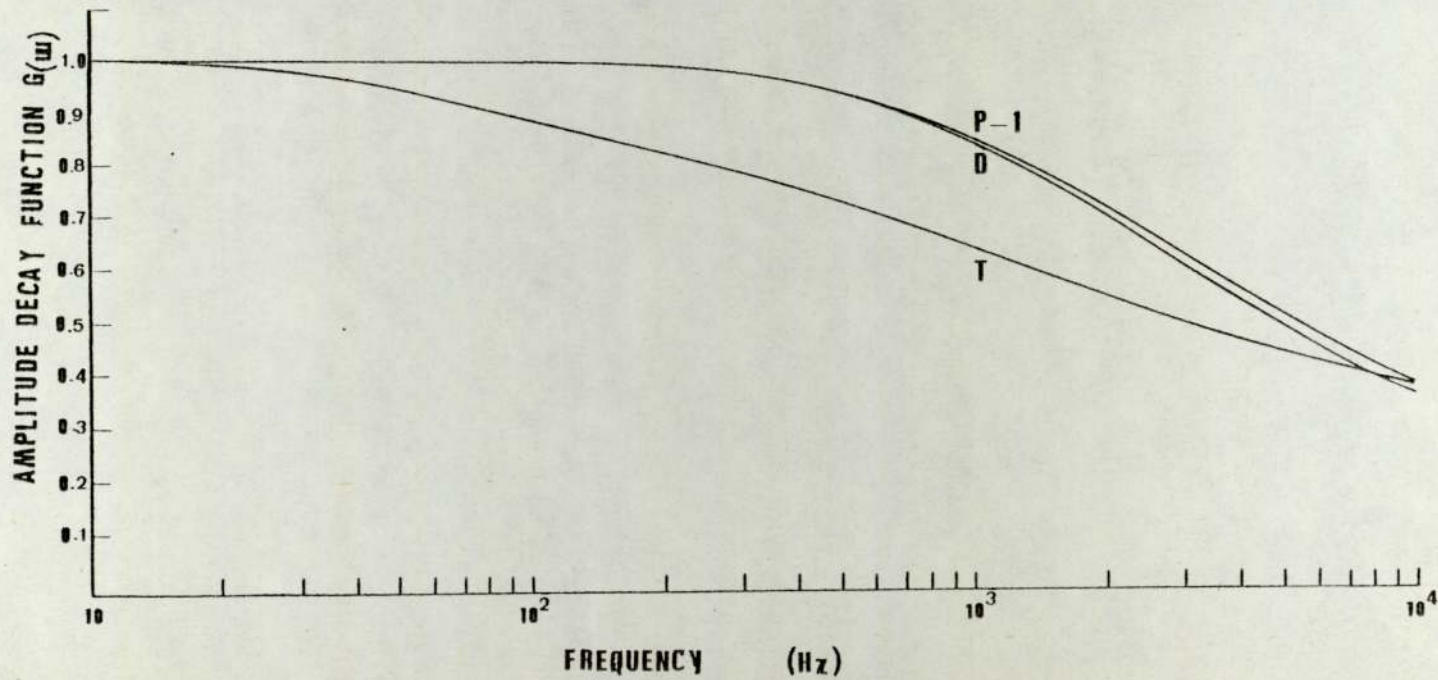


Fig. 7.1. COMPUTATION OF AMPLITUDE DECAY BY DIFFERENT THEORETICAL MODELS FOR WATER WITHOUT VOIDS

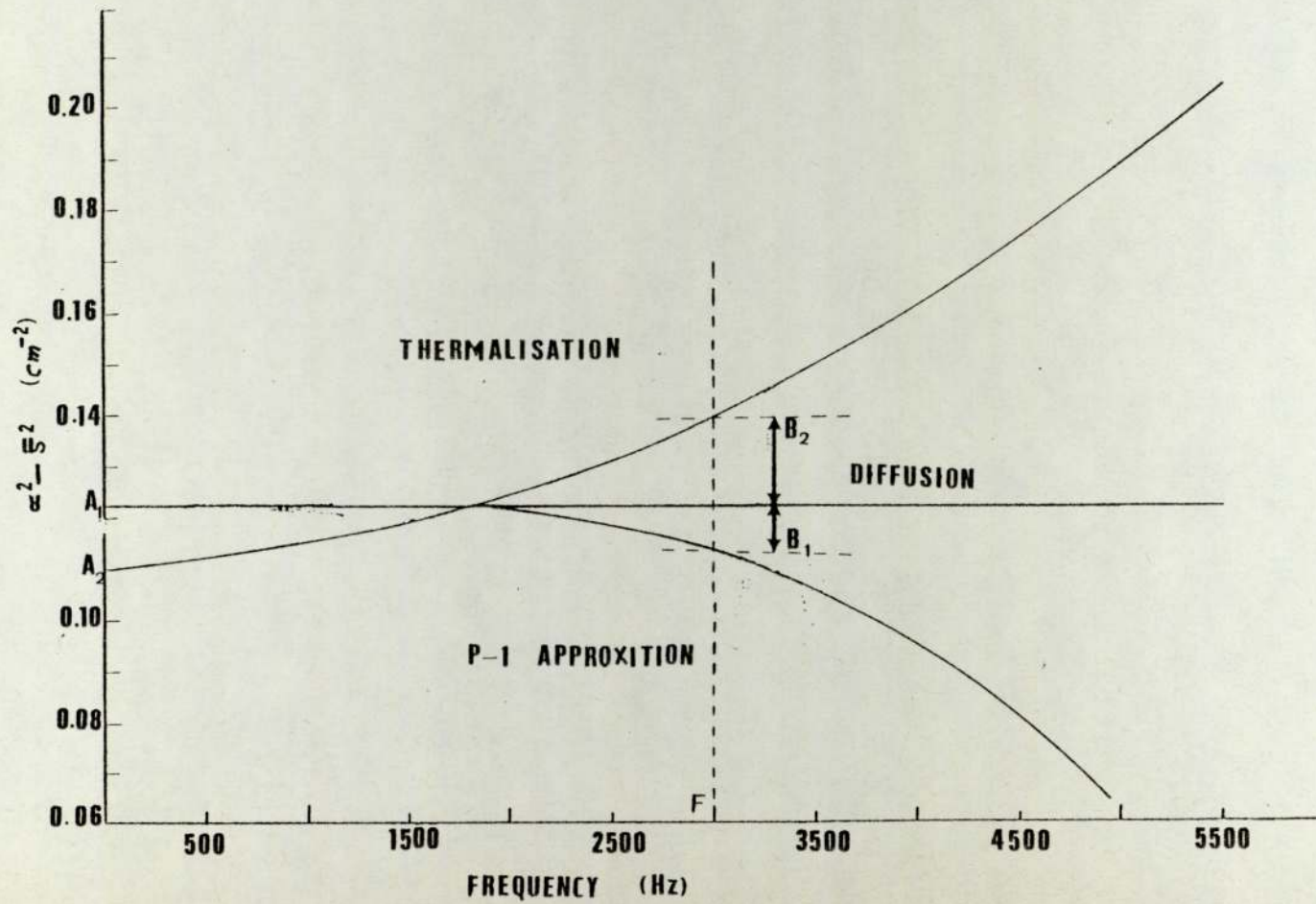


Fig.7.2. COMPARISON OF THEORETICAL MODELS, ($\alpha^2 S^2$ VERSUS FREQUENCY)

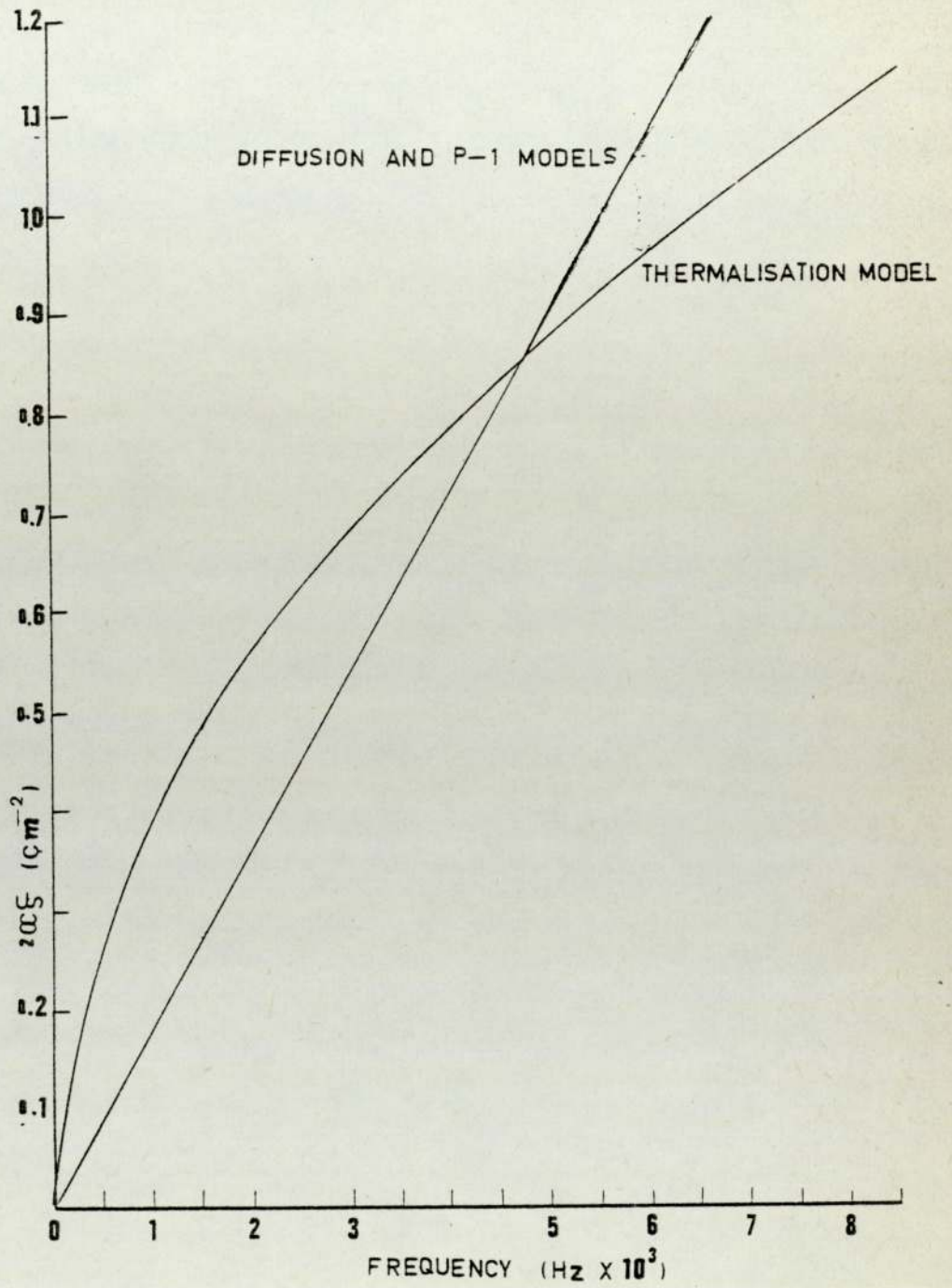


Fig.7.3. COMPARISON OF THEORETICAL MODELS, (200ξ AND FREQUENCY).

The diffusion theory predicts a constant value for $(\alpha_{\omega}^2 - \xi^2)$ over all ranges of frequency, while the P-1 results coincide with the diffusion results up to 1500 Hz. Beyond this frequency $(3 \frac{\omega^2}{v^2})$ effectively reduces the values of $(\alpha_{\omega}^2 - \xi^2)$.

For the thermalisation theory calculations, the zero frequency intercept (A_2) is:

$$A_2 = B_1^2 + \frac{\sqrt{\pi}}{2L^2} \left(1 + \frac{\pi C}{4vD_0 L^2}\right)$$

which is smaller than (A_1) predicted by diffusion and P-1 approximations. However, the values of $(\alpha_{\omega}^2 - \xi^2)$ increase with frequency by a factor of $(\frac{\sqrt{\pi}}{2vD_0})^3 C$.

It can be seen from Figure 7.2 that the corrections to the diffusion theory introduced by the transport effects in the P-1 approximation, (B_1), and the correction due to the non-Maxwellian energy distribution introduced by the thermalisation theory, (B_2), are in opposite sense. At a given frequency, (F), $B_2 > B_1$, which indicates that the thermalisation effects are more important than the transport effects in a large-size moderator.

In Figure 7.3 the values of the function $(2 \alpha_{\omega} \xi_{\omega})$ for the diffusion and the P-1 calculation almost coincide in a linear variation with modulation frequency. The slope of the straight line for the diffusion results is $(\frac{1}{vD_0})$ and for P-1 is $(\frac{1 + 3D_0 \sum a}{vD_0})$. The thermalisation results show a considerable deviation from a linear relationship. The quasi-exponential rise in the values of $(2 \alpha_{\omega} \xi_{\omega})$ with frequency is reported by GOYAL (1971) following a different theoretical approach. However, it must be mentioned that the thermalisation theory developed in this work predicts a larger deviation from the linearity than that reported by Goyal.

7.2 Comparison between the theoretical and the experimental results,
- water moderator without voids -

The experimentally measured amplitude and phase shift of the thermal neutron wave, excited by a modulated source and propagating in the axial direction of the water moderator without voids, are listed in Table 5.1. These values are compared with the theoretical values predicted by each model and the results are shown in Figures 7.4 and 7.5. It can be seen from Figure 7.4 that both the diffusion and the P-1 approximation predictions underestimate the amplitude decay over the whole range of frequencies. The thermalisation theory prediction of the amplitude decay is fairly accurate for frequencies below 750 Hz.

It can be seen from Figure 7.5, in which the calculated and the measured phase shifts are compared, that the diffusion and the P-1 calculations underestimate the phase lag up to frequencies around 1000 Hz. and overestimate it at larger frequencies. The thermalisation calculation provides good agreement with the observed values in frequency range 75 Hz to 750 Hz.

An alternative approach is to compare the theoretical results with those obtained experimentally the two independent wave parameters, $2\alpha_{\omega}\xi_{\omega}$ and $\alpha^2 - \xi^2$. This approach allows the diffusion effects, which are the main contributors the wave function ($2\alpha_{\omega}\xi_{\omega}$), to be separated from the thermalisation effects which determine the values of ($\alpha_{\omega}^2 - \xi^2$). Figure 7.6 shows the measured and the calculated ($2\alpha_{\omega}\xi_{\omega}$) functions versus frequency. It can be seen that the diffusion and P-1 approximations fail to describe the experimental observations, while the thermalisation calculations show a good agreement with the experimental values in the frequency range (0 - 1250 Hz).

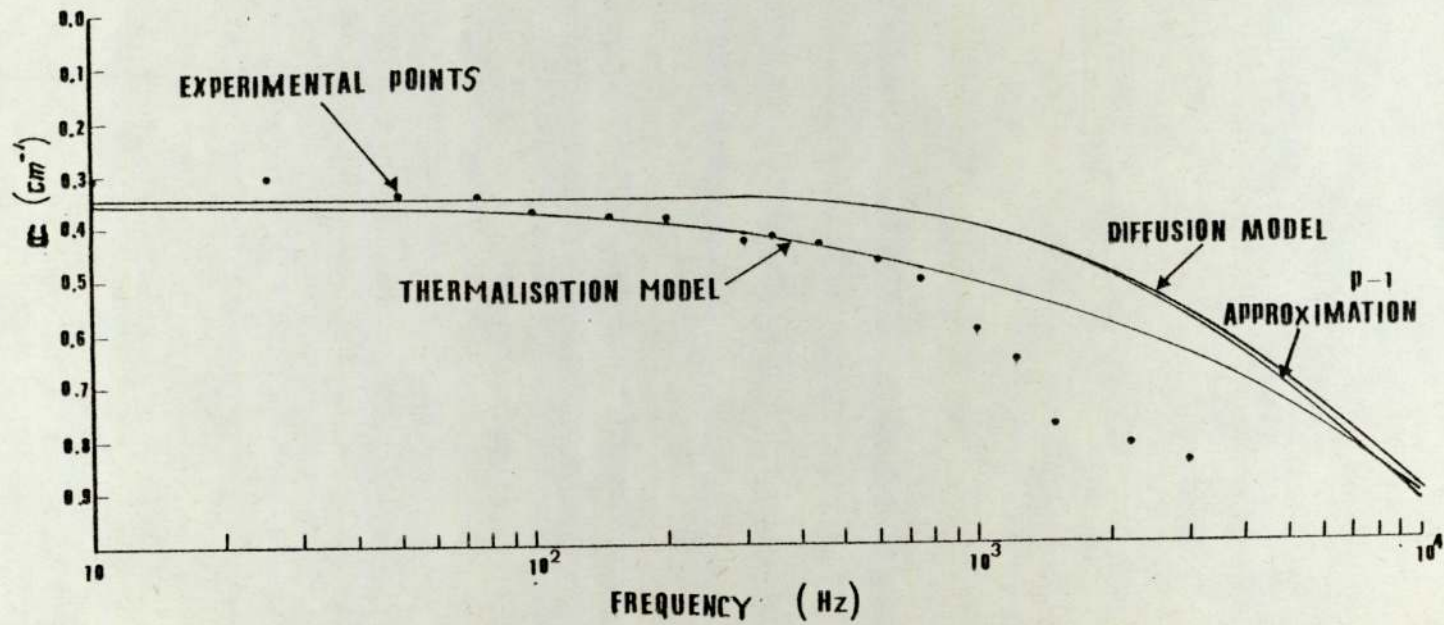


FIG. 7.4. CALCULATED AND MEASURED AMPLITUDE ^{PARAMETER} OF THERMAL NEUTRON WAVE IN WATER ASSEMBLY WITHOUT VOIDS.

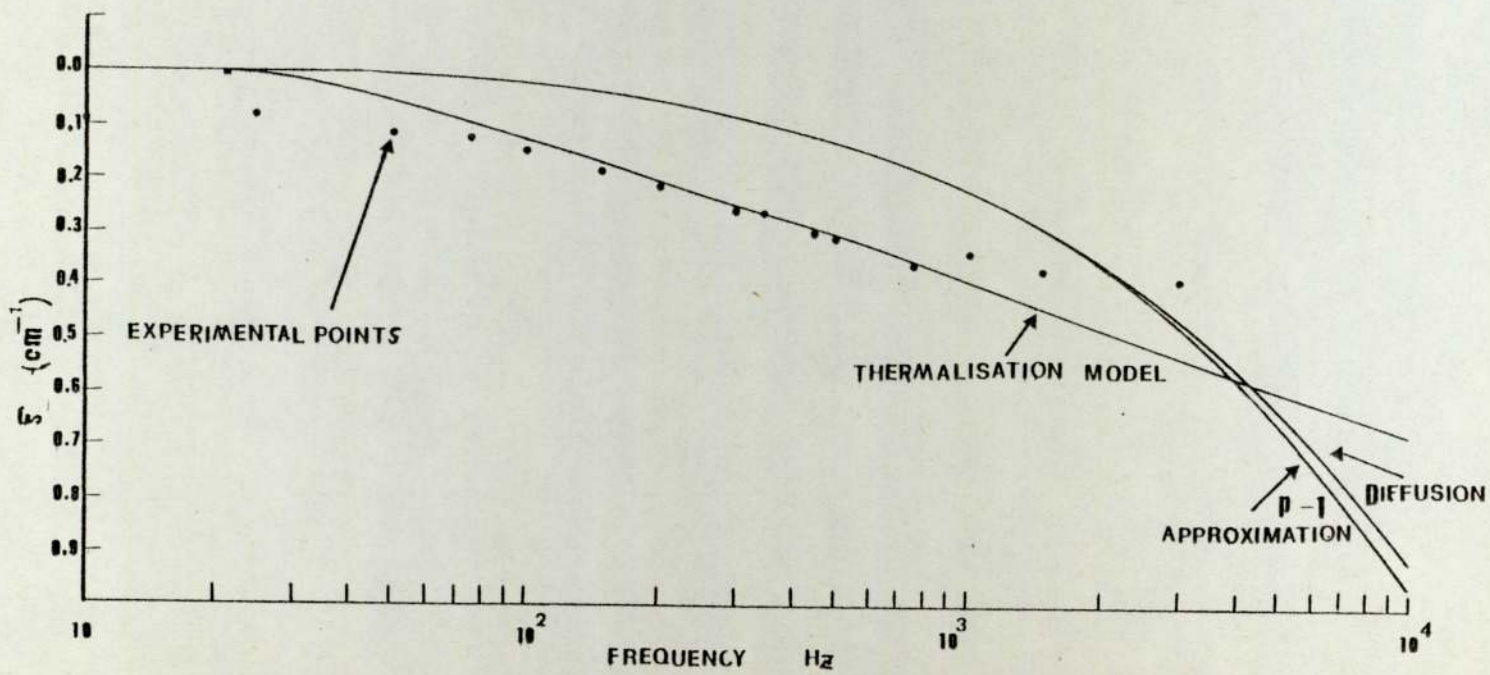


FIG.7.5. CALCULATED AND MEASURED PHASE SHIFT OF THERMAL NEUTRON WAVE IN A WATER ASSEMBLY WITHOUT VOIDS.

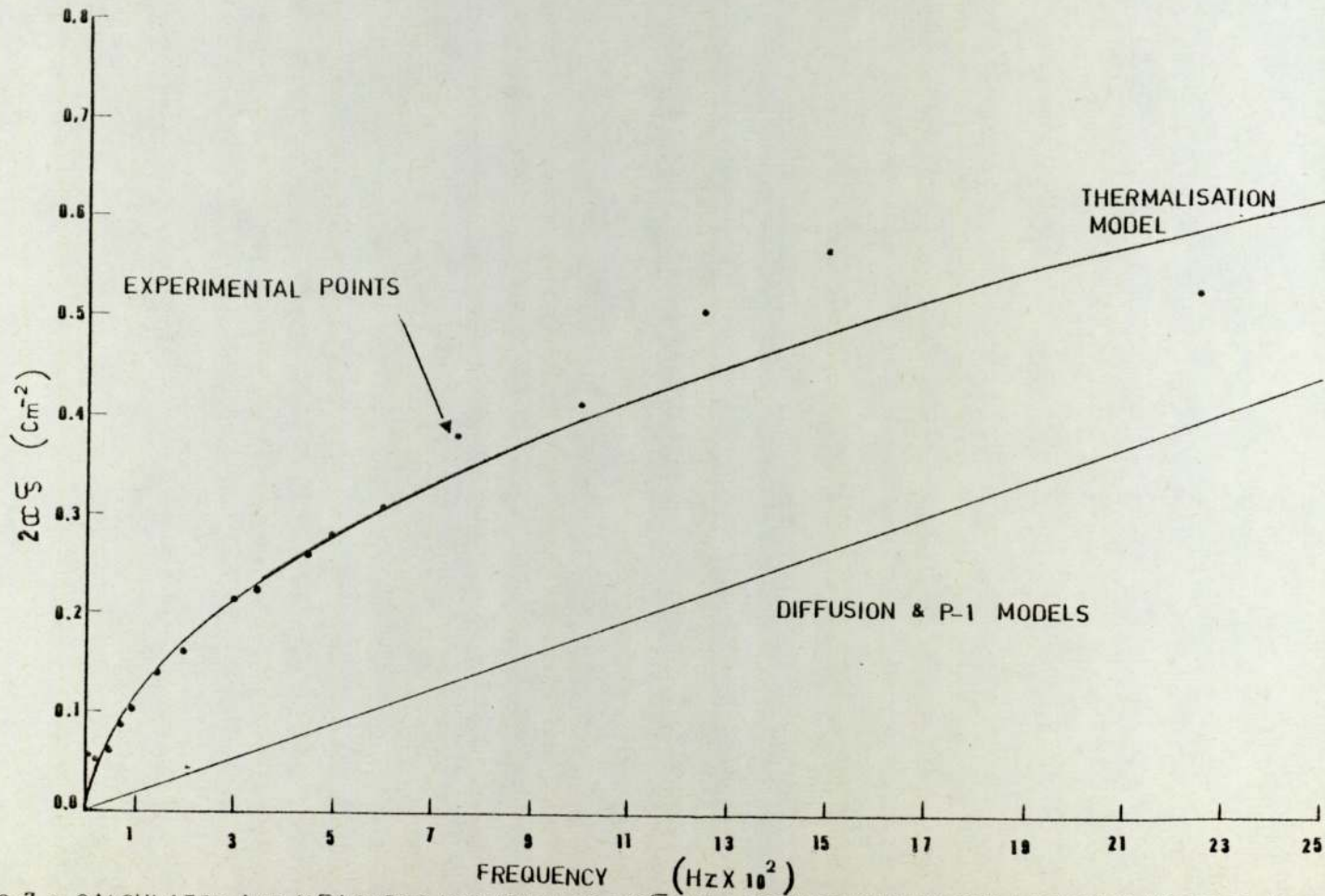


FIG.7.6. CALCULATED AND MEASURED VARIATION OF $2\alpha C_5$ WITH FREQUENCY IN WATER ASSEMBLY WITHOUT VOIDS.

Figure 7.7 shows the calculated and the measured variation of the function $(\alpha_{\omega}^2 - \xi_{\omega}^2)$ with the modulation frequency. The experimental values do not agree with the constant values predicted by the diffusion theory or with the P-1 predictions, which indicate that the transport effects are not important in determination of the function $(\alpha_{\omega}^2 - \xi_{\omega}^2)$. The thermalisation predictions are plotted over two frequency range, first, (0 - 1250 Hz), which is the experimental range, and second, (0 - 8000 Hz). The second range is presented (the dashed curve in Figure 7.7) to contrast it with the least squares fit of the experimental data and indicates that the thermalisation calculation predicts the general trend of the variation of $(\alpha_{\omega}^2 - \xi_{\omega}^2)$ with frequency but is in disagreement with experimentally-measured values. The calculated values of $(\alpha_{\omega}^2 - \xi_{\omega}^2)$ do not increase with frequency as fast as the experimental results. The apparent agreement in the $(2\alpha_{\omega}\xi_{\omega})$ plot with the thermalisation calculations and the disagreement in the $(\alpha_{\omega}^2 - \xi_{\omega}^2)$ plot can be explained by the fact that small errors in determination of the experimental and theoretical values of (α_{ω}) and (ξ_{ω}) tend to cancel in the $(2\alpha_{\omega}\xi_{\omega})$ plot but re-inforce the disagreement in the $(\alpha_{\omega}^2 - \xi_{\omega}^2)$ plot.

A third method for comparing the experimental results with the theoretical results is to present the first order, or (ρ) dispersion law, (i.e. the plot of α_{ω} versus ξ_{ω}), and the second order, or (ρ^2) dispersion law, (i.e. the plot of $2\alpha_{\omega}\xi_{\omega}$ versus $\alpha_{\omega}^2 - \xi_{\omega}^2$). This method was first used by PEREZ (1968) to investigate the nature of wave propagation in graphite.

The calculated and the measured (ρ) and (ρ^2) laws for water are shown in Figures 7.8 and 7.9. Inspection of these figures reveals that all theoretical models predict the experiment fairly well up to

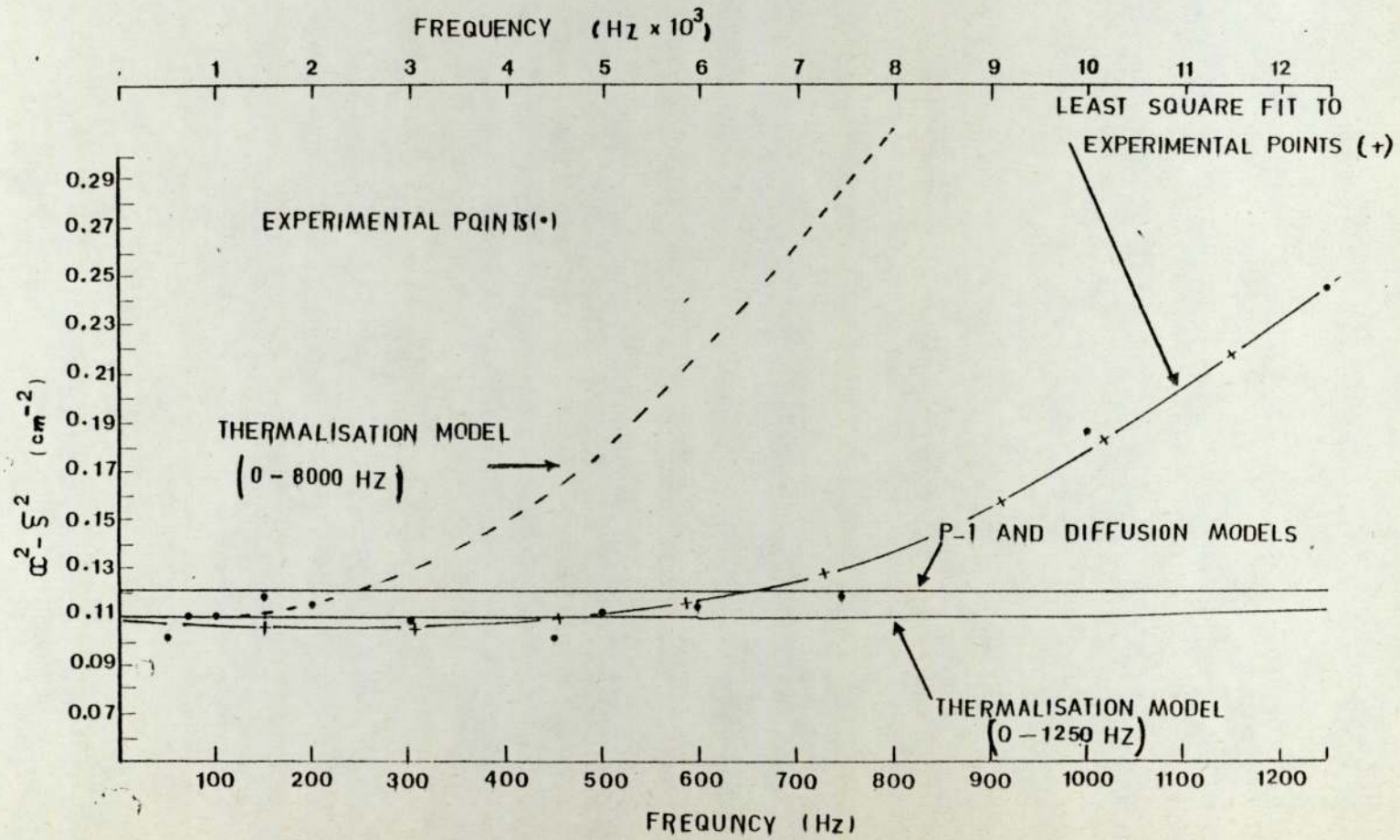


FIG. 7.7. CALCULATED AND MEASURED VARIATION OF $(\alpha^2 S^2)$ WITH FREQUENCY IN WATER ASSEMBLY WITHOUT VOID.

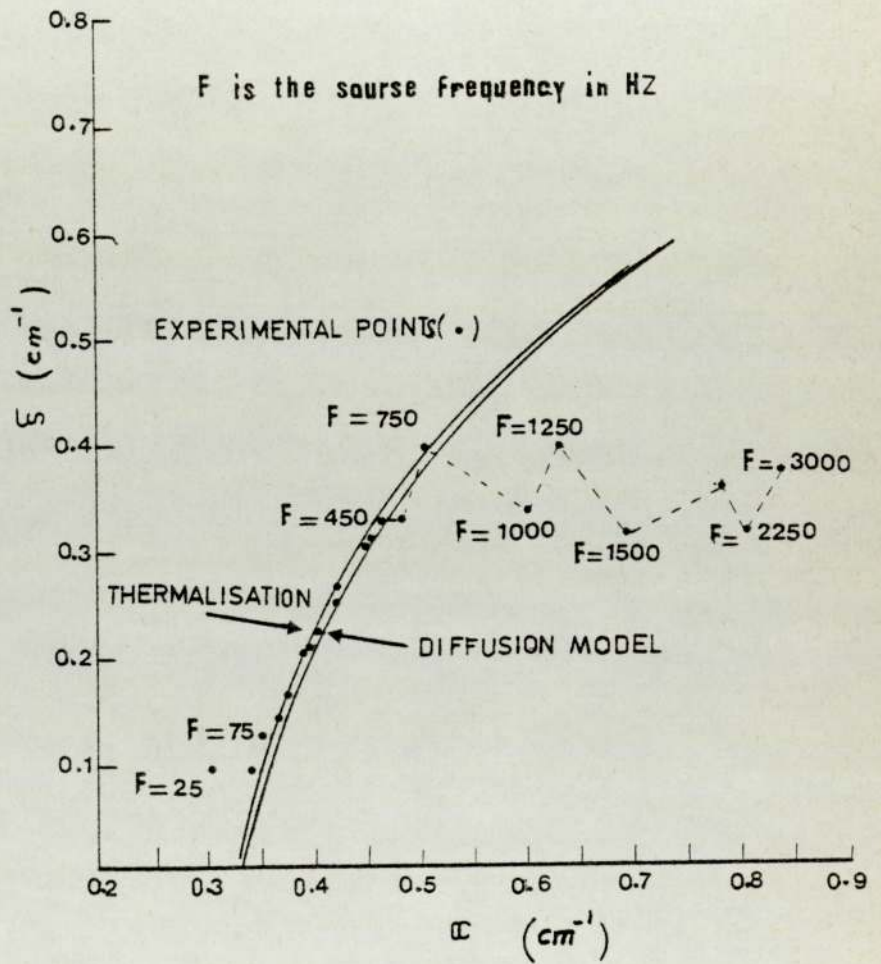


FIG. 7.8 . CALCULATED AND MEASURED (β) DISPERSION RELATIONS FOR WATER ASSEMBLY WITHOUT VOIDS.

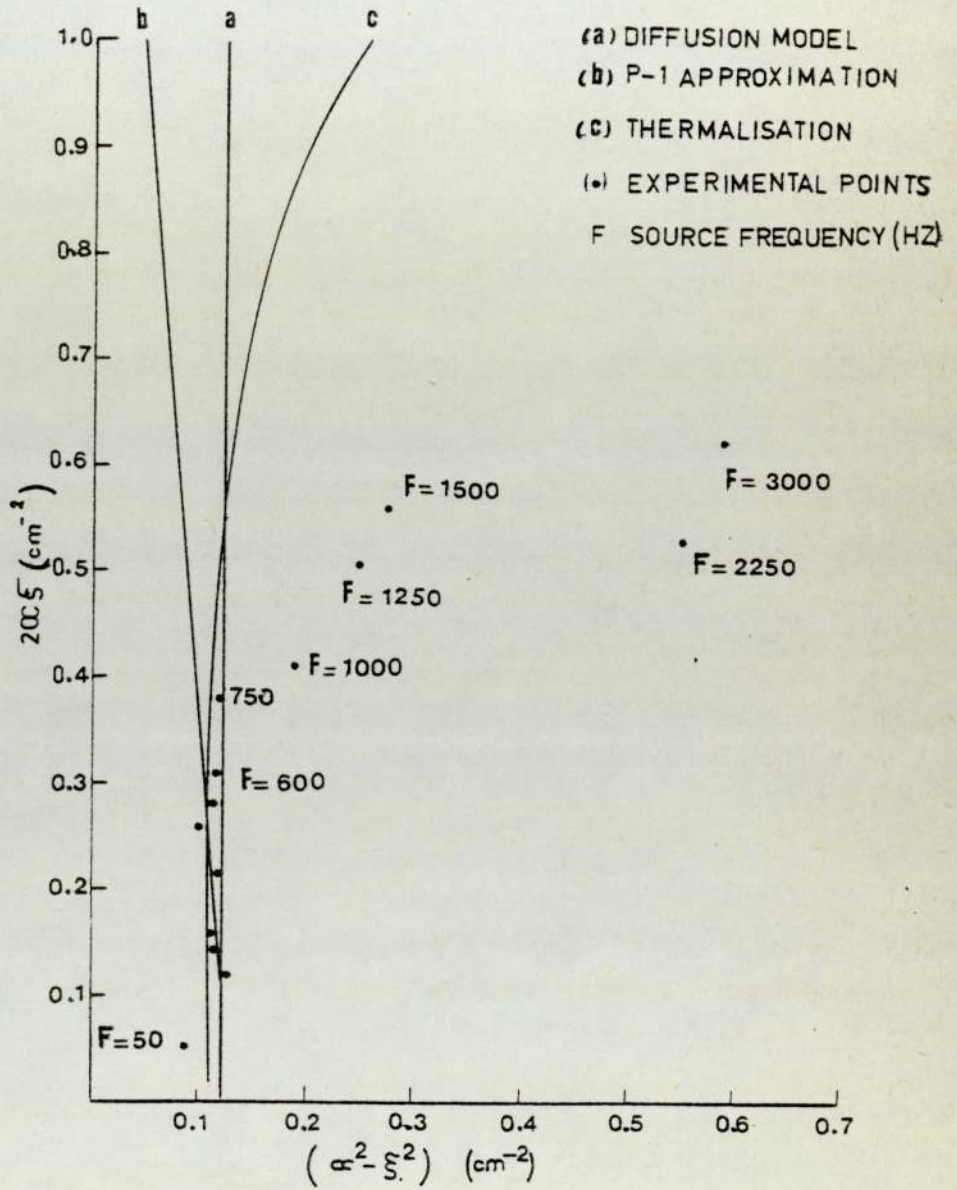


FIG.7.9. CALCULATED AND MEASURED (ρ^2) DISPERSION RELATION FOR WATER ASSEMBLY WITHOUT VOIDS.

750 Hz. At frequencies above 750 Hz the experimental results depart considerably from the theoretical predictions. This departure has been noticed in crystalline moderators by many workers (e.g. TAKAHASHI (1968) in graphite, RITCHIE and WHITTLESTONE (1973) in beryllium oxide and GOYAL (1975) in beryllium. The common interpretation was to attribute the disagreement to the presence of a strong sub-Bragg continuum at high frequencies.

In the present work, the theoretical models dealt with the neutron wave as of a single discrete mode but higher spatial modes of the wave do exist, and the dispersion laws can be generalised to include these spatial modes. The continuum concept can be illustrated by the one-group and one-dimensional neutron transport equation given by LAMARSH (1967) as:

$$\frac{1}{v} \frac{\partial \phi(z, \mu, t)}{\partial t} + u \frac{\partial \phi(z, \mu, t)}{\partial z} + \sum_t \phi(z, \mu, t) = \frac{1}{2} \sum_s \int_{-1}^1 \phi(z, \mu, t) d\mu \quad \dots\dots\dots 7.2$$

where $\phi(z, \mu, t)$ is the number of neutrons per unit volume having a velocity vector with a direction cosine between u and $u+du$. The continuum corresponds to the vanishing of the operator on the left of Eq. (7.2), i.e.

$$\frac{1}{v} \frac{\partial \phi(z, \mu, t)}{\partial t} + \mu \frac{\partial \phi(z, \mu, t)}{\partial z} + \sum_t \phi(z, \mu, t) = 0 \quad \dots\dots\dots 7.3$$

If the flux is assumed to be of the form:

$$\phi(z, \mu, t) = e^{-\rho z + j\omega t} \quad \dots\dots\dots 7.4$$

Then by introducing Eq. (7.4) into Eq. (7.3) putting ($\rho = \alpha_{\omega} + j\xi_{\omega}$) and separating the real and imaginary parts yields:

$$\left. \begin{aligned} \alpha &= \frac{1}{\mu} \Sigma_{\neq} \\ \xi_{\omega} &= \frac{\omega}{\mu v} \end{aligned} \right\} \dots\dots\dots 7.5$$

which indicates that the continuum corresponds to neutrons with direction cosine (μ) and whose attenuation is dictated by the total removal cross section. HETRICK (1971) showed that the continuum contribution increases with higher excitation frequencies.

The main factors influencing the magnitude of the sub-Bragg continuum contributions are:

- i. The energy distribution of the thermal neutron source. A source of higher thermal-to-fast ratio will increase the sub-Bragg continuum contribution, GOYAL (1975).
- ii. The choice of the diffusing medium, i.e. whether it is a crystalline or non-crystalline moderator. The sub-Bragg continuum contribution is relatively small in non-crystalline moderators, WARNER and ERDMANN (1969b).
- iii. The transverse buckling of the assembly which reduces the discrete part and hence increase the continuum contribution. HETRICK (1971) suggested that at high frequencies there is no detectable discrete mode in small assemblies.

It appears from i - iii that in the present work, (where the neutron wave propagates in a non-crystalline and large size moderator and the thermal neutron source cannot be regarded as ^(OVER-THERMALISED) the sub-Bragg continuum cannot be held entirely responsible for the considerable deviation from the theory at frequencies larger than 750 Hz.

Moreover, for frequencies larger than 750 Hz, in both (ρ) and (ρ^2) plane, a quasi-cyclic behaviour is observed.

At frequencies (700 - 2000 Hz) the attenuation of the discrete and higher spatial modes components of the wave are the same, (since they are propagate in the same medium), for the same detector location. The magnitude of the discrete mode dominates the experimental results until frequencies around 750 Hz. Above 750 Hz, the magnitude of the sub-Bragg continuum becomes more and more prominent. Hence, for high frequencies there are two waves of approximately the same amplitude, attenuated with distance, and with the same frequency. Under these conditions the phase relationship of the two waves may give rise to constructive or distructive interference, which may explain the cyclic behaviour in the (ρ) and (ρ^2) planes. This phenomenon is reported by many workers and at different frequency ranges. TAKAHASHI (1968) refers to interference between the forward propagating pulse (+Z) and the backward reflected pulse (-Z) from the end surface. GOYAL (1975) refers to the interference between the discrete mode and the sub-Bragg continuum. However, no other explanation can be cited for non-crystalline moderators.

In view of the possible contribution from the sub-Bragg continuum, the present results should be interpreted as the measurement of the 'effective' phase shift and attenuation. Therefore, the measured (ρ) and (ρ^2) dispersion laws confirm that below 750 Hz the neutron wave has the properties of discrete mode and the theory predicts the experimental results fairly well. At higher frequencies wave interference appears as a strong possibility which the theory fails to predict. However, no firm explanation can be given for the data fluctuation without critical information about the source energy distribution, WOOD (1971), and the other factors affecting the degree of sub-Bragg contribution.

7.3 Determination of the diffusion and thermalisation parameters for water assembly without voids

From the previous section it can be concluded that there is a good agreement between the measured and calculated results at frequencies lower than 750 Hz. Therefore, the diffusion and the thermalisation parameters of the system were derived from the experimental data below 750 Hz.

The diffusion parameter (vD_0) is calculated from the slope of the linear fitting of the experimental data in the $2\alpha_\omega \xi_\omega$ versus frequency plot shown in Figure 7.6. The linear fitting was performed by a computer routine with data in the frequency range (50 - 750 Hz). The values of L^2 were found, from the zero frequency intercept, by linear fitting of the $\alpha_\omega^2 - \xi_\omega^2$ versus frequency results.

The diffusion parameter, and hence the diffusion constant was found to be considerably higher than the accepted values (13.9%), while the error in the measured values of L^2 does not exceed 2%. The considerably high error in the diffusion parameter and the comparatively lower error in the thermalisation parameter can be attributed, in addition to the experimental errors, to the presence of the sub-Bragg neutrons.

The sub-Bragg neutrons will shift the energy spectrum towards a region of larger mean free path and, hence, produce an effective D_0 greater than that associated with discrete mode propagation.

Table 7.2

Numerical results for the water assembly without voids

Parameter	Experimental values	Calculated values at 22°C	Percentage error
$vD_o \text{ cm}^2 \text{ s}^{-1}$	40900 \pm 850	35106	13.9%
$D_o \text{ cm}$	0.183	0.159	15%
$L^2 \text{ cm}^2$	8.145	8.245	1%

7.4 Theoretical results for water-void assemblies (Computer Programme VOID)

The thermal neutron wave parameters for a wave propagating in a water-void assembly have been calculated for four assemblies of different void channel radii, (1.55 cm, 1.75 cm, 2.40 cm and 3.55 cm). These calculations were performed by means of a FORTRAN computer code, VOID, to:

- i. Calculate a streaming factor for each water-void assembly according to the streaming formula given in Eq. (6.67).
- ii. Calculate α_ω and ξ_ω for each assembly over the frequency range 50 - 10000 Hz, in steps of 50 Hz.
- iii. Calculate the wave functions $\alpha_\omega^2 - \xi_\omega^2$ and $2\alpha_\omega \xi_\omega$ over the same frequency range.
- iv. Calculate the amplitude decay function $G_{(\omega)}^V$ as a measure of the amplitude damping with frequency, similar to the function $G_{(\omega)}$ explained in Eq. 7.1.
- v. Steps ii and iii were repeated for the diffusion theory model in accordance with Eqs. (6.69) and (6.70) and for the thermalisation model in accordance with Eqs. (6.79) and (6.80).

A listing of the code VOID is provided in Appendix III together with a sample of the input and output data.

Figure 7.10 is a plot of the variation of the amplitude decay function G_{ω}^V with modulation frequency. The results presented are those of water-void assembly with void channel radius of 1.75 cm. As it was the case in the homogeneous assembly, the diffusion theory underestimates the amplitude decay compared to thermalisation theory predictions.

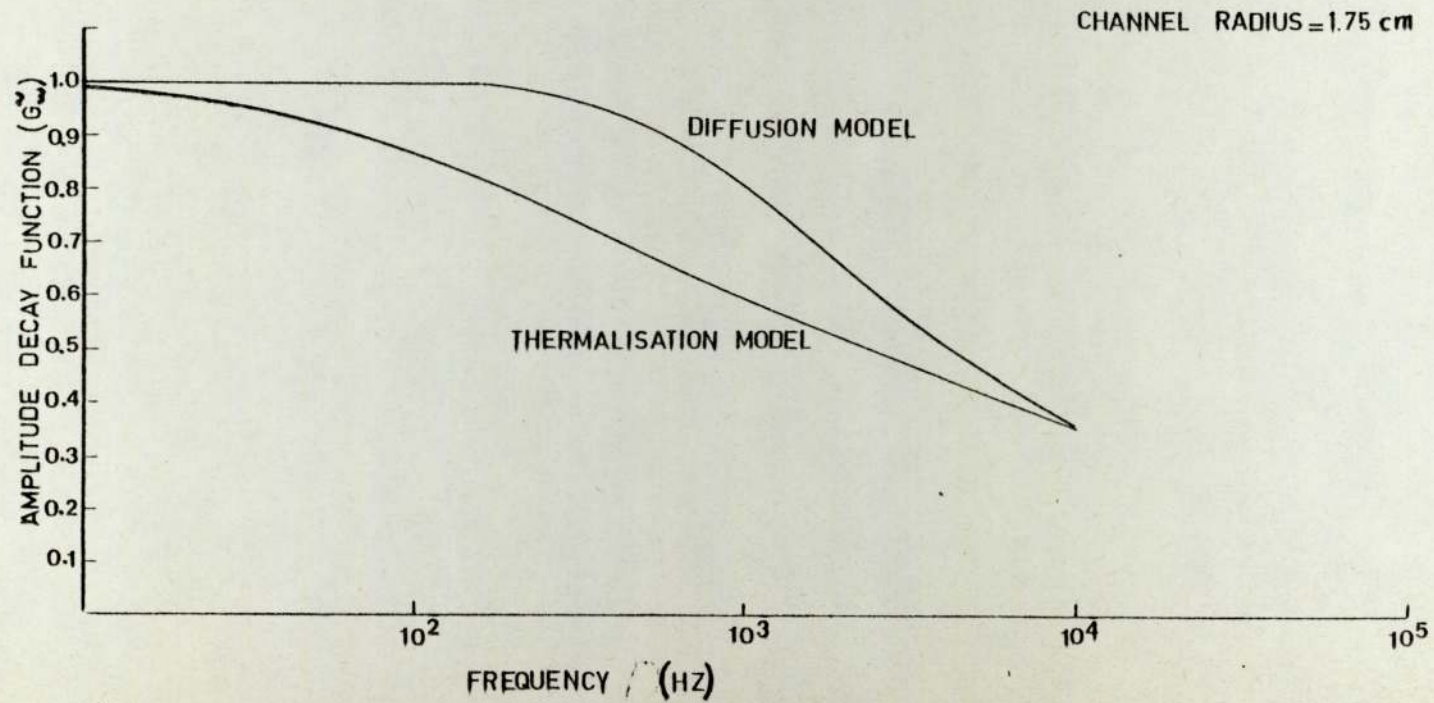


FIG 7)10. CALCULATED AMPLITUDE DECAY RESPONSE OF WATER-VOID ASSEMBLY

Figure 7.11 shows the measured and calculated amplitude decay of the thermal neutron wave propagating in a water-void assembly with void channel radius 1.75 cm, from the data given in table 5.3. As expected, the thermalisation results give a better prediction of the experiment for frequencies less than 1000 Hz, while the diffusion results fail totally to predict the experiment. The reason for the diffusion theory failure is that the diffusion assumption is no longer valid; with the presence of voids, isotropic scattering in the medium cannot be assumed and the changes in the flux gradient are rapid.

The thermalisation theory extends the diffusion theory to an energy-dependent problem which, in the present work, is dealt with by considering the deviation from a Maxwellian energy spectrum. The Maxwellian spectrum is highly distorted when void channels are present in the moderator, due to the anisotropic leakage which affects the high energy end of the Maxwellian spectrum and due to diffusion cooling. In a moderator-void assembly the neutrons with relatively low velocities, i.e. low-energy end of the Maxwellian spectrum, will be trapped in the void gap for longer time than higher velocity neutrons. Therefore, the spectrum near the void channel suffers more cooling than the spectrum far from the void-moderator interface.

For these reasons the thermalisation calculations shows a better agreement with the experimental observations. A similar agreement was observed in phase shift-frequency relationship.

The effect of the void channel dimensions on the calculated amplitude decay function G_{ω}^V variation with frequency is shown in Figure 7.12. The calculations were performed using the thermalisation model. It can be seen from Figure 7.12 that for larger channel radii the theory predicts lower values of the amplitude decay function, the sensitivity to channel radius increasing with frequency. Since G_{ω}^V is defined as the ratio of amplitude at a given frequency to the

parameter (α_{ω})

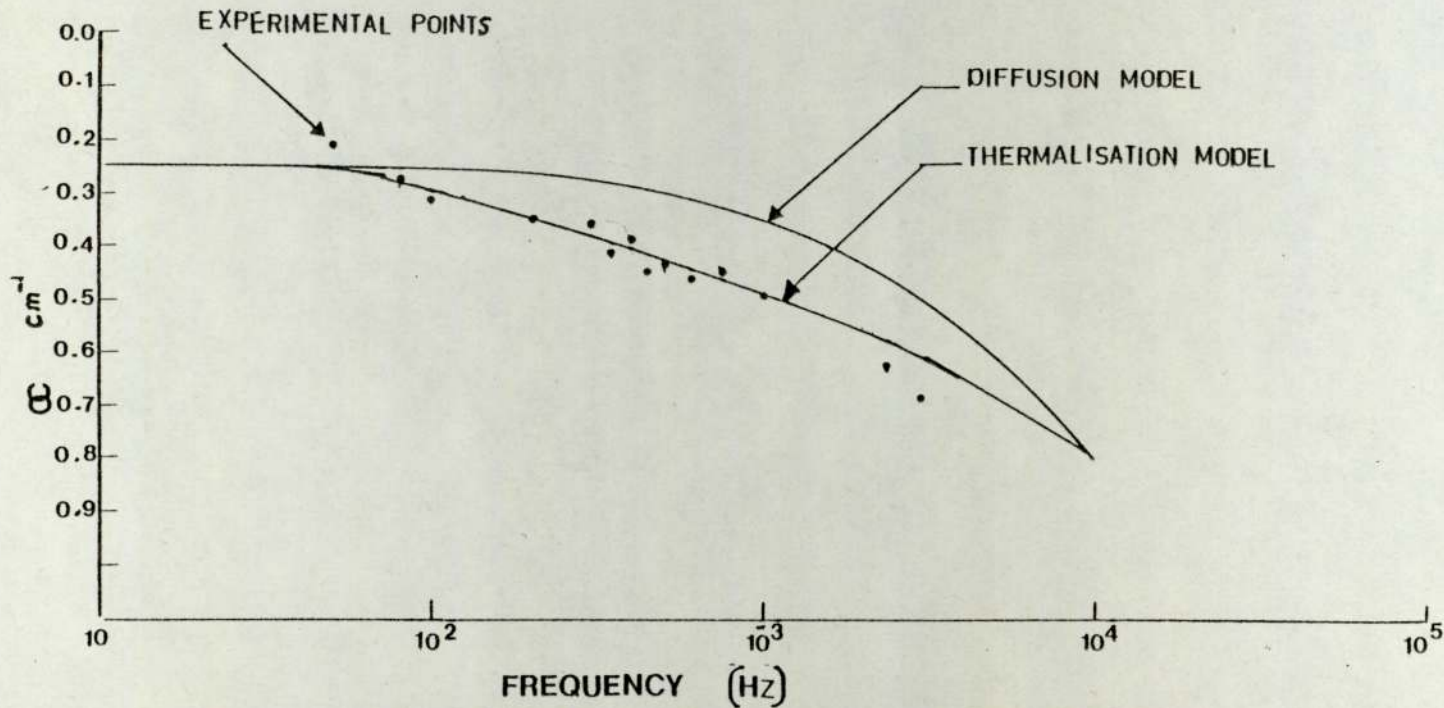


FIG. 7.11. CALCULATED AND MEASURED AMPLITUDE RESPONSE IN WATER-VOID ASSEMBLY (VOID RADIUS = 1.75 cm.)

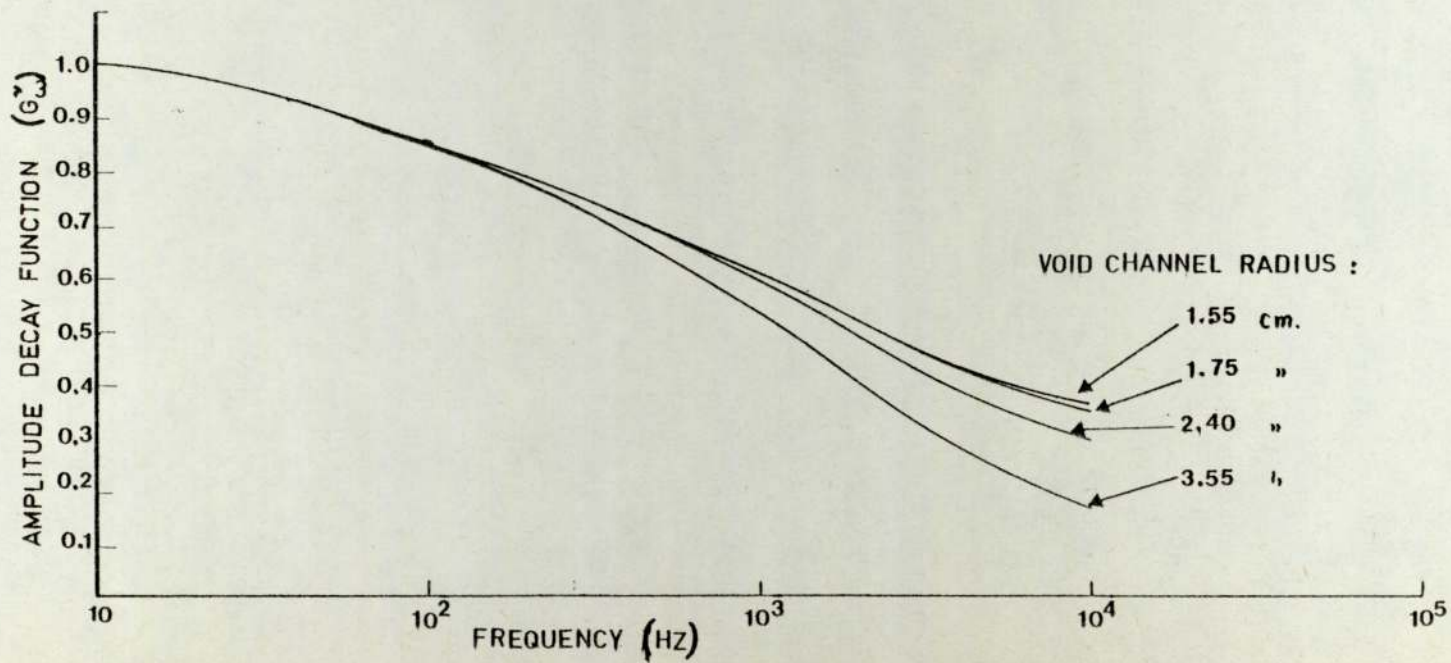


FIG. 7.12. THE EFFECT OF CHANNEL RADIUS ON THE CALCULATED AMPLITUDE FREQUENCY RESPONSE

Parameter (α_ω)
amplitude at zero frequency, (Eq. (7.1)), Figure 7.12 can be interpreted as giving lower values for (α_ω^v) for larger void dimensions at a given frequency. To check this result experimentally, a plot of the amplitude decay parameter (α_ω^v) versus frequency for two different void dimensions is shown in Figure 7.13. The calculated and measured values of (α_ω^v) are presented as a function of frequency for two water-void assemblies with void channel radii of 1.75 cm and 3.55 cm. The experimental results seem to confirm the theoretical prediction of lower wave attenuation at a given frequency for the larger void dimensions. For the larger void there is greater leakage and, therefore, greater anisotropy, which results in further deviation from the Maxwellian distribution. However, for both assemblies the experimental results are lower than the theoretical predictions. This is because the values of the calculated streaming factor incorporated in thermalisation calculations is rather higher than the actual values. Other experimental errors are also present and these will be detailed in a separate section of this chapter.

The variation with frequency of the real and imaginary parts of the (ρ^2) dispersion law for water-void assembly are presented in Figures 7.14 and 7.15. In Figure 7.14 the calculated and the measured values of the wave function ($\alpha_\omega^2 - \xi^2$) is plotted for two water-void assemblies, (void channel radii 1.75 cm and 3.55 cm). The theoretical results for the homogeneous water assembly is also presented. Although the theory predicts correctly the general trend of the variation with frequency, it underestimates the values of ($\alpha_\omega^2 - \xi^2$) considerably. This underestimation increases with both void dimensions and modulation frequency. There is greater disagreement with water-void assemblies due to the overestimation of the leakage and the streaming factors incorporated in the thermalisation calculation. Both experimental and theoretical values of ($\alpha_\omega^2 - \xi^2$)

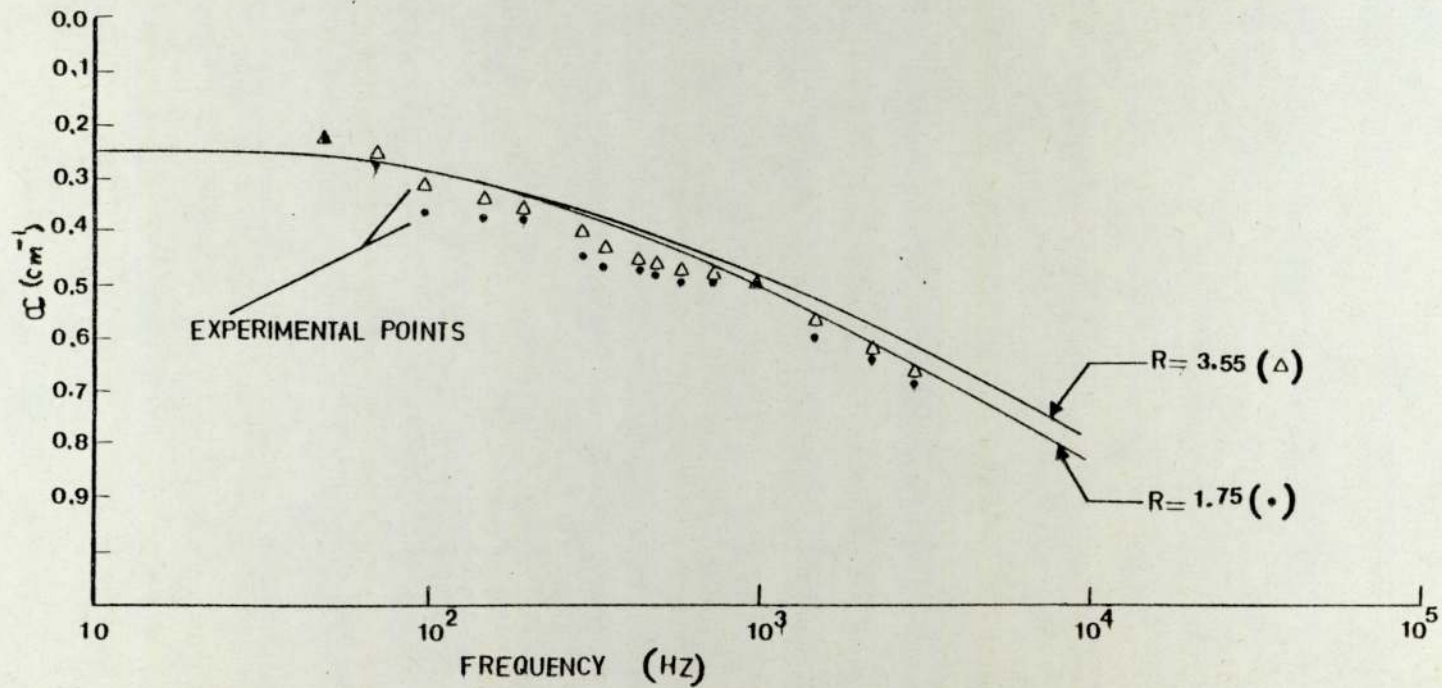


FIG. 7. 13. CALCULATED AND MEASURED EFFECT OF VOID RADIUS (R) ON THE AMPLITUDE DECAY WITH FREQUENCY.

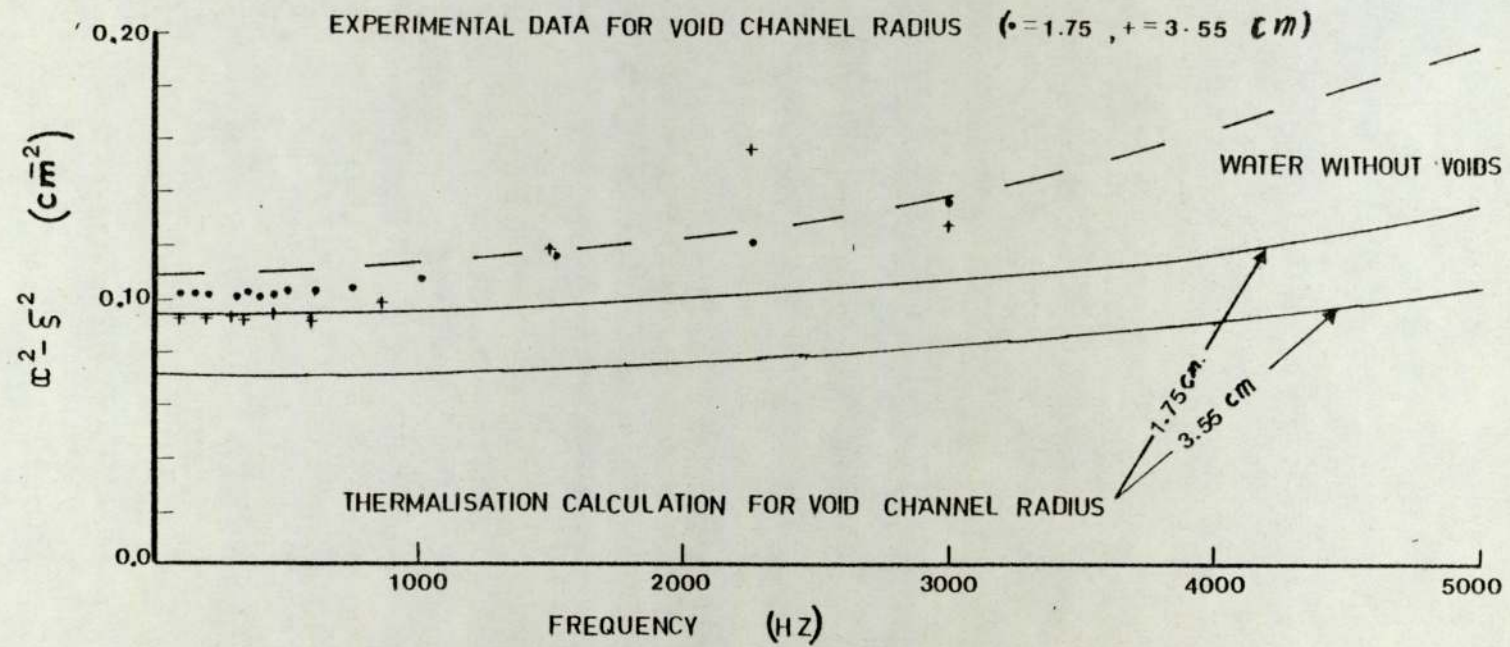


FIG. 7.14. CALCULATED AND MEASURED $(\alpha^2 - \xi^2)$ FOR TWO VOID CELLS.

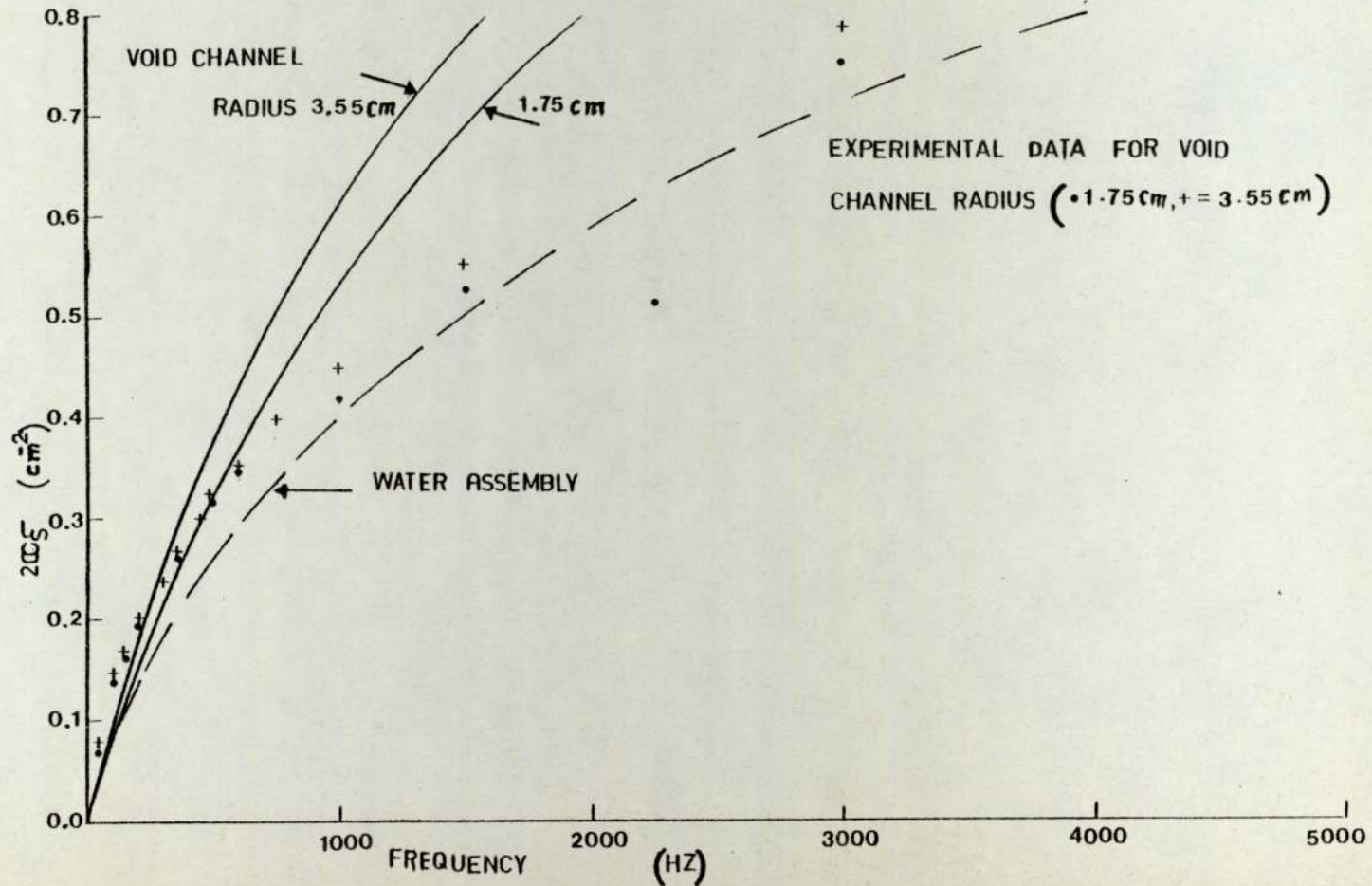


FIG. 7.15 CALCULATED AND MEASURED (200ξ) FOR TWO VOID CELLS

fall below those of the homogeneous water assembly since the voids cause a considerable increase in the diffusion area in the direction of the void channel, producing a lower zero frequency intercept value on the $(\alpha_{\omega}^2 - \xi_{\omega}^2)$ axis. Since $L_{||}^2 = \frac{D_{o||}}{\Sigma_a}$, the increase in L^2 should be interpreted as increase in D_0 in the void channel direction. However, the experimental results show that the increase in $L_{||}^2$ is lower than the increase in $\frac{D_{||}}{D_{\perp}}$, which means that Σ_a suffers considerable reduction, not only because of an overall reduction in density but because of energy spectrum variations in the vicinity of the void channel.

In Figure 7.15 the agreement between the calculated and the measured values of $(2\alpha_{\omega}\xi_{\omega})$ is better than in the $(\alpha_{\omega}^2 - \xi_{\omega}^2)$ curves. The theoretical results predict correctly the increased slope of the $(2\alpha_{\omega}\xi_{\omega})$ curve for a larger void dimension. The agreement is observed until the frequency reaches 750 Hz, which indicates that the energy spectrum variation is less important than the change in the diffusion parameter (vD_0) on which the function $(2\alpha_{\omega}\xi_{\omega})$ is highly dependent.

The measured and the calculated first order, or (ρ) dispersion law for a water-void assembly with void channel radius 2.40 cm is presented in Figure 7.16, together with the measured dispersion laws for a water moderator without voids. The theoretical dispersion law for a water-void assembly predicts the experimental observations up to 500 Hz. At larger frequencies the experimental results depart considerably from theoretical predictions. The deviation from the theory cannot be attributed totally to the quantitative effects of anisotropy and to the changes in the neutron energy distribution caused by the presence of void channels. The deviation from the theory can be explained by the nature of the wave propagation, i.e. the discrete-continuum modes relation. This relation is much

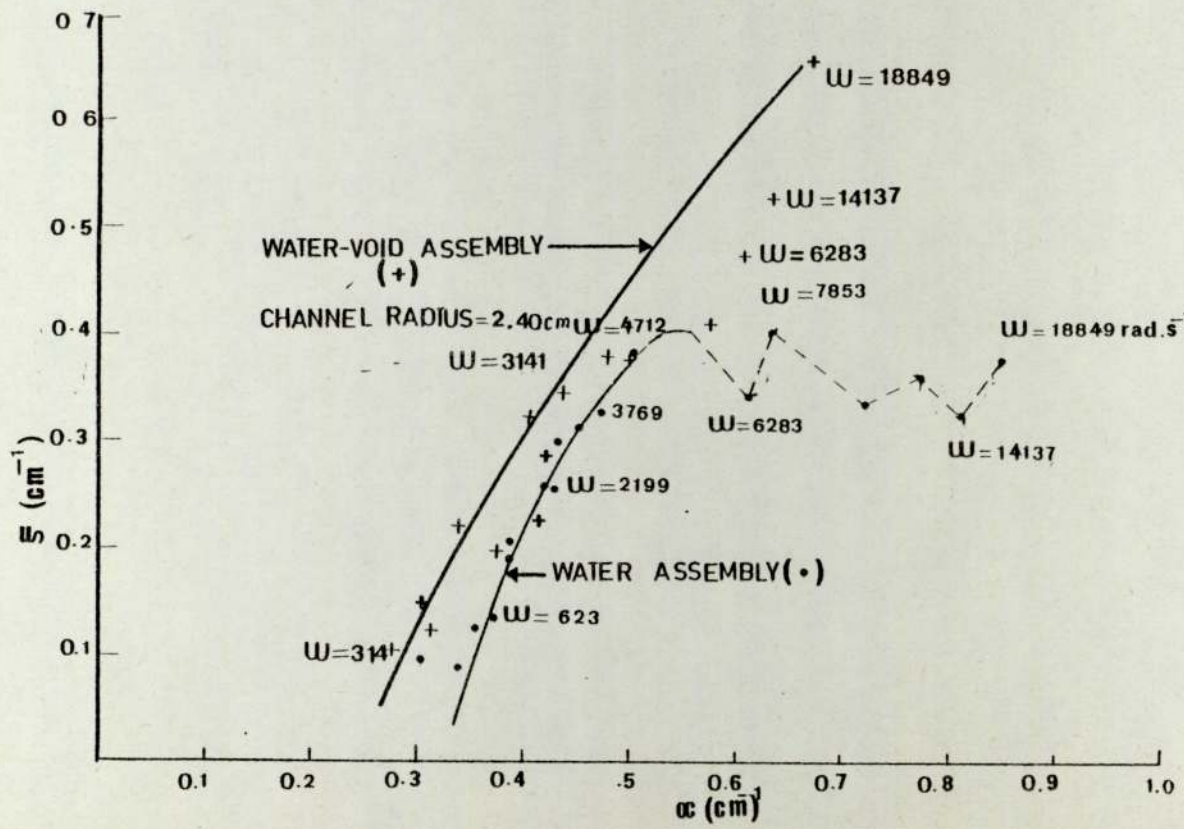


FIG. 7.16. COMPARISON BETWEEN CALCULATED AND MEASURED (ρ) DISPERSION LAWS FOR WATER AND WATER-VOID ASSEMBLIES.

more complicated than the one in homogeneous moderators, (the detailed analysis of this relation is given qualitatively by DANCE and CONNOLLY (1971) and quantitatively by VAN BINNBECK (1974)). Both works indicated that the continuum conditions given by Eq. (7.5) are not applicable in a system containing voids. Physically, all neutron wave modes cannot propagate with characteristic frequency greater than the minimum interaction frequency, $(v \Sigma_t)_{\min.} \cdot \left(\frac{\omega}{v \Sigma_t}\right)$ must be less than unity for discrete mode propagation. The same condition can be extended to systems containing voids. Since in a void region $(v \Sigma_t)$ approaches zero, (for an air-filled void), then $\left(\frac{\omega}{v \Sigma_t}\right)$ will be very large and a smaller discrete mode part should be expected than in homogeneous systems.

However, the theoretical models consider the problem as if the wave consists of a single discrete mode, which is why the calculated dispersion law shows singularity over the complete frequency range.

It can be seen from Figure 7.16 that for a system without voids, the departure from the theory starts at 750 Hz., ($\omega = 4712 \text{ rad. s}^{-1}$), while for a void system considerable deviation starts at about 500 Hz., ($\omega = 3141 \text{ rad.s}^{-1}$). This indicates that the continuum is more effective in void containing systems.

The experimental dispersion law for a water-void assembly does not show the cyclic behaviour which was observed in the water assembly without voids. In homogeneous systems this was interpreted as wave interference between the discrete and the continuum modes. However, due to the negligible contribution of the discrete mode at high frequency in a water-void assembly, no interference can be expected.

7.5 Determination of the diffusion and thermalisation parameters
for water-void assemblies

The previous section showed that the theory adopted in this work predicted the experimental measurements of the thermal neutron wave parameters in water-void assemblies for frequencies less than 600 Hz. The diffusion and thermalisation parameters of each assembly for this frequency range have been determined from the experimental data. For each assembly the diffusion parameter (vD_0), and consequently (D_0), were obtained from a linear fit of the experimental data in the $(2\alpha \frac{\xi}{\omega})$ versus frequency plot. The values of $(\frac{1}{L^2})$ or, $(\frac{\sum a}{D_0})$ were determined from the zer-frequency intercept in the $(\alpha \omega^2 - \xi^2)$ versus frequency plot. The axial streaming factor (at zero frequency), ($S_{0||}$), was obtained as the ratio of the axial diffusion area of water-void assembly, $(L_{||}^2)$, to the diffusion area of water assembly without voids, (L^2) . The numerical values of the diffusion and the thermalisation parameters for each assembly are listed in table 7.3.

The measured axial streaming factor was found to be smaller than the ^{from Eq.(6.67)} calculated values, (13.5% smaller for void channel radius 1.55 cm, 8.4% smaller for void channel radius 1.75 cm., 4.0% smaller for void channel radius 2.40 cm and 2.8% smaller for void channel radius 3.55 cm). This is due to the assumption in the theoretical calculation of uniform distribution of void channels throughout the moderator, in addition to other sources of error which will be discussed later.

Table 7.3

Diffusion and thermalisation parameters of
water-void assemblies

Void channel radius (cm)	$(\alpha^2 - \xi^2)_{\omega=0}$ (cm ⁻²)	L_{11}^2 (cm ²)	$D_0 = L^2 \sum_a$ (cm)	$S_{ }$ measured	$S_{ }$ calculated
1.55	0.112	8.928	0.196	1.115	1.290
1.75	0.105	9.523	0.209	1.190	1.300
2.40	0.097	10.309	0.226	1.288	1.342
3.55	0.091	10.989	0.241	1.375	1.415

It was found that the measured axial streaming factor increases with modulation frequency for all water-void assemblies. A typical illustration is given in Figure 7.17, where the axial streaming of the water-void assembly with void channel radius 2.40 cm is shown. Figure 7.17 indicates that the increase in the modulation frequency has the same effect as the increase in the void dimension, (or the axial leakage). This demonstrates that the use of a modulated source of neutrons is equivalent to poisoning the moderator medium, (or increasing neutron absorption), a characteristic feature of neutron wave experiments.

7.6 Discussion of errors

The errors affecting the experimental measurements and those associated with theoretical calculations are outlined in this section. The magnitude of individual error is also evaluated.

7.6.1 Errors associated with experimental technique

7.6.1.1 The changes in detection efficiency

The changes in the detection efficiency at high count rates are accounted for by compensating for detector dead time and analyser memory transfer time. These corrections were incorporated in the computation of the amplitude and the phase shift of the neutron waves by the computer code DATACOR detailed in Section 5.1. However, changes in detection efficiency can be expected at all count rate levels due to changes in the E.H.T., drift in amplifier gain and in discrimination level. The magnitude of these errors increases with the count rate level and modulation frequency, KERLIN (1974). The combined effects of these errors can be evaluated statistically following the method given by UHRIG (1970). It was found that for an average count rate of 10^3 counts per channel per second and

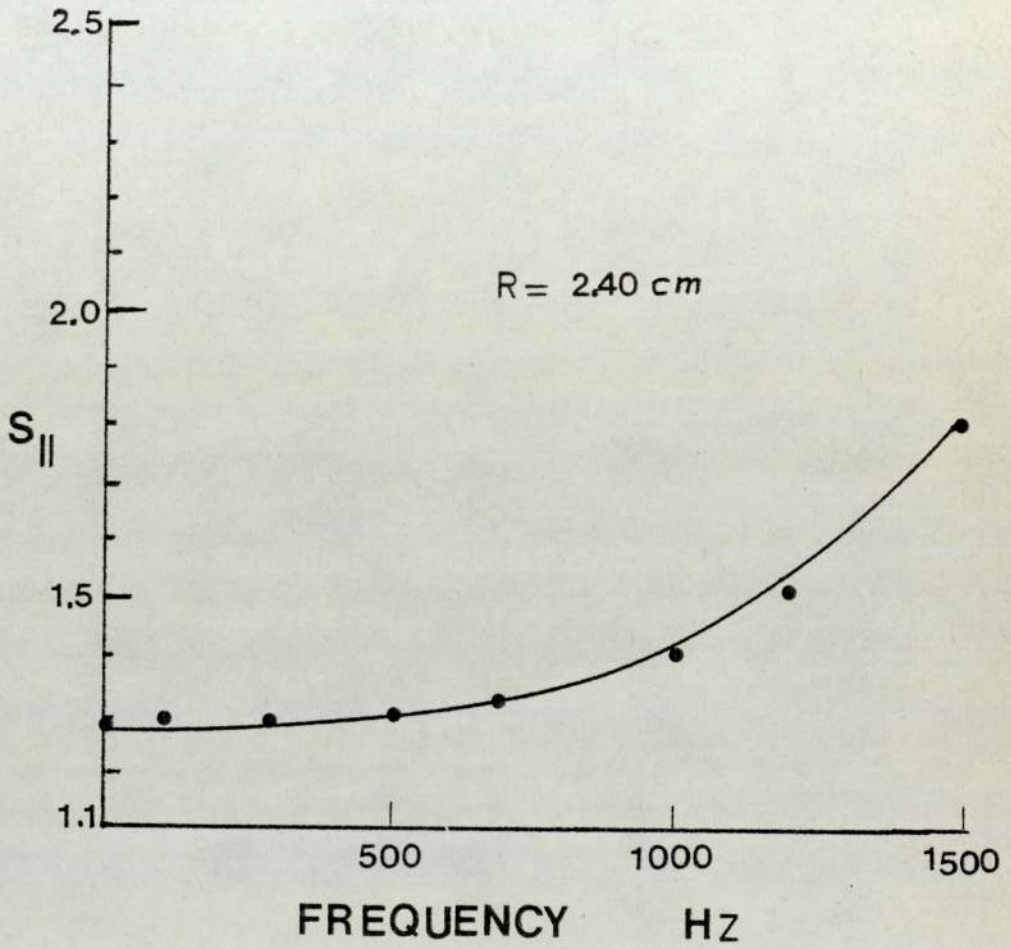


FIG.7.17. EFFECT OF FREQUENCY ON THE AXIAL STREAMING.

modulation frequencies less than 1000Hz, these errors are of the order of 0.1%.

7.6.1.2 Errors in detector positions

The accuracy in detector position was ± 3 mm. This gives rise to errors over the experimental frequency range of between 0.25% and 0.35% in amplitude measurements and between 0.05% and 0.15% in the phase measurements.

7.6.2 Systematic errors

There were three major sources of systematic errors associated with the measurement of the thermal neutron wave amplitude and phase constants. These errors are dependent on each other and can be described as:

- i. errors associated with the co-existence of a discrete mode of the wave with higher spatial modes and continuum. The decay of the higher spatial mode at large distances from the source leads to smaller values of the attenuation constant if the points close to the source are included in the analysis.
- ii. errors associated with the change in the neutron energy distribution along the axial distance. Generally, the neutron energy distribution in a moderator will be shifted toward the higher energy end of the spectrum at large distances from the source due to changes in the energy dependent scattering and absorption processes. Therefore, changes in (α_{ω}) and (ξ_{ω}) will be expected if there is to be any changes in the energy-dependent cross section, $\Sigma_{(E)}$ and diffusion coefficient $vD_{o(E)}$. Water shows a strong variation of cross section with

energy in the thermal range, and therefore, considerable changes in the values of (α_ω) and (ξ_ω) are expected for any spectrum changes.

iii. errors associated with the deviation from plane wave source conditions. It was pointed out by SOBHANA (1973) that the effect of a non-planar source is that the relaxation length of the wave tends to increase as the curved wavefronts progress. Since away from the source the wavefronts become more planar, then the inverse relaxation length, (ρ) , and hence, (α_ω) and (ξ_ω) are expected to have lower values.

The systematic errors associated with (i), (ii) and (iii) are all spatially dependent. Therefore, the combined effect of these errors was estimated by evaluating (α_ω) and (ξ_ω) from a set of measurements close to the source, (axial distances 5, 9, 15 and 20 cm) and from another set at large distances from the source, (axial distances 40, 45, 50, 55 and 60 cm). It was found that over all experimental frequencies the values of (α_ω) and (ξ_ω) close to the source are 0.5% - 3.5% and 0.075% - 0.150%, respectively, smaller than those measured at larger distances. This conclusion is illustrated in Figure 7.18 for the water moderator without voids. The amplitude gain is plotted versus the axial distance for two frequencies and the difference in the slope of the linear fit to the experimental data is taken as the magnitude of the total error. It must be mentioned that, throughout the present work, the experimental data for distances 5 cm, 55 cm and 60 cm showed some inconsistency and were not included in the analysis.

7.6.3 Statistical errors

The values of (α_ω) and (ξ_ω) were determined from a linear least squares fit of the measured amplitude or phase of the thermal wave

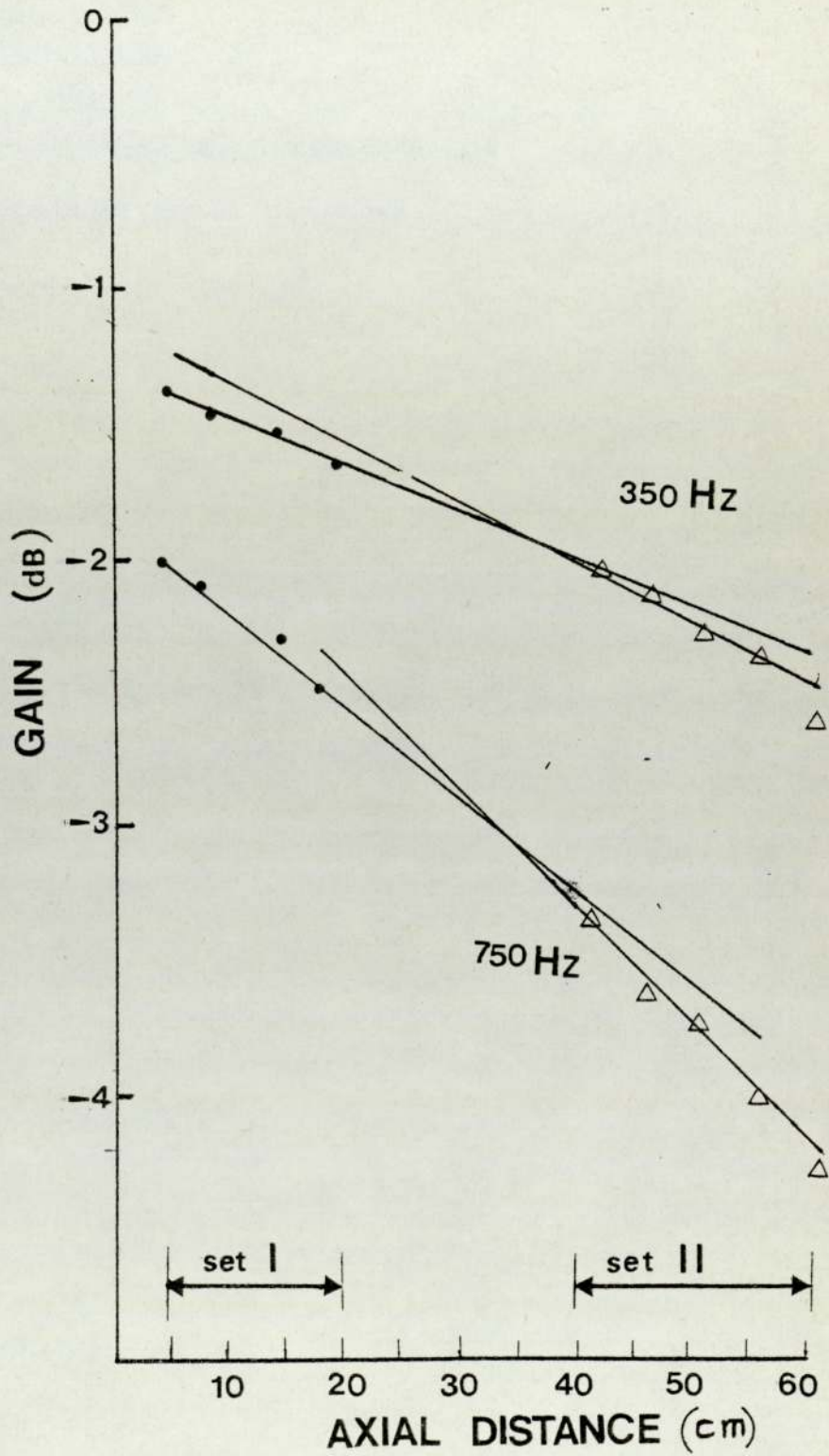


FIG. 7.18. EFFECT OF SPATIAL ERRORS ON THE WAVE ATTENUATION MEASUREMENTS

versus the axial distance from the source. The statistical errors associated with the curve fitting routine is calculated by the fitting code UAO1. Over the experimental frequency range these errors were found to vary from 1.5% in the determination of (α) and (ξ) to 5.5% in determination of the diffusion and thermalisation parameters.

7.6.4 Errors associated with the theoretical calculations

7.6.4.1 The energy-dependence of the system nuclear parameters

The exact treatment of neutrons diffusion in water at thermal energies, (0.01 eV - 1.0 eV), is a complicated problem (GODDART et al (1968)). Nevertheless, it is a common practice to approximate the neutron behaviour in the thermal region by considering the average values of the diffusion and scattering cross sections in low absorption moderators.

To account for energy dependence, the average value of the diffusion coefficient can be calculated from the energy dependent diffusion equation. Assuming that the flux $\phi(z,E)$ can be written as a separable function of (z) and (E), it can be shown that (\bar{D}) can be defined as:

$$\bar{D} = \frac{\int D_{(E)}\phi_{(E)} dE}{\int \phi_{(E)} dE} \dots\dots\dots 7.6$$

The diffusion coefficient is primarily a function of scattering cross section and for many moderators this is constant at thermal energies. However, water is an exception since its scattering cross section decreases with increasing energy (E), given by LAMARSH (1967) as:

$$\sum s_{(E)} = \sum s_{(E_0)} \left(\frac{E_0}{E}\right)^{0.470} \dots\dots\dots 7.7$$

where $E_0 = 0.0253$ eV. Since the diffusion coefficient varies inversely with the scattering cross section it follows that:

$$D(E) = D(E_0) \left(\frac{E}{E_0} \right)^{0.470} \dots\dots\dots 7.8$$

To illustrate the effects of the energy variation on the system nuclear parameters, and hence, on the calculated values of (α_w) and (ξ_w) , the constant values of total cross section of water are used in this work are compared in Figure 7.19 with values obtained from the empirical formula in Equation (7.7), and from the experimentally-measured values presented in Neutron Cross Sections Tables, HUGHES (1958).

The errors arising from the energy dependence of cross-section was estimated to affect the calculated values of (α_w) and (ξ_w) for homogeneous water assemblies by $\pm 0.01\%$ in the energy range between 0.01 eV to 1.0 eV. However, when dealing with water-void assemblies this error is more important and increases to about 0.5% in (α_w) and (ξ_w) . This error is increased further in calculation of $(2\alpha_w\xi_w)$ and $(\alpha_w^2 - \xi_w^2)$ because the elastic part of the total cross section is associated with $(2\alpha_w\xi_w)$ and the inelastic part is associated only with $(\alpha_w^2 - \xi_w^2)$.

7.6.4.2 Errors associated with streaming calculations

In water-void assemblies, the discrepancy between the theoretical predictions and the experimental observations can be attributed to some assumptions involved in the development of the theoretical models. These assumptions were:

- i. In the calculation of axial streaming by Eq. (6.67) it was assumed that the void channels were uniformly distributed throughout the moderator. In the

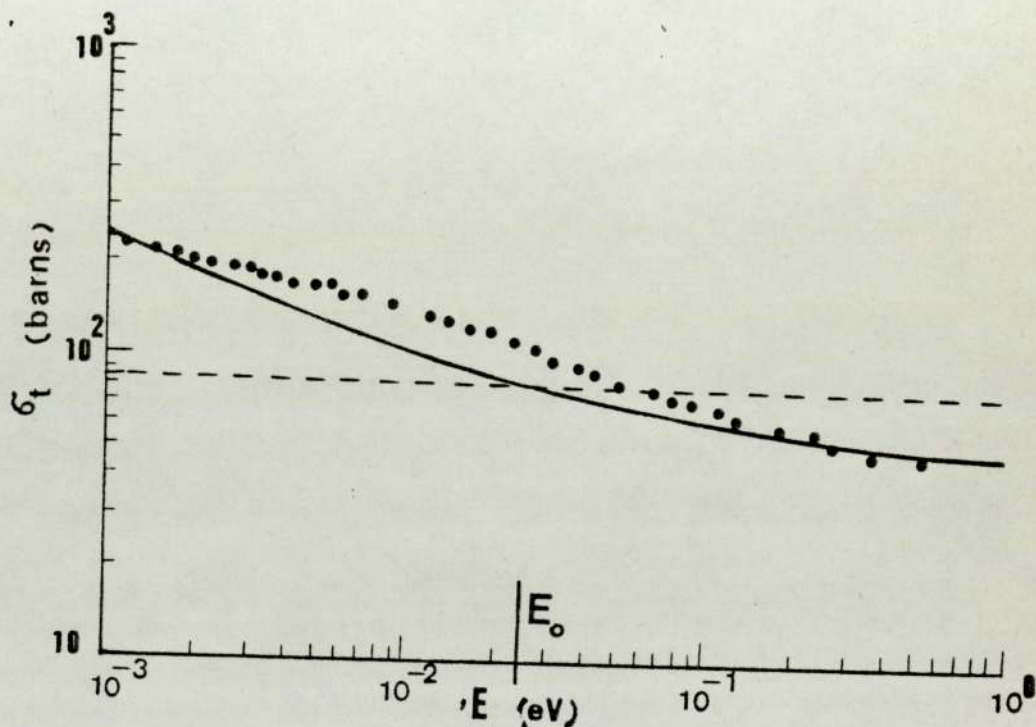


FIG. 7.19. WATER MICROSCOPIC TOTAL CROSS SECTION,
----- PRESENT WORK
———— EMPIRICAL VALUES
..... EXPERIMENTAL, (BNL-325).

experimental arrangement six void channels were placed to form a hexagonal array with a seventh channel in its centre. To approximate to a uniformly distributed arrangement, the detectors were placed in such a way that they were surrounded by equally spaced void channels, (as in Figure 3.1.). This arrangement was chosen for simplicity and practical resemblance in nuclear systems. This approximation gives rise to higher values of the calculated axial streaming factors. However, it was found that for larger void channel radius the error is minimised, as was shown in Table 7.3.

- ii. It was assumed that the insertion of void channels in the moderator leaves the radial buckling, (B_1^2) , unchanged. Although this assumption can be tolerated for a large system with few channels and small void channel radius, it becomes a serious source of error when the total void dimensions are comparable to the radial dimension of the water assembly, due to radial leakage. To minimise this effect the void cells were placed in the centre of the water assembly surrounded by a minimum of 35 cm of water.

- iii. It was assumed that the macroscopic absorption cross section of a void system is $(1+X)$ times lower than that without voids, where X is the void to moderator ratio, i.e.

$$\sum_a^v = \frac{\sum_a^m}{1 + X} \dots\dots\dots 7.9$$

The application of this relation requires a constant neutron flux and neutron energy distribution. It can be shown that the presence of voids perturbs the flux distribution and near the void boundaries shifts the energy spectrum towards higher energies, i.e. \sum_a^v becomes an energy and space dependent function.

PAGE (1967) checked the validity of Eq. (7.9) in pulsed source experiments. His results showed that the approximation holds satisfactorily when the void radius does not exceed, considerably, the transport mean free path of the system. PAGE determined the fluxes in the void channel and in the moderator and calculated flux coupling coefficients which were a function of \sum_a^v and the pulse decay constant. It can be shown that by following the analytical approach of PAGE and by using the analogy between PST and NWT, (MICHAEL and MOORE 1968), that Eq. (7.9) is frequency dependent and \sum_a^v increases with frequency.

It is very difficult to assess exactly the error in the values of α_u^v and ξ_u^v which arise from i, ii and iii. In large systems, error (i) and (ii) act to cancel each other. However, when these errors become frequency dependent, in neutron wave experiments, further complications arise in the computation of the net effects of these errors.

CHAPTER EIGHT

CONCLUSIONS AND RECOMMENDATIONS

A summary of the principal conclusions reached in this work are presented in this chapter. Some experimental and analytical studies to extend and compliment the present work are suggested.

8.1 Conclusions

8.1.1 Frequency response measurements

The spatial variation of the amplitude decay and the phase angle of the thermal neutron wave as a function of the source frequency were used in the present work to characterise the frequency response of the nuclear system. A comparison of the frequency response curves of a water moderator with and without voids indicated that the presence of the void channels in the moderator reduces the frequency at which the neutron wave suffers larger amplitude attenuation and phase lag. These effects can be amplified by increasing the void dimensions. The presence of voids also make the spatial differences in the measured frequency response more noticeable.

8.1.2 Thermal neutron wave parameters measurements

The use of three independent theoretical models for the calculation of the frequency dependent amplitude decay and phase lag of a thermal neutron wave has made it possible to isolate the diffusion, transport and thermalisation effects in interpretation of the propagation of thermal neutron wave in moderators. The calculation of the (ρ) and (ρ^2) dispersion laws by each model

showed their dependence on the source frequency and the nuclear parameters of the system in which the wave propagates. The use of a modulated source of neutrons and the measurement of the time-dependent component of the flux is then equivalent to performing a poisoning experiment.

At frequencies where the time between successive neutron collisions is comparable to the reciprocal of the source frequency, (500 Hz), higher modes of the wave affect the measured values of the real and the imaginary components of (ρ) and (ρ^2) dispersion laws. At these frequencies, the use of a P-1 approximation model showed better agreement with the experimental observations than the diffusion model predictions. However, as the frequency increased beyond 500 Hz the present work has shown that the correction due to the non-Maxwellian neutron energy distribution, as introduced by the thermalisation theory model, is more important than the improvements achieved by the use of P-1 approximation transport corrections.

Further interpretation of the experimental results has been achieved by defining two wave functions, $(2\alpha_{\omega}\xi_{\omega})$ and $(\alpha_{\omega}^2 - \xi_{\omega}^2)$. This approach offered the advantage of separating the diffusion effects associated with the function $(2\alpha_{\omega}\xi_{\omega})$ from thermalisation effects associated with the function $(\alpha_{\omega}^2 - \xi_{\omega}^2)$. The plots of these two function versus frequency again showed the failure of the diffusion theory in predicting the experiment. The present results have shown that the correction to the diffusion theory introduced by the P-1 and the thermalisation models are acting in an opposite sense and that the non-Maxwellian neutron energy distribution corrections are more important.

In the view of the possible contribution from the presence

of neutron continuum, the present results should be interpreted as the measurements of the effective phase shift and attenuation constants of the thermal neutron wave in water with and without voids. The present results confirm that below 500 Hz a mode of wave propagation existed with discrete mode properties.

The extension of the theoretical models to a moderator with voids involved a mathematical coupling between parameters of the buckling expansion in the pulsed source technique and those of frequency expansion in the neutron wave experiments. Experimental results indicated that such coupling is possible for frequencies below 500 Hz in a large nuclear systems, i.e. systems with small radial and axial bucklings. This approach is applied to evaluate the anisotropic diffusion and thermalisation parameters of a large system with voids. This approach has the advantage of linking the neutron streaming to the source frequency. In the water moderator with voids the thermalisation model offered better prediction of the experiment. This is due to the important deviation from the Maxwellian energy distribution caused by the presence of voids. The thermalisation model predicts correctly the general trend of the variation with frequency but overestimates the numerical values of the diffusion and the thermalisation parameters in a homogeneous moderating medium by up to 15%. However, the numerical values in a heterogeneous medium are found to be closer to the calculated values.

The axial streaming of thermal neutrons along the channels axis was found to increase with the modulation frequency. This indicated that the increase in the source frequency is equivalent to an increase in the void dimensions. This can be regarded as another way of showing the equivalence between the neutron wave

technique and poisoning experiments, with the neutron losses by leakage along the void channel regarded as the neutron losses by the absorption by the poison.

8.2 Recommendations for future work

The application of the neutron wave technique to study the anisotropic neutron diffusion in nuclear system requires more experimental and theoretical work. The theoretical models presented in the present work can be refined to investigate the nature of the wave propagation through a homogeneous or a heterogeneous moderators. The use of multi-group treatment may offer more information about the nature of neutron slowing down and the scattering process as a function of the source frequency. More work is also needed to investigate the continuum contribution to the measured wave parameters. The introduction of the higher spatial modes of the wave propagation in the analysis will offer more information about continuum contribution and frequency limitation of the discrete mode calculation presented in the present work.

It may be of interest to check the validity of the coupling between the frequency and the buckling expansions, (as used in the present work to investigate the anisotropic diffusion), in a multiplying medium containing void regions. This will have many practical application in studying power oscillation in reactors.

The water-void assemblies used in the present work can be used to study the possibility of thermal neutron wave reflection. This can be done by filling the empty channels with materials of different scattering and absorption properties. Information obtained about wave reflection can assist in conclusions about the possibility of wave interference, a phenomenon which was not possible to evaluate in the present work.

APPENDIX I

COMPUTER PROGRAMME - BROAD -

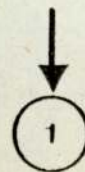
APPENDIX I

COMPUTER PROGRAMME "BROAD"

START

TRACE 1
TRACE 2
MASTER BROAD

```
C *****  
C CALCULATION OF PULSE BROADENING IN DIFFERENT MODERATING *  
C MATERIALS *  
C THIS PROGRAMME NEEDS THE FOLLOWING INPUT DATA *  
C N IS NUMBER OF EXPERIMENTS *  
C M IS NUMBER OF THE CYCLES IN EACH EXPERIMENT *  
C NM IS THE NUMBER OF CHANNELS PER CYCLE *  
C IBA IS THE BACKGROUND OF DETECTOR A *  
C IBB IS THE BACKGROUND OF DETECTOR B *  
C X IS THE COUNT PER CHANNEL *  
C *****
```



1



```

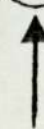
DIMENSION Y(10,40),A(10),B(10),TAW(10),D(10)
READ(1,12) H,H,HH,IBA,IBB
12 FORMAT(5I40)
DO 11 I1=1,H
READ(1,1) ((Y(I,J),J=1,40),I=1,10)
1 FORMAT(10F0.0)
DO 2 I=1,H
    SUMX=0.0
    SUMZ=0.0
    SUMXZ=0.0
    SUMX2=0.0
    ASUM=0.0
    BSUM=0.0
        JJ=0
    DO 5 J=21,HH
        X=J-20
        YY=Y(I,J)
        JJ=JJ+1
        ASUM=ASUM+Y(I,J-20)
        BSUM=BSUM+YY
        IF (I.LE.5) YY=YY-IBA
        IF (I.LE.10) YY=YY-IBB
        IF (YY.EQ.0.0) YY=1.0
10 Z=ALOG(YY)
        SUMX=SUMX+X
        SUMZ=SUMZ+Z
        SUMXZ=SUMXZ+X*Z
        SUMX2=SUMX2+X*X
    5 CONTINUE

```

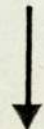
2



1



2



2



2

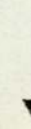


```
TERII=J.I*SUMX2-SUMX*SUMX
B(I) =-(J.I*SUMXZ-SUMX*SUMZ)/TERII
A(I)=EXP((SUMX2*SUMZ-SUMX*SUMXZ)/TERII)
TAW(I)=-ALOG(Y(I,21)/(2*A(I)))/B(I)
C   TAU IS A MEASURE OF PULSE DECAY TIME
    D(I)=ASUM/BSUM
C   D IS THE DISTORTION OF THE PULSE
    IF(D(I).GT.1.0) D(I)= BSUM/ASUM
        WRITE(2,4) I,A(I),B(I),TAW(I),D(I)
4   FORMAT(1H ,1",I2,5X,'A=',F12.4,5X,/,
*     'B=',F12.4,6X,'TAW=' ,F12.4,'DISTORTION FACTOR D = ',F16.6)
    IF(I.NE.5) GO TO 9
    SUHTAU = 0.0
    SUMD=0.0
    DO 5 K=1,5
    SUHTAU=SUHTAU+TAU(K)
    SUMD=SUMD+D(K)
5   CONTINUE
```

3



3



3

```
TAMHEAN=SUMTAW/5.0
WRITE(2,6) TAMHEAN
6  FORMAT(1H,'MEAN OF DETECTOR A TAWS IS ',F7.4)
   WRITE(2,20) DHEAN
20  FORMAT(1H,'MEAN OF DETECTOR A DISTORTION IS = ',F7.4)
9   IF(I.NE.10) GO TO 2
      SUHTAW=0.0
      SUMD=0.0
          DO 7 K=6,10
              SUHTAW=SUHTAW+TAW(K)
              SUMD=SUMD+D(K)
7   CONTINUE
      TAMHEAN=SUMTAW/5.0
      DHEAN=SUMD/5.0
   WRITE(2,8) TAMHEAN
8   FORMAT(1H,'MEAN OF DETECTOR B TAWS IS =',F7.4)
   WRITE(2,30) DHEAN
30  FORMAT(1X,'MEAN OF DETECTOR B DISTORTION',
*    F7.4//1X,'NEXT FREQUENCY'//)
2   CONTINUE
11  CONTINUE
    STOP
    END
```

3

↓

STOP

LINEPRINTER OUTPUT EXAMPLE

NEXT FREQUENCY 200 Hz

I= 1	A=	2185.8075	B=	0.2385
I= 2	A=	2450.5829	B=	0.2426
I= 3	A=	2441.8331	B=	0.2416
I= 4	A=	2191.4263	B=	0.2423
I= 5	A=	2166.6351	B=	0.2348
MEAN OF THE DETECTOR A TAWS IS 2.9104				
MEAN OF DETECTOR A DISTORTION 0.2391				
I= 6	A=	2414.0710	B=	0.2443
I= 7	A=	2493.6153	B=	0.2397
I= 8	A=	2446.9361	B=	0.2448
I= 9	A=	2407.3294	B=	0.2448
I=10	A=	2432.9092	B=	0.2444
MEAN OF THE DETECTOR B TAWS IS 3.4237				
MEAN OF DETECTOR B DISTORTION 0.2707				

TAW=	2.9138	DISTORTION FACTOR D =	0.239375
TAW=	2.9474	DISTORTION FACTOR D =	0.241978
TAW=	2.9883	DISTORTION FACTOR D =	0.238630
TAW=	2.9112	DISTORTION FACTOR D =	0.235543
TAW=	2.7911	DISTORTION FACTOR D =	0.240059

TAW=	3.5035	DISTORTION FACTOR D =	0.268557
TAW=	3.4934	DISTORTION FACTOR D =	0.274888
TAW=	3.3634	DISTORTION FACTOR D =	0.272925
TAW=	3.2088	DISTORTION FACTOR D =	0.268294
TAW=	3.5494	DISTORTION FACTOR D =	0.268946

I. is the cycle number

A and B are constants of the equation:

$$h = A \text{ Exp}(- Bx)$$

TAW is a measure of the pulse broadening

D is the distortion factor

APPENDIX II

COMPUTER CODE - WAVE -

START

TRACE 2
MASTER WAVES

```

C *****
C * CALCULATION OF THERMAL NEUTRON WAVE PROPAGATION *
C * CONSTANTS IN WATER AS A DIFFUSING MEDIUM BY *
C * 1= DIFFUSION THEORY MODEL *
C * 2= P-1 APPROXIMATION THEORY MODEL *
C * 3= THERMALISATION THEORY MODEL *
C *****

```

```

10 READ(1,10)B,SIG,DC,DA,V,CC
10 FORMAT(4F10.8,2F10.2)
C B IS THE TRANSVERSE BUCKLING OF THE ASSEMBLY
C SIG IS THERMAL MACROSCOPIC CROSS SECTION OF THE MEDIUM
C DC IS THE THERMAL DIFFUSION COEFFICIENT OF THE MEDIUM
C DA IS THE THERMAL DIFFUSION AREA OF THE MEDIUM
C V IS THE THERMAL NEUTRON VELOCITY CORRECTED TO 22 C
C CC IS THE DIFFUSION COOLING CONSTANT OF THE MEDIUM

```

```

DIMENSIONE(100),A1(100),G1(100),P1(100),F(100),
*Q(100),R(100),A2(100),G2(100),P2(100),
*SUM1(100),SUM2(100),A3(100),G3(100),P3(100),
*CA12(100),CA13(100),CA32(100),
*CP12(100),CP13(100),CP32(100)
DIMENSION ALFA1(100),ALFA2(100),ALFA3(100),
*BETA1(100),BETA2(100),BETA3(100)

```

```

X=B+(SIG/DC)
A01=SQRT(X)
A02=A01
H=SQRT(3.1415926)/2.0
Z=H/(V*DC)
T1=H*(SIG/DC)
T2=CC*(H**2)/(V*DC*DA)
A03=SQRT(B+T1*(1+T2))
T3=(1+3*DC*SIG)**2

```

```

DO 3 N=1,100
F(N)=N*100.0

```

```

C F IS THE SOURCE MODULATION FREQUENCY
E(N)=((2*3.1415926*F(N))/(V*DC))**2
A1(N)=SQRT((SQRT(X**2+E(N))+X)/2)
P1(N)=SQRT((SQRT(X**2+E(N))-X)/2.0)
G1(N)=A01/A1(N)
R(N)=E(N)*(DC**2)
A2(N)=SQRT((SQRT((X-3*R(N))**2+E(N)*T3)+X-3*R(N))/2.0)
P2(N)=SQRT((SQRT((X-3*R(N))**2+E(N)*T3)-X+3*R(N))/2.0)
G2(N)=A02/A2(N)
SUM1(N)=B+T1*(1+T2)+(Z**3)*CC*(2*3.1415926*F(N))**2
SUM2(N)=Z*(1-T2)*(2*3.1415926*F(N))
A3(N)=SQRT((SQRT(SUM1(N)**2+SUM2(N))+SUM1(N))/2.0)
P3(N)=SQRT((SQRT(SUM1(N)**2+SUM2(N))-SUM1(N))/2.0)
G3(N)=A03/A3(N)

```



①

①

```
CA12(N)=A1(N)/A2(N)
CA13(N)=A1(N)/A3(N)
CA32(N)=A3(N)/A2(N)
CP12(N)=P1(N)/P2(N)
CP13(N)=P1(N)/P3(N)
CP32(N)=P3(N)/P2(N)
ALFA1(N)=2*A1(N)*P1(N)
BETA1(N)=A1(N)**2-P1(N)**2
ALFA2(N)=2*A2(N)*P2(N)
BETA2(N)=A2(N)**2-P2(N)**2
ALFA3(N)=2*A3(N)*P3(N)
BETA3(N)=A3(N)**2-P3(N)**2
```

3 CONTINUE

```
WRITE(2,5)
5 FORMAT(1X,20X,'AMPLITUDE DECAY AND PHASE SHIFT WITH FREQUENCY'//
*1X,11X,'DIFFUSION THEORY CALCULATIONS',10X,
*5X,'P-1 THEORY CALCULATIONS',5X,
* 'THERMALISATION THEORY CALCULATIONS',///
*1X,'FREQUENCY',5X,'AMPLITUDE',5X,'GAIN',5X,'PHASE',
*7X,'AMPLITUDE',2X,'GAIN',5X,'PHASE',5X,
*5X,'AMPLITUDE',4X,'GAIN',8X,'PHASE'///)
WRITE(2,13)((F(I),A1(I),G1(I),P1(I),A2(I),G2(I),P2(I),A3(I),
*G3(I),P3(I)),I=1,100)
13 FORMAT(1X,F7.1,9X,F7.5,6X,F7.5,2X,F7.5,
*5X,F7.5,4X,F7.5,3X,F7.5,
*5X,F7.5,6X,F7.5,4X,F7.5)
```

↓
②

↓
②

②



②



```
WRITE(2,26)
26 FORMAT(1X,25X,'COMPARISON OF THEORETICAL METHODS'///
*1X,20X,'AMPLITUDE COMPARISON',40X,'PHASE COMPARISON'///
*1X,'FREQUENCY',6X,'DIF/P-1',5X,'DIF/THER',5X,'THER/P-1',15X,
*'DIF/P-1',5X,'DIF/THER',5X,'THER/P-1'///)
WRITE(2,35)((F(I),CA12(I),CA13(I),CA32(I),
*CP12(I),CP13(I),CP32(I)),I=1,100)
35 FORMAT(1X,F7.1,9X,F8.6,5X,F8.6,5X,F8.6,
*17X,F8.6,4X,F8.6,5X,F9.6)
C DISPERSION LAWS CALCULATIONS FOR DIFFIRENT MODELS
WRITE(2,40)
40 FORMAT(1X,10X,'DISPERSION LAWS PARAMETERS',///
*20X,'DIFFUSION THEORY MODEL'///,
*10X,'FREQUENCY',5X,'ALFA1',5X,'BETA1'///)
WRITE(2,41)((F(I),ALFA1(I),BETA1(I)),I=1,100)
41 FORMAT(1X,10X,F7.1,7X,F6.4,4X,F6.4)
WRITE(2,42)
42 FORMAT(1X,10X,'DISPERSION PARAMETERS BY P-1 THEORY'///,
*10X,'FREQUENCY',5X,'ALFA2',5X,'BETA2'///)
WRITE(2,43)((F(I),ALFA2(I),BETA2(I)),I=1,100)
43 FORMAT(1X,10X,F7.1,7X,F6.4,4X,F6.4)
WRITE(2,44)
44 FORMAT(1X,10X,'DISPERSION PARAMETERS BY THERMALISATION THEORY'///,
*10X,'FREQUENCY',5X,'ALFA3',5X,'BETA3'///)
WRITE(2,45)((F(I),ALFA3(I),BETA3(I)),I=1,100)
45 FORMAT(1X,10X,F7.1,7X,F6.4,4X,F6.4)
STOP
END
```

END

AMPLITUDE DECAY AND PHASE SHIFT WITH FREQUENCY

DIFFUSION THEORY CALCULATIONS

P-1 THEORY CALCULATIONS

THERMALISATION THEORY CALCULATIONS

FREQUENCY	AMPLITUDE	GAIN	PHASE	AMPLITUDE	GAIN	PHASE	AMPLITUDE	GAIN	PHASE
100.0	0.35057	0.99735	0.02553	0.35056	0.99740	0.02576	0.37195	0.89188	0.16813
200.0	0.35329	0.98967	0.05066	0.35322	0.98986	0.05113	0.39910	0.83121	0.22160
300.0	0.35761	0.97772	0.07507	0.35746	0.97814	0.07579	0.42038	0.78912	0.25766
400.0	0.36326	0.96251	0.09854	0.36299	0.96322	0.09951	0.43820	0.75703	0.28542
500.0	0.36997	0.94506	0.12094	0.36955	0.94612	0.12218	0.45369	0.73118	0.30821
600.0	0.37747	0.92628	0.14224	0.37689	0.92772	0.14377	0.46750	0.70959	0.32766
700.0	0.38555	0.90687	0.16247	0.38477	0.90871	0.16429	0.48001	0.69109	0.34469
800.0	0.39403	0.88735	0.18169	0.39304	0.88959	0.18381	0.49151	0.67492	0.35987
900.0	0.40278	0.86807	0.19996	0.40155	0.87073	0.20240	0.50218	0.66058	0.37359
1000.0	0.41170	0.84927	0.21736	0.41022	0.85234	0.22014	0.51216	0.64771	0.38612
1100.0	0.42071	0.83108	0.23398	0.41895	0.83456	0.23711	0.52156	0.63604	0.39767
1200.0	0.42975	0.81359	0.24988	0.42771	0.81747	0.25337	0.53046	0.62536	0.40838
↓	↓	↓	↓	↓	↓	↓	↓	↓	↓
9700.0	0.96505	0.36231	0.89948	0.90782	0.38514	0.96491	0.92377	0.35911	0.66673
9800.0	0.96966	0.36058	0.90443	0.91155	0.38357	0.97087	0.92760	0.35762	0.66739
9900.0	0.97425	0.35888	0.90935	0.91526	0.38202	0.97681	0.93142	0.35616	0.66803
10000.0	0.97882	0.35721	0.91424	0.91893	0.38049	0.98272	0.93525	0.35470	0.66865

COMPARISON OF THEORETICAL METHODS

AMPLITUDE COMPARISON

PHASE COMPARISON

FREQUENCY	AMPLITUDE COMPARISON			PHASE COMPARISON		
	DIF/P-1	DIF/THER	THER/P-1	DIF/P-1	DIF/THER	THER/P-1
100.0	1.000050	0.942533	1.061024	0.990897	0.151824	6.526599
200.0	1.000197	0.885233	1.129869	0.990751	0.228610	4.333802
300.0	1.000433	0.850685	1.176033	0.990517	0.291360	3.399631
400.0	1.000746	0.828989	1.207188	0.990207	0.345238	2.868184
500.0	1.001123	0.815463	1.227674	0.989835	0.392391	2.522574
600.0	1.001552	0.807431	1.240419	0.989410	0.434119	2.279125
700.0	1.002024	0.803208	1.247528	0.988945	0.471367	2.098035
800.0	1.002530	0.801675	1.250543	0.988446	0.504876	1.957800
900.0	1.003062	0.802068	1.250596	0.987921	0.535240	1.845754
1000.0	1.003617	0.803848	1.248516	0.987375	0.562943	1.753952
1100.0	1.004190	0.806634	1.244914	0.986812	0.588380	1.677167
1200.0	1.004777	0.810149	1.240238	0.986235	0.611877	1.611819
1300.0	1.005377	0.814191	1.234818	0.985646	0.633700	1.555384
1400.0	1.005987	0.818610	1.228896	0.985049	0.654071	1.506027
1500.0	1.006605	0.823295	1.222654	0.984444	0.673175	1.462389
1600.0	1.007231	0.828162	1.216224	0.983832	0.691166	1.423438
1700.0	1.007863	0.833147	1.209706	0.983215	0.708175	1.388378
1800.0	1.008500	0.838201	1.203172	0.982594	0.724313	1.356588
1900.0	1.009142	0.843286	1.196678	0.981969	0.739673	1.327572
2000.0	1.009789	0.848375	1.190262	0.981340	0.754337	1.300931
2100.0	1.010439	0.853444	1.183954	0.980709	0.768374	1.276344
2200.0	1.011092	0.858477	1.177774	0.980075	0.781845	1.253542
2300.0	1.011748	0.863460	1.171737	0.979440	0.794803	1.232305
↓						
9700.0	1.063033	1.044677	1.017571	0.932188	1.349093	0.690974
9800.0	1.063745	1.045345	1.017602	0.931563	1.355163	0.687418
9900.0	1.064458	1.045982	1.017664	0.930940	1.361230	0.683896
10000.0	1.065171	1.046589	1.017755	0.930316	1.367295	0.680407

DISPERSION LAWS PARAMETERS

DISPERSION PARAMETERS BY P-1 THEORY

DISPERSION PARAMETERS BY THERMALISATION THEORY

DIFFUSION THEORY MODEL		
FREQUENCY	ALFA1 $2\alpha\xi$	BETA1 $\alpha^2 - \xi^2$
100.0	0.0179	0.1223
200.0	0.0358	0.1223
300.0	0.0537	0.1223
400.0	0.0716	0.1223
500.0	0.0895	0.1223
600.0	0.1074	0.1223
700.0	0.1253	0.1223
800.0	0.1432	0.1223
900.0	0.1611	0.1223
1000.0	0.1790	0.1223
1100.0	0.1969	0.1223
1200.0	0.2148	0.1223
1300.0	0.2327	0.1223
1400.0	0.2506	0.1223
1500.0	0.2685	0.1223
1600.0	0.2864	0.1223
1700.0	0.3043	0.1223
1800.0	0.3222	0.1223

FREQUENCY	ALFA2 $2\alpha\xi$	BETA2 $\alpha^2 - \xi^2$
100.0	0.0181	0.1222
200.0	0.0361	0.1222
300.0	0.0542	0.1220
400.0	0.0722	0.1219
500.0	0.0903	0.1216
600.0	0.1084	0.1214
700.0	0.1264	0.1211
800.0	0.1445	0.1207
900.0	0.1626	0.1203
1000.0	0.1806	0.1198
1100.0	0.1987	0.1193
1200.0	0.2167	0.1187
1300.0	0.2348	0.1181
1400.0	0.2529	0.1175
1500.0	0.2709	0.1168
1600.0	0.2890	0.1160
1700.0	0.3070	0.1152
1800.0	0.3251	0.1144
1900.0	0.3432	0.1135

FREQUENCY	ALFA3 $2\alpha\xi$	BETA3 $\alpha^2 - \xi^2$
100.0	0.1251	0.1101
200.0	0.1769	0.1102
300.0	0.2166	0.1103
400.0	0.2501	0.1106
500.0	0.2797	0.1108
600.0	0.3064	0.1112
700.0	0.3309	0.1116
800.0	0.3538	0.1121
900.0	0.3752	0.1126
1000.0	0.3955	0.1132
1100.0	0.4148	0.1139
1200.0	0.4333	0.1146
1300.0	0.4510	0.1154
1400.0	0.4680	0.1163
1500.0	0.4844	0.1172
1600.0	0.5003	0.1182
1700.0	0.5157	0.1192

APPENDIX III

COMPUTER CODE - VOID -

1

1

```
C   DISPERSION PARAMETERS CALCULATIONS
C   DIFFUSION AND THERMALISATION THEORETICAL MODELS.
C   ALFA= = A**2-P**2
ALFA1(N,I)=A1V(N,I)**2-P1V(N,I)**2
ALFA2(N,I)=A2V(N,I)**2-P2V(N,I)**2
C   BETA= 2*A*P
BETA1(N,I)=2*A1V(N,I)*P1V(N,I)
BETA2(N,I)=2*A2V(N,I)*P2V(N,I)
12 CONTINUE
6 CONTINUE
WRITE(2,30)
30 FORMAT(1X,10X,'VOID CELL STREAMING FACTORS'//)
WRITE(2,31)SF
31 FORMAT(1X,10X,F8.6)
WRITE(2,32)
32 FORMAT(1X,'CALCULATION OF AMPLITUDE AND PHASE VARIATION WITH'//,
*10X,'FREQUENCY BY DIFFUSION APPROXIMATION THEORY'//)
WRITE(2,33)
33 FORMAT(1X,15X,'AMPLITUDE CHANGE WITH FREQUENCY'//)
WRITE(2,34)
34 FORMAT(1X,5X,'FREQUENCY',10X,'A1',10X,'A2',12X,'A3',10X,'A4'//)
WRITE(2,35)(F(I),(A1V(N,I),N=1,4),I=1,100)
35 FORMAT(1X,5X,F7.1,15X,F8.5,5X,F8.5,5X,F8.5,5X,F8.5)
WRITE(2,36)
36 FORMAT(1X,15X,'AMPLITUDE GAIN CHANGE WITH FREQUENCY'//)
WRITE(2,37)
37 FORMAT(1X,5X,'FREQUENCY',10X,'G1',10X,'G2',12X,'G3',10X,'G4')
WRITE(2,38)(F(I),(G1V(N,I),N=1,4),I=1,100)
38 FORMAT(1X,5X,F7.1,15X,F8.5,5X,F8.5,5X,F8.5,5X,F8.5)
WRITE(2,39)
39 FORMAT(1X,15X,'PHASE ANGLE CHANGE WITH THE FREQUENCY'//)
WRITE(2,40)
40 FORMAT(1X,5X,'FREQUENCY',10X,'P1',10X,'P2',12X,'P3',10X,'P4'//)
WRITE(2,41)(F(I),(P1V(N,I),N=1,4),I=1,100)
41 FORMAT(1X,5X,F7.1,15X,F8.5,5X,F8.5,5X,F8.5,5X,F8.5)
WRITE(2,44)
44 FORMAT(1X,10X,'THERMALISATION THEORY CALCULATIONS'//)
WRITE(2,45)
45 FORMAT(1X,5X,'FREQUENCY',10X,'A21',10X,'A22',10X,'A23',10X,'A24')
```

2

2

2

2

```
WRITE(2,46)(F(I),(A2V(N,I),N=1,4),I=1,100)
46 FORMAT(1X,5X,F7.1,15X,F8.5,5X,F8.5,5X,F8.5,5X,F8.5)
WRITE(2,47)
47 FORMAT(1X,15X,'AMPLITUDE GAIN CHANGE WITH FREQUENCY'//)
WRITE(2,48)
48 FORMAT(1X,5X,'FREQUENCY',10X,'G21',10X,'G22',9X,'G32',9X,'G24'//)
WRITE(2,49)(F(I),(G2V(N,I),N=1,4),I=1,100)
49 FORMAT(1X,5X,F7.1,15X,F8.5,5X,F8.5,5X,F8.5,5X,F8.5)
WRITE(2,50)
50 FORMAT(1X,15X,'PHASE ANGLE CHANGE WITH FREQUENCY'//)
WRITE(2,51)
51 FORMAT(1X,5X,'FREQUENCY',9X,'P21',9X,'P22',9X,'P23',9X,'P24'//)
WRITE(2,52)(F(I),(P2V(N,I),N=1,4),I=1,100)
52 FORMAT(1X,5X,F7.1,15X,F8.5,5X,F8.5,5X,F8.5,5X,F8.5)
WRITE(2,42)
42 FORMAT(1X,10X,'DISPERSION PARAMETERS CALCULATIONS',//
*'CALCULATUON BY DIFFUSION APPROXIMATION THEORY',//
*10X,'FREQUENCY',15X,'ALFA11',15X,'ALFA12',15X,'ALFA13',10X,
*'ALFA14'//)
WRITE(2,43)(F(I),(ALFA1(N,I),N=1,4),I=1,100)
43 FORMAT(1X,10X,F10.2,10X,F10.6,10X,F10.6,10X,F10.6,10X,F10.6)
WRITE(2,53)
53 FORMAT(1X,10X,'CALCULATIONS OF BETA1',//
*10X,'FREQUENCY',15X,'BEAT11',15X,'BETA12',15X,'BETA13',10X,
*'BETA14',//)
WRITE(2,54)(F(I),(BETA1(N,I),N=1,4),I=1,100)
54 FORMAT(1X,10X,F10.2,10X,F10.6,10X,F10.6,10X,F10.6,10X,F10.6)
WRITE(2,55)
55 FORMAT(1X,10X,'DISPERSION CALCULATIONBY THERMALISATION THEORY',//
*10X,'FREQUENCY',15X,'ALFA21',15X,'ALFA22',15X,'ALFA23',10X,
*'ALFA24',//)
WRITE(2,56)(F(I),(ALFA2(N,I),N=1,4),I=1,100)
56 FORMAT(1X,10X,F10.2,10X,F10.6,10X,F10.6,10X,F10.6,10X,F10.6)
WRITE(2,57)
57 FORMAT(1X,15X,'FREQUENCY',15X,'BETA21',15X,'BETA22',10X,'BETA23'
*,10X,'BETA24',//)
WRITE(2,58)(F(I),(BETA2(N,I),N=1,4),I=1,100)
58 FORMAT(1X,10X,F10.2,10X,F10.6,10X,F10.6,10X,F10.6,10X,F10.6)
STOP
END
```

END

VOID CELL STREAMING FACTORS

1.290644
1.300081
1.341883
1.415232

CALCULATION OF AMPLITUDE AND PHASE VARIATION WITH
FREQUENCY BY DIFFUSION THEORY

AMPLITUDE CHANGE WITH FREQUENCY

FREQUENCY	CELL 1 A1	CELL 2 A2	CELL 3 A3	CELL 4 A4
100.0	0.28384	0.28328	0.27907	0.27223
200.0	0.28688	0.28630	0.28204	0.27511
300.0	0.29164	0.29102	0.28667	0.27959
400.0	0.29773	0.29706	0.29261	0.28535
500.0	0.30480	0.30408	0.29951	0.29204
600.0	0.31254	0.31178	0.30707	0.29938
700.0	0.32073	0.31991	0.31506	0.30714
800.0	0.32918	0.32831	0.32332	0.31517
900.0	0.33778	0.33686	0.33173	0.32334
1000.0	0.34644	0.34548	0.34020	0.33157
1100.0	0.35510	0.35409	0.34868	0.33981
1200.0	0.36372	0.36267	0.35711	0.34801
1300.0	0.37228	0.37118	0.36548	0.35615
1400.0	0.38074	0.37961	0.37377	0.36421
1500.0	0.38911	0.38794	0.38196	0.37218
1600.0	0.39737	0.39616	0.39006	0.38005
1700.0	0.40553	0.40427	0.39804	0.38781
1800.0	0.41357	0.41228	0.40591	0.39547
1900.0	0.42149	0.42017	0.41368	0.40303
2000.0	0.42931	0.42795	0.42133	0.41048
2100.0	0.43701	0.43562	0.42888	0.41782
2200.0	0.44461	0.44318	0.43632	0.42506
2300.0	0.45210	0.45064	0.44366	0.43220
2400.0	0.45948	0.45800	0.45090	0.43925
2500.0	0.46677	0.46525	0.45804	0.44619
2600.0	0.47396	0.47241	0.46508	0.45305
2700.0	0.48105	0.47948	0.47204	0.45982
2800.0	0.48806	0.48645	0.47890	0.46649
2900.0	0.49497	0.49333	0.48567	0.47309
3000.0	0.50180	0.50013	0.49236	0.47960
3100.0	0.50854	0.50685	0.49897	0.48603
3200.0	0.51520	0.51348	0.50550	0.49230
↓				
9900.0	0.85298	0.84996	0.83666	0.81478
10000.0	0.85703	0.85400	0.84063	0.81864

AMPLITUDE GAIN CHANGE WITH FREQUENCY

FREQUENCY	G1	G2	G3	G4
100.0	0.99629	0.99631	0.99633	0.99635
200.0	0.98570	0.98580	0.98584	0.98594
300.0	0.96963	0.96982	0.96991	0.97011
400.0	0.94979	0.95008	0.95023	0.95053
500.0	0.92776	0.92815	0.92835	0.92876
600.0	0.90478	0.90525	0.90549	0.90599
700.0	0.88169	0.88224	0.88252	0.88309
800.0	0.85905	0.85966	0.85997	0.86061
900.0	0.83718	0.83784	0.83817	0.83887
1000.0	0.81625	0.81695	0.81730	0.81804

PHASE ANGLE CHANGE WITH THE FREQUENCY

FREQUENCY	P1	P2	P3	P4
100.0	0.02443	0.02430	0.02390	0.02323
200.0	0.04834	0.04808	0.04729	0.04597
300.0	0.07132	0.07096	0.06979	0.06785
400.0	0.09315	0.09268	0.09116	0.08864
500.0	0.11374	0.11318	0.11133	0.10826
600.0	0.13311	0.13247	0.13031	0.12673
700.0	0.15133	0.15061	0.14817	0.14411
800.0	0.16851	0.16773	0.16501	0.16050
900.0	0.18474	0.18390	0.18093	0.17600
1000.0	0.20014	0.19924	0.19603	0.19071
1100.0	0.21478	0.21383	0.21039	0.20469
1200.0	0.22875	0.22775	0.22409	0.21804
1300.0	0.24212	0.24108	0.23721	0.23081
1400.0	0.25495	0.25386	0.24979	0.24306
1500.0	0.26729	0.26615	0.26189	0.25485
1600.0	0.27918	0.27800	0.27356	0.26621
1700.0	0.29066	0.28945	0.28482	0.27718
1800.0	0.30178	0.30052	0.29573	0.28780
1900.0	0.31255	0.31126	0.30630	0.29810
2000.0	0.32301	0.32160	0.31656	0.30800
9700.0	0.79609	0.79312	0.78063	0.76005
9800.0	0.80043	0.79744	0.78488	0.76419
9900.0	0.80474	0.80174	0.78911	0.76831
10000.0	0.80903	0.80601	0.79332	0.77240

THERMALISATION THEORY CALCULATIONS

AMPLITUDE CHANGES WITH FREQUENCY

FREQUENCY	A21	A22	A23	A24
100.0	0.32868	0.32806	0.32413	0.31773
200.0	0.35713	0.35646	0.35252	0.34607
300.0	0.37876	0.37806	0.37405	0.36750
400.0	0.39657	0.39583	0.39176	0.38508
500.0	0.41188	0.41111	0.40697	0.40016
600.0	0.42540	0.42460	0.42039	0.41347
700.0	0.43757	0.43675	0.43247	0.42543
800.0	0.44869	0.44785	0.44350	0.43634
900.0	0.45895	0.45808	0.45367	0.44640
1000.0	0.46850	0.46762	0.46314	0.45576
1100.0	0.47746	0.47655	0.47201	0.46453
1200.0	0.48590	0.48498	0.48037	0.47279
1300.0	0.49390	0.49297	0.48829	0.48061
1400.0	0.50152	0.50056	0.49583	0.48804
1500.0	0.50879	0.50782	0.50302	0.49514
1600.0	0.51576	0.51477	0.50991	0.50193
1700.0	0.52245	0.52144	0.51653	0.50845
1800.0	0.52889	0.52787	0.52290	0.51472
1900.0	0.53512	0.53408	0.52905	0.52077
2000.0	0.54113	0.54008	0.53499	0.52662

AMPLITUDE GAIN CHANGE WITH FREQUENCY

FREQUENCY	G21	G22	G32	G24
100.0	0.86036	0.86032	0.85782	0.85367
200.0	0.79182	0.79178	0.78875	0.78377
300.0	0.74659	0.74655	0.74334	0.73807
400.0	0.71307	0.71302	0.70974	0.70436
500.0	0.68657	0.68653	0.68322	0.67781
600.0	0.66475	0.66471	0.66140	0.65600
700.0	0.64626	0.64622	0.64293	0.63756
800.0	0.63025	0.63021	0.62695	0.62162

PHASE ANGLE CHANGE WITH FREQUENCY

FREQUENCY	P21	P22	P23	P24
100.0	0.16748	0.16718	0.16655	0.16545
200.0	0.21798	0.21760	0.21657	0.21482
300.0	0.25172	0.25127	0.24998	0.24776
400.0	0.27761	0.27712	0.27560	0.27302
500.0	0.29884	0.29831	0.29662	0.29374
600.0	0.31696	0.31640	0.31455	0.31142
700.0	0.33283	0.33224	0.33027	0.32691
800.0	0.34700	0.34639	0.34429	0.34075
900.0	0.35982	0.35919	0.35699	0.35327
1000.0	0.37155	0.37090	0.36861	0.36473
1100.0	0.38237	0.38170	0.37933	0.37532
1200.0	0.39244	0.39175	0.38930	0.38516
1300.0	0.40184	0.40114	0.39862	0.39436
1400.0	0.41068	0.40997	0.40738	0.40301
1500.0	0.41902	0.41829	0.41565	0.41118
1600.0	0.42692	0.42618	0.42348	0.41892
1700.0	0.43442	0.43367	0.43092	0.42628
1800.0	0.44156	0.44081	0.43801	0.43329
1900.0	0.44839	0.44762	0.44479	0.43999
2000.0	0.45492	0.45415	0.45127	0.44641
2100.0	0.46118	0.46041	0.45749	0.45257
2200.0	0.46720	0.46642	0.46347	0.45849
2300.0	0.47300	0.47221	0.46923	0.46419
2400.0	0.47858	0.47778	0.47478	0.46969
2500.0	0.48396	0.48316	0.48013	0.47499
2600.0	0.48917	0.48836	0.48531	0.48013
2700.0	0.49420	0.49339	0.49032	0.48510
2800.0	0.49908	0.49826	0.49517	0.48991
2900.0	0.50380	0.50299	0.49987	0.49458
3000.0	0.50838	0.50757	0.50444	0.49912
3100.0	0.51283	0.51201	0.50887	0.50352
3200.0	0.51716	0.51633	0.51318	0.50781
3300.0	0.52136	0.52054	0.51737	0.51198
3400.0	0.52545	0.52462	0.52145	0.51604

DISPERSION PARAMETERS CALCULATIONS

CALCULATUON BY DIFFUSION APPROXIMATION THEORY

FREQUENCY	ALFA11	ALFA12	ALFA13	ALFA14
100.00	0.079966	0.079657	0.077311	0.073570
200.00	0.079966	0.079657	0.077311	0.073570
300.00	0.079966	0.079657	0.077311	0.073570
400.00	0.079966	0.079657	0.077311	0.073570
500.00	0.079966	0.079657	0.077311	0.073570
600.00	0.079966	0.079657	0.077311	0.073570
700.00	0.079966	0.079657	0.077311	0.073570
800.00	0.079966	0.079657	0.077311	0.073570
900.00	0.079966	0.079657	0.077311	0.073570
1000.00	0.079966	0.079657	0.077311	0.073570
1100.00	0.079966	0.079657	0.077311	0.073570
1200.00	0.079966	0.079657	0.077311	0.073570
1300.00	0.079966	0.079657	0.077311	0.073570
1400.00	0.079966	0.079657	0.077311	0.073570
1500.00	0.079966	0.079657	0.077311	0.073570
1600.00	0.079966	0.079657	0.077311	0.073570
1700.00	0.079966	0.079657	0.077311	0.073570
1800.00	0.079966	0.079657	0.077311	0.073570
1900.00	0.079966	0.079657	0.077311	0.073570
2000.00	0.079966	0.079657	0.077311	0.073570
2100.00	0.079966	0.079657	0.077311	0.073570
2200.00	0.079966	0.079657	0.077311	0.073570
2300.00	0.079966	0.079657	0.077311	0.073570
2400.00	0.079966	0.079657	0.077311	0.073570
2500.00	0.079966	0.079657	0.077311	0.073570
2600.00	0.079966	0.079657	0.077311	0.073570
2700.00	0.079966	0.079657	0.077311	0.073570
2800.00	0.079966	0.079657	0.077311	0.073570
2900.00	0.079966	0.079657	0.077311	0.073570
3000.00	0.079966	0.079657	0.077311	0.073570
3100.00	0.079966	0.079657	0.077311	0.073570

CALCULATIONS OF BETA1

FREQUENCY	BEAT11	BETA12	BETA13	BETA14
100.00	0.013867	0.013767	0.013338	0.012646
200.00	0.027734	0.027533	0.026675	0.025293
300.00	0.041602	0.041300	0.040013	0.037939
400.00	0.055469	0.055066	0.053351	0.050586
500.00	0.069336	0.068833	0.066689	0.063232
600.00	0.083203	0.082600	0.080026	0.075879
700.00	0.097071	0.096366	0.093364	0.088525
800.00	0.110938	0.110133	0.106702	0.101172
900.00	0.124805	0.123899	0.120040	0.113818
1000.00	0.138672	0.137666	0.133377	0.126465
1100.00	0.152540	0.151432	0.146715	0.139111
1200.00	0.166407	0.165199	0.160053	0.151758
1300.00	0.180274	0.178966	0.173391	0.164404
1400.00	0.194141	0.192732	0.186728	0.177050
1500.00	0.208009	0.206499	0.200066	0.189697
1600.00	0.221876	0.220265	0.213404	0.202343
1700.00	0.235743	0.234032	0.226741	0.214990
1800.00	0.249610	0.247799	0.240079	0.227636
1900.00	0.263478	0.261565	0.253417	0.240283
	↓	↓	↓	↓
9800.00	1.358990	1.349125	1.307098	1.239353
9900.00	1.372858	1.362892	1.320436	1.252000
10000.00	1.386725	1.376659	1.333773	1.264646

DISPERSION CALCULATION BY THERMALISATION THEORY

FREQUENCY	ALFA21	ALFA22	ALFA23	ALFA24
100.00	0.079981	0.079672	0.077324	0.073581
200.00	0.080025	0.079715	0.077363	0.073614
300.00	0.080099	0.079787	0.077429	0.073671
400.00	0.080202	0.079888	0.077521	0.073749
500.00	0.080335	0.080018	0.077639	0.073850
600.00	0.080498	0.080177	0.077784	0.073973
700.00	0.080690	0.080365	0.077955	0.074119
800.00	0.080911	0.080582	0.078152	0.074287
900.00	0.081162	0.080828	0.078375	0.074477
1000.00	0.081443	0.081102	0.078625	0.074690
1100.00	0.081753	0.081406	0.078901	0.074925
1200.00	0.082093	0.081738	0.079203	0.075183

FREQUENCY	BETA21	BETA22	BETA23	BETA24
100.00	0.110092	0.109692	0.107970	0.105134
200.00	0.155693	0.155127	0.152692	0.148682
300.00	0.190685	0.189991	0.187009	0.182098
400.00	0.220184	0.219383	0.215939	0.210269
500.00	0.246173	0.245278	0.241427	0.235088
600.00	0.269669	0.268688	0.264470	0.257526
700.00	0.291276	0.290217	0.285661	0.278159
800.00	0.311387	0.310255	0.305384	0.297365
900.00	0.330276	0.329075	0.323909	0.315403
1000.00	0.348141	0.346875	0.341430	0.332464
1100.00	0.365134	0.363806	0.358094	0.348691
1200.00	0.381370	0.379983	0.374017	0.364196
1300.00	0.396942	0.395499	0.389290	0.379067
1400.00	0.411926	0.410428	0.403985	0.393377
1500.00	0.426384	0.424834	0.418164	0.407184
1600.00	0.440368	0.438766	0.431878	0.420538
1700.00	0.453921	0.452270	0.445170	0.433480
1800.00	0.467080	0.465382	0.458076	0.446047
1900.00	0.479880	0.478135	0.470628	0.458270
2000.00	0.492346	0.490556	0.482854	0.470175
2100.00	0.504505	0.502670	0.494779	0.481786
2200.00	0.516377	0.514499	0.506422	0.493124
2300.00	0.527982	0.526062	0.517804	0.504207
2400.00	0.539338	0.537377	0.528941	0.515051
2500.00	0.550460	0.548458	0.539848	0.525672
2600.00	0.561361	0.559320	0.550539	0.536082
2700.00	0.572054	0.569974	0.561026	0.546294
2800.00	0.582552	0.580433	0.571321	0.556319
2900.00	0.592863	0.590707	0.581434	0.566166
	↓	↓	↓	↓
9700.00	1.084280	1.080337	1.063377	1.035454
9800.00	1.089854	1.085891	1.068844	1.040777
9900.00	1.095401	1.091418	1.074283	1.046074
10000.00	1.100919	1.096916	1.079695	1.051344

BIBLIOGRAPHY

- AHMED, M. 1969, "Neutron Streaming and Isotropic Effects in Diffusing Medium With Empty Channels", Part I, The Nucleus, 6, pp 200 - 205.
- ARFKEN, A. 1973, "Mathematical Methods for Physicists" 1st.Ed., Academic Press, New York.
- BEHRENS, D.J. 1949, "The Effect of Holes In A Reacting Material On The Passage Of Neutrons", Proc. Phys.Soc. London, A62, pp 607 - 616.
- BEHRENS, D.J. 1959, "The Effects Of Holes In A Moderator On Neutron Slowing Down", A.E.R.E., U.K., (T/R 103).
- BENOIST, P. 1968, "Streaming Effects And Collision Probabilities In Lattices", Nucl.Sci.Engng., 34, pp 285 - 307.
- BEYNON, T.D. and MONDAL, M.A.W. 1971, "On The Effect Of Accelerator Pulse Shape On Neutron Slowing Down Time" J.Nucl.Energy, Vol.25, pp 391-395.
- BIRKS, J.B. 1964, "The Theory Of Scintillation Counting", Pergmann Press, London.
- BOOTH, R.S. and PEREZ, R.B. 1967, "Propagation Of Thermal Neutron Wave In Hetrogeneous Media", Proc.Symp.Neutron Noise,Wave and Pulse Propagation, Division Of Technical Information, USAEC.
- BULL, S.R. et al 1970, "Pulsed Source Investigation On Graphite Systems", J.Nucl.Energy, Vol.24, pp 473-477.
- BULL S.R. and CONNOLLY, W. 1971 "Pulse-Source Investigation II, The Effect Of Cylindrical Void Channels In A Neutron Diffusing Medium", J.Nucl.Energy, Vol.25, pp 179-187.
- CARTER, C. 1961, "Influence Of Cylindrical Channels On A Neutron Flux", J.Nucl.Energy, Part A/B, Vol.15, pp 113-119.
- CARTER, C. 1961, "Streaming Due To Holes In A Reactor" J.Nucl.Energy, Vol.15, pp 76-80.

- COATES, M.S. et al 1974, "Measurement Of Relative ${}^6\text{Li}(n,\alpha)\text{T}$ Cross Section In The Energy Range 1 keV-500 keV", Proc. Symp. Neutron Standard Reference Data, I.A.E.A., Vienna .
- COOPER, P.N. and DOUKAS, L. 1971, "External Pulsing Of An Accelerator", Nucl. Instr. Methods, 92, pp 581 - 582.
- CORNGOLD, N. 1965, "Theoretical Interpretation Of Pulsed Neutron Phenomena", Proc. Symp. Pulsed Neutron Research, Vol. I, I.A.E.A., pp 199-218.
- DANCE, T. and CONNOLLY, W. 1971, "Pulsed-Source Investigation -I, The Effect Of Voids On Neutron Transport In a Diffusing Medium", J. Nucl. Energy, Vol. 25, pp 155-177.
- DANSO, T. 1969, "Investigation Of Neutron Diffusion Parameters In Liquid Moderator and Liquid-Moderated Multiplying Systems" A Ph.D. Dissertation, Dept. of Physics, The University of Aston in Birmingham, U.K.
- DAUGHTRY, J.W. and WALTNER, A.W. 1965, "The Diffusion Parameters Of Heavy Water", Proc. Symp. Pulsed Neutron Research, Vol. I, I.A.E.A., pp 65-88.
- DENIZ, V. 1968, "Study Of Lattice Of Graphite With Empty Channels by Means Of The Pulsed Source Technique" Nucl. Sci. Engng., 32, pp 201-224.
- DOUKAS, L. 1971, "Reactivity Investigation Using A Periodic Neutron Source In A Sub-Critical Assembly", A Ph.D. Dissertation, Dept. of Physics, The University of Aston In Birmingham, U.K.
- ETEMAD, A. and PICTET, J.M. 1964, "PENETRATION OF NEUTRONS IN CYLINDRICAL AIR DUCTS IN DIFFUSING MEDIA", 3rd. U.N. Inter. Conf. on the Peaceful Uses of Atomic Energy, Report No. A/Conf.28/P/688.
- FORT, E. and MARQUETTE, J.P. 1974, "Experimental Methods Used

- To Determine The ${}^6\text{Li}(n, \gamma)\text{T}$ Cross Section Between 20 keV and 1700 keV", Proc. Symp. Neutron Standard Reference Data, I.A.E.A., Vienna.
- GIL RAMOS, A. 1974, "The Spatial Response Of A Multiplying System To A Periodic Neutron Source", A Ph.D. Dissertation, Dept. of Physics, The University of Aston in Birmingham, U.K.
- GIL RAMOS, A. and COOPER, P.N. 1974, "Improvements To A Method Of Externally Pulsing An Accelerator", Nucl. Instr. and Methods, 109, pp 617-618.
- GOYAL, I.C. et al 1971, "The Decay Of Neutron Pulse In A Multiplying Assembly Using A Simple Kernel", J.Nucl.Energy, 25, pp 121-128.
- GRANT, J.S. 1958, "Neutron Streaming In Gas-Cooled Reactors", A.E.R.E., Report No. R/R 2568, Harwell, U.K.
- HENRY, A.F. 1972, "Review Of Computational Methods For Space Dependent Kinetics", Dynamics of nuclear systems, Ed. D.L. Hetrick, University of Chicago Press, pp 9-21.
- HETRIC, D.L. 1971, "Dynamics of Nuclear Reactors", The University of Chicago Press, Chicago and London.
- HINO, T. and OZAWA, Y. 1974, "Analysis Of Fast Neutron Pulse By Superposition of Wave Modes", J. Nucl. Sci. and Technology, 11, 4, pp 119-124.
- HUGHES, D.J. et al 1958, "Neutron Cross Sections", BNL-325, 2nd edition, U.S.A.E.C.
- JOSHI, A. et al 1965, "Diffusion Parameters Of BeO By Pulsed Neutron Method", Proc. Symp. Pulsed Neutron Research, Vol. I, pp 105-121, I.A.E.A., Vienna.
- KANEKO, Y. et al 1974, "Measurements of Anisotropic Neutron Diffusion Coefficients In Square Lattice Of Aluminum In Light Water By The Pulsed Neutron Method", Nucl. Sci. Engng., 55, pp 89-116.

- KERLIN, T.W. 1972, "Method For Frequency Response Measurements In Power Reactors", Dynamics Of Nuclear Systems, D.L.Hetrick, (Ed.), University Of Arizona Press.
- KERLIN, T.W. 1974, "Frequency Response Testing In Nuclear Reactors", Academic Press, New York.
- KUNAISH, H.E. 1967, "Consistent P-3 Theory Of Neutron Wave Propagation", Proc. Symp. Neutron Noise, Wave And Pulse Propagation, Division of technical information, U.S.A.E.C.
- LALETIN, N.I. 1958, "Passage Of Neutrons In A Hetrogeneous Medium", 2nd. Inter. Conf. On Peaceful Application Of Atomic Energy, Vol.16, pp 601-610.
- LAMARSH, R.J. 1967, "Introduction To Nuclear Reactor Theory" Addison-Wesley Publishing Compony, Inc. Reading, U.S.A.
- MARTI, J.T. and SCHNEEBERGER, J.P. 1962, "The Reactivity Effects Of A regular Array Of Empty Channels In A Critical Systems", Nucl. Sci. Engng., 13, pp 1-13.
- MEGAHID, R. 1975, "Fast Neutron Attenuation And Energy Loss In Extended Shields", A Ph.D. Dissertation, Dept. Of Physics, University Of Aston In Birmingham, U.K.
- MICHAEL, P. and MOORE, M.N. 1968, "Relationship Between Pulsed And Wave Experiments", Proc. Symp. Neutron Thermalisation And Reactor Spectra, Vol.I, pp 125-142, I.A.E.A., Vienna.
- MOORE, M.N. 1965, "The Determination Of Reactor Dispersion Laws From Modulated Neutron Experiment", Nucl. Sci. Eng., 21, pp 565-572.
- MOORE, M.N. 1966, "The Dispersion Law Of A Moderator", Nucl. Sci. Engng., 26, pp 354-361.
- MOORE, M.N. 1967, "The General Theory Of Excitation Experiments In Space Dependent Kinetics", Proc. Symp. Neutron Noise, Wave And Pulse Propagation, Division Of Technical Information, U.S.A.E.C.

- PAGE, R.W. 1967, "An Investigation Of Neutron Streaming Using The Pulsed-Neutron Source Technique", J.Nucl.Energy, 21, pp 403-415.
- PAIANO, M.C. and PAIANO, S. 1968, "Pulsed Neutron Measurement In Water", Proc. Symp. Neutron Thermalisation And Reactor Spectra, Vol.II, pp 395-410, I.A.E.A., Vienna.
- PEREZ, R.B. and BOOTH, R.S. 1965, "Excitation Of Neutron Waves By Modulated And Pulsed Sources", Proc.Symp. Pulsed Neutron Research, Vol.II, pp 701-728, I.A.E.A., Vienna.
- PEREZ, R.B. and UHRIG, R.E. 1963, "Propagation Of Neutron Waves In Moderating Media", Nucl. Sci. Engng., 17, pp 90-100.
- PEREZ, R.B. and UHRIG, R.E. 1967, "Development Of Neutron-Wave and Neutron-Pulse Propagation", Proc. Symp. Neutron Noise, Wave And Pulse Propagation, Division of Technical Information, U.S.A.E.C.
- POOLE, M.J. 1965, "Review Of The Application Of Pulsed Source To The Measurement Of Neutron Spectra In Moderators And Reactor Lattice", Proc. Symp.Pulsed Neutron Research, Vol.I, pp 425-464, I.A.E.A., Vienna.
- PRICE, W.J. 1964, "Nuclear Radiation Detectors", McGraw-Hill Book Company, New York.
- PUROHIT, S.N. 1965, "Time-Dependent Neutron Thermalisation In Liquid Moderators H_2O and D_2O ", Proc. Symp. Pulsed Neutron Research, Vol.I, pp 273-288, I.A.E.A., Vienna.
- QUDDUS, M.A. et al 1969, "Axial Propagation Of Neutron Waves In Hetrogeneous Media", Nucl. Sci. Engng., 35, pp 342-349.
- RITCHIE, A.I.M. and WHITTLESTONE, S. 1972, "Measurement Of The Thermal neutron Wave Dispersion Relations In BeO ", J.NUCL. Energy, Vol. 26, pp 27-41.
- RITCHIE, A.I.M. and WHITTLESTONE, S. 1973, "Measurement Of Thermal Neutron Waves At High Frequencies In BeO ", J. Nucl. Energy, Vol. 27, pp 335-350.

- SCHAEFER, C. and PARKYN, D. 1958, "A Monte Carlo Study Of Thermal Utilization Factor And Diffusion Area : Gas-Cooled Graphite-Moderated Lattice", Proc. 2nd. Inter. Conf. Peaceful Uses Of Atomic Energy, Vol. 16, pp 496-503.
- SOBHANA, S. et al 1973, "Study of Neutron Wave Propagation Through A Subcritical Assembly", J. Nucl. Energy, 27, pp 441-447.
- UHRIG, R.E. 1967, "Neutron Noise, Wave And Pulse Propagation", (Ed), Division of technical information, U.S.A.E.C.
- UHRIG, R.E. 1965, "Techniques Closely Related To Pulsed Neutron Research", Proc. Symp. Pulsed Neutron Research, Vol.I, pp 657- 699, I.A.E.A., Vienna.
- UHRIG, R.E. 1970, "Random Noise Technique In Nuclear Reactor Systems", Ronald Press Company, New York.
- UTZINGER, F. et al 1965, "Pulsed-Source Experiments with A Multiplying And Non-Multiplying Heavy Water Systems", Proc. Symp. Pulsed Neutron Research, Vol.II, pp 119-131, I.A.E.A., Vienna.
- VAN BINNBECK, K. 1974, "A Theory For Pulsed-Neutron Experiments In Reactor Lattice", Nucl. Sci. Engng., 54, pp 341-352.
- WARNER, J.H.Jr. and ERDMANN, R.C. 1969a, "Infinite Medium Neutron Wave Propagation - Theory", J. Nucl. Energy, Vol.23, pp 117-134.
- WARNER, J.H.Jr. and ERDMANN, R.C. 1969b, "Inifinite Neutron Wave Propagation - Numerical Results For Water And Graphite", J. Nucl. Energy, Vol.23, pp 135-145.
- WAGNER, R. 1970, "Neutron Wave Experiment In A Heavy Water - Natural Uranium Subcritical Assembly", J. Nucl. Energy, Vol.24, pp 71-84.

- WILLIAMS, M.M.R. 1968, "Existence Of A Diffusion Length In A Finite Prism Of Pure Moderator", Proc. Symp. Neutron Thermalisation And Reactor Spectra, Vol.I, pp 27-43, I.A.E.A., Vienna.
- WOOD, J. 1965, "Time And Space Eigenvalues Of The Boltzmann Equation", Proc. Symp. Pulsed Neutron Research, Vol.I, pp 219-238, I.A.E.A., Vienna.
- WOOD, J. 1969, "An Interpretation Of Neutron Wave Experiment", J. Nucl. Energy, Vol.23, pp 17-28.
- WOOD, J. and LAWRENCE, E.W. 1971, "Neutron Wave Interference Effects In Beryllium Oxide", J.Nucl.Energy, Vol 25, pp 525-529.

- COHN, C.E. et al. (1968), "Calculation of Space-Dependent Transfer Function Using Static Technique", Nucl. Sci. and Engng., 26, pp 198-206
- GODDART, J., (1968), "Measurement of neutron Spectra In Light water-Uranium Systems", Proc.Symp.Neutron thermalisation and Reactor Spectra, Vol.I pp 58-71
- KOBAYASHI, K. (1975), "A Numerical study on Application of Benoist's Anisotropic Diffusion Coefficients", J.Nucl.Sci. and Technology, 12(7), pp 456-459
- MILES, R.E. et al (1974), "Neutron Wave in Beryllium", Annals of Nucl.Sci. and Engng. Vol.I pp 365-376.
- PEREZ, R.B. and OHANIAN, M.J. (1968), "Propagation of Monochromatic Neutron Wave in Non-Multiplying Media", Proc.Symp. Neutron Noise, Wave and Pulse Propagation, Division of Technical Information, U.S.A.E.C.
- TAKASHAHI, K. (1968), "A Simple Pulsed Neutron Source For Neutron Propagation Experiments", Proc.Symp.Neutron Thermalisation and Reactor Spectra, Vol.I, pp 161-172, I.A.E.A., Vienna.